2015

Behaviour of geocell-reinforced subballast under cyclic loading in plane strain condition

M Mahdi Biabani
University of Wollongong

UNIVERSITY OF WOLLONGONG

Department of Engineering

School of Civil, Mining and Environmental Engineering

Behaviour of Geocell-Reinforced Subballast under Cyclic Loading in Plane Strain Condition

M. Mahdi Biabani

(BScEng, MScEng)

This thesis is presented as part of the requirement for the

Award of the Degree of the Doctor of Philosophy

of the

University of Wollongong

2015

CERTIFICATION

I, M. Mahdi Biabani, declare that this thesis, submitted in fulfilment of the requirements for the award of Doctor of Philosophy, in the Department of Civil Engineering, University of Wollongong, is wholly my own work unless otherwise referenced or acknowledged. The results, ideas and convictions presented are those of the author, except when stated otherwise, and only he us accountable for them. The document has not been submitted for qualification at any other academic institution.

M. Mahdi Biabani

February 2015

ABSTRACT

Ballasted rail tracks have gained a competitive edge over other modes of transportation systems in terms of long term performance, better ride quality, higher safety, lower cost of construction and relatively acceptable speed and efficiency of services. In order to keep rail infrastructure costs minimal, the railway industry needs to use locally available materials during track construction, some of which do not have sufficient shear strength. At times owing to use of poor quality material, ballast and subballast cause excessive lateral spreading that leads to differential track settlement, cases of derailment and regular costly maintenance. In addition, presence of soft estuarine clay deposits along the coastal belt of Australia pose serious concerns on track stability. On other hand, considering significant demand for urban transportation, substantial urban growth, the construction of new tracks as well as the maintenance and modernisation of existing tracks have been more challenging. As result, other engineering solutions should be pursued to improve ballasted rail track substructure, which can help to maintain railways as the most economical and safest mode of transportation in Australia.

In the view of above, reinforcing the subballast is an economical alternative for stabilizing the track substructure. Unlike conventional rigid reinforcement such as steel and timber, flexible geosynthetics have shown a promising approach for improving the performance of granular media (ballast and subballast) placed over weak and soft subgrade. In the recent past, different varieties of geosynthetics, including planar (two dimensional) and cellular (three dimensional) geosynthetics, have been successfully employed. Geosynthetics have been proven to be effective in terms of reducing the settlements and enhancing track stability. Nevertheless, among different types of reinforcement, a geocell mattress due to its unique honeycomb shape, provides an effective cellular confinement, to reduce lateral displacement. Additional confinement induced by the geocell, mobilized by the tensile stresses of the membrane (i.e. hoop stress), arrests almost all lateral spreading of the infill material and increases the overall material stiffness.

It is important to note that the potential use of geocells to stabilise the ballast layer has often been regarded with some scepticism from a track maintenance point of view. In other words, cleaning and replacement of spent material is not convenient if a geocell mattress interferes with the tamper 'tines'. In this context, Australian rail organisations have now made attempts to use geocells and other methods of stabilisation to improve the subballast that rarely requires maintenance, rather than the overlying ballast. This study was the result of applied research undertaken within the Cooperative Research Centre for Rail Innovation in collaboration with the rail organisations, namely ARTC and Sydney Trains.

In this study, triaxial tests were conducted to characterize the behaviour of reinforced and unreinforced subballast under cyclic loading using large-scale process simulation prismoidal triaxial apparatus (PSPTA) designed and built at the University of Wollongong, Australia. The laboratory tests were conducted in plane strain condition and stress controlled mode. Cyclic loading with different frequencies under very low confining pressure was applied to study the performance of subballast. Granular material with an average particle size of 3.3 mm and a geocell system with a depth of 150 mm and a nominal area of 46×10^3 mm^2, made from high density polyethylene (HDPE) material, were used in this study. The laboratory results revealed that subballast stabilisation was influenced by the number of cycles, the confining pressure and the frequency.

The results proved that the geocell reinforcement is an ideal technique to improve subballast performance under very low confining pressure. The outcome of this investigation confirmed that the geocell could effectively arrest lateral spreading and reduce excessive settlement of the subballast under cyclic loading, hence increase track longevity. The results also showed that the geocell performs effectively, especially under low confining pressure ($5 \leq \sigma'_3 \leq 30$ kPa) and higher frequencies ($10 \leq f \leq 30$ Hz). Moreover, the geocell increased the resilient modulus of the composite layer, providing enhanced track stability of increased train speed. An optimum confining pressure required to reduce excessive volumetric dilation of the subballast was also identified in this study.

The interface shear resistance developed between the subballast and geocell has important consequences on the shear behaviour of the geocell reinforced soil. In this regard, the interface shear resistance of unreinforced and reinforced subballast with different types of geosynthetics was also investigated using a large-scale direct shear box apparatus (DSBA). The results showed that the loading mechanism had a significant impact on the interface shear strength of the subballast.

A new analytical model was developed to calculate the additional confining pressure induced by the geocell mattress. The proposed model investigate the influence of several factors i. e. (a) frequency (b) confining pressure (c) number of cycles (d) the tensile strength on the behaviour of geocell reinforced subballast. Practical design guidelines in terms of allowable train speeds for different levels of confining pressure are provided for unreinforced and geocell reinforced subballast.

Finally, a three-dimensional numerical analysis was developed for unreinforced and geocell-reinforced subballast to simulate practical or real-life railroad conditions to support experimental observations. The numerical predictions indicated that the load-distribution mechanism of subballast could be improved by the geocells. The finite element predictions were found to be in good agreement with the laboratory data. This numerical analysis can be used as a primary tool in the design of geocell-reinforced granular material with known shear strength, subjected to cyclic loading in typical railway environments.

ACKNOWLEDGEMENTS

I wish to express my sincere gratitude to Professor Indraratna for his valuable discussions, patient guidance and enthusiastic encouragement throughout this study. I also extend my sincere thanks to my co-supervisors, Dr. Sanjay Nimbalkar and A/Prof. Cholachat Rujikiatkamjorn for their assistance at all times and constructive comments.

I would like to acknowledge the American Society of Civil Engineers for allowing me to use the technical data presented in numerous Figures, Tables, and some technical discussions in the journal paper published in the *Journal of Geotechnical and Geo-environmental Engineering*.

I also wish to express my great appreciation to the CRC for Rail Innovation and to the Australian Postgraduate Award (APA), which without their sponsorship, this project would not have been possible. The author is grateful to the University of Wollongong and Centre for Geomechanics and Railway Engineering (GRE) for continuing the financial support of the study through this study.

I thank all technical staff who assisted me during laboratory work, especially Alan Grant for his assistance, planning and understanding of the experimental requirements. I also would like to thank Ritchie McLean, Fernando Escribano, Cameron Neilson and Bob Rowlan for their contribution to various aspects of the project.

I wish to extend my sincere gratitude to my wife Saeideh Mashayekhi for her continual love, encouragement and my sweet girl, Romina, who without their help this study would not have been possible.

Thank you my friends and fellow PhD student who celebrated the great time and endured bad times with me.

LIST OF PUBLICATIONS

The following publications are related with this PhD thesis.

Indraratna, B., **Biabani, M. M.** and Nimbalkar, S. (2015). "Behavior of geocell-reinforced subballast subjected to cyclic loading in plane strain condition." *Journal of Geotechnical and Geoenvironmental Engineering*, 141(1): 04014081.

Indraratna, B., **Biabani, M. M.** and Nimbalkar, S. (2015). Closure to Discussion of "Behavior of geocell reinforced subballast subjected to cyclic loading in plane strain condition". *Journal of Geotechnical and Geoenvironmental Engineering ASCE*.

Biabani M. M., Indraratna, B. (2014). "An evaluation of the interface behaviour of rail subballast stabilised with geogrids and geomembranes." *Journal of Geotextiles and Geomembranes* 43(3): 240-249

Biabani, M. M., Indraratna, B. and Nimbalkar, S. (2015). "Improved performance of subballast stabilized using geocell for high speed train." *4th International conference on Recent Advance in Rail engineering, Tehran, Iran*. (accepted)

Biabani, M. M., Indraratna, B. and Nimbalkar, S. (2015). "Behaviour of geocell-reinforced subballast under cyclic loading." *XV Pan American Conference on Soil Mechanics and Geotechnical Engineering. Buenos Aires, Argentina*. (Abstract accepted, technical paper under review)

Biabani, M. M., Indraratna, B. and Nimbalkar, S. (2016). "Additional confinement induced by the geocell mattress under cyclic loading." *Geotechnical and Structural Engineering Congress, Phoenix, Arizona, USA, 2016,* Technical Paper. (Abstract submitted)

List of symbols

A	=	shearing area in direct shear (mm^2)
A', B', C', D'	=	model parameters relating resilient modulus
a', b', c', d'	=	model parameters relating permanent deformation
a , b	=	mohr-coulomb experimental parameters (dimensionless)
B	=	footing width (mm)
b	=	geocell mattress width (mm)
B_S	=	width of sleeper (mm)
ΔB	=	wide slab effect (mm)
B_g	=	width of the grid (mm)
C	=	non-dimensional factor (≈ 0.3)
c	=	super elevation (mm)
c, d	=	experimental parameters for plastic work (dimensionless)
C_c	=	coefficient of curvature (dimensionless)
C_r	=	apparent cohesion (kPa)
C_u	=	uniformity coefficient (dimensionless)
D	=	loading plate diameter (mm)
D_0	=	initial diameter of geocell pocket (mm)
d	=	diameter of an equivalent circular area of geocell pocket (m)
d_S	=	distance between the rail head center and edge of the sleeper (mm)
D_{10}	=	diameter for 10% fine by weight (mm)
D_{20}	=	diameter for 20% fine by weight (mm)
D_{30}	=	diameter for 30% fine by weight (mm)
D_{50}	=	average particle size (mm)
D_{60}	=	diameter for 60% fine by weight (mm)
D_{max}	=	maximum particle size (mm)
D_{min}	=	minimum particle size (mm)
D_p	=	dilation factor for maximum shear stress (dimensionless)
d_q, S_q *and* S_γ	=	bearing capacity parameters
D_R	=	relative density (%)
D_r	=	depth of reinforcement (mm)
D_w	=	wheel diameter (m)
E	=	elastic modulus (MPa)
e *and* f'	=	model parameters
F_2	=	factor depending on track maintenance and sleeper type (dimensionless)
f	=	frequency (Hz)
f_b	=	interface coefficient (dimensionless)
$F(M_R)$	=	improved resilient modulus (%)
$F(S_a,_p)$	=	settlement reduction factor (%)
F_v	=	speed improvement factor (%)
g	=	gravity acceleration (m/s^2)
G	=	horizontal distance between rail and centreline (mm)
h	=	geocell height (mm)
d *and* b	=	dimension of geocell mattress(mm)
J_2	=	first stress invariant (kPa)
k_1, k_2, k_3	=	resilient modulus constants
k'_1, k'_2, k'_3	=	model parameters relating resilient modulus

g', h', i, j and k' = model parameters relating permanent deformation

k = ratio, $(\varepsilon_c^p / \varepsilon_3^p)$ (dimensionless)

k_σ = normalized confinement ratio (dimensionless)

k_τ = interface shear strength ratio

I_f = bearing capacity improving factor (dimensionless)

I_L = lateral spreading reduction factor (%)

l, b, h = dimension of cubical triaxial chamber (mm)

L = total length of sleeper (mm)

$L_a \times W_a \times H_a$ = dimension of the large-scale equipment (mm)

L_e = effective length of sleeper supporting the load (mm)

L_f = footing length (mm)

M = geocell modulus (kN/m)

m = vertical distance from top of the rail to the centre of the vehicles mass (mm)

M_m = mobilized geocell modulus (kN/m)

M_R = resilient modulus (MPa)

N = number of cycles

n = material porosity (%)

n' = super-elevation deficiency (mm)

n_c = cell number

n_{max} = maximum porosity (%)

N_q and N_γ = bearing capacity parameters (dimensionless)

OA = percentage of opening area (%)

ΔP_1 = bearing capacity due to wide slab (kPa)

ΔP_2 = bearing capacity due to membrane effect (kPa)

ΔP_3 = bearing capacity due to planar geogrid (kPa)

P_a = average contact pressure between sleeper and ballast (kPa)

P_{atm} = atmosphere pressure (kPa)

P_d = design wheel load (kN)

P_r = applied vertical stress (kPa)

PRS = settlement reduction factor

P_s = static wheel load (kN)

$P_{s'}$ = shear resistance in direct shear (kPa)

q_0 = footing pressure for unreinforced soil (kPa)

q and p = stress (kPa)

q_c = footing pressure for reinforced soil (kPa)

q_{max} = maximum amplitude (kPa)

q_{mean} = mean load (kN)

q_{min} = minimum amplitude (kPa)

q_r = maximum rail seat load (kN)

q_u = bearing capacity (kN/m^2)

R = radius of curvature (mm)

r = coefficient of regression (dimensionless)

S_1 = vertical deformation in first cycle (mm)

S = opening size of the grid (mm)

S/B = ratio of footing settlement (%)

S_0 = settlement of unreinforced soil (mm)

S_L = lateral spreading (mm)

S_N = axial permanent deformation (mm)
S_R = shear displacement rate (mm/min)
S_r = settlement of reinforced soil (mm)
S_v = vertical deformation (mm)
T = tensile strength of geosynthetic (kN.m)
t = footing thickness (mm)
u = depth of embedment (mm)
V = train velocity (km/h)
W_{box} = chamber width (mm)
W_p = plastic work (kN.m$\times 10^{-5}$)
x = function of settlement under given load (degree)
y = model parameters relating permanent deformation
ΔY_B = rut depth (mm)

Greek symbols

α, β = empirical parameters
α', β' = parameters related to mean value of the impact factor (dimensionless)
α_b = fraction of geosynthetic width available for bearing
α_{ds} = ratio of shear area between reinforcement and total shear area
α_s = fraction of geosynthetic area that is solid
γ' = parameter related to standard deviation of impact factor (dimensionless)
γ = unit weight (kN/m^3)
γ_d = dry unit weight of the soil (kN/m^3)
γ_{max} = maximum unit weight of the soil (kN/m^3)
γ_{min} = minimum unit weight of the soil (kN/m^3)
δ = interface friction angle of subballast-geosynthetic (degree)
δ/B = ratio of surface settlement (%)
δ_x = horizontal strain increment
δ_y = vertical strain increment
$\varepsilon_0 / \varepsilon_r, \beta'', \rho''$ = Empirical parameters relating permanent deformation with number of load cycles
ε_1 = vertical strain (%)
ε_1^e = elastic vertical strain (%)
ε_1^p = plastic vertical strain (%)
$\varepsilon_{1,1}^p$ = settlement after first load cycle (mm)
ε_2 = lateral strain parallel to intermediate principal stress (%)
ε_3 = radial strains (%)
ε_3^e = elastic strain parallel to minor principal stress (%)
ε_3^p = plastic radial strain (%)
ε_a = axial strain of geocell (%)
ε_c = circumferential strain (%)
ε_c^p = plastic circumferential strain (%)

ε_e = elastic strain (%)

$d\varepsilon_{ij}^{e}$ = elastic strain increment

$d\varepsilon_{ij}^{p}$ = plastic strain increment

ε_n = normal strain (%)

ε_h = horizontal strain (%)

ε_v = volumetric strain (%)

ε_v^p = plastic volumetric strain (%)

η = dimensionless footing coefficient

θ = bulk stress (kPa)

λ = distance between axles (mm)

υ_g = Poisson's ratio of geocell

ρ' = percentage of open area of geogrid (%)

ρ = density (kg/m^3)

σ_1 = major principal stress (kPa)

σ_2' = intermediate principal stress (kPa)

σ_3' = minor principal stress (kPa)

$\Delta\sigma_3'$ = additional confining pressure (kPa)

σ_c = circumferential stress (kPa)

σ_c' = uniaxial compressive strength of parent rock (MPa)

σ_b'/σ_n' = normalised bearing ratio (dimensionless)

σ_{cyc} = cyclic deviator stress (kPa)

σ_n = effective normal stress (kPa)

σ_{max} = maximum stress (kPa)

σ_{mean} = mean stress (kPa)

σ_{min} = minimum stress (kPa)

τ = interface shear strength (kPa)

τ/σ_n = stress ratio

$(\tau/\sigma_n)_{peak}$ = peak stress ratio

τ_{fri} = frictional resistance between soil and reinforcement (kPa)

τ_{int} = particles internal resistance (kPa)

τ_{oct} = shear stress (kPa)

τ_p = passive resistance (kPa)

τ_{peak} = peak shear stress (kPa)

$\tau_{sb\text{-}r}$ = peak shear stress of reinforced subballast (kPa)

ϕ = dimensionless impact factor

$\phi_{apparent}$ = apparent friction angle of unreinforced soil (degree)

ϕ_{ds} = apparent friction angle of soil obtained from direct shear test (degree)

$\phi_{unre\,inf}$ = internal friction angle of unreinforced soil (degree)

ϕ_m = mobilized friction angle (degrees)

ϕ_p = peak friction angle (degrees)

$\phi_{p(u\text{-}sb)}$ = peak friction angle of unreinforced subballast (degrees)

ψ = dilation angle (degrees)

ψ_m = mobilized dilation angle (degrees)

Abbreviations

AREA = American railway engineering association
APT = accelerated pavement testing
ASCE = American society of civil engineering
CMD = cross machine direction
DSBA = large-scale direct shear box apparatus
FRAP = fraction recycled asphalt material
GC1 = geomembrane
GC2 = modified geomembrane
GG1 = geogrid with triangle aperture shape
GG2 = geogrid with square aperture shape
GG3 = geogrid with rectangle aperture shape
GG4 = geogrid with square aperture shape
HDPE = high density polyethylene
LVDT = linear voltage differential transformer
MD = machine direction
OMC = optimum moisture content (%)
ORE = office of research experiments
PE = polyethylene
PET = poly Ester
PP = polypropylene
PRS = percentage reduction in footing settlement (%)
PSD = particle size distribution
PSPTA = process simulation prismoidal test apparatus
RAP = recycled asphalt material
USACE = US army corps of engineering
WES = waterways experiment station

TABLE OF CONTENTS

LIST OF FIGURES

LIST OF TABLES

CHAPTER 1

1. INTRODUCTION

1.1 Background

Rapid urbanization and subsequent frequent congestion of major highways have caused greater demand on railways to convey passengers and bulk freight commodities. In Australia, in order to maintain its effectiveness over other modes of transportation and to encourage more people to use railways, train speeds are required to be elevated to at least about 150 km/h. On the other hand, due to the limited supply of high strength igneous rock aggregates, majority of tracks are forced to be built using locally available materials, and some of these have micro-fissures, which would inhibit elevated train speeds. Under such circumstances, innovative ground improvement techniques such as the use of geosynthetics in two dimensional form (geogrids, geotextils, geocomposites) or in three dimensional form (geocells) are necessary to increase track resiliency, reduce maintenance costs, and increase operational safety and customer satisfaction.

Railway organisations often do not wish to use geocells to confine the ballast layer because of practical difficulties encountered with the use of tamping machine during track maintenance. However, reinforcing the underlying subballast with geocells is an economical and feasible alternative. Geocells were originally developed by the U.S. Army Corps of Engineers to improve vehicular mobility over loose sandy subgrade (Webster and Alford 1977). Since then, improved performance by geocells has been well recognized, and it is mainly attributed to increased confinement. During loading, an additional hoop stress is mobilised in the geocell that helps to

increase the confining pressure, hence arrest the granular mass from spreading laterally. By increasing the in-fill rigidity, geocells also improve the load carrying capacity, which in turn improves track performance. Accordingly, train speed can also be increased for tracks with enhanced resiliency even if they are constructed over soft estuarine clays. The geocell-reinforced subballast was tested using the large-scale triaxial and process simulation chambers.

The triaxial apparatus was first developed to study soil characteristics mainly under compression (Bishop and Henkel, 1976). Since then, conventional triaxial apparatus has been widely used to investigate the shear strength of various types of the material under different load applications. However, large size aggregates require large –scale testing rigs. Accordingly, as a versatile apparatus, large-scale cylindrical triaxial apparatus (Indraratna et al. 1998) and large-scale process simulation prismoidal triaxial apparatus (Indraratna et al. 2013) were designed and built at UOW and they have been successfully employed to study the behaviour of both unreinforced and reinforced granular material under monotonic and cyclic load conditions. Numerous studies have been carried out to investigate the behaviour of reinforced granular media under monotonic and cyclic loading in cylindrical triaxial chambers. However, the effect of the intermediate stress in plane strain condition has received less attention in all previous studies, because the intermediate stress could not be controlled independently in conventional triaxial equipment. In a conventional triaxial apparatus, the lateral deformation of reinforced material is the same in all horizontal directions, but this is unrealistic in practice when considering the directions parallel and perpendicular to a sleeper. Although, a limited number of studies have investigated the behaviour of subballast under axisymmetric condition, the performance of geocell-reinforced subballast in plane strain condition subjected to the cyclic loading is not yet fully understood.

In order to obtain a more realistic understanding of subballast, subjected to cyclic load application, the experiments needed to be conducted in an environment similar to field conditions, where the intermediate stress differs from the minor principal stress $\left(\sigma_2' \neq \sigma_3'\right)$. As a result, the large-scale process simulation prismoidal triaxial

apparatus (PSPTA) designed and built at the University of Wollongong was deployed to investigate the stress-strain behaviour of the unreinforced and geocell-reinforced subballast subjected to cyclic loading. In addition, the lateral displacement of the specimen in both parallel and perpendicular direction to the sleeper can be controlled separately, to simulate realistic field conditions.

In the current thesis, a comprehensive laboratory study was carried out to study the geocell-reinforced subballast under cyclic loading. An analytical model was proposed to capture the additional confining pressure developed by the geocell mattress. The influence of various critical factors such as external confining pressure, frequency of cyclic loading as well as number of load cycles on the performance of subballast with and without geocells was studied. Three-dimensional finite element simulations were carried out using ABAQUS and an analytical approach for determining additional confinement induced by geocells was implemented. The numerical predictions were in good agreement with the laboratory data.

1.2 Research Motivation (Statement of problem)

The main motivation behind the current study was the urgent need to construct a high speed train network as well as upgrading of heavy haul freight in Australia. The adoption of high speed passenger trains (speeds exceeding 200 km/h) and heavy haul freight network (axle loads exceeding 30 tones), cause large cyclic stresses on the track substructure. Under these high cyclic loads, ballast and subballast spread laterally due to the low confinement prevailing in a typical tracks, causing excessive settlement, thereby leading to frequent track maintenance. In view of this, adoption of ground improvement techniques becomes necessary for sustainable development of modern rail infrastructure. Reinforcing the track substructure using planar reinforcement is an established practice to control the lateral spreading of ballast and subballast, and to improve the stability of the track respectively during high speed cyclic loading. However, recent studies have shown that geocells can provide increased track confinement compared to planar reinforcement such as geogrid.

The majority of investigations have been carried out on the monotonic behaviour of geocell-reinforced foundations. Numerous studies are available in the current literature devoted to the impact of the physical and mechanical properties of geocell mattress, depth of embedment and material type, and mainly focussing on monotonic loading (Sitharam and Hegde 2013; Biswas et al. 2013; Dash 2010; Dash 2001). Monotonic loading does not fulfil the design criteria required for high speed trains, where high frequency of cyclic loading leads to completely different volumetric changes of track materials. Due to cyclic loading, granular materials undergo extensive particle rearrangement and densification. Only a limited number of researches have been carried out to examine the performance of reinforced sub-ballast under cyclic loading. Therefore this study is dedicated to evaluating the behaviour of geocell-reinforced subballast under cyclic loading.

1.3 Objectives and Scopes of this thesis

The key objective of this study is to investigate the behaviour of geocell-reinforced subballast subjected to cyclic loading in plane strain condition and under a large number of cycles (N = 500,000 cycles). The outcomes of the current study will assist to develop a new approach for designing geocell reinforcement of subballast for providing extra confinement during cyclic loading. The ultimate research goal is to provide an economical and safe technique to increase train speed (frequency of laboratory). The current thesis focuses on an analytical approach and experimental testing to assess the behaviour of subballast with and without geocells under high frequency cyclic loading. The laboratory findings are used to calibrate and validate the numerical model. A design approach is proposed to assist railway engineers for upgrading the existing railways in terms of geosynthetics improvement of track materials.

In the current study, numerical simulations are performed using a commercial finite element method, ABAQUS in three dimensions. A cyclic loading with a periodic, positive full-sine waveform is adopted for modelling geocell-reinforced subballast. The numerical simulations are able to capture:

1. The behaviour of unreinforced and reinforced subballast under cyclic loading at different confining pressures ($5 \leq \sigma'_3 \leq 30$ kPa) and number of cycles (N = 10,000 cycles).
2. The permanent vertical and lateral deformation of both unreinforced and geocell-reinforced subballast
3. The behaviour of geocell mattress under cyclic loading.
4. The behaviour of unreinforced and reinforced subballast at different subballast strength and geocell stiffness.

1.4 Organisation of the Thesis

This dissertation is divided into 7 chapters. Chapter 1 introduces the background and motivation of the study. It also specifies the organization of the thesis.

Chapter 2 provides a comprehensive review of the current state of research on the performance of unreinforced and geocell-reinforced subballast subjected to the different load applications. By summarising various investigations carried out on different types of granular soil and geocell, this chapter provides insights into the role of geocells in stabilising granular material, especially under cyclic loads

Chapter 3 explains the properties of the materials that were used in this investigation. It also defines the methodology and discusses the experimental results of large-scale direct shear box employed for investigating the behaviour of reinforced subballast in this study with several geosynthetics under different conditions (i.e. various strain rates, normal load and relative density). This chapter highlights the impact of interfacial friction resistance on the behaviour of geocell-reinforced subballast.

Chapter 4 describes the methodology and discusses the experimental results obtained from conducting tests in a large-scale prismoidal triaxial apparatus, which is capable of maintaining plane strain condition (i.e. true triaxial nature). The

specimens were tested in plane strain condition, under cyclic loading in a stress controlled fashion, at a relatively very low confining pressure, and the axial stress applied at different frequencies.

Chapter 5 outlines the analytical model proposed in this study to calculate the additional confining pressure induced by the geocell mattress.

Chapter 6 presents the numerical simulation of the unreinforced and geocell-reinforced subballast subjected to the cyclic loading with different confining pressures. The behaviour of geocell-reinforced subballast is investigated through different subballast strength and geocell stiffness.

Chapter 7 provides the summary of this study and gives recommendations for future work, whilst also recognising its limitations.

CHAPTER 2

2. LITERATURE REVIEW

2.1 General

Railway plays a key role operating heavy freight transport and passenger services in large and rapidly growing countries such as Canada, Unite States, Australia, India and China. Considering an acceptable ride quality, relatively low cost, compatibility with the environment, and growing demand from industry and commuters, railway has become more popular than other modes of transportation. However, the sustainable development of rail infrastructure does require a significant amount of funding. In order to minimise these costs, innovative ground improvement solutions are necessary. To date, reinforcing track substructure, using planar reinforcement, is commonly used to controlling the lateral spread of ballast and subballast and improving the stability of the track during cyclic loading. However, recent studies have shown that geocell can provide much better lateral confinement to infill soil than planar reinforcement.

A conventional ballasted track foundation consists of granular material overlying a subgrade. In order to have long term satisfactory performance, the granular material

must possess high shear strength and acceptable permanent deformations. This necessitates a comprehensive knowledge of the loading and mechanical behaviour of material under cyclic loading conditions. The objective of this chapter is to present the current state of knowledge related to the deformation and densification of unreinforced soil and soil reinforced with geocell. This chapter begins with a brief review of ballasted rail track, and then, by introducing the concepts of reinforced soil, discusses the implication of using geocell-reinforced soil for applications such as embankments, roads, and railways. This discussion covers the factors that are needed to improve the performance of geocell composite soil such as the type of loading, its relative density, the geocell infill material, and the properties of geocell and depth of its embedment. It also examines the analytical and numerical studies carried out while investigating the stress-strain behaviour of geocell-reinforced soil. The knowledge presently available is summarised and then the contribution made by this current study is outlined.

2.2 Ballasted Track Substructure

Ballasted track that consists of superstructure and substructure is the most conventional and popular track system throughout the world (Selig and Waters 1994). The track superstructure consists of sleepers, rails, and a fastening system. The track substructure is divided into three layers (shown in Figure 2.1): (i) ballast, i.e. coarse angular aggregates (size = 10-70 mm), (ii) subballast, containing finer aggregates (size = 0.3-20 mm), and (iii) subgrade (soil or rock). Subballast typically consists of a broadly graded sand-gravel mixture (Selig and Waters 1994; Dahlberg 2001; Indraratna et al. 2015), designed to reduce the cyclic stress being transmitted to the subgrade. Depending on the type of subgrade, subballast may vary in thickness, unlike the consistent thickness of ballast (i.e. 300 mm in Australia) usually adopted in track construction and maintenance practices.

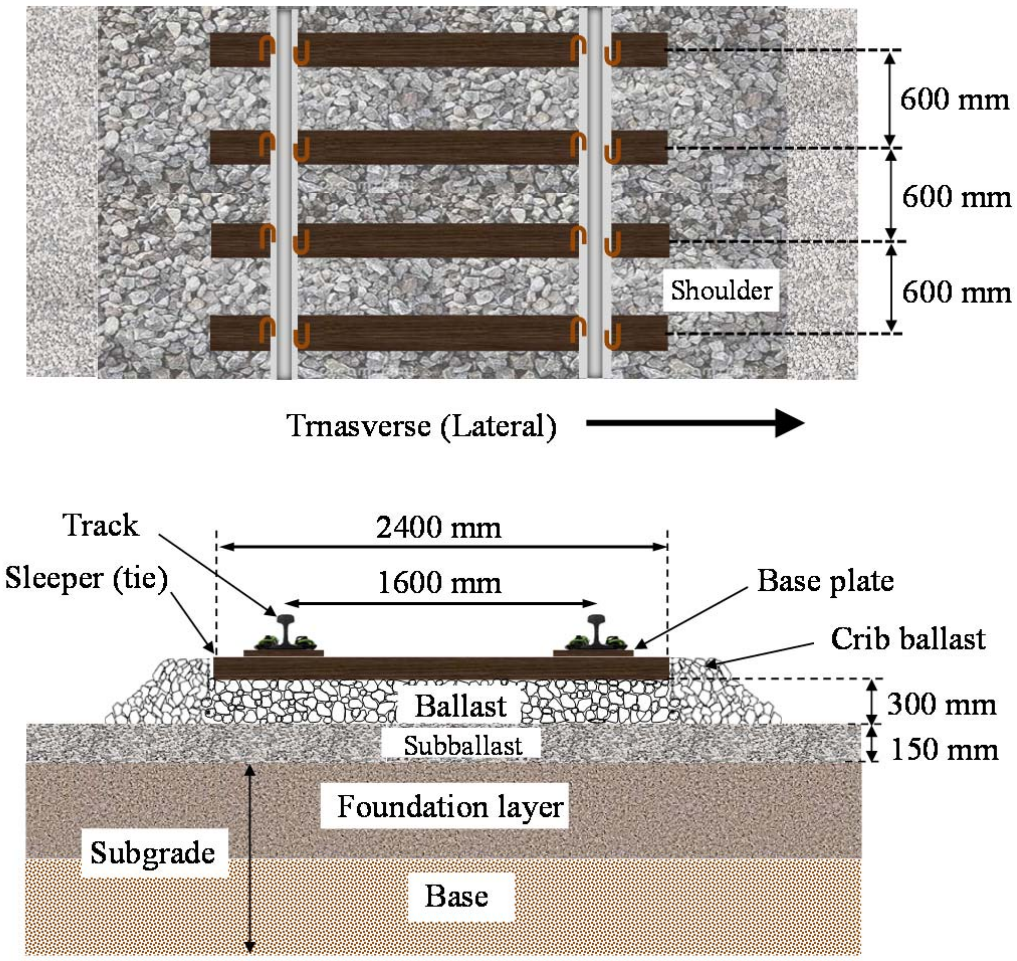

Figure 2.1. Typical geometry of ballasted rail track

2.2.1 Ballast

Different modes of transportation, such as highways, rail tracks and airport (runways), rely almost entirely on the quality of the granular materials used in their foundations. In railways, the longevity of the tracks largely depends on the quality of granular material used for the supporting tracks, and to have a maximum response to cyclic loading, granular material with a higher shear strength must be used. The ballast layer should be thick enough to absorb the stresses applied during train passage. The vital functions of ballast are (Indraratna et al. 2011):

- Providing a platform that is stiff and stable enough to support sleepers from the cyclic stresses developed by train passage.
- Effectively propagating induced stresses to the underlying layers of subballast and subgrade at an acceptable stress level.
- Maintaining track geometry by minimising the permanent axial, lateral, and longitudinal forces applied to the sleepers.
- Providing adequate hydraulic conductivity to maintain free drainage of water during flooding.
- Minimising the lateral buckling and vertical deformation of track, thus maintaining its longevity and reducing maintenance costs.
- Providing enough rigidity and resiliency for track subjected to cyclic loading in order to maintain its alignment.

A typical load distribution under sleepers is illustrated in Figure 2.2.

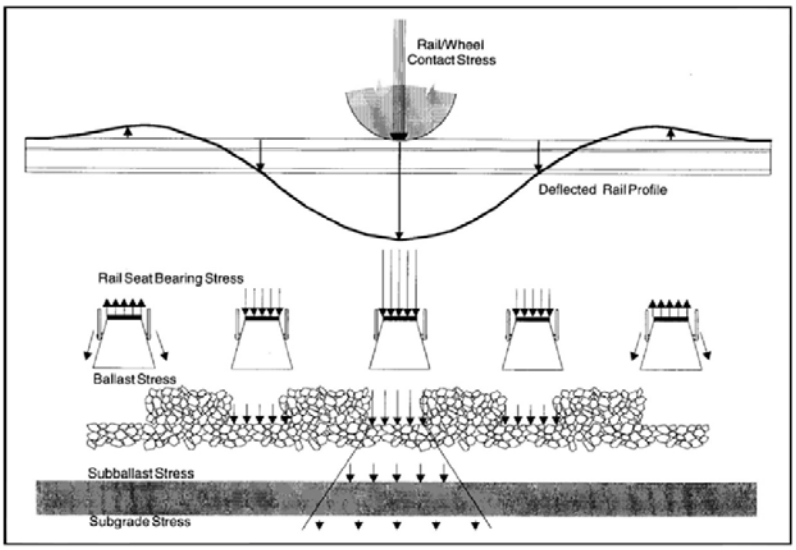

Figure 2.2. Typical load distribution in ballasted track (After Selig and Waters, 1994)

2.2.2 Subballast

Subballast, also known as the capping layer, is an important sub-structural layer that helps distribute further applied cyclic stress to the foundation. It usually has the same source as ballast, (crushed basalt), but it contains much finer aggregates that have several key functions in track stability, i.e., (Indraratna et al. 2011):

- Reducing the stress induced from cyclic loading to an acceptable degree, such that it does not lead to exceed the allowable plastic deformation of subgrade.
- Preventing mud-pumping from the subgrade layer to the ballast.
- Acting as a filter layer to shed water coming from the ballast
- Extending the frost protection of the subgrade
- Acting as a blanket to prevent inter-penetration from the ballast and subgrade
- Facilitating the drainage of water that might exist in subgrade and prevent it from flowing to the upper layer ballast
- Avoiding the attrition of subgrade by ballast which leads to the formation of slurry in the presence of water.

2.2.3 Subgrade

The lowest layer in track substructure is the subgrade soils, which has a significant impact on the permanent settlement of the track. Subgrade is not considered as supporting a large cyclic stress and therefore it does not usually require very much maintenance. However, due to heavy freight network, the magnitude of cyclic stress eventually exceeds the allowable limits of subgrade and that promotes the loss of track geometry. This means that material with enough bearing capacity and stiffness must be selected for the subgrade layer. Common practice for improving the performance of subgrade under cyclic loading is as follows:

- Providing vertical drains to facilitate the dissipation of pore water
- Compacting the subgrade to increase its rigidity

- Improving the performance of the upper layers (ballast and subballast) to reduce the stress transmitted to the subgrade layer by increasing the thickness of the ballast or reinforcing the ballast and subballast with suitable reinforcement
- Using lime-cement, coal wash-steel slag or lignosulfonates as stabilisers to improve the performance subgrade with lower shear strength.

Table 2.1 summarises the mechanical properties of subballast and subgrade.

Table 2.1. Mechanical properties of subballast and subgrade (Esveld 2001)

Parameters	**Design required values**	
	Subballast	**Subgrade**
Compaction by Proctor (%)	100	97
Maximum deviation from design subgrade profile (mm)	< 10	< 10
Modulus of elasticity (MPa)	100	35
California Bearing Ratio (%)	> 25	> 5

2.3 Cyclic Loading Mechanism

Perhaps the most important factor associated with the safe and economical design of rail tracks is traffic forces. The forces applied to the track can be divided into static and dynamic components. There are several factors that influence the amplitude of cyclic loading, and they are:

(a) Wheel diameter
(b) Train speed
(c) Track condition
(d) Maximum traffic load
(e) Static axle load

There are several methods available, used by practicing engineers to calculate static and dynamic loading, and they are briefly discussed in the following.

2.3.1 Atalar et al. method (Equivalent dynamic wheel load)

Based on recommendations by Atalar et al. (2001), the design wheel load can then be calculated using (Li and Selig 1998):

$$P_d = \phi \cdot P_s \tag{2.1}$$

$$\phi = \left((1 + \frac{V}{100}) (1 + C) \right) \tag{2.2}$$

where P_s is the static wheel load (kN), P_d is the design wheel load (kN), ϕ is the impact factor (dimensionless), V, is the train speed (km/h) and C is non-dimensional factor (≈ 0.3).

2.3.2 ORE method

Another method for determining the impact factor was introduced by the Office of Research and Experiments (ORE) of the International Union of Railways (ORE 1965, Jeffs and Tew 1991). In this method the forces applied to the track by passing trains is used to calculate the impact factor; this method has several dimensionless speed factors such as α', β' and γ', and they are given by the following relationship:

$$\phi = 1 + \alpha' + \beta' + \gamma' \tag{2.3}$$

where α', β' are related to the mean value of the impact factor and γ' is related to the standard deviation of the impact factor. These dimensionless factors can be calculated based on following equations:

$$\alpha' = 0.04 \left(\frac{V}{100} \right)^3 \tag{2.4}$$

$$\beta' = \frac{2n'.m}{G^2} \tag{2.5}$$

$$\beta' = \frac{V^2(2m+c)}{127RG} - \frac{2cm}{G^2} \tag{2.6}$$

$$\gamma' = 0.10 + 0.017\left(\frac{V}{100}\right)^3 \tag{2.7}$$

where m is the vertical distance from the top of the rail to the centre of the vehicle's mass (mm), R is the radius of curvature, g is gravity acceleration (m/sec^2), n' is super-elevation deficiency (mm), G is the horizontal distance between the rail and centreline (mm), and c is the super elevation (mm).

2.3.3 AREA manual method

Based on recommendations by the American Railway Engineering Association (AREA), the design wheel load can then be calculated using (Li and Selig 1998):

$$P_d = \phi \cdot P_s \tag{2.8}$$

$$\phi = 0.0052V \big/ D_W + 1 \tag{2.9}$$

where D_w is the diameter of the wheel (mm). Table 2.2 shows the nominal axle loads applied onto the rail track in the USA and Australia.

Table 2.2. Nominal axle loads applied to the track (Esveld 2001)

Rolling type	Number of axles	Empty (kN)	Loaded (kN)
Trams	4	50	70
Light-rail	4	80	100
Passenger coach	4	100	120
Passenger motor coach	4	150	170
Locomotive	4 or 6	215	-
Freight wagon	2	120	225
Heavy haul (USA and Australia)	2	120	250-350

2.4 Track Substructure Problems

Under high cyclic loading, tracks gradually lose their geometry. To restore and maintain track geometry, requires specific and expensive machinery for tamping, which imposes significant maintenance costs to the railway industry. Also, there are frequent and common problems, which promote track instability, and they are explained as follows:

2.4.1 Differential settlement of track

Perhaps the most critical problem associated with cyclic loading is the differential settlement of rail tracks. Constructing rail tracks on poor quality locally available granular material can help to promote differential settlement. This problem will be intensified when the rail track is subjected to trains with higher speeds. Also, exceeding the permissible load onto the substructure, localised lateral displacement, rapid crushing of ballast, exceeding the allowable permanent deformation of subgrade, and mud pumping from the subgrade into the upper layers are other factors that increase differential settlement and also cause vertical and horizontal track derailment.

2.4.2 Lateral spreading

Another issue that has a major influence on track stability is lateral spreading. Commuting heavy freight or passenger trains at high speed causes high cyclic stress to the rail tracks. Under these high cyclic loads, ballast and subballast spreads laterally due to low confinement exerted by the ballast shoulder usually available in the field. Continuing lateral spreading means that permanent vertical deformation will occur at a faster rate and this will lead to a decreasing tamping period.

2.4.3 Ballast crushing

Another problem that impacts on the service life of rail tracks is the crushing of ballast particles. This happen, due to high angularity of ballast particles. This degradation of ballast stems from weathering, the use of compaction machines, and tamping (Selig and Waters 1994). Consequently, other problems will be initiated as the particles are reduced in size and angularity. While reducing the angularity of ballast particles has a significant impact on the internal friction angle of ballast, it causes ballast become fouled, which in turn reduces its permeability. This leads to regular and costly maintenance.

2.4.4 Poor drainage

One of the most important factors in maintaining rail track stability is drainage, because inadequate drainage causes other problems such as:

- Substantial reduction in strength due to increasing pore water pressure
- Promoting ballast degradation, owing to interaction with chemical components in the water, and freezing.
- Propagating the migration of finer material from the lower subgrade layer
- Accelerating the permanent vertical deformation of the track which leads to a substantial reduction in its bearing capacity

2.4.5 Mud pumping or foundation liquefaction

One of the most common problems found in coastal regions is mud pumping in saturated subgrade, known as foundation liquefaction that causes the lower subgrade layer to migrate between the ballast particles. This problem will be exacerbated where subballast is not used under the ballast. Without a subballast layer, and under cyclic loading, saturated particles from the subgrade migrate to the ballast and fill the

void spaces between the particles of ballast which in turn reduces its permeability and causes undrained shear failure.

2.4.6 Flood damage

Flooding is a major problem for railways because the sudden and rapid forces exerted by the massive volumes of flood water wash out the granular particles and severely damage the substructures layers. This leads to a significant increase in maintenance or the cost of reconstructing the rail tracks. The problem will probably increase in countries where rail track are constructed near the ocean, including Australia, and in countries affected by rainy seasons.

2.4.7 Ballast fouling

Ballast fouling is one of the most critical problems experience by ballasted rail track, causes significant reduction in bearing capacity. Moreover, ballast fouling can initiate other problems that affect its performance; the fouling material fills the space between the ballast particles which in turn reduces the drainage capacity of the granular materials and hence, decreases the internal friction angle, compromises track stability and reduces its longevity under high cyclic loading.

2.5 Fundamental of Reinforced Soil

The concept of stabilising soil by utilising the tensile element within the soil mass is not a new idea it began more than 3000 years ago, where various techniques (i. e. utilising palm branches and straw) were used to reinforce the soil and improve its performance (Jha 1988; Haeri et al. 2000). However, in the past recent decades, due to increasing demand for constructing of highways and railways on subgrade soil with poor shear strength, reinforcing soil with different types of geosynthetics has

taken more attention (Vidal 1969). New and modern geosynthetics such as geotextile, geogrid, geocell have offered an economical way to improve the performance of soil by reducing the thickness of the foundation and increasing the life of the reinforced layer.

Planar geogrid has been used in railway foundations as a filtration system to help dissipate excessive pore water pressure, reduce particle breakage, and reduce differential settlements (Indraratna 2006; Indraratna et al. 2011; Indraratna et al. 2015). However, unlike planar reinforcement, geocell offers all round cellular confinement to the infill soil and arrests its tendency to spread laterally. The early generation of geocell was made by coating hexagonal shaped craft paper soaked in phenolic resistant resin (Rea and Mitchell 1979). Later geocell was made from aluminium, but its high manufacturing cost and handling difficulties made it impractical. The current modern concept of cellular confinement began with the US Army Corps of Engineering (USACE) (Webster and Alford 1978; Bathurst 1988) and the Presto Products Company, a division of Reynolds Packaging Group in the late 1970's. This newly developed confining system known as geocell was introduced to improve the performance of poorly graded sand subjected to the repeated loading of military vehicles. The first generation of modern geocell mattresses (or geoweb) consisted of three dimensional plastic tubes with a depth of 300 mm that were filled with granular materials and placed over soft clay foundation subjected to repetitive truck wheel loads at the Waterways Experiment Station (WES). The experimental results showed a significant improvement in the performance of this reinforced soil; indeed its performance was comparable with an unreinforced subgrade foundation with a depth of 500 mm (Webster and Watkins 1977; Bathurst 1988). Since then the geocell mattress has proved to be a promising approach and has been used for various applications (such as railways, highways, and embankments) to improve the performance of soil and increase its stability under different load applications. The commercial concept of geocells were made from polyethylene strips with different widths (i. e. 100, 150 and 200 m), which were welded by ultrasound and connected at the joints to provide a cellular expandable mattress. In this current study the pocket size (d) of the geocell was taken as the

diameter of an equivalent circular area of the geocell pocket. The configuration of the geocell-reinforced soil discussed in this chapter is shown in Figure 2.3.

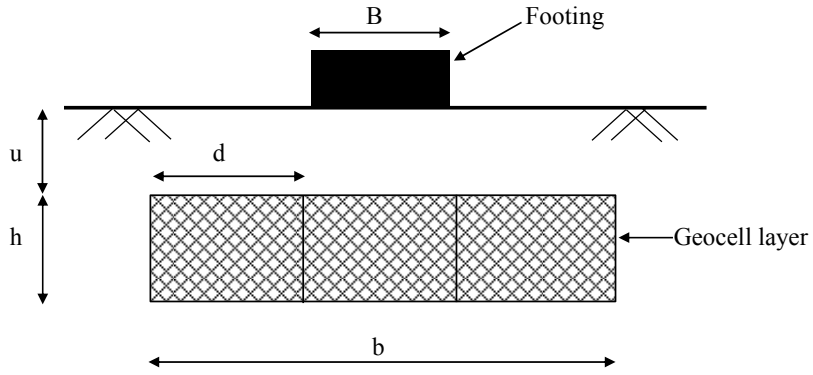

Figure 2.3. Geometric parameters of apparent geocell-reinforced foundation bed

In order to study the behaviour of geocell-reinforced soil, factors such as the load application, relative density of the in-fill material, the height and diameter of the geocell mattress, including its depth of embedment, must be carefully considered. Accordingly, numerous studies have been carried out to investigate the behaviour of geocell-reinforced soil, most of which are discussed in this chapter.

2.6 Fundamentals of Geocell-Reinforced Soil

Stabilizing subballast with a geocell mattress can provide following benefits for the railway substructure:

- By confining the infill material, geocell offers additional confinement and helps minimise the excessive lateral and differential settlement that leads to having to maintain trail track alignment.

- Geocell mattress acts like a semi-rigid mattress and distributes load to a wider and deeper depth. As a result, the magnitude of cyclic loading is transferred to the subgrade is reduced markedly, which means the vertical deformation of subballast can be maintained at the allowable degree of deformation.

- In addition, using geocell mattress causes local failure occurred, rather than global failure, leads to reducing punching effect on the footing, and thus heaving on the soil, shown in Figure 2.4.

- Having some aperture in the strips, as shown in Figure 2.5, means that geocell can provide enough drainage to dissipate any pore water pressure that might develop in the subgrade. Also it promotes drainage during flooding while helping to maintain the bearing capacity of the rail track foundation.

- Geocell mattress can act like a barrier to stop fine particles migrating from the subgrade to the upper layer; this also helps to maintain ballast permeability and reduce mud pumping.

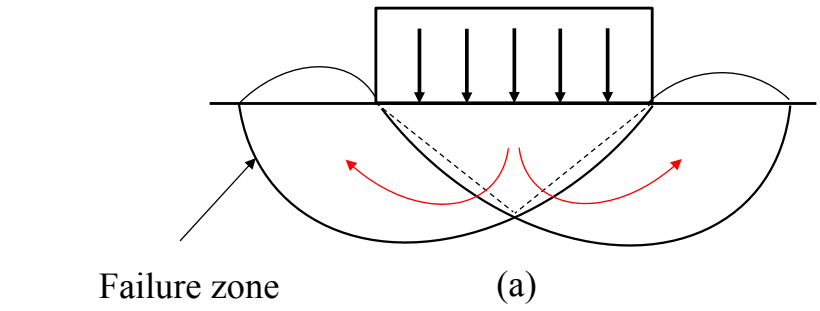

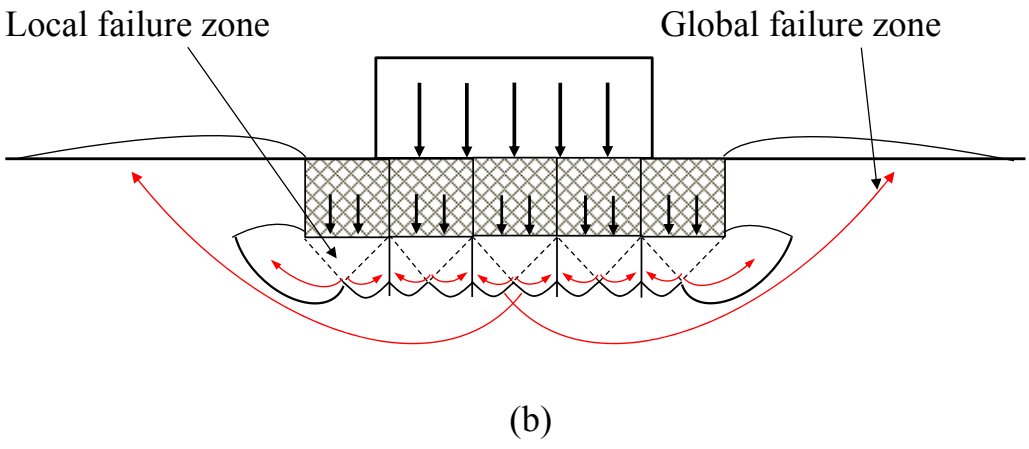

Figure 2.4. Typical failure plane under (a) unreinforced and (b) geocell-reinforced foundation

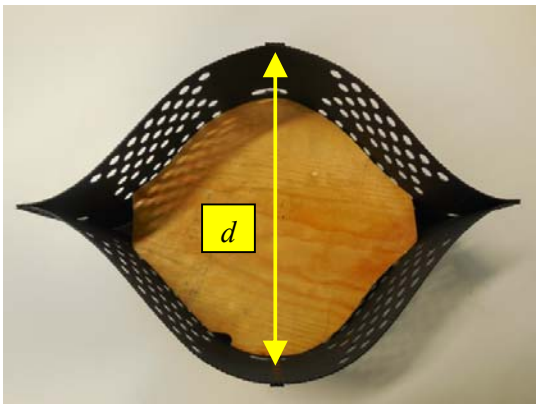

Figure 2.5. Illustration of geocell pocket

2.7 Bearing capacity of unreinforced and reinforced soil

Certainly the main parameter impacted by utilising reinforcement is the bearing capacity of the soil. Due to its unique honeycomb like structure, geocell can effectively confine the infill material, minimise lateral displacement and thus increases its rigidity. As a result, the bearing capacity of the reinforced layer can be significantly increased, compared to unreinforced soil. One of the earliest studies in large-scale model tests (3.6 m × 2.4 m × 1.8 m) was carried out by Bathurst (1988). The performance of a reinforced gravel base was improved by geocell mattresses and the outcome was compared to an unreinforced gravel base at different depths (Bathurst 1988; Bathurst 1993). It was shown that by using geocell mattress as reinforcement (i.e. depth of geocell = 150 and 300 mm), the thickness of the gravel base could be markedly reduced. The permanent deformation was also reduced because the geocell mattress increased the stiffness of the soil, as shown in Figure 2.6. This implied that for geocell-reinforced soil, the magnitude of loading can be substantially increased. Also, it was shown that the reinforced soil performance is improved by increasing the depth of the geocell mattress reinforcement.

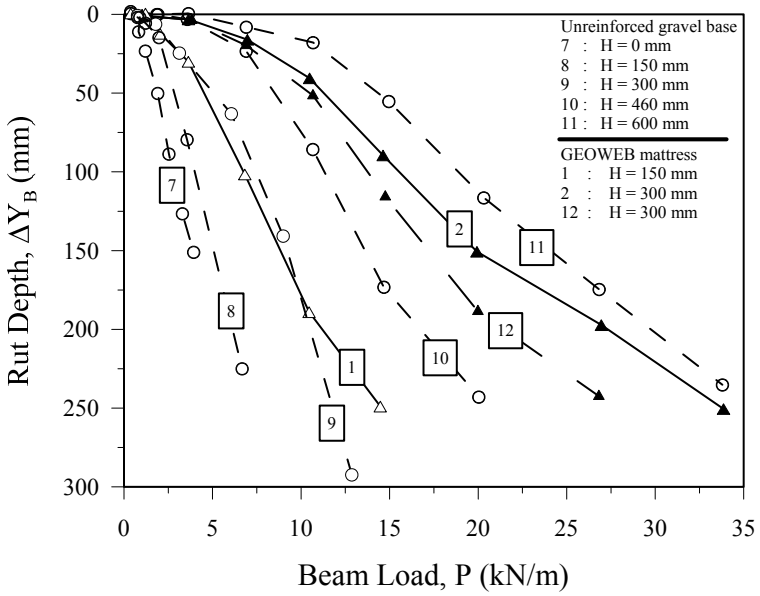

Figure 2.6. Load-deformation results for experiments on unreinforced and geocell mattress reinforced gravel base (Modified after Bathurst, 1988)

The behaviour of a single cell of unreinforced and reinforced specimens with different aspect ratios (i. e. h/d = 1& 2.2) and different confining pressures (σ'_3) was also investigated in a conventional triaxial apparatus (Bathurst 1993). The reinforced specimens showed a remarkable improvement in behaviour in terms of improving their shear strength and reducing their volumetric dilation. It was assumed that in the reinforced specimens the internal friction angle would remain constant, so the improved performance was attributed to the apparent cohesion developed at the interface between the infill material and reinforcement. Additional confinement developed in reinforced specimen using hoop tension theory (Henkel and Gilbert 1952) as:

$$\Delta\sigma_3 = \frac{2M\varepsilon_c}{D_0}\frac{1}{(1-\varepsilon_a)} \tag{2.10}$$

where ε_c is the circumferential strain, ε_a is the axial strain, M is the modulus of membrane and D_0 is the initial diameter of the specimen. Accordingly, the apparent cohesion was quantified as:

$$C_r = \frac{\Delta\sigma_3}{2}\tan(\frac{\pi}{4} + \frac{\phi_{unreinf}}{2}) \tag{2.11}$$

where, $\phi_{unreinf}$ is the internal friction angle of unreinforced soil. The beneficial effect of using geocell reinforcement was also highlighted when geocell reinforcement was used in a large-scale implementation (Bush et al. 1990). A large-scale geocell mattress was used to construct embankment overlying soft clay, as shown in Figure 2.7, and it was reported that about 31% of the cost was obtained compared to conventional construction methods.

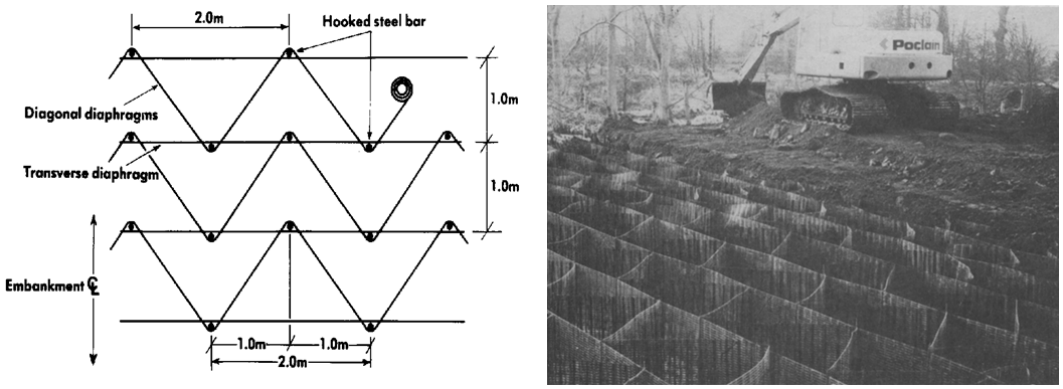

Figure 2.7. Geocell-reinforced mattress used for constructing an embankment (Bush et al. 1990)

Improvements in the bearing capacity of soil reinforced by geocell have been the subject of investigation by many studies (Binquet and Lee 1975; Huang and Tatsuoka 1988 ; Bush et al. 1990; Huang and Tatsuoka 1990; Mandal and Gupta 1993; Huang and Menq 1997; Patra et al. 2005; Soleimanbeigi and Hataf 2006; Chen et al. 2009; Mohamed 2010). The bearing capacity has been investigated in terms of a wide-slab mechanism. It was stated that utilising reinforcement under footings resulted in increasing their width at a depth (D_r) from the ground surface. So, the bearing capacity can be determined as (Schlosser et al., 1983):

$$q_{u(nrein)} = 0.5 \cdot (B + \Delta B) \cdot \gamma \cdot N_\gamma S_\gamma + \gamma \cdot D_r \cdot N_q \cdot S_q \cdot d_q \tag{2.12}$$

where, B is the width of footing, γ is the unit weight of sand, d_q, N_q, S_q, S_γ and N_γ are the bearing capacity parameters, D_r is the depth of footing, and ΔB is the wide slab effect, which is an increase in the width of a footing by using reinforcement, as shown in Figure 2.8.

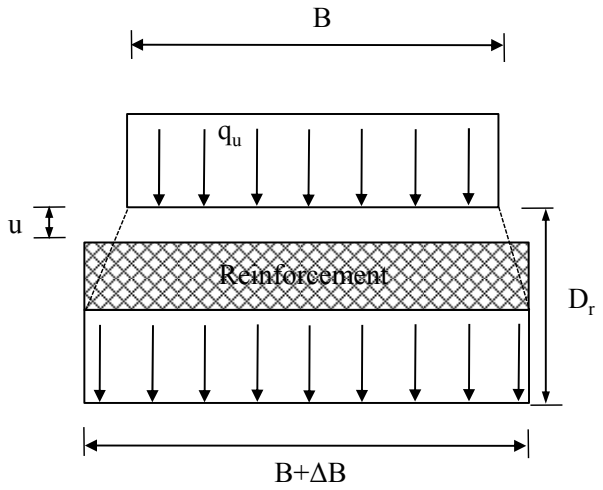

Figure 2.8. Failure mechanism for reinforced soil (Modified after Schlosser et al., 1983)

This improved performance was justified because a quasi-rigid region was created under the foundation from the reinforced layer, known as deep-foundation. Also, extending the reinforcement beyond the footing width $(B + \Delta B)$, lead to the creation of a wide-slab that helped to distribute the footing load over a larger area (Huang and Menq 1997). Following the same concept, a modified bearing capacity relationship for a deep footing was proposed as follows (Huang and Menq 1997):

$$q_{u(rein)} = q_{u(unrein)} + q_{u(slab)} \tag{2.13}$$

where, $q_{u(slab)} = \eta \cdot \Delta B \cdot \gamma \cdot N_\gamma$. The performance of an embankment supported by a geocell-reinforced foundation over soft settled red mud has been studied (Sitharam and Hegde 2013). It was reported that due to the beam effect, there was no distinct failure even with a very large settlement. This occurred because the geocell mattress acts like a very stiff and rigid beam which supported the footing even after soil failed. By utilising the geogrid, the performance of the reinforced footing was further

improved. The improvement factor of the bearing capacity (I_f) had increased to the degree of I_f = 4 and 5 for geocell-reinforced and geocell with additional geogrid reinforcement respectively. An analytical model was proposed to determine the bearing capacity ratio offered by geosynthetics with respect to wide slab mechanism (Binquet and Lee 1975), and the membrane effect where (Sitharam and Hegde 2013):

$$\Delta P_1 = 2P_r \tan^2\left(45 - \phi_{unreinf}/2\right)\tan\delta \tag{2.14}$$

Reduction of pressure due to the geocell:

$$\Delta P_2 = P_r\left(1 - \frac{B}{B + 2D_r \tan\beta}\right) \tag{2.15}$$

The improved bearing capacity due to the membrane effect offered by a planar geogrid:

$$\Delta P_3 = \frac{2T \sin x}{B} \tag{2.16}$$

where $\phi_{unreinf}$ is the internal friction of unreinforced soil, P_r is the vertical stress applied onto he geocell mattress, δ is the angle of interface shear resistance between the infill soil and geocell wall, x is a function of settlement under the given load, B is the width of the footing, D_r is the depth of reinforcement, and T is the tensile strength of the planar geogrid.

2.8 Resilient Modulus

Rapid urbanisation and the subsequent increasing demand for more land has caused a lot of pressure on the railway industry to build their infrastructures on locally available material, some of which have very low shear strength. Using subgrade with low strength and insufficient confinement, lead to poor quality material spread laterally, causes excessive vertical deformation of the granular material in the substructure and thus increasing tamping of the rail tracks. Based on theory of

elasticity, the elastic properties of materials can be defined by the elastic modulus (E) and Poisson's ratio (υ). However, in cyclic loading the modulus of elasticity can be replaced by the resilient modulus to account for the nonlinearity and stress dependency during cyclic loading. As result the resilient modulus was used to address the cyclic response of the granular material of substructure layers subjected to cyclic loading (Selig 1987; Selig and Waters 1994; Indraratna et al. 2009). The resilient modulus (M_R), known as the elastic modulus in monotonic loading, can be calculated as:

$$M_R = \frac{\sigma_{\text{cyc}}}{\varepsilon_{\text{e}}} \tag{2.17}$$

where, M_R is the resilient modulus for each cycle, σ_{cyc} is the cyclic deviatoric stress and ε_e is elastic strain or recoverable strain, known also as resilient strain, in a single cycle, as shown in Figure 2.9. (a & b)

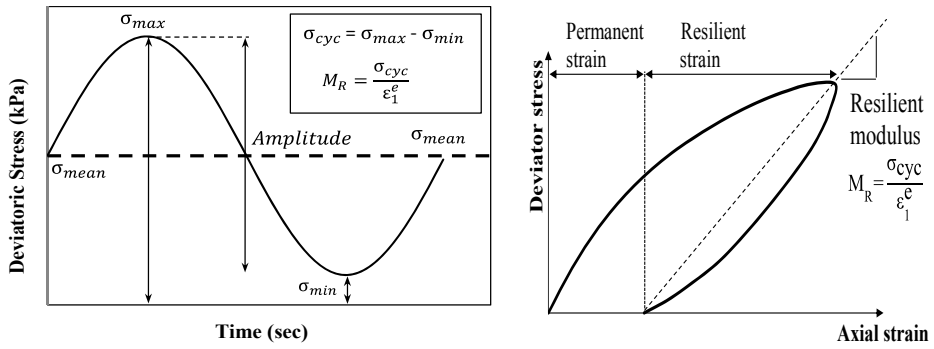

(a) (b)

Figure 2.9. (a) Cyclic loading curve with maximum and minimum deviator stress and (b) demonstration of strain in one single cycle

Numerous studies have been devoted to investigate the influence of different factors on the resilient modulus of various types of soil. The impact of factors such as the degree of stress, the load duration and frequency, the number of load cycles, the degree of confining pressure, material density, and degree of moisture content, have already been investigated. It has long been recognised that the resilient modulus is affected mainly by the degree of stress applied under variable and constant confining pressure (Hicks 1970; Uzan 1985; Sweere 1990; Lekarp et al. 2000). Indeed it has

been reported that the resilient increased by about 50% by increasing the degree of principal stress from 70 to 140 kPa (Smith and Nair, 1973).

The confining pressure is another important factor that has a remarkable impact on the resilient modulus. By conducting triaxial testing on constant and variable confining pressures, the result confirmed that experiments with constant confining pressure led to a higher degree of resilient modulus (Allen and Thompson 1974). A similar result was reported by Monismith et al. (1967), who showed that an increase of about 500% in resilient modulus occurred when confinement was changed from 20 to 200 kPa. Moreover, by comparing the results obtained from large-scale triaxial subjected to cyclic loading, it was reported that, the degree of resilient modulus was markedly influenced by the confining pressure in a railway environment (Indraratna et al. 2005; Lackenby et al. 2007; Indraratna et al. 2009). Table 2.3 summarises the main analytical models available in literature, and which captured the resilient modulus of the unreinforced soil subjected to different load applications.

Table 2.3. Summary of model based on resilient modulus for unreinforced soil

Model	**Model to predict Resilient modulus**	**Symbols defined**
(Dunlap 1963)	$M_R = k_1' \sigma_3'^{k_2'}$	k'_1, k'_2 model parameter
(Monismith et al. 1967)	$M_R = k_1' \left(\frac{\sigma_3'^{k_2'}}{p_{atm}} \right)$	P_{atm}=atmospheric pressure
Seed et al., (1967); Brown and Pell (1967); Hicks, 1970	$M_R = k_1' \left(\frac{\theta}{p_{atm}} \right)^{k_2'}$	θ = bulk stress = $3p$
Hicks and Monismith (1971)	$\nu_R = A' + B' \left(\frac{\sigma_1}{\sigma_3'} \right) + C' \left(\frac{\sigma_1}{\sigma_3'} \right)^2 + D' \left(\frac{\sigma_1}{\sigma_3'} \right)^3$	A', B', C', D' model parameters
(Uzan 1985)	$M_R = k_1' p_{atm} \left(\frac{\theta}{p_{atm}} \right)^{k_2'} \left(\frac{\tau_{oct}}{p_{atm}} \right)^{k_3'}$	k'_1, k'_2 and k'_3 model parameter
Johnson et al., 1986	$M_R = k_1' \left(\frac{J_2}{\tau_{oct}} \right)^{k'2}$	First stress invariant: $J_2=\sigma_1\sigma'_2+\sigma'_2\sigma'_3+\sigma'_3\sigma_1$ τ_{oct} = shear stress= $(2/3)^{0.5}q$

(Thom and Brown 1988)	$M_R = \left(\frac{p}{q}\right)^{k'_2}$	$P = (\sigma_1 + \sigma'_2 + \sigma'_3)/3$ $q = \sigma_1 - \sigma'_3$
Nataatmadja and Parkin (1989) Nataatmadja (1992)	$M_R = \frac{\theta}{\sigma_1}(C' + D'q)$, $\sigma'_3 \neq$ constant $M_R = \frac{\theta}{q}(A' + B'q)$, σ'_3 = constant	A', B', C', D' model parameters
Karasahin (1993)	$M_R = A' \times \left(\frac{p_m}{p_u}\right)^{B'} \left(\frac{p_u}{\delta p}\right)^{C'}$ $M_R = A' \times \left(\frac{q_m}{p_u}\right)^{B'} \left(\frac{p_u}{p_m}\right)^{C'} \left(\frac{p_u}{\delta p}\right)^{D'}$	A', B', C', D' model parameter $\delta p = p_{max} - p_{min}$ $p_m = (p_{max} - p_{min})/2$ p_u=unit pressure (1kPa)
(Pezo 1993; Garg and Thompson 1997)	$M_R = N_1 q^{N2} \sigma'^{N3}_3$	N_1-N_3=(10-A), (1-k'_1) and(-k'_2), respectively in $\log(\varepsilon_{1,e}) = A + k'_1 \log \sigma_1 + k'_2 \log \sigma'_2$
Kolisoja (1997)	$M_R = A'(n_{\max} - n) p_0 \left(\frac{\theta}{p_{atm}}\right)^{0.5}$ $M_R = B'(n_{\max} - n) p_{atm} \left(\frac{\theta}{p_{atm}}\right)^{0.7} \left(\frac{q}{p_{atm}}\right)^{-0.2}$	n= material porosity; n_{max}=maximum porosity
Andrei (1999)	$M_R = k'_1 p_{atm} \times \left(\frac{\theta - 3k_6}{p_{atm}}\right)^{k'_2} \left(\frac{\tau_{oct}}{p_{atm}} + k'_3\right)^{k'_4}$	k'_1, k'_2, k'_3 and k'_4 model parameter
(Lekarp et al. 2000)	$M_R = \frac{\Delta(\sigma_1 - \sigma'_3) \times \Delta(\sigma_1 + 2\sigma'_3)}{\varepsilon_{1e} \times \Delta(\sigma_1 - \sigma'_3) - 2\varepsilon_{3e} \times \Delta\sigma'_3}$	

It is well known that utilising the geocell in soil helps to increase the resilient modulus and enhance the performance of soil under cyclic loading. As a result, cellular confinement has been used in railways and pavements to increase the stiffness of the subgrade layer and reduces lateral and vertical deformation. By confining the infill material, a geocell mattress improves the shear strength of the soil and improves the resilient modulus (M_R) of infill soil subjected to various load applications.

To investigate the influence of different factors (such as confinements and number of cycles), a series of experiments with coarse grained and fine grained materials and a

single geocell were carried out (Mengelt et al. 2006). These experiments were performed at a conventional 2500 cycles and an extended 12,500 cycles. It was reported that the infill coarse grained material had less effect on the resilient modulus, but there was a significant improvement when fine grained material was used. Furthermore, reinforcing the soil led to a marked reduction in the accumulation of irrecoverable strain (Mengelt et al. 2006). The results showed that by increasing the confining pressure the resilient modulus also increased, as shown in Figure 2.10.

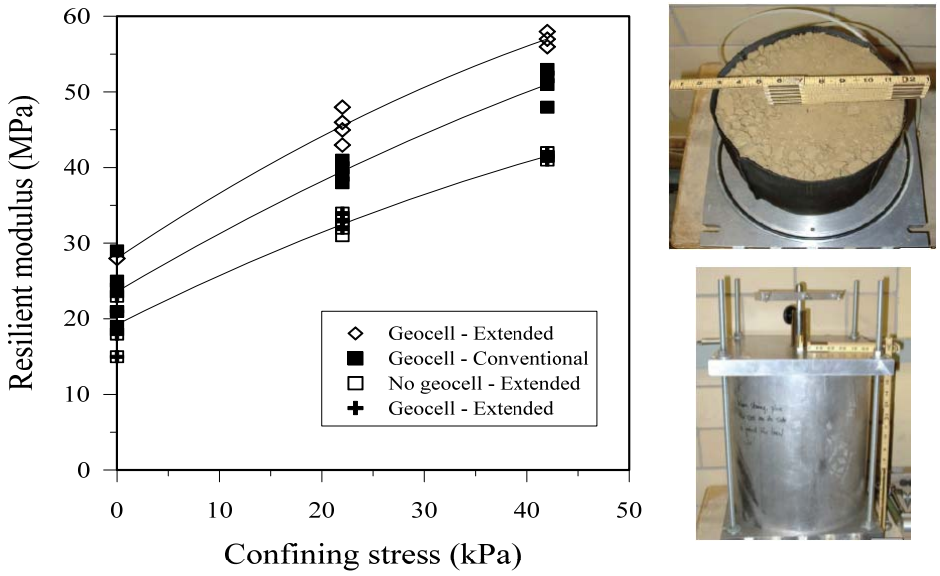

Figure 2.10. Resilient modulus of unreinforced and geocell-reinforced Antigo silt load (OMC = 2%) at different confining pressures (Modified after Mengelt et al. 2006).

To examine the improved performance of geocell-reinforced soil, a relationship for the additional confinement induced by the geocell mattress need be established. The influence of hoop stress on the residual modulus was investigated by developing an analytical model to predict the resilient modulus and permanent deformation of unbound granular media reinforced by geocell (Yang and Han 2013). Although there are several analytical models in the literature, which capture the hoop stress, only a limited number have considered the influence of factors such as the number of load cycles, frequency, and confining pressure in a railway environment (plane strain condition). Table 2.4 summarises the main research outcome, which captures the resilient modulus of reinforced soil.

Table 2.4. Summary of resilient modulus of geocell-reinforced soil

details	Resilient modulus equation	Symbols definition
MEPDG, Research Board (TRB), USA	$M_R = k_1 p_{atm}\left(\frac{\theta}{p_{atm}}\right)^{k2}\left(\frac{\tau_{oct}}{p_{atm}}+1\right)^{k3}$	k_1, k_2 and k_3 model parameter
(Perkins et al. 2004)	$M_R = E_{t(\sigma_2=\sigma_3)} \times \left[1-(\sigma_1-\sigma_3')\left[\frac{k_2}{\theta}+\frac{\sqrt{2}k_3}{3(\tau_{oct}+p_{atm})}\right]\right]$	τ_{oct} = octahedral shear stress
(Yang 2010)	$M_{R,re\inf} = \frac{\sigma_1-\sigma_3'}{\frac{\Delta\sigma_3'}{M_{R,1}}+\frac{\sigma_1-(\sigma_3'+\Delta\sigma_3')}{M_{R,2}}}$	
(Yang et al. 2013)	$M_R = E_t \times \left[1-(\sigma_1-\sigma_3')\left[\frac{k_2}{\theta}+\frac{k_3(2\sigma_1-\sigma_2'-\sigma_3')}{9\tau_{oct}(\tau_{oct}+p_{atm})}\right]-(\sigma_2'-\sigma_3')\left[\frac{k_2}{\theta}+\frac{k_3(2\sigma_2'-\sigma_1-\sigma_3')}{9\tau_{oct}(\tau_{oct}+p_{atm})}\right]\right](\tau_{oct}\neq 0)$	τ_{oct} = octahedral shear stress
(Yang and Han 2013)	$\Delta\sigma_3 = \frac{M}{D}\left[-\frac{\Delta\sigma_3'}{M_{R,1}}+\frac{\sigma_1-(\sigma_3'+\Delta\sigma_3')}{M_{R,2}}\right]\times\left(\frac{\varepsilon_0}{\varepsilon_r}\right)e^{-\left(\rho''/N_{\lim it}\right)^{\beta''}}\left(\frac{1+\sin\psi}{1-\sin\psi}\right)$	ρ'' and β'' permanent deformation parameter

2.9 Long term axial deformation

The need to maintain the superiority of railways over other transportation systems, has intensified the pressure on the railway industry to increase train speed, improve its efficiency, and reduce the cost of maintenance. Indeed to maintain this competitive edge, train speeds are expected to exceed over 150 km/hr, which imparts high cyclic stress onto the tracks. Under these high cyclic loads, rail track experiences a significant derailment that requires frequent track maintenance. As a result, understanding the long term behaviour of rail track substructure is a key requirement for designing substructure layers, which has long been of interest to many researches. Developing a constitutive model that can accurately predict the long term stress-strain behaviour of granular material subjected to different load applications has been one of the main objectives of the researches.

The linear elastic model was one of the earliest and most straightforward models developed, such that by using a generalised Hook's law and only considering two of the four elastic properties of the material, the elastic stress-strain behaviour of any material can be determined. However, there are several factors such as the number of cycles, the stress level, and the confining pressure influence the behaviour of reinforced granular material under cyclic loading. Because the soil is complex in its behaviour, the elastic relationship cannot satisfy the prediction of soil performance under different load applications. Moreover, there are additional factors such as the reinforcement interface resistance, hoop stress, and passive resistance induced by the geosynthetic aperture in reinforced soil that needs careful consideration. Because most of the constitutive relationships are complex, several analytical model were developed that can predict the permanent deformation of granular material with respect to the number of cycles. Table 2.5 summarises the models developed to predict the permanent deformation of rail-track substructure granular material subject to cyclic loading.

Table 2.5. Summary of models based on permanent deformation of soil subjected to cyclic loading

Reference	Axial deformation under cyclic loading	Parameters
(Raymond and Gaskin 1975)	$S_N = S_1(1 + a' \log N)$	a'
(Khedr 1985)	$\frac{S_n}{N} = A'.N^{-b'}$	A', b'
(Jeffs 1987)	$S_N = g' + h'(\log N) + k'N$, $N \leq 200{,}000$ $S_N = i + jN$, $N \geq 200{,}000$	g', h', i, j and k'
Paute et al., (1988)	$S_N = \frac{A'\sqrt{N}}{\sqrt{N} + D'}$	A' and D'
(Sweere 1990)	$\varepsilon_{1,p} = a'(N^{b'})$	a' and b'
Paute et al., (1996)	$S_N = A'\left(1 - \left(\frac{N}{100}\right)^{-B'}\right)$	S_N=permanent deformation after N=100 A' and B'
Vuong (1994)	$S_N = \varepsilon_1^r \left(\frac{a'}{b'}\right) N^{c'}$	a', b', c'
Wolff and Visser (1994)	$S_N = (a'N + b')(1 - e^{-c'N})$	a', b', c'
(Sato 1995)	$S_N = C'(1 - e^{-A'N}) + B'N$	A', B', C'
Huurman (1997)	$S_N(N) = A'\left(\frac{N}{1000}\right)^{B'} + C'(e^{D'\frac{N}{1000}} - 1)$	A', B', C', D'
Neidhart (2001)	$S_N = S_1 + \frac{e \log N}{1 + f' \log N}$	e, f'
(Indraratna et al. 2007)	$S_N = S_1(N^y)$	y
(Indraratna et al. 2011)	$\varepsilon_{1,p} = c' + d'(\ln N)$	c', d'
(Indraratna and Nimbalkar 2013)	$S_N = S_1(1 + a' \ln N + 0.5b' \ln N^2)$	a', b'
(Yang et al. 2013)	$\Delta_p = a'\varepsilon_v h\left(\frac{\varepsilon_0}{\varepsilon_r}\right) e^{-\left(\frac{b'}{N}\right)^{c'}}$	a', b', c'

2.10 Physical and Mechanical Properties of Geocell

The load-deformation geocell-reinforced soil depends on several important physical and mechanical properties, such as: (i) the number of cells, (ii) the dimensions of the cells, (iii) the depth of embedment, (iv) the in-fill material, and (v) the ultimate tensile strength of the reinforcement. A lot of researches have performed different experiments and compared the results of unreinforced and geocell-reinforced soil. As results there are too many studies available in the literature, which have investigated the physical properties of the geocell and their influences on the performance of reinforced soil. In this section a brief review of these studies is reported and compared for available studies.

2.10.1 Physical properties

2.10.1.1 Number of cells

It is commonly accepted in engineering in the cellular mattress, the cells effectively confine the infill material and prevent lateral spreading, hence reduce axial deformation. There are several investigations that have studied the behaviour of soil reinforced with a geocell mattress (Bathurst 1988; Bush et al. 1990; Cowland and Wong 1993; Tetsudo Gijutsu 1994; Raymond 2001; Han et al. 2011; Xiaoming et al. 2012; Yang et al. 2012). However, the numbers of cell that can be used in the experiments were usually limited due to the size of the apparatus, so the number of cells needed must be selected thoughtfully to satisfy the practical implication. A few studies have investigated the impact of the number of cells on the behaviour of reinforced cells, including the use of single cells and multi cells (i.e. n_c = 1, 3 and 5 cells) (Pokharel et al. 2010). It was reported that increasing the number of cells, had a remarkable impact on improved the performance of reinforced soil. The improved performance was attributed to apparent cohesion induced in the soil and cell interface. Marginal improvement was observed by increasing number of cell beyond three cells. This was because there was not a significant improvement of the soil area confined from three to five cells. This investigation also highlighted that cell geometry also affected the behaviour of reinforced soil, as a circular geocell was

compared to an elliptical geocell and it was reported that the circular cell performed better than the elliptical cell.

The influence of hoop stress and lateral earth resistance were also investigated by comparing the performance of sand reinforced with geocell pocket and unreinforced sand (Emersleben and Meyer 2010). Different types of geocells with numbers of cells (i.e. n_c = 1, 9 and 25) were used to examine how the number of cells affected the performance of reinforced sand. It was reported that the horizontal pressure and earth resistance increased as the number of cells increased.

The impact of the number of the cells (i.e. n_c = 1, 2, 3 and 4 cells) was also highlighted in the triaxial apparatus (d = 100 mm), as shown in Figure 2.11. It was reported that the geocell improved the performance of the soil quite significantly, and this improvement was attributed to apparent cohesion between the infill material and geocell interface, whereas the internal friction resistance of the material was not affected (Rajagopal et al. 1999).

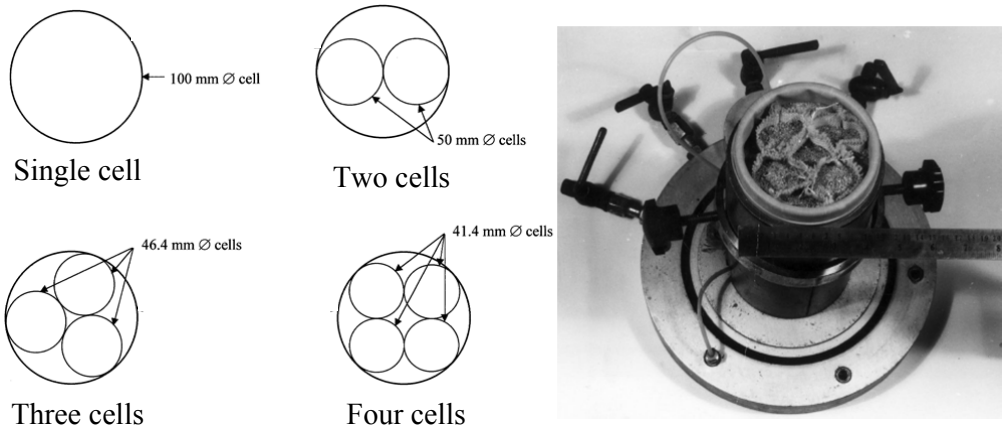

Figure 2.11. Schematic of cells used in the triaxial (Modified after Rajagopal et al. 1999)

It was also stated that the shear strength of the reinforced soil improved as the number of cell increased to three, but there was only a marginal improvement of the number of cells was increased further (Figure 2.12). This can be justified because increasing the number of cells, increased the ratio of the confinement area of the soil

over the total area of the triaxial cell, which in turn markedly improved the stiffness of the soil and thus enhanced specimen behaviour (Rajagopal et al. 1999). This result indicated that increasing the number of cell from three to four (i.e. n_c = 4) did not improve the area of confined soil, thereby did not provided a significant overall improvement.

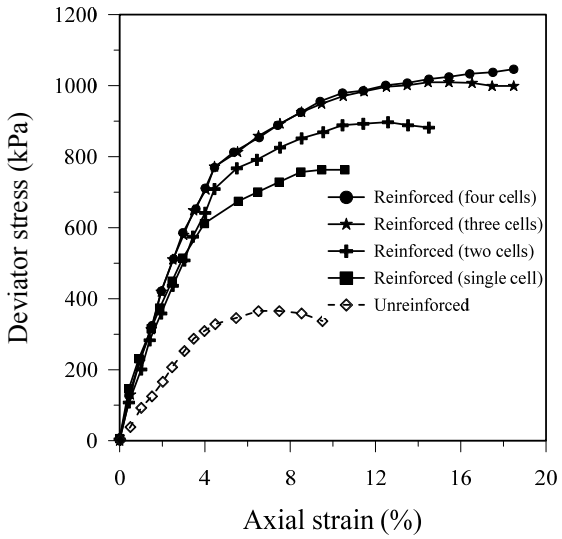

Figure 2.12. Load-deformation curve for geocell with different number of cells at σ_3' = 100 kPa (Modified after Rajagopal et al. 1999)

2.10.1.2 Infill material

It is well known that the improved performance of geocell-reinforced soil is attributed to additional confinement induced by the geocell walls, so several investigations were carried out to study how infill soil affects the performance of geocell-reinforced soil (Pokharel et al. 2010). In order to compare the infill material, an experiment was carried out using clay and clayey sand as infill material (Krishnaswamy et al. 2000). It was reported that a geocell-reinforced layer, using clay or clayey sand as infill, improved the load bearing capacity compared to the unreinforced specimen, as shown in Figure 2.13.

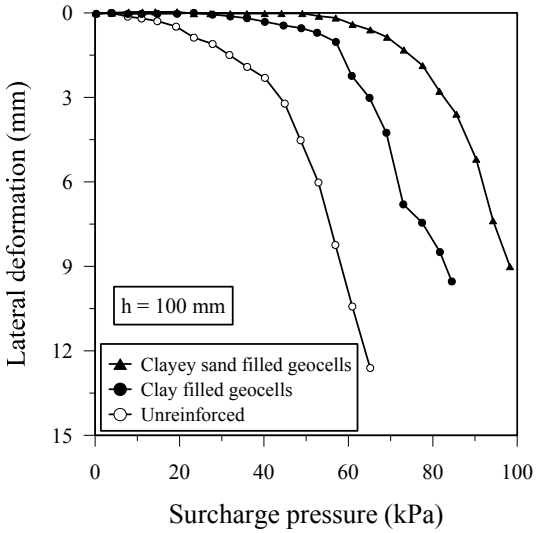

Figure 2.13. Influence of infill material used in geocell-reinforced soil (Modified after Krishnaswamy et al. 2000)

By using recycled asphalt pavement material (RAP) and fraction recycled asphalt pavement (FRAP) as infill material, the performance of geocell reinforcement for unpaved soil under a repeated wheel load was investigated (Han et al. 2011). The results showed that even recycled material can significantly improve geocell-reinforced soil under repeated loads. In fact, it was also reported that recycled material reinforced with the geocell substantially reduced the vertical pressure applied to lower layer of soil. As shown in Figure 2.14, the depth of the rut caused by repeated loading was also markedly reduced (Han et al. 2011).

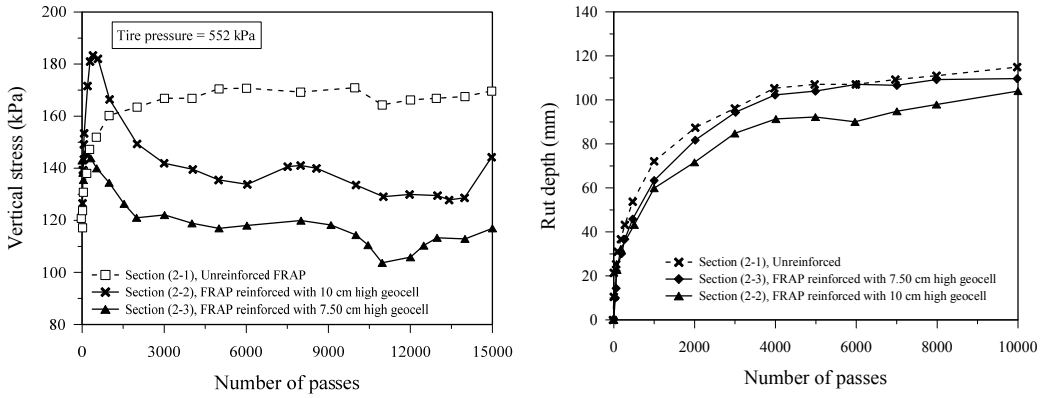

Figure 2.14. Vertical stress and rut depth in geocell-reinforced in-filled with FRAP at different number of load cycles (Modified after Han et al. 2011)

The impact of infill material was also investigated by using three different infill soils including local red soil, sand, and aggregate. The load bearing capacity of the geocell-reinforced soil improved remarkably and there was a significant reduction in settlement for different infill materials, as shown in Figure 2.15 (Hegde and Sitharam 2014). It was concluded that the infill material has a marginal impact on the final performance of geocell-reinforced soil.

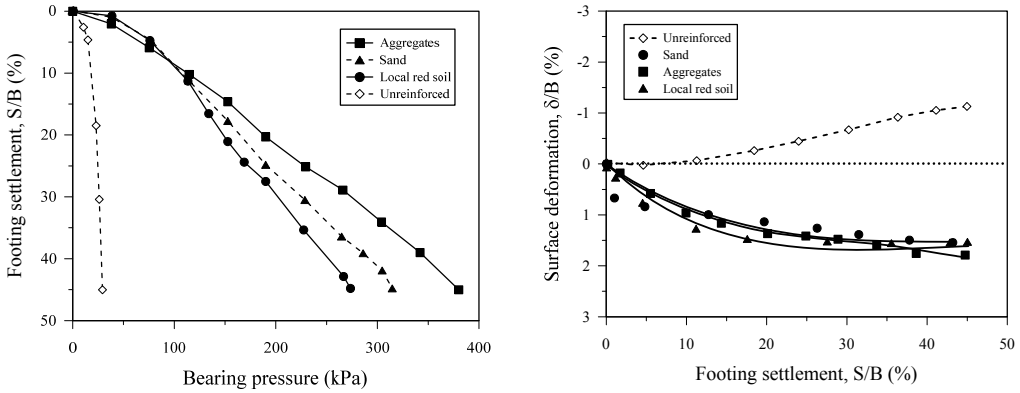

Figure 2.15. Variation of load capacity and settlement in geocell-reinforced soil (Modified after (Hegde and Sitharam 2014)

2.10.1.3 Geocell Tensile Strength

The influence of tensile strength of geocell on the reinforced soil performance has investigated by several researches. By conducting experiments using different types of geocell, it was soon recognised that geocell with a higher modulus provides a better performance (Rajagopal et al. 1999; Dash et al. 2001; Rajagopal et al. 1999; Latha et al. 2006; Krishnaswamy et al. 2000; Madhavi Latha and Somwanshi 2009). This result occurred because by improving geocell's modulus, the rigidity of the reinforced soil layer will increase and thus improve the load bearing capacity of the mattress. In another study, it was reported that the degree of improvement in geocell-reinforced soil changed significantly after the modulus of the geocell was increased (Pokharel et al. 2010). This can be explained by the fact that higher tensile strength mobilised in the geocell strips under higher load.

Emersleben and Meyer (2010) conducted an experiment to evaluate the impact of factors such as geocell stiffness on hoop stress and lateral earth resistance in geocell-reinforced sand. Different types of geocell with different modulus were used for the experiment. Regardless of the number of cells, it was found that by increasing the modulus of the geocell the horizontal pressure transferred to surrounding cells was significantly reduced.

2.10.2 Physical Properties

The physical properties of geocell such as its height, width and size of pockets, have been investigated by several researches (Dash et al. 2001; Mandal and Gupta 1993; Tetsudo Gijutsu 1994; Thallak et al. 2007; Emersleben and Meyer 2008; Han et al. 2011; Biswas et al. 2013; Tanyu et al. 2013). Significant improvements have been reported by changing the physical properties of geocell in reinforced soil. Of these different physical properties, the height of geocell markedly improved the performance of reinforced soil. It has long been recognised that by increasing the cell height, and hence the aspect ratio of the cell (h/d), the confinement offered by the geocell increases and that leads to a better performance by the reinforcement. This occurs because increasing the height of the cell confines more soil in the geocell pocket which in turn leads to a higher interface friction over a larger area. Accordingly, the lateral spreading of the infill soil diminishes significantly (Dash et al. 2001), and there is a reduction in settlement in the layer of reinforced soil. This can be explained by the fact that by increasing the height of the geocell, the reinforced layer acts like a rigid mattress with higher stiffness than unreinforced soil. There is also a reduction in the intensity of pressure applied to the lower layers of soil as the load is distributed over a wider area; this also reduces any vertical and lateral deformation and hence the load bearing capacity increases. The impact of the height of a geocell mattress in terms of the percentage reduction in settlement (PRS) was investigated in a surface footing reinforced by geocell reinforcement, made from geogrid, on soft clay beds (Thallak et al. 2007). In a similar previous study (Mandal and Sah 1992), the percentage of reduction in a footing settlement was introduced as;

$$PRS = \frac{S_0 - S_r}{S_0} \times 100 \tag{2.18}$$

where, S_o and S_r are settlements of unreinforced and reinforced soil at the same footing pressure. Similar to previous studies (Binquet and Lee 1975), a non-dimensional improved performance coefficient was also introduced to compare the performance of unreinforced soil and soil reinforced with a geocell mattress as:

$$I_f = \frac{q_c}{q_0} \tag{2.19}$$

where, q_c and q_o are the footing pressures of reinforced and unreinforced soil at the same settlement. It was observed that by using geocell with various aspect ratios, the surface deformation and vertical settlement had reduced markedly compared to the unreinforced specimen. It was also reported that by increasing the height of the geocell (h/d = 2.4) the improvement factor was increased to about I_f = 4.40. Furthermore, when the reinforcement with a smaller ratio of $b/d \leq 2$, (b and d are shown in Figure 2.16), the layer of geocell reinforcement acted like a relatively deep footing so it was better at transferring the load to deeper depths. Furthermore, by increasing the width of the apparent footing (geocell-reinforced clay) to $b/B \geq 4$, means there will be a remarkable improvement in the behaviour of reinforced soil in terms of percentage reduction in footing settlement (PRS), and increasing the bearing ratio (I_f).

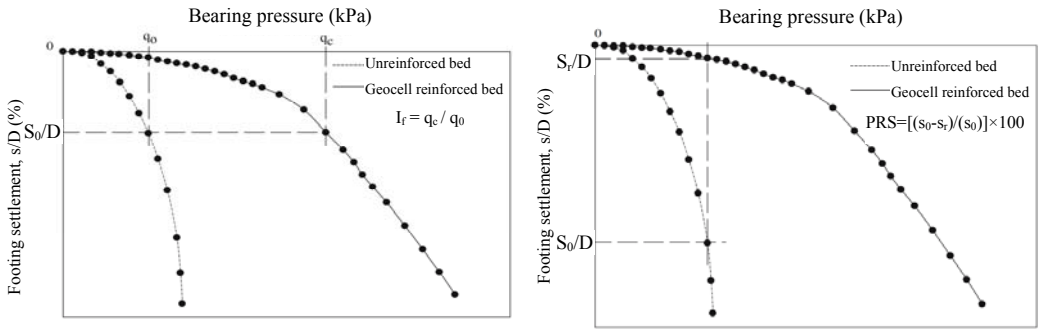

Figure 2.16. Improvement factor and percentage reduction in footing settlement (Modified after Thallak et al. 2007)

In this study the depth at which the geocell layer was embedded was also investigated. It was observed that the bearing capacity of the footing was improved by increasing the depth of the geocell mattress to about $u \leq 0.5B$. This was explained by the fact that increasing the depth of embedment to this ratio (known as the active zone), most of the slip planes beneath the footing will be ceased and hence the performance of the footing will be increased.

There are numerous studies which were carried out to investigate the properties of geocell and its influence on the performance of geocell-reinforced soil. Table 2.6. summarises some of these studies and highlights the outcome of investigations and shows the recommendations suggested for designing geocell-reinforced soil.

Table 2.6. Summary of case study of geocell-reinforced soil

Reference	**Experiment scale $L_a \times W_a \times H_a$ (mm)**	**Footing type $L_f \times B \times t$ (mm)**	**Geocell shape**	**Variables**	**Infill material**	**Type of loading**	**Research Highlights**
(Mandal and Gupta 1993)	610×310×400	Square	Hexagon	h/B = 0.75-1.5 Geocell opening size = 24, 32 and 40 mm	Sand	Monotonic	1- Improving of bearing capacity of reinforced layer. 2- Reducing of settlement. 3- Further improvement of bearing capacity obtained by increasing geocell thickness and opening size.
(Mandal and Gupta 1993)	7000×3500×2500 (full size model)	Railway track with sleeper	Elliptical	q = 30-90 kN N = 1,500,000	Crushed stone	Monotonic and cyclic	1- Geocell has significant effect when subgrade has low bearing capacity. 2- Deformations of subgrade layer reduced significantly.
(Dash et al. 2001)	1200×332×700	Square, 330×100×25	Chevron pattern	u/B = 0.1 h/B =1.2-2.75 b/B = 8	Poorly grade river sand	Monotonic	1- providing geogrid the base of geocell help to improve soil performance 2- Optimum height h/B = 2
(Krishnaswamy et al. 2000) (Latha et al. 2006)	1800×800×1200	Square	Chevron, diamond pattern	u/B = 0.57 h/d = 0.25-0.625	Clayey sand	Monotonic	1- The geocell has the most benefit when h/d = 0.5 2- Both chevron and diamond pattern shown almost same performance. 3- Materials with poor quality also can be used also as infill material

(Thallak et al. 2007)	900×900×600	Circular	Chevron pattern	u/d = 0-1.0 b/d = 1.3-5.5 h/d = 0.6-2.4	Silty clay	Monotonic	1- The geocell has the most benefit when b/D = 4.9, u/D = 0, h/D = 2.4 2- The beneficial effect of planar geogrid reduces by increasing geocell height.
(Dash et al. 2001)a	1200×332×700	Square, 330×100×25	Chevron, diamond pattern	u/B = 0-1.5 h/B = 0.8-3.14 b/B = 1-12	River sand	Monotonic	1- By utilizing geocell, settlement reduced by 50% and load bearing capacity of reinforce soil increased by 8 times of the unreinforced soil. 2-The geocell has the most benefit when u/B = 0.1**,** h/B = 2, b/B = 4
(Madhavi Latha et al. 2008)	1200×332×700	Square, 330×100×25	Chevron, diamond pattern	u/B = 0-0.75 h/B = 0.8-2.75 d/B = 1.2-2.7	Uniformly graded river sand	Monotonic	1- Shear stress transmitted to lower soil layer. 2- The potential failure planes under footing arrested by the geocell.
(Leshchinsky 2011)	1524×1524×546	Square, 356×356×25	Elliptical	─	Poor graded gravel	Monotonic & Cyclic	1- Provision of geocell lead to significant increasing in strength and decreasing in deformation was observed.
(Dash et al. 2003)	900×900×600	Circular	Chevron pattern	u/d = 1.0 b/d = 1.2-5.6 h/d = 0.42-2.52	Soft clay	Monotonic	1-Using the geocell lead to significant reduction in surface heaving and increased bearing capacity. 2- The geocell has the most

							benefit when b/D = 5, h/D = 2.1
(Dash et al. 2007)	1200×332×700	Square, 330×100×25	Chevron pattern	u/B = 0-1.5 h/B = 0.8-3.14 d/B = 1.2-2.7 b/B = 1-12	Angular dry river sand	Monotonic	1-The load dissipation factor found influenced by pocket size, height and width of the geocell. 2- The geocell has the most benefit when u/B = 0-0.1, h/B =1.2, d/B = 1.2, b/B = 4
(Emersleben and Meyer 2008)	2000×2000×2000	Circular, 300 mm	Elliptical	h/d = 0.43-0.87 h/d = 0.67-1.25	Sand	Monotonic	Due to using geocell stress over subgrade layer was significantly reduced
(Sireesh et al. 2008)	900×900×900	Circular, 150×30	Chevron pattern	h/d = 0.6-3.6 b/d = 1.3-5.5	Silty clay	Monotonic	1- The rigidity of the geocell-reinforced layer increased by increasing the height of the geocell. 2- The geocell has the most benefit when b/D = 4.9
(Dash 2010)	1200×332×700	Square, 330×100×25	Chevron pattern	D_R(%) = 30-70	Poorly graded sand	Monotonic	Stiffness of reinforced soil layer increased by increasing relative density
(Yang et al. 2012)	6100×4900×1800 full size model	Wheel load	Elliptical	h(Geocell height)	Sand	APT	1- Increasing shear strength of reinforced soil layer 2- Rut depth was markedly reduced in reinforced soil.
(Biswas et al. 2013)	1000×1000×1000	Circular, D = 150	Chevron pattern	h/d=0.63-2.19 C_u=7-30 kPa	Sand	Monotonic loading	Geocell shown better performance in subgrade with lower shear strength

(Leshchinsky and Ling 2013)	1524×1524×546	Square, 356×356×25	Sinusoidal diamond	*h(Geocell height)*	Poor graded gravel	Monotonic & Cyclic	1- By increasing apparent confinement, geocell reduces lateral and axial deformation under both monotonic and cyclic loading. 2-Using geocell lead to uniform distribution of load over subgrade layer.
(Tanyu et al. 2013)	3000×3000×3500	Circular, D = 250	Sinusoidal diamond	D=200, 300 mm h =150, 200 mm	Gravel	Cyclic loading	1- Plastic deformation if geocell-reinforced layer reduced to %50 of unreinforced soil layer. 2- By using geocell, the modulus of subgrade increased.
(Tafreshi et al. 2014)	Full scale model	Circular, D = 300	Sinusoidal diamond	*Load* = 150-800 kPa	Sandy soil	Repeated loading	1- Plastic deformations increase with increasing N. 2- Use of rubber soil mixture layer is effective under cyclic loading. 3- By increasing N, the rate of strain increments decrease.

Note: h = geocell height (depth) (mm), B = width of footing (mm), b = geocell mattress width (mm), d = pocket size (mm), D = footing diameter (mm), APT: Accelerated pavement testing

2.11 Interface shear strength

Among of the different physical and mechanical properties of geosynthetics, the contribution made by the interface friction angle between the reinforcement and soil, in improving the performance of reinforced soil has been highlighted in literature. Due to very small opening area in geotextiles, shear resistance is barely associated with shear resistance between reinforcement and soil particles. Nevertheless, in case of larger openings in geogrid or geocell, this mechanism is distinctive. It is well known that skin friction or the interface friction angle has a remarkable impact on the performance of reinforced soil, and it must be known accurately. The direct shear apparatus and pull-out box have been widely used to investigate the shear behaviour of soil-geosynthetics and determine the interface friction resistance (Jewell and Wroth 1987; Jewell 1990; Swan et al. 1991; Moraci and Recalcati 2006; Wang et al. 2008; Khedkar and Mandal 2009; Liu et al. 2009; Anubhav and Basudhar 2010; Arulrajah et al. 2014; Ezzein and Bathurst 2014). Due to difficulties associated with determination of interface coefficient, a conservative value of (1/2-2/3) of soil friction angle is generally used. However, the interface friction angle is influenced by factors such as effective normal stress (σ_n), the shearing displacement rate (S_R), relative density (D_R) and geosynthetic type (variations in aperture size and shape as well as material type). A limited number of studies dealing with the effects of these factors on the strength of the interface are currently available, and they will be discussed in this section.

Perhaps one of the earliest studies which investigated the influence of interface friction angle between geosynthetic and soil was done by Jewell (Jewell and Wroth 1987). It was reported that the inclusion of reinforcement in soil leads to substantial reduction of stress distributed on the soil which increases its shearing resistance. Also, by conducting a pull out test, it was stated that the maximum interface friction angle between reinforcement and sand can be equal to the apparent friction angle between sand particles (Jewell 1990). As a result, a bond coefficient was proposed for reinforced materials that depended on skin friction as (Jewell and Milligan 1984):

$$f_b = \alpha_s \left(\frac{\tan \delta}{\tan \phi_{unrein}} \right) + \left(\frac{\alpha_b B_g}{S} \right) \left(\frac{\sigma'_b}{\sigma'_n} \right) \frac{1}{2 \tan \phi_{unrein}} \tag{2.20}$$

where S is the opening size of the grid, σ'_b / σ'_n is the normalised bearing stress, α_s is fraction of geosynthetic area that is solid, α_b is the fraction of geosynthetic width available for bearing, B_g is the width of the grid, ϕ_{unrein} and δ are the apparent friction angle and skin friction angle between the material and reinforcement respectively.

A later work included an investigation of the load mechanism between soil and reinforcement. The interaction between cohesive frictional soil and different types of reinforcement such as steel grids, bamboo grids, and polymer geogrids has been investigated in both large scale direct shear and pull out test (Bergado et al. 1993). It was reported that the improved performance of reinforced soil can be explained by three main components as (1) passive resistance associated with transverse ribs, (2) frictional resistance between soil particles and reinforcement, and (3) internal resistance between the soil particles (Liu et al. 2009). In order to calculate the direct shear resistance, the following relation was proposed as (Bergado et al. 1993; Liu et al. 2009):

$$P_{s'} = \sigma_n A' \left[\alpha_{ds} \tan(\delta + (1 - \alpha_{ds}) \tan \phi_{ds}) \right] \tag{2.21}$$

$$\tau_{sand-geogrid} = (1 - \rho')\tau_{san-geosynthetic} + \rho' \tan \tau_{sand} \tag{2.22}$$

where σ_n is normal stress, A' is the shearing area, δ is the friction angle between soil and reinforcement, α_{ds} is the ratio of shear area between reinforcement and total shear area, ϕ_{ds} is the apparent friction angle of soil obtained from direct shear test, and ρ' is the percentage of open area of geogrid. The impact of passive resistance was highlighted by comparing the peak shear strength of different types of reinforcement (Liu et al. 2009). It was observed that due to the higher percentage of transvers ribs, passive resistance contributed more to the overall shear resistance, and was associated with larger displacement.

The impact of compaction, water content, and dry unit weight of cohesive soil on the interface shear strength of reinforced soil has been also investigated (Swan et al. 1991). It was reported that the peak shear stress increased by increasing the compaction effort. Also, it was observed that peak shear stress improved by increasing the water content and dry unit weight of the soil.

By using different types of geosynthetics, the influence of relative density (D_R = 50 and 80%) and normal stress (σ_n = 50, 100, 200, 300 kPa) were investigated using a large-scale direct shear box (Lee 2000). It was observed that reinforced soil provided a greater initial modulus (stiffness) than unreinforced soil. Also, it was reported that the reinforced soil exhibited a higher peak shear strength at larger shear displacement than the unreinforced specimen. Moreover, the peak shear strength was increased by increasing the relative density.

By using fly ash and a smooth and textured geomembrane, the impact of material's density was investigated. Standard and modified compaction employed to study the impact of compaction on the interface shear resistance. It was reported that due to better interlocking, textured geomembrane exhibited significantly higher shear strength than smooth geomembrane. The same results were also observed by other researches (Anubhav and Basudhar 2010). Moreover, the reinforced specimens showed relatively small difference between residual and peak strength, whereas this difference was much higher for unreinforced ash.

2.12 Geocell application in cyclic loading and Railway

Although there are numerous literatures available with regards to the behaviour of geocell-reinforced soil under monotonic loading, only a few have been devoted to the cyclic performance of geocell-reinforced media (Kief et al. 2014). By performing full-scale moving wheel tests, the influence of a geocell mattress on the performance of an unpaved road under a large number of cycles was investigated. It was found that by utilising the geocell mattress the thickness of an unpaved road can be reduced and still perform the same as an unpaved road. It was also observed that the

magnitude of stress transferred to the lower soil layer had decreased, which led to a substantial reduction of vertical stress (Kief et al. 2014).

The benefit of using a geocell mattress has been highlighted by using a large-scale model experiment (Tanyu et al. 2013). In this experiment the impact of cyclic loading on the geocell-reinforced gravel overlying uniform sand was investigated using geocell with different heights (i.e. 150 and 200 mm). The geocell had a remarkable impact on the resilient modulus and permanent axial deformation of reinforced soil. Indeed the total axial deformation of geocell-reinforced gravel was about 20-30% less than the unreinforced specimen, as shown in Figure 2.17. It was also found that the rate of axial deformations decreased by increasing the number of cycles. Furthermore, the resilient modulus of subgrade improved by about 40-50% when geocell reinforcement was used, as shown in Figure 2.17 (Tanyu et al. 2013).

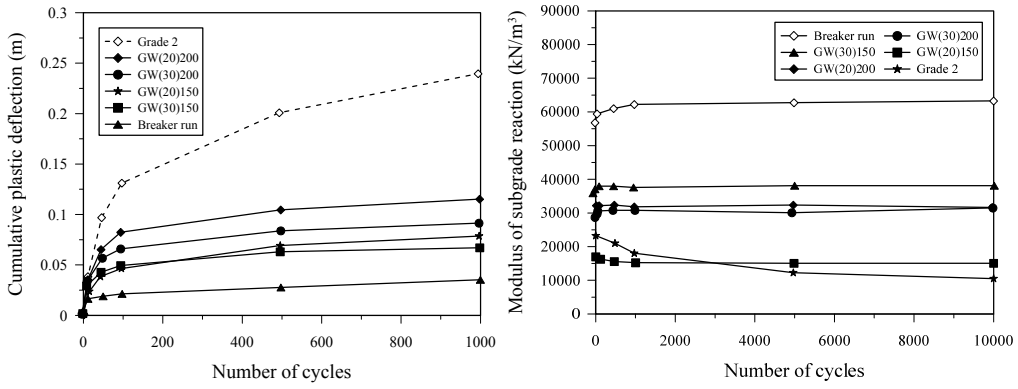

(a) (b)

Figure 2.17. (a) Plastic deformation and (b) modulus of subgrade for 450 mm subbase thickness during traffic loading (Modified after Tanyu et al. 2013).

The performance of geocell reinforcement was investigated using 300 mm diameter plate subjected to cyclic loading (Tafreshi et al. 2014). It was found that the plastic deformation was significantly influenced by the number of cycles. It was observed that most of the plastic deformation occurring at the initial cycles, as shown in Figure 2.18 (a & b). It was reported that the vertical permanent deformation increased by

increasing the number of cycles. The rates of axial deformation diminished in the following cycles where the specimen experienced a shakedown stage. An optimum depth of u/D=0.2 was recommended for the geocell mattress when it was embedded beneath the footing (Tafreshi et al. 2014), where D is diameter of footing and u is depth of embedment.

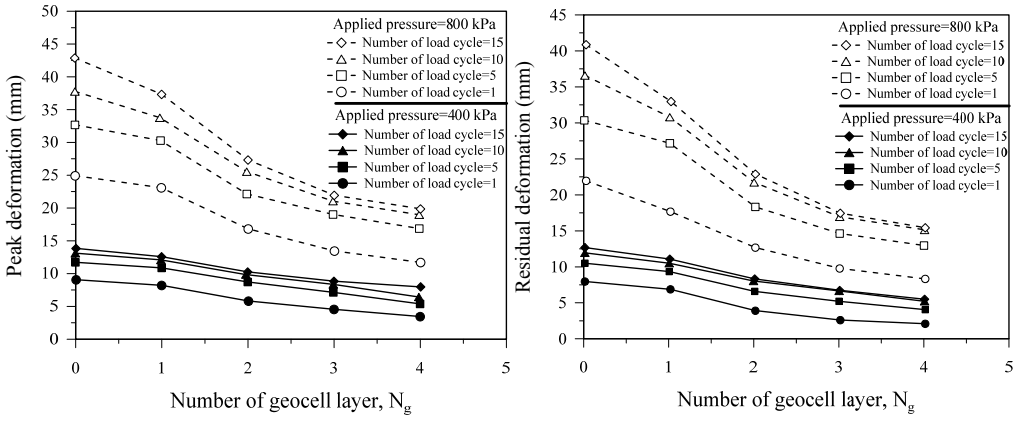

(a) (b)

Figure 2.18. (a) Maximum and (b) residual deformation of geocell-reinforced soil at different number of cycles (q = 400 and 800 kPa) (Modified after Tafreshi et al. 2014).

2.13 Numerical modelling

A numerical approach is inevitable to provide a clear resolution of geocell-reinforced soil. Several investigations were conducted to simulate geocell-reinforced soil under monotonic loading. Influence of geocell properties on reinforced sand and clay was investigated using FLAC (Saride et al. 2009), and it was reported that increasing the geocell geometry had a significant impact on the behaviour of reinforced soil. It was also proven that using planar geogrid to reinforce sand and clay soil improved further their performance. By adopting the Mohr-Coulomb yield criterion, the behaviour of a single pocket of geocell was investigated using FLAC 3D (Yang et al. 2010). It was observed that due to the confining infill soil, the stress inside the pocket was higher than outside the pocket. The behaviour of geocell-reinforced sand subjected to monotonic loading was also investigated (Hegde and Sitharam 2014). The Mohr-

Coulomb yield criterion was used to predict the dilation and interface between geocell and infill soil. Numerical analysis was also used to evaluate the impact of geocell modulus, height of the mattress, friction angle, and pocket size. It was reported that geocell-reinforced soil performed better when the height and pocket size of geocell was increased (Hegde and Sitharam 2014). It was also observed that the interface friction angle and geocell modulus had a significant impact on the performance of reinforced soil, as shown in Figure 2.19.

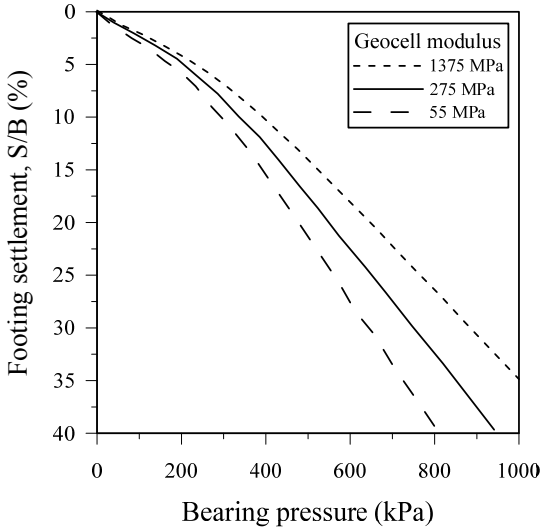

Figure 2.19. Footing settlement against bearing pressure (Modified after Hegde and Sitharam 2014

Large-scale laboratory equipment has been used to investigate the behaviour of an embankment reinforced with ballast (Leshchinsky and Ling 2013). In this experiment, the ballast was examined via monotonic and cyclic loading with a large number of cycles. The test confirmed that the geocell mattress embedded into the ballast layer provided additional confinement that helped increase the apparent confining pressure applied to the ballast. As a result, this cellular confinement successfully arrested most of the lateral spreading of ballast subjected to cyclic loading. Furthermore, it also minimised the axial deformation of ballast in the reinforced layer (Leshchinsky and Ling 2013). A numerical simulation was adopted to validate experimental results, and based on the results, the performance of geocell reinforcement was further improved by increasing the ballast and geocell properties

such as the friction angle, the modulus of ballast and the geocell, as shown in Figure 2.20, (Leshchinsky and Ling 2013).

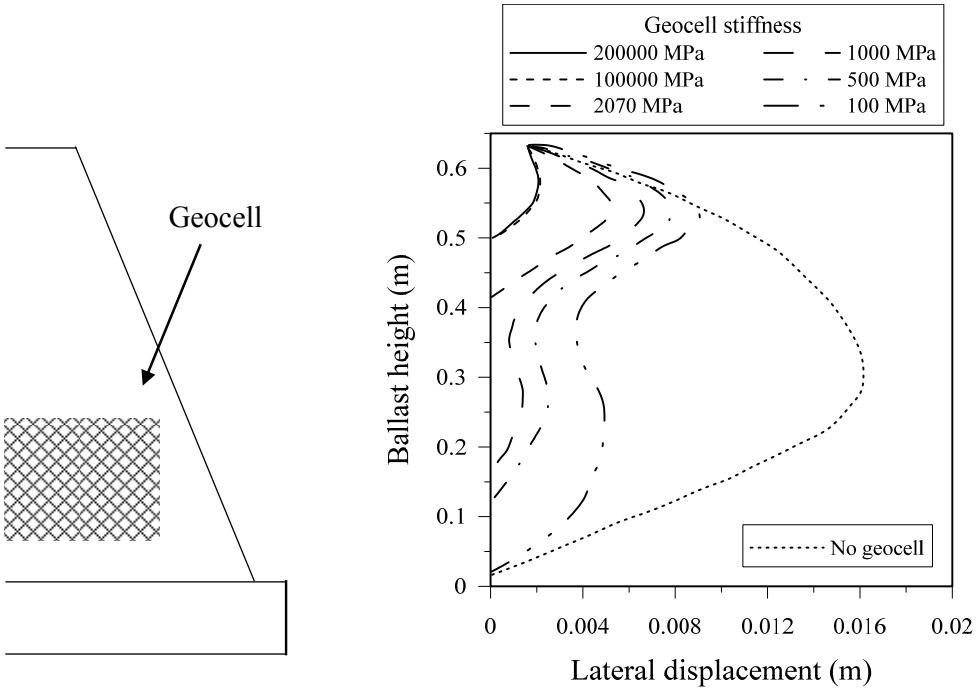

Figure 2.20. Lateral displacement of geocell-rienforced ballast (Modified after Leshchinsky and Ling 2013)

During this literature review there was no study available which investigated the behaviour of geocell-reinforced subballast subjected to cyclic loading with a full sinewave in plane strain condition, and which was similar to a railway environment.

2.14 Critical Review of Literature

The literature review discussed in this chapter addressed the latest available investigations related to the current study. It was highlighted that a geocell mattress significantly improved the behaviour of soil subjected to different load applications. The beneficial impact of geocell reinforcement can be summarised as follows:

(a) Acting as semi-rigid slab, geocell mattress distributes the applied load over a wider area and to a deeper depth.

(b) It minimises lateral and vertical displacement and helps to increase the rigidity of infill material under different stress levels.
(c) It reduces the intensity of applied stress over the deeper layers of soil and helps reduce their settlement.
(d) It confines the infill material, which accelerates the material densification and improves the stiffness of the geocell-reinforced layer of soil.
(e) The performance of a geocell mattress can be improved further by increasing its height.
(f) In order to achieve maximum benefit, the geocell reinforcement needs to be placed beneath the footing at an embedment depth of $u/B = 0.1$.

Most of the available literatures have studied the impact of cyclic loading under a relatively small number of cycles (N). Nevertheless, under small number of cycles, the granular material does not experience a shakedown stage. A larger number of cycles are needed to reach the shakedown stage, where the volumetric changes are almost negligible. As a result, experiments with a large number of cycles (i.e. $N \geq$ 100,000 cycles) are must be carried out to capture the behaviour of geocell-reinforced subballast.
During this study period, no major study was carried out to investigate the performance of unreinforced and geocell-reinforced subballast subjected to cyclic loading in a stress controlled fashion, or in plane strain condition. Most studies were carried out using large-scale cylindrical triaxial or plate load test. Nevertheless, in a conventional triaxial test the intermediate stress (σ'_2) cannot be controlled. Thereby, conventional triaxial apparatus cannot be used to investigate geocell-reinforced subballast. As a result, appropriate equipment is needed to investigate the performance of geocell-reinforced soil that simulates a railway environment ($\sigma'_2 \neq \sigma'_3$). The main contribution of this current study is to address the impact that geocell reinforcement has on the implementation of rail track substructure under a large number of cycles and conditions that are similar to the field. Providing railway field conditions will lead to a better understanding and more accurate data of the vertical and lateral displacement of unreinforced and geocell-reinforced subballast.

CHAPTER 3

3. AN EVALUATION OF THE INTERFACE BEHAVIOUR OF RAIL SUBBALLAST STABILISED WITH GEOGRID AND GEOMEMBRANES

3.1 General

One of the most important design parameters that must be known accurately is the shearing resistance between the aggregates and geocell material. Due to difficulties associated in determining the interface coefficient, a conservative value of half to two-third of the soil friction angle is generally used (Indraratna and Nimbalkar 2013; Leshchinsky and Ling 2013). However, the interface friction angle is influenced by several factors such as the effective normal stress (σ_n), the shearing displacement rate (S_R), the relative density (D_R), and type of geosynthetic (i.e., variations in the size and shape of the aperture and the type of material). In this regard, conducting large-scale direct shear test to evaluate the interface friction angle between the subballast and the geocell membrane was considered blatantly advantageous (Jewell and Wroth 1987; Swan et al. 1991; Anubhav and Basudhar 2010), given the immense benefits to the rail industry, as many rail organisations worldwide are now looking at effective ways of stabilising subballast.

The shearing rate in a railway embankment may differ because it is subjected to various cyclic stress levels, depending on the train speeds. Moreover, to maximise the benefits of reinforcement in the field the infill soil needs to be compacted to an optimum density. However, under a typical rail environment, this optimum density is not always achieved. The interface shear strength is also governed by geosynthetic characteristics such as the percentage of open area (*OA*). Therefore, a comprehensive study of the effect of effective normal stress, shearing rate, relative density, and *OA* on the shear strength is both timely and imperative. Despite these advances, only

limited number of studies have examined the influence of the size and shape of geogrid apertures on the performance of ballast (Brown et al. 2007; Indraratna et al. 2012). Moreover, no comprehensive study on investigating the influence of these parameters on the behaviour of rail subballast has yet been reported.

To design rail tracks stabilised with geocell, it is imperative to determine the frictional interaction between the aggregates and the geocell membrane in both lateral and vertical directions. However, given the highly random nature of particle orientation within the subballast assembly, it is anticipated that the angle of shearing resistance between the aggregates and the membrane could be isotropic, assuming that the membrane texture is usually uniform. A series of large-scale direct shear tests were carried out to investigate the interface shear strength of subballast stabilised with geogrids and geomembranes. The beneficial effects of these two different types of geosynthetics on the stress-strain behaviour of unreinforced and reinforced subballast were also investigated. The influences of effective normal stress (σ_n), relative density (D_R), and the shearing displacement rate (S_R) were studied.

3.2 Experimental procedure

3.2.1 Materials

3.2.1.1 Subballast

The subballast material (crushed basalt) used in this study was collected from a local quarry near Wollongong, NSW Australia. Prior to the experiments, the material was carefully sieved to meet the Australian standard. Then, the aggregates were mixed based on the proposed particle size distribution (PSD), as shown in Figure 3.1. The current PSD was similar to current Australian practices in the states of Queensland and Victoria. Specimens were oven dried prior to the experiment. Table Properties of subballast used in current study are presented in Table 3.1.

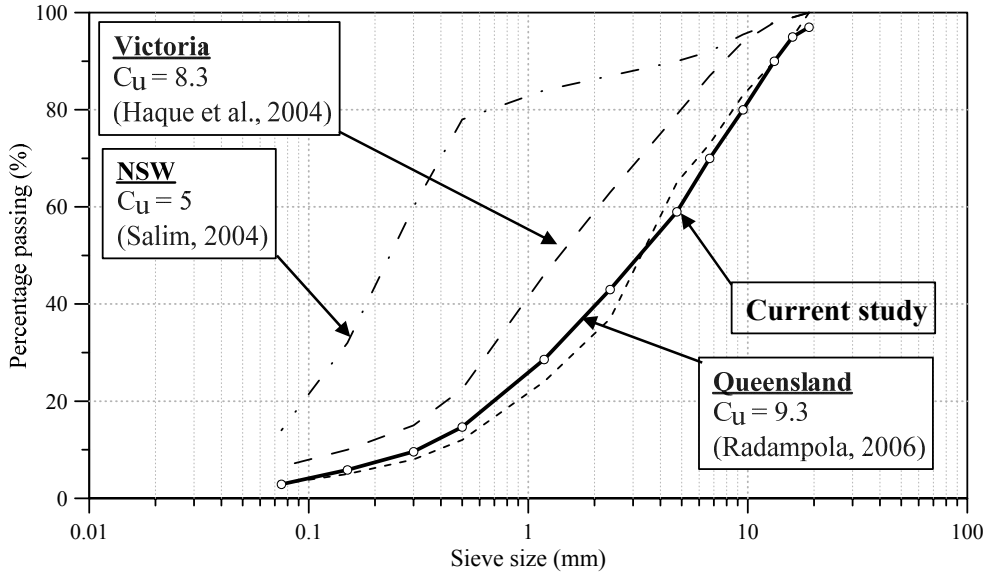

Figure 3.1. Particle size distribution of subballast used in the current study compared to typical materials used in track in various states of Australia

Table 3.1. Properties of subballast used for conducting the experiments in this study

Main particles size (mm)	D_{max}	D_{min}	D_{50}	D_{30}
	19	0.075	3.3	1.4
Coefficient	C_u	C_c		
	16.3	1.3		
Dry unit weight (kN/m^3)	**Max**	**Min**		
	21.22	15.68		
Dry unit weight (kN/m$^{3)}$	20.58			
Void ratio (e)	0.29			
Specific gravity	2.7			

3.2.1.2 Geosynthetics

In order to investigate the interface friction of subballast and geosynthetics, three types of geosynthetics (Figure 3.2) were used to reinforce the subballast: (i) geomembrane (GC1 and GC2), (ii) triaxial geogrid with a triangular opening (GG1), and (iii) biaxial geogrid (GG2, GG3 and GG4). By selecting different types of geogrid and geomembrane, the influence of the open area (*OA*%) on the interface shear strength was examined. Table 3.2 summarises the physical and mechanical properties of these geosynthetics.

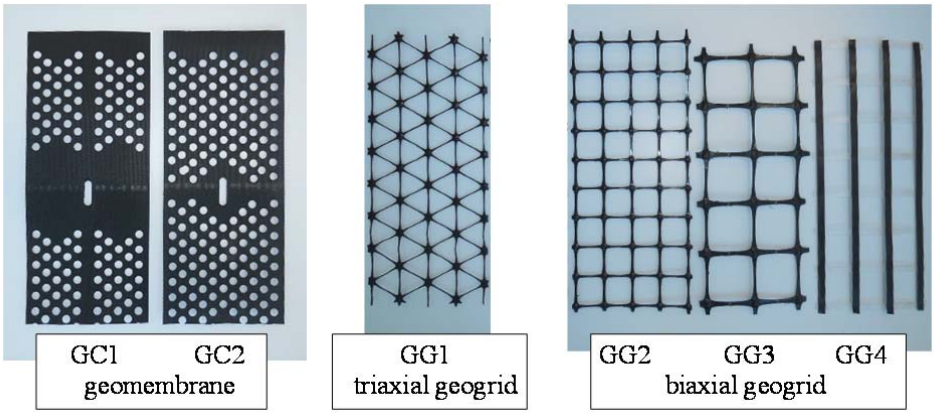

Figure 3.2. Different types of geosynthetic used in large-scale direct shear testing

Table 3.2. Physical characteristics and technical specification of geosynthetics used for the study

Geosynthetic type	Geomembrane		Geogrid			
	GC1	GC2	GG1	GG2	GG3	GG4
Material	PE	PE	PP	PP	PP	PP
Structure	Perforated, textured strip	Perforated, textured strip	Triaxial	Biaxial	Biaxial	Biaxial
Physical Characteristics						
Open Area (%)	19.19	29.65	65.74	78.9	84.01	81.03
A/D_{50}	3.03	3.03	10.90	11.21	19.54	13.33
Aperture shape	circle	circle	Triangle	Square	Rectangle	Square
Aperture size (mm)	10	10	37	37	63.5×64.5	44
Cell depth (mm)	150	150	—	—	—	—
Thickness (mm)	1.5[c]	1.5[c]	—	—	—	—
Rib thickness (mm) (MD/CMD)	-/-	-/-	2[c]/2[c]	2.2[c]/1.3[c]	2.3[c]/1.3[c]	1.0[c]/1.0[c]
Technical Characteristics						
Tensile strength at 5% strain (kN/m)	7.5	5	11	16.5	17.5	15.5
Ultimate strength (kN/m) (MD/CMD)	9.5[a]/-	6.5[a]/-	19[b]/19[b]	30[b]/30[b]	30[b]/30[b]	30[b]/30[b]

Note: PP: *polypropylene, PE:* Polyethylene, MD: Machine Direction, CMD: Cross Machine Direction Note: [a]ASTM 4885; [b]ASTM 6637; [c]ASTM 5199

3.2.2 Testing program

Experiments were carried out using a large-scale direct shear box which consisted of two square units (300 × 300 mm). The upper box (100 mm in height) was fixed, while the lower box (90 mm in height) was free to move, as shown in Figure 3.3. An electric motor with a set of gears was used to control the displacement of the lower box. A predetermined amount of subballast was placed inside the shear box and compacted in several layers to achieve the desired density that represented field conditions (ρ = 2100 kg/m^3).

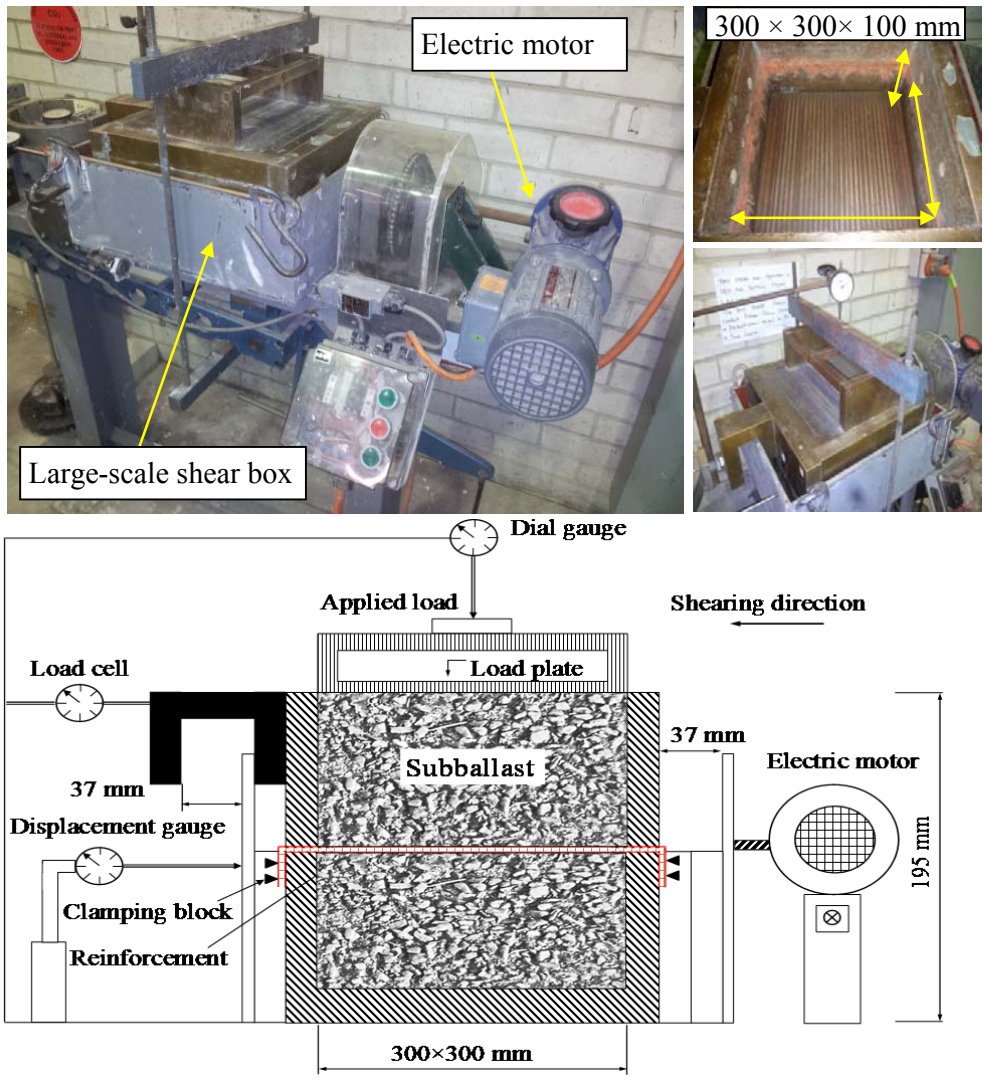

Figure 3.3. Schematic illustration of large-scale direct shear apparatus.

For the reinforced subballast, one layer of geogrid (biaxial and triaxial) (300 × 300 mm) or two layers of geomembrane (150 × 300 mm), were placed at the interface of upper and lower boxes, along the shearing direction (Figure 3.4). Several clamping blocks were used to clamp each end of the geosynthetics and the front edge of the lower shear box, and then the upper boxed was filled with subballast. In the field, only a small confining pressure (hence effective normal stress) exerted by the ballast shoulder ($\sigma_3' \leq 30$ kPa), is usually available (Indraratna et al. 2015). The experiments were conducted at relatively low effective normal stresses ($1 \leq \sigma_n \leq 45$ kPa), to simulate a realistic track environment (i.e. with less confining pressure).

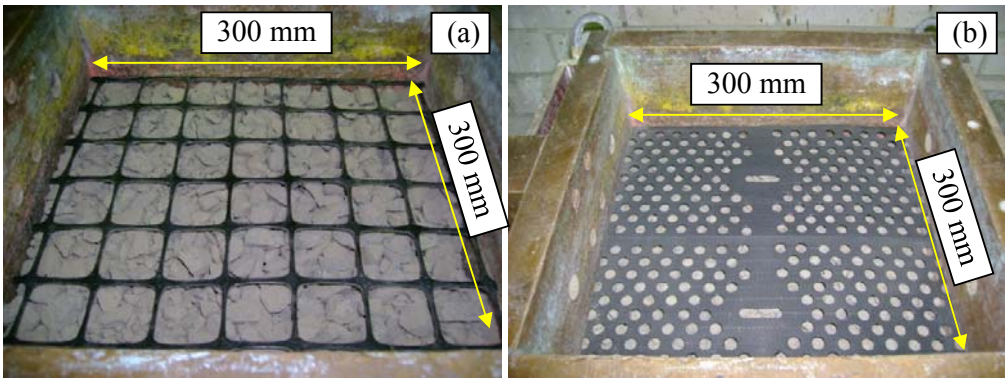

Figure 3.4. Subballast reinforced with (a) geogrid and (b) geomembrane in the direct shear box

A total of 60 tests were carried out with 15 unreinforced and 45 reinforced specimens under different effective normal stresses (σ_n), as summarised in Table 3.3. To investigate the influence of relative density, 12 tests were carried out with different relative densities (i.e. D_R = 40, 50, 60, 70, 77 and 85 %). In addition, the impact of the rate of shearing was analysed by varying the shear displacement rate (i.e. S_R = 1, 2, 4, 8 and 12 mm/min) for both unreinforced and reinforced subballast with GC1 at selected relative density (D_R) of about 77 % and at an effective normal stress of σ_n = 20.5 kPa. The type of geomembrane GC1 was selected because it is used in the manufacture of geocell mattresses (Indraratna et al. 2015). For the remaining investigations, the specimens were compacted in a dry condition to a relative density (D_R) of about 77 % and sheared at a constant shearing rate of 1 mm/min (ASTM D5321-2012). Shearing continued during these experiments until a maximum horizontal strain (ε_h) of 10 % was reached. Three mechanical gauges were used to record the shear force, and the vertical and horizontal displacements.

Table 3.3. Summary of test programming in current study using direct shear apparatus

Test details	Effective normal stress σ_n (kPa)	Shearing rate S_R (mm/min)	Relative density D_R (%)
Subballast (SB)			
	1, 6.7, 11.5, 20.5, 29.5, 45	1	77
	20.5	1	40, 50, 60, 70, 85
	20.5	2, 4, 8, 12	77
Subballast-geomembrane (SB-GC1)			
	1, 6.7, 11.5, 20.5, 29.5, 45	1	77
	20.5	1	40, 50, 60, 70, 85
	20.5	2, 4, 8, 12	77
Subballast-geomembrane (SB-GC2)			
	1, 6.7, 11.5, 20.5, 29.5, 45	1	77
Subballast-geogrid			
SB-GG1	1, 6.7, 11.5, 20.5, 29.5, 45	1	77
SB-GG2	1, 6.7, 11.5, 20.5, 29.5, 45	1	77
SB-GG3	1, 6.7, 11.5, 20.5, 29.5, 45	1	77
SB-GG4	1, 6.7, 11.5, 20.5, 29.5, 45	1	77

3.3 Results and Discussion

3.3.1 Interface shear characteristics Stress ratios

To study the impact of effective normal stress on the shear strength, the stress ratio (τ/σ_n) and normal strain (ε_h) are plotted against the horizontal strain (ε_h) as shown in Figure 3.5(a & b). Higher stress ratios occurred at low effective normal stress, and this is in accordance with earlier studies as the (τ/σ_n) ratio represents the apparent friction angle of granular materials (Suiker et al. 2005, Indraratna et al. 2011). The stress ratio (τ/σ_n) showed a non-linear variation with the horizontal strain (ε_h), as shown in Figure 3.5a (i) and Figure 3.5b (i). As expected, by increasing σ_n, the peak value of τ/σ_n decreased, due to diminished dilation at increased levels of effective normal stress [Figure 3.5a (ii) and 4b (ii)].

For the subballast reinforced with geomembrane, $(\tau/\sigma_n)_{peak}$ exhibited relatively stable behaviour over a larger range of horizontal strain (2-6 %), compared to the unreinforced subballast (2-4 %), before strain softening occurred. Although a slight increase in the initial modulus is observed, it was found that the geomembrane (GC1) did not provide a remarkable increase in the value of τ/σ_n. This indicated that the interface shear strength (τ) is less affected by the geomembrane. The results also showed that the unreinforced subballast underwent excessive volumetric dilation, while the reinforced specimens showed a decreased magnitude and rate of dilation. Figure 3.5a (ii) and Figure 3.5b (ii) clearly indicated that for the same applied horizontal strain, the dilation of the geomembrane-reinforced subballast was much less.

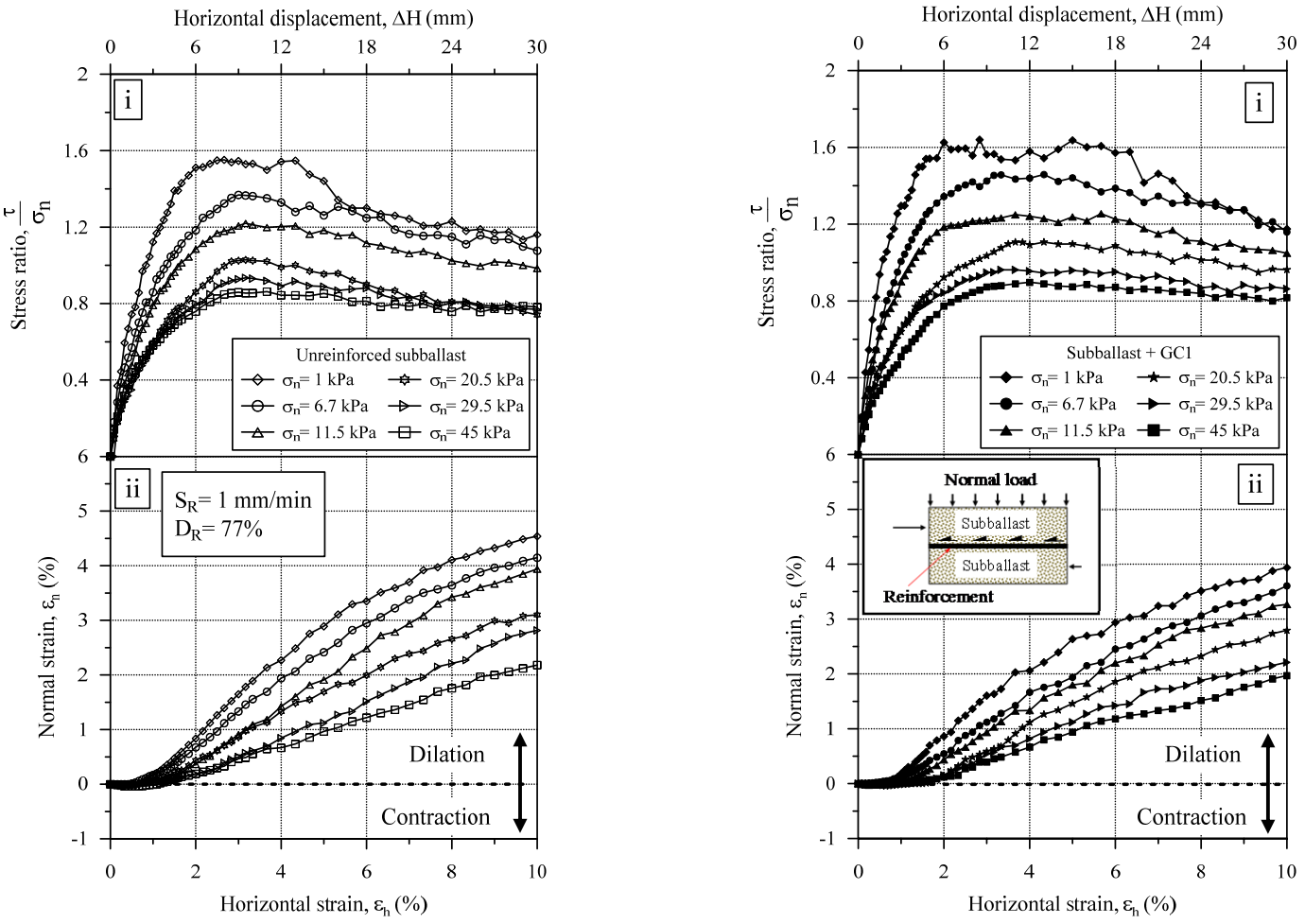

Figure 3.5. Comparison of Stress-strain behaviour of (a) unreinforced and (b) reinforced subballast tested in large-scale shear box

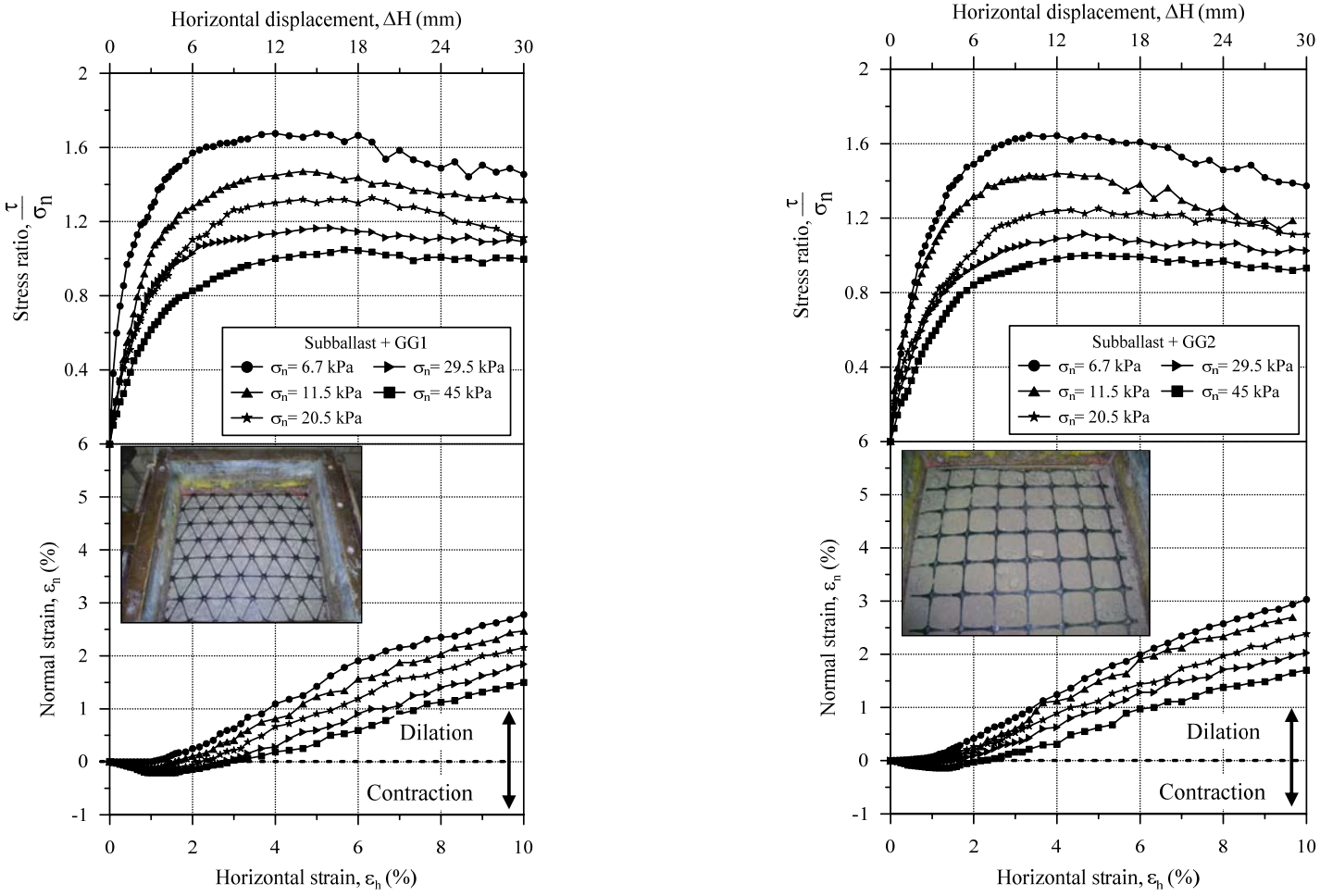

Figure 3.6. Comparison of Stress-strain behaviour of reinforced-subballast with (a) GG1 and (b) GG2 tested in large-scale shear box

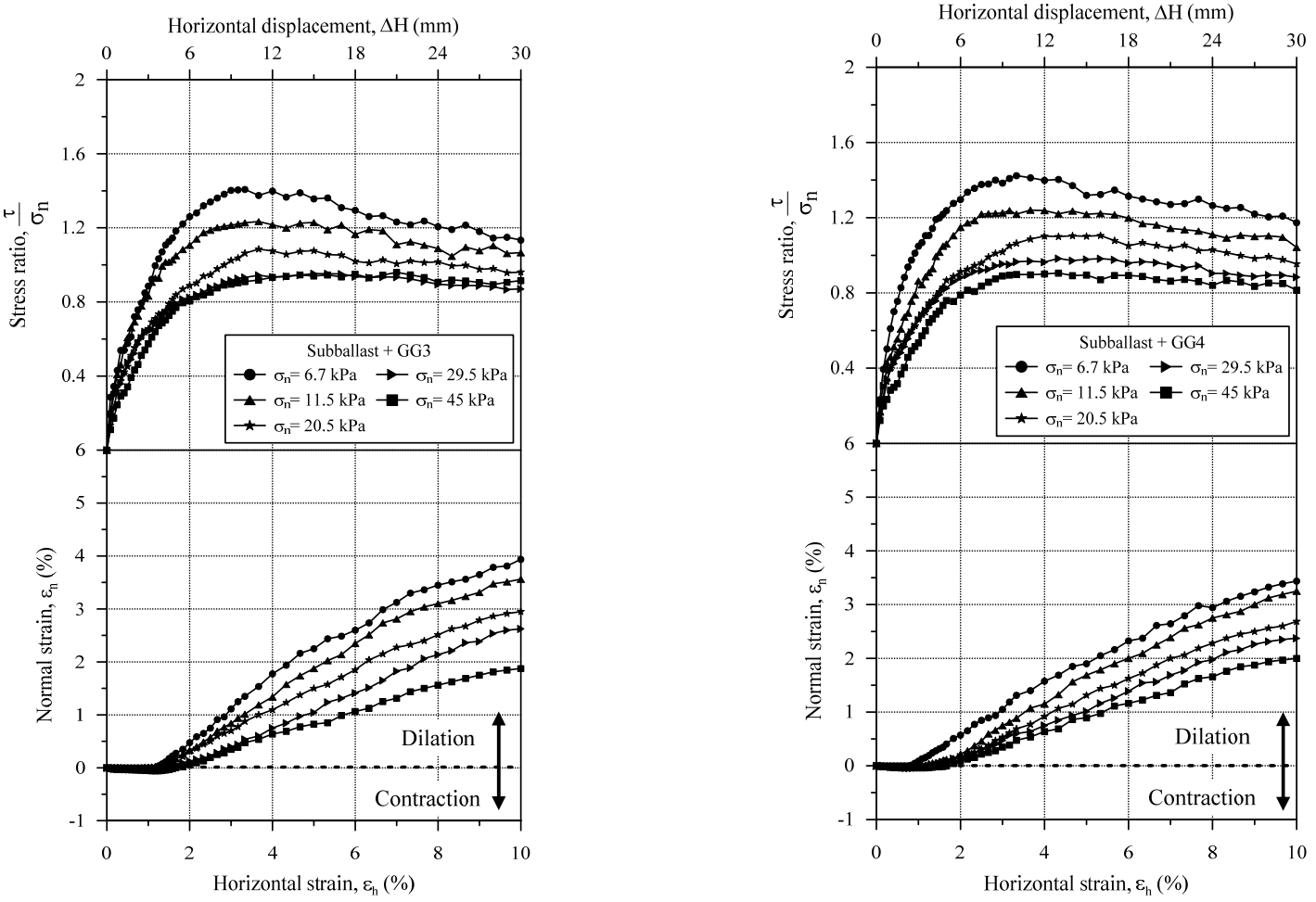

Figure 3.7. Comparison of Stress-strain behaviour of reinforced-subballast with (a) GG3 and (b) GG4 tested in large-scale shear box.

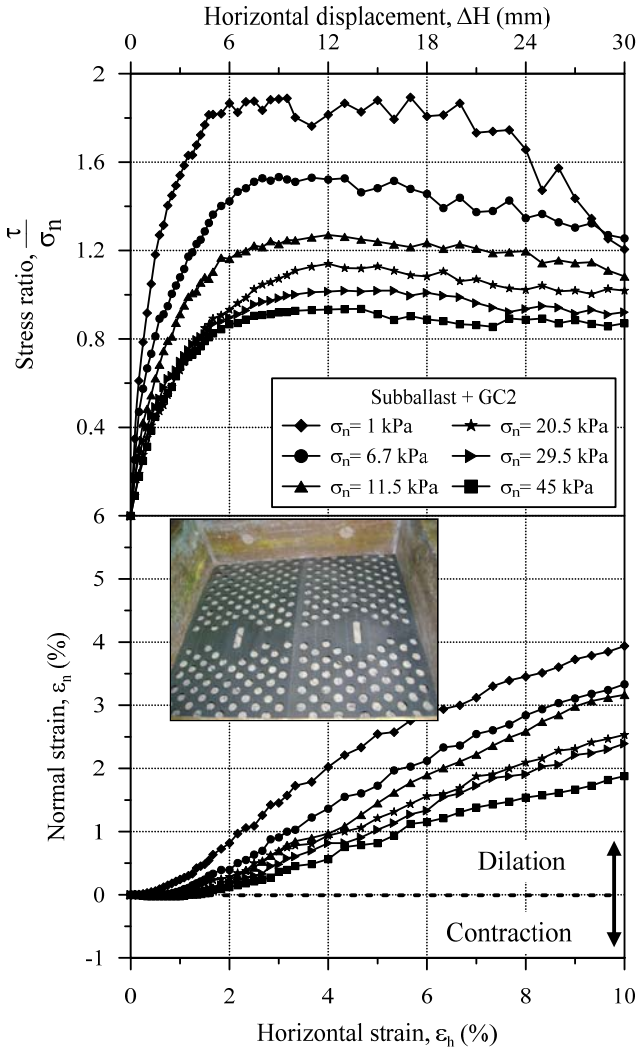

Figure 3.8. Comparison of Stress-strain behaviour of reinforced-subballast with GC2

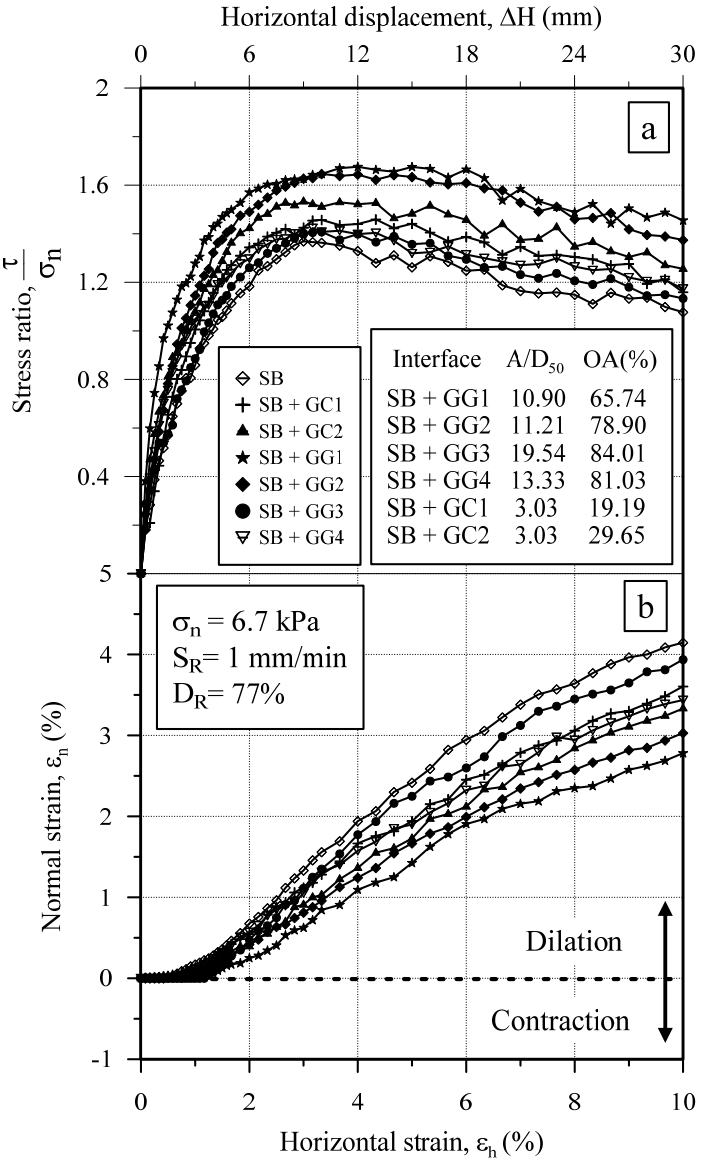

Figure 3.9. Plots of (a) stress ratios (τ/σ_n) and (b) normal strain (ε_n) of different types of geosynthetic conducted in large-scale direct shear box.

Figure 3.6 (a & b), Figure 3.7 (a & b) Figure 3.8 show the experimental results of reinforced subballast with different types of geosynthetics. The influence of effective normal stress on unreinforced and reinforced subballast with different types of geosynthetics can best be evaluated by comparing the stress ratio (τ/σ_n) and normal strain (ε_n) at a desired effective normal stress (σ_n = 6.70 kPa) shown in Figure 3.9 (a). It was observed that all these artificial inclusions led to an improved initial elastic

modulus and increased shear stress, albeit at different magnitudes. As Figure 3.9 (a) shows, the triaxial geogrid (GG1) provided the highest ratio of τ/σ_n, as well as the highest initial modulus (gradient). GG1 with triangular apertures exhibited the lowest magnitude and rate of dilation compared to other geosynthetics (Figure 3.9 b). This can be justified due to better particle interlock, due to optimum aperture size with respect to subballast gradation. Also, triaxial ribs facilitate a more uniform or isotropic stress distribution. In contrast, GG3 provided the lowest ratio of τ/σ_n. This can be attributed to the size of the aperture in geogrid GG3, which was too large to provide an optimum interlock with the particles. To highlight the effectiveness of the reinforcement, an interface shear strength ratio (k_τ) was proposed in accordance with previous studies (Bergardo et al. 1993; Tatlisoz et al. 1998; Liu at al. 2009; Puppala 2010) that is:

$$k_\tau = \frac{\tau_{p(reinforced)}}{\tau_{p(unreinforced)}} \tag{3.1}$$

where τ_p is the interface peak shear strength. In reinforced subballast, the peak stress (τ_{peak}) was attained at a larger horizontal strain compared to unreinforced subballast. The geogrid GG1 and geomembrane GC2 performed better, in spite of their lower ultimate tensile strengths compared to GG2 and GC1 (i.e. higher values of τ_{peak} and k_τ). This clearly indicated that the ultimate tensile stress of the geosynthetics was not reached during testing. It can be concluded that the improved performance was only governed by the mobilised tensile stress (i.e. particle-grid frictional interlocking) rather than its ultimate value.

The impact of reinforcement on the performance of subballast can be highlighted by plotting the peak shear strength vs. shear strain at the peak, as shown in Figure 3.10. Based on the laboratory results, it was found that peak shear strength (τ_{peak}) of the reinforced subballast will occur at a larger shear strain (ε_h) compared to unreinforced specimen at different σ_n. As shown in this figure, the peak shear strength in GG1 occurred at the largest shear strain. Nevertheless, the τ_{peak} in GG3 was found to be occur at the lowest ε_h. As this figure shows, the inclusion of geosynthetics postponed

the softening behaviour of reinforced subballast, indicating the beneficiary effects of geosynthetics.

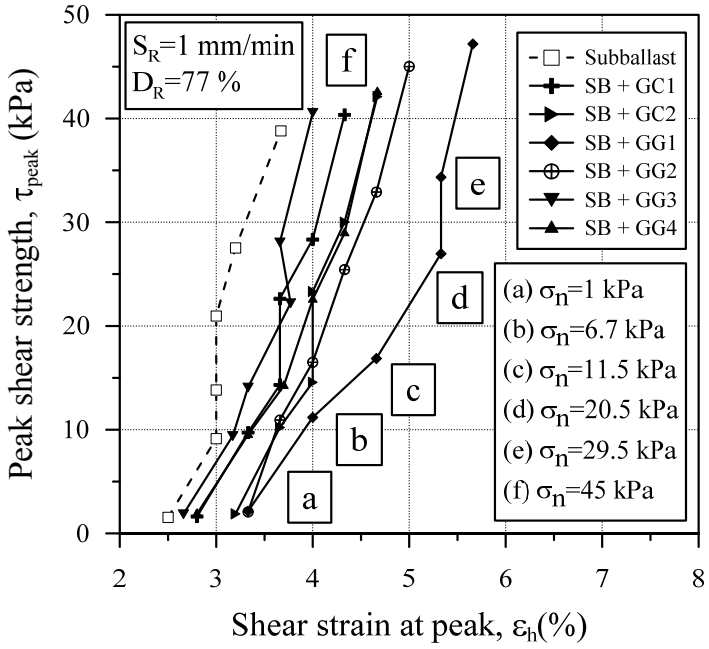

Figure 3.10. Variation of peak shear strength (τ_{peak}) against peak shear strain (ε_h) for different effective normal stresses

3.3.2 Generalised equation for shear stress

The influence of effective normal stress on the shear strength of unreinforced and reinforced subballast could be well represented by the conventional Mohr circles plotted in Figure 3.11. Based on these experimental outcomes, the values of τ_p can be calculated for different specimens using the values of a and b, which are shown in Figure 3.11 for unreinforced and reinforced subballast. At very low effective normal stress ($\sigma_n \leq 25$ kPa), the shear strength envelope is curved and passes through the origin. However, the curvature of the strength envelope is reduced by the increasing effective normal stress. This trend follows the non-linear strength envelope proposed by De Mello (1977) for various rockfills. As shown in this figure, the value of b increases from 0.791 to about 0.811, as effective normal stress increased. As expected, the results also showed that k_τ increased gradually with the effective

normal stress. This was attributed to an improved interlock resulting from increased contact area upon shearing. This was also observed in previous studies (Hebeler et al. 2005, Bacas et al. 2011). The results also showed that geogrid GG1 followed by GG2 had the highest value of k_τ. Nevertheless, having a larger aperture than GG1 and GG2, GG3 offered the lowest k_τ.

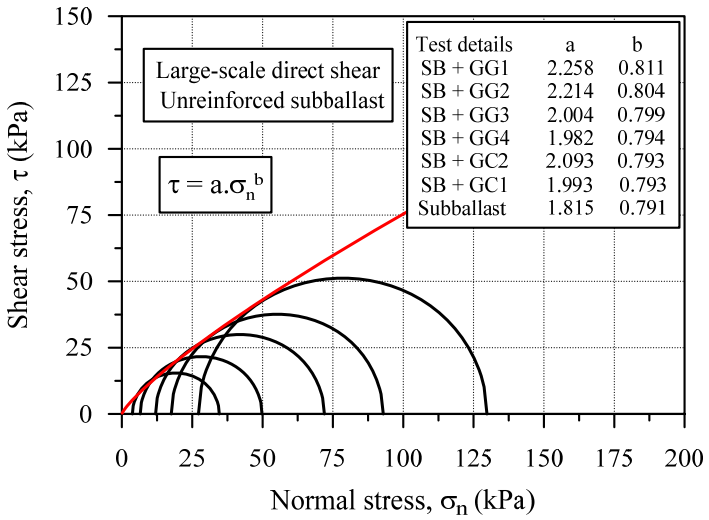

Figure 3.11. Mohr-Coulomb failure envelopes for unreinforced subballast.

In the absence of an apparent cohesion intercept (c), the normalised shear strength of rockfills can be expressed by (Indraratna et al. 1993, 1998):

$$\left(\frac{\tau}{\sigma_c}\right) = \alpha\left(\frac{\sigma_n}{\sigma_c}\right)^{\beta} \tag{3.2}$$

where τ/σ_c = the normalised shear strength ratio, σ_c = the uniaxial compressive strength of the parent rock, σ_n/σ_c = the normalised stress, α and β = empirical parameters. The merit of Eq. (3.2) is that by knowing the value of σ_c, the shear strength of the subballast can be estimated based on the recommended values of α and β, as given in Figure 3.12 and plotted on a log-log scale. It is evident that the non-linearity or curvature of the envelopes is controlled by the value of β. The maximum (initial) curvature of the shear envelopes is attributed to the dilation

behaviour of the subballast at very low effective normal stress. Accordingly, β approaches unity and α approaches the tangent of the interface peak friction angle (Indraratna et al. 2012).

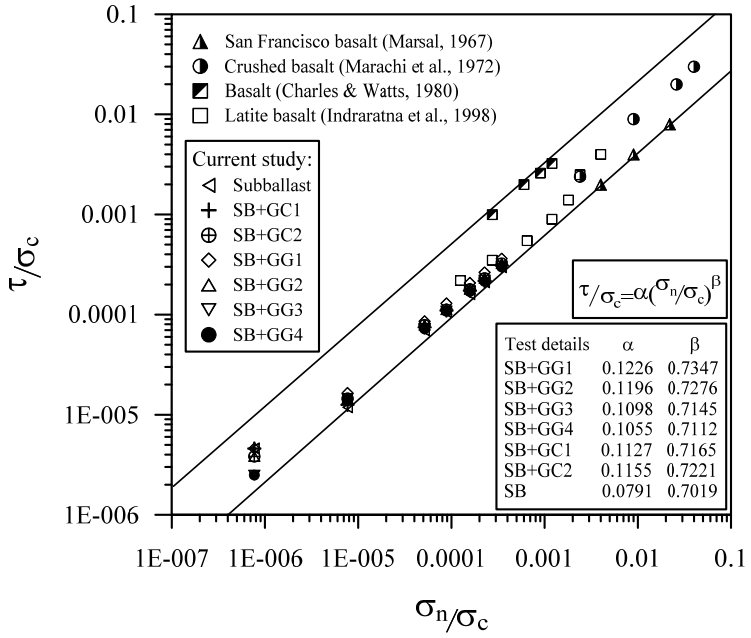

Figure 3.12. Normalised shear strength vs. effective normal stress relation

Figure 3.12 shows that all the experimental results of the subballast were within the same range of other rockfill and ballast. This was because the subballast material was sourced from similar parent rock (i. e. basalt).

Table 3.4. summarises the values of k_τ for the different types of geosynthetics tested in the current study, with respect to the shearing rate and relative density, were compared with previous studies. It is noted that most of these studies were carried out at relatively small strain rates ($S_R \leq 5$ mm/min). Table 3.4. also shows that compacted subballast gives slightly higher values of k_τ than sand and gravel when the most appropriate geosynthetics are used.

Table 3.4. Summary of interface shear strength ratio (k_τ) obtained from large-scale direct shear

Soil type	Relative density (D_R) %	Reinforcement type	Material type	Aperture shape	Shearing rate (S_R) mm/min	Interface ratio (k_τ)	Reference
Ballast							
	75	Geogrid	PP	Square, triangle and rectangle	2.75	0.90-1.16	Indraratna et al. (2012)
Gravel							
	—	Uniaxial and biaxial Geogrid	HDPE	Square and rectangle	0.1-5.0	0.83–0.90	Cazzuffi et al. (1993)
	80	Geogrids, Geotextile	PET	square and rectangle	1	0.89–1.01	Liu et al. (2009)
Sand							
	—	Uniaxial and biaxial Geogrid	HDPE	Square and rectangle	0.1-5.0	0.95-1.04	Cazzuffi et al. (1993)
	50 and 80	Geotextile	PET	—	1	0.61-0.66	Lee and Manjunath (2000)
	80	Geogrids, Geotextile	PET	Square and rectangle	1	0.93-1.01	Liu et al. (2009)
	45	Geotextile	Jute/PP	—	1	0.91-0.95	Sayeed et al.

							(2014)
Clay							
	95	Tensar geogrids, steel geogrids and bamboo grids	HDPE	—	1.0	1.00-1.20	Bergado et al. (1993)
	80	Geogrids, Geotextile	PET	Square and rectangle	1	0.92-0.99	Liu et al. (2009)
Subballast (sand + gravel)							
	77	Geogrid	PET (GG1 to GG4)	Square, triangle and rectangle	1	1.01-1.29	Current study
	40, 50, 60, 70, 77, 85	Geomembrane	PE (GC1)	Circle	1, 2, 4, 8, 12	1.03-1.08	Current study
	77	Geomembrane	PE (GC2)	Circle	1	1.05-1.12	Current study
Construction and demolition aggregate							
	98	Biaxial and Triaxial Geogrid	PP	Square and triangle	0.025	0.66-1.60	Arulrajah et al. (2014)

Note: HDPE: high density polyethylene, PP: *polypropylene, PET: Poly Ester, PE:* Polyethylene

3.3.3 Apparent friction and dilation angle

Considering the low lateral (confining) pressure prevalent in a typical track environment, the effective normal stresses typically applied on the geomembrane would be small. As a result, the apparent peak friction angle becomes very high (i.e. ϕ_p > 55 degree) for σ_n < 10 kPa (Figure 3.13). As expected, the peak friction angle ϕ_p decreases with the increase in effective normal stress (σ_n). There was a marginal improvement in the peak friction angle for GG3 and GC1-reinforced subballast. This can be attributed to a lower shear resistance between the geomembrane and particles (δ). However, by changing the type of reinforcement and increasing the aperture size of the geogrid GG1, ϕ_p could be increased by enhanced particle interlocking. In the stress-dilatancy approach originally proposed by Rowe 1962, the internal friction angle also depends on the shearing resistance and dilatancy.

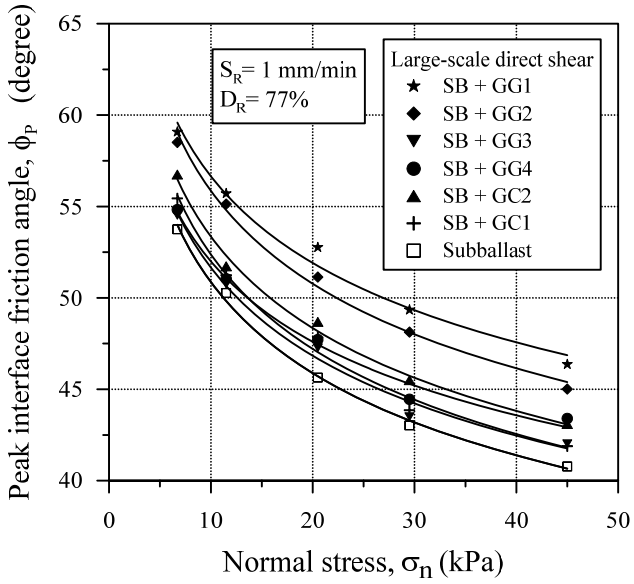

Figure 3.13. Variation of peak interface frction angle (ϕ_p) at different effective normal stresses (σ_n)

To highlight the benefits of using geosynthetics in reducing the extent of dilation, the angle of dilation (ψ) was plotted against the peak interface friction angle (ϕ_p) as shown in Figure 3.14. The angle of interface shear resistance decreases as a result of

increasing the effective normal stress. This was also accompanied by a reduction in the dilation angle of about 10° for reinforced aggregates. A similar observation was also found in several past studies, including Bolton (1986), Indraratna et al. (1993), Schanz and Vermeer (1996) and Been and Jefferies (2004). It is worth noting that the dilation angle was considerably suppressed (approaching zero) when σ_n was increased. This was also accompanied with a reduction of ϕ_p to about 38-39° for unreinforced subballast and to about 44-46° for reinforced subballast.

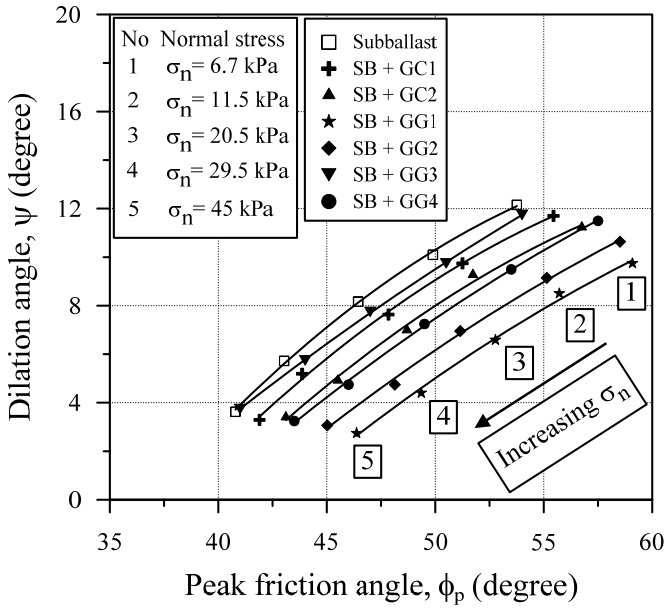

Figure 3.14. Variation of (b) dilation angle (ψ) against peak friction angle (ϕ_p).

3.3.4 Plastic work

To highlight the influence of geosynthetic reinforcement on the plastic work and dilation, W_p is plotted against the dilatancy factor, which is defined as $D_p = 1 - (\delta y / \delta x)_p$ (Rowe 1962; Indraratna et al. 1998), as shown in Figure 3.15. By increasing the effective normal stress, the ratio of dilation was decreased. However, in reinforced

subballast, the dilation factor is larger than for unreinforced subballast. This is due to better interlocking induced by the geosynthetic. It also shows that the relationship between plastic work (W_p) and the dilation factor (D_p) for unreinforced and reinforced subballast are nonlinear. Using the hyperbolic fit, the following equation can be derived to measure the dilatancy factor for reinforced subballast with respect to the dissipation of plastic work in large-scale direct shear as (Indraratna et al. 1998):

$$D_p = \frac{1}{c + d/W_p} \tag{3.3}$$

where D_p is the dilatancy factor, W_p is the plastic work, and c and d are experimental parameters (c = 0.2 and d = 0.83). It can be seen that the nonlinear curve of the plastic work and dilation factor tended to become asymptotic at about D_p = 0.92.

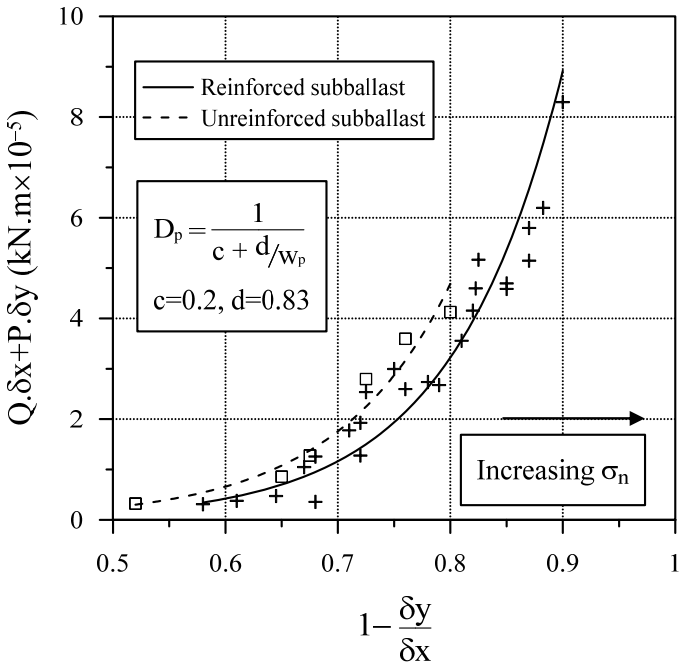

Figure 3.15. Dissipation of plastic work in large-scale direct shear

3.3.5 Effect of open area and aperture size

The effect of aperture size for reinforced soil has already been investigated in the literature. In this regards, the effect of the A/D_{50} ratio on the interface shear strength of subballast reinforced with different geosynthetics is shown in Figure 3.16. Geomembrane GC2 performed better than GC1, while GG2 provided the highest degree of k_τ followed by GG1. As Figure 3.16 shows, no significant difference was observed between GG3 and GG4. Nevertheless, the effect of different geosynthetics could also be highlighted by plotting the open area (OA%) versus k_τ, shown in Figure 3.17. The magnitude of k_τ increased with an increase in OA. Although having the same A/D_{50} ratio, the geomembrane GC2 showed an increased value of k_τ compared to GC1 (Figure 3.17). This could be attributed to the increased percentage of open area (OA%), which had resulted in all improved the grid-particle interlock.

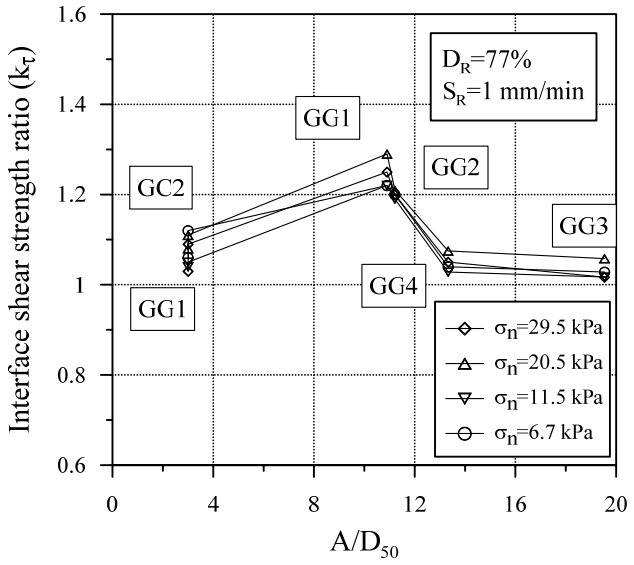

Figure 3.16. Interface shear strength ratio (k_τ) versus (a) A/D_{50}

Moreover, Figure 3.17 shows that GG1 has the maximum value of about k_τ = 1.29. This indicates the optimum opening area required to provide the most effective particle interlocking with subballast particles. The optimum opening area for

reinforcing subballast is when *OA* = 50-80 %. In contrast, a rapid decreased was observed for k_τ when *OA* was increased beyond 80 %. Slight improvement was observed when *OA* was changed from GG3 to GG4. As shown in Figure 3.17, none of the geosynthetics provided a value of k_τ less than unity. This highlighted how effectively geosynthetics improved the performance of subballast, irrespective of the aperture size.

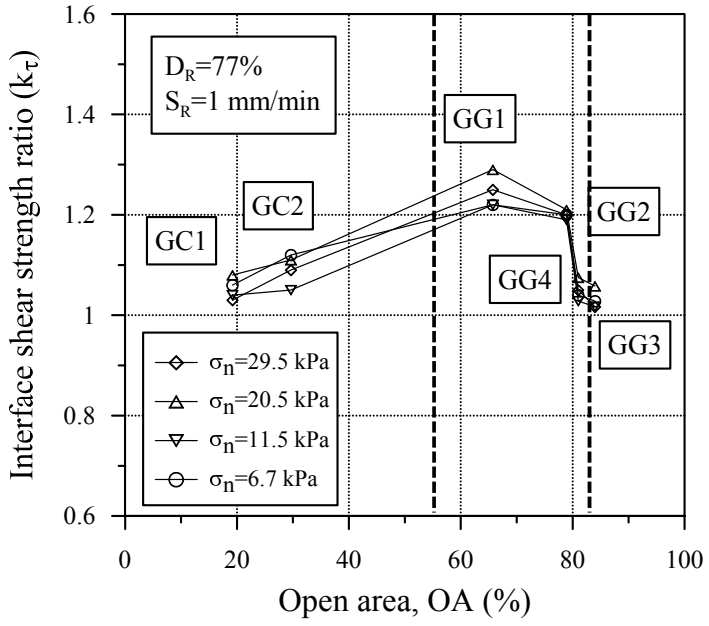

Figure 3.17. Interface shear strength ratio (k_τ) versus open area (*OA)* (%)

3.3.6 Relative density and shear displacement rate

The influence of the relative density (D_R) and shear displacement rate (S_R) was investigated for unreinforced and reinforced subballast, shown in Figure 3.18 (a-d) and Figure 3.19 (a-d), respectively. Marginal improvement was observed in reinforced-subballast when compacted at a lower D_R. In contrast, improving D_R led to a significant increase in the behaviour of geocell-reinforced subballast, as shown

in Figure 3.18. There was also a marginal improvement in geocell-reinforced subballast at various shear displacement rates compared to unreinforced specimen, shown in Figure 3.19. This can justified due to the lower particles interlocking at higher rates of shear displacement.

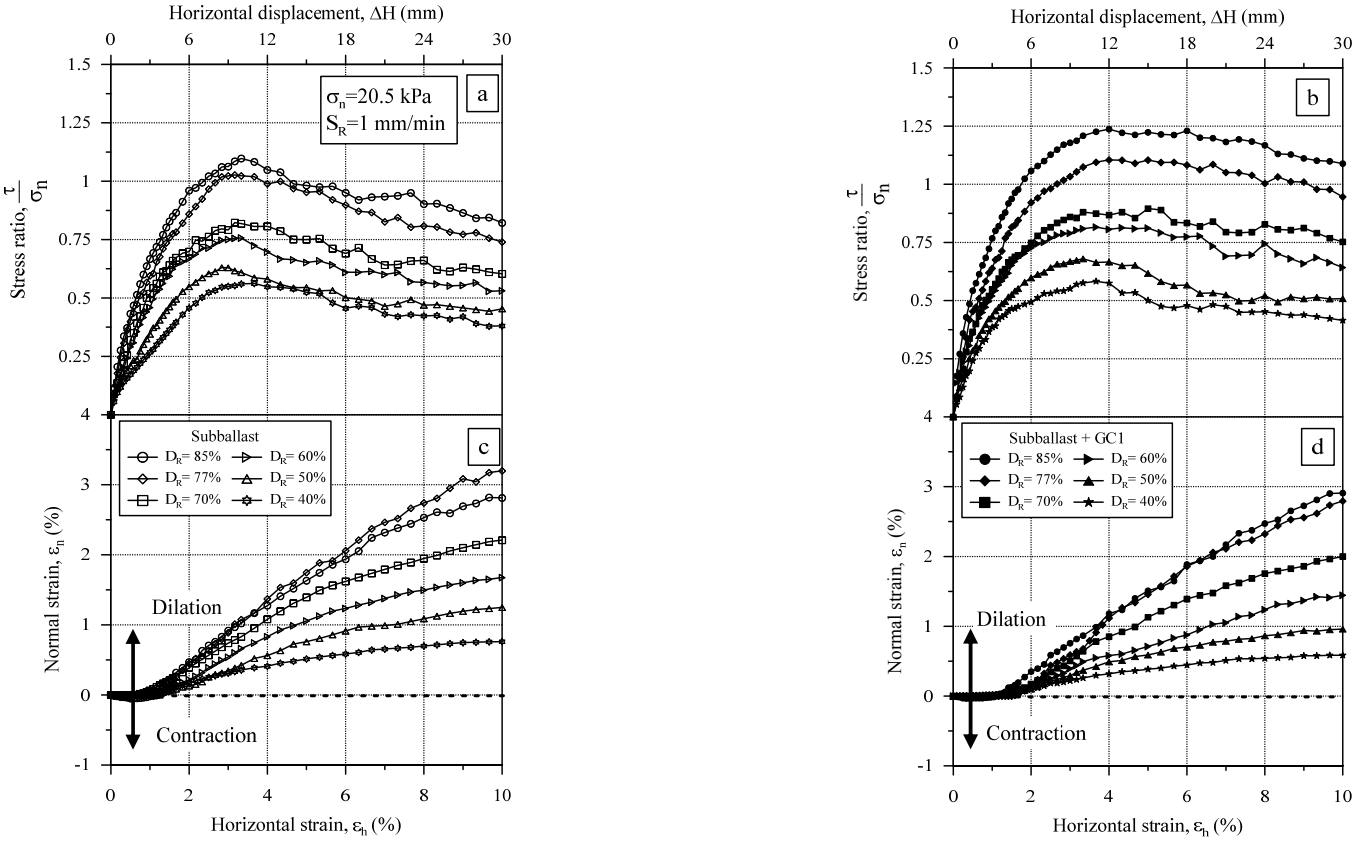

Figure 3.18. Comparison between stress ratios (τ/σ_n) of (a) unreinforced subballast, (b) reinforced subballast and normal strain (ε_n) of (c) unreinforced subballast, (d) reinforced subballast at different shear strain (ε_h) with different relative densities (D_R)

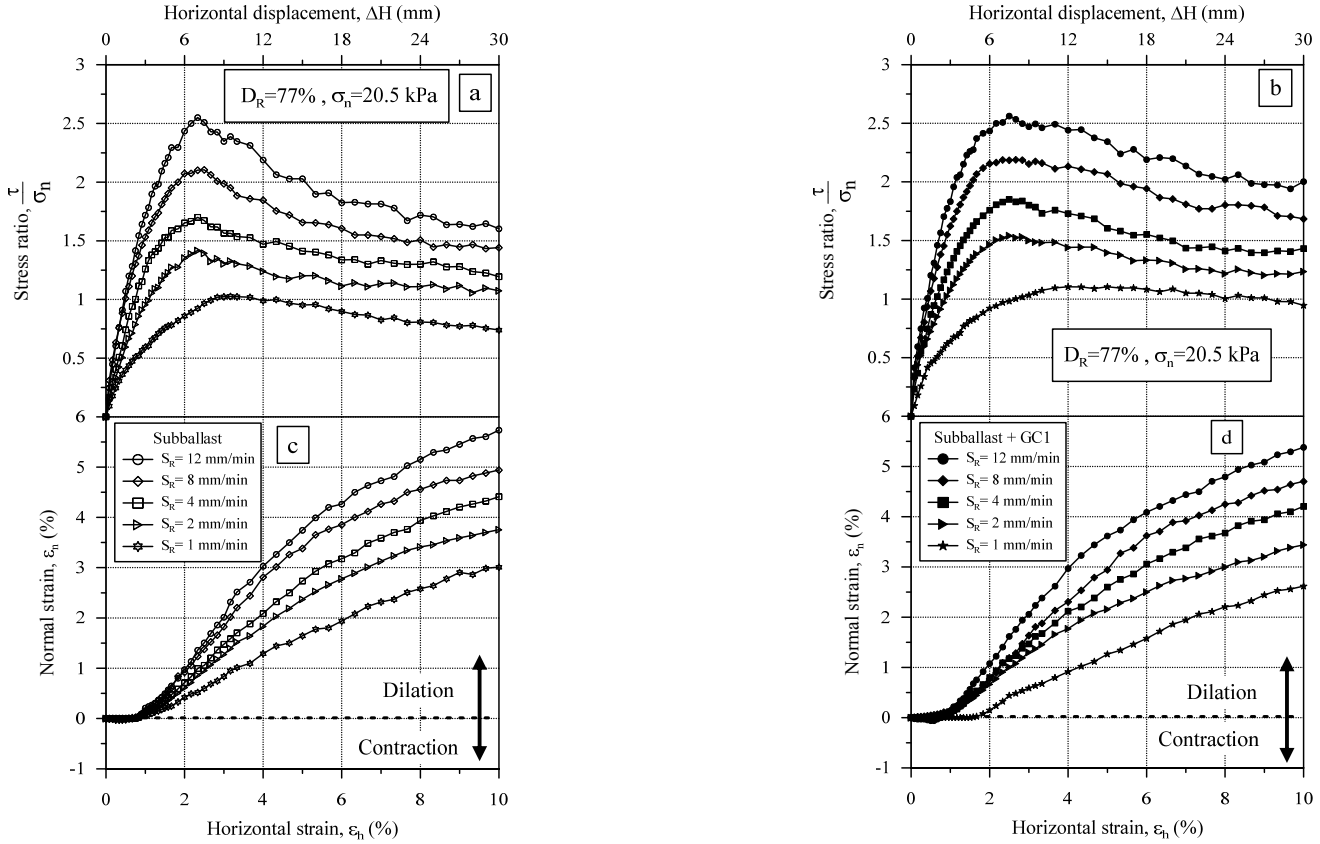

Figure 3.19. Comparison between stress ratios (τ/σ_n) of (a) unreinforced subballast, (b) reinforced subballast and normal strain (ε_n) of (c) unreinforced subballast, (d) reinforced subballast at different shear strain (ε_h) at different sheaing displacement rates

The influence of relative density and the rate of shear displacement can best be evaluated by comparing the value of k_τ at the peak shear strength for different densities and shear displacement rates (Figure 3.20). At a lower relative density, only marginal improvement in performance was observed for reinforced subballast (GC1) compared to the unreinforced specimen (k_τ = 1.04). This is due to low particle interlock that developed with the geomembrane (GC1) at relatively low densities. By increasing the relative density (D_R = 40-77%), the performance could be improved substantially. However, by further increasing the relative density from 77% to 85%, diminishing returns were observed, where only a marginal improvement was observed in the reinforced subballast (k_τ = 1.098-1.101). Based on these results, a relative density of about 77% could be considered to be an optimum density to provide acceptable interface resistance between the subballast aggregates and geosynthetics.

The influence of the shearing rate can be evaluated by varying it (S_R = 1, 2, 4, 8 and 12 mm/min) at a relative density of D_R = 77% and at an effective normal stress of σ_n = 20.5 kPa. Figure 3.20 shows that by increasing the shearing rate, the value of k_τ decreased in reinforced subballast for geomembrane GC1 (k_τ = 1.10-1.025). This is because at a higher displacement rate, the particles were exposed to considerable densification which in turn increased the contact area and reduced the stress concentrations. Figure 3.20 also shows that increasing the shearing rate significantly reduced the influence the geomembrane had on the performance of the subballast. A minimum value of k_τ was obtained at a shearing rate of 12 mm/min. It can be concluded that at higher shearing rates, the interface shear strength ratio is expected to decrease significantly.

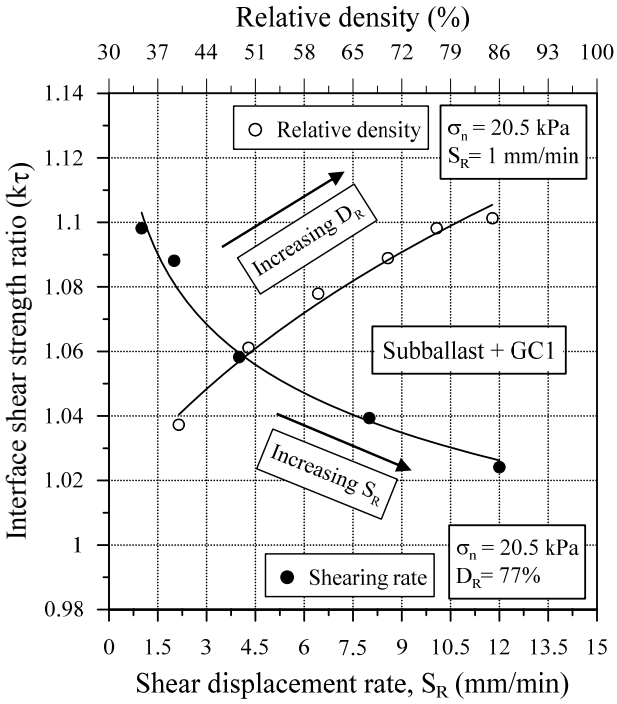

Figure 3.20. Interface shear strength ratio (k_τ) versus shearing rate and placement density (S_R)

3.3.7 Frictional and passive resistance

It is well known that the shear strength (τ) developed between the reinforcement and soil consists of: (i) internal resistance between the soil particles, τ_{int}, (ii) frictional resistance between the soil and reinforcement, τ_{fri} (Tatlisoz et al. 1998; Liu at al. 2009), and (iii) passive resistance due to transverse ribs, τ_p (Bergado et al. 1993; Liu et al. 2009; Sieira et al. 2009). It is also well known that τ_{fri} and τ_p have a significant impact on the interface shear strength of a reinforced soil. The shear strength of subballast-geosynthetics interface by direct shear testing can be determined from (Bergado et al. (1993); Liu et al. (2009):

$$\tau_{\text{int}erface} = \sigma_n \times \left[(1-OA)\tan\delta + OA \times \tan\phi_{p(u-sb)}\right] \tag{3.4}$$

where OA (%) is the open area of the geosynthetic, δ is interface friction angle of subballast-geosynthetic (degree), σ_n is effective normal stress (kPa) and $\phi_{p(u\text{-}sb)}$ is peak friction angle of unreinforced subballast obtained from direct shear test (degree). Passive resistance can be obtained by subtracting the frictional resistance

(τ_{fri}) and subballast internal resistance (τ_{int}) from the total shear strength ($\tau_{sb\text{-}r}$) of reinforced subballast, thus,

$$\tau_p = \tau_{sb-r} - (\tau_{fri} + \tau_{\text{int}}) \tag{3.5}$$

In order to investigate the influence of passive resistance on different subballast reinforcement, the variation of τ_{fri} and τ_p for different types of geosynthetics is plotted against the open area (OA) in Figure 3.21 (a & b). It was found that the frictional resistance decreased when the open area was increased at different effective normal stresses. Nevertheless, due to a higher contact area with the aggregates, the geomembrane GC1 had the highest degree of frictional resistance (τ_{fri}), as shown in Figure 3.21 (a). Moreover, GG3 provided the lowest degree of τ_{fri} due to its large aperture size compared to the particle sizes.

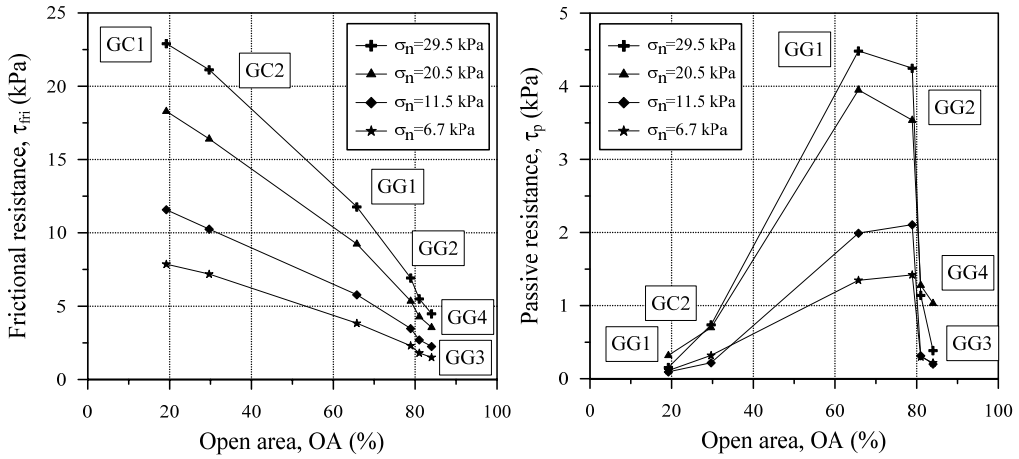

(a) (b)

Figure 3.21. Computation of (a) frictional resistance (τ_{fri}), and (b) passive resistance (τ_p) at different opening area (OA) of different geosynthetics.

As Figure 3.21 (b) shows, the geomembrane GC1 had the lowest degree of passive resistance. Nevertheless, by improving the opening area (i.e. changing from GC1 to GC2), the results show that the passive resistance is improved. Passive resistance has the most dominant effect on the performance of geogrids. Although having an aperture the same size as GG2, GG1 offered the maximum passive resistance (τ_p), which was attributed to its favourable opening area and shape, as well as the

effectiveness of its transverse ribs. Moreover, the triaxial grid provided more passive resistance than the biaxial geogrid.

3.4 Summary

The behaviour of unreinforced and reinforced subballast was investigated using large-scale direct shear testing under low effective normal stresses ($1 \leq \sigma_n \leq 45$ kPa). Also, the effects of relative density, shearing displacement rate and open area of geosynthetics were investigated. In all of cases, inclusion of geosynthetics led to improved performance of subballast. Also, using geosynthetics in the subballast, caused the peak shear strength to occur at a larger shear strain (ε_h). No compression behaviour was observed for unreinforced and reinforced subballast under low effective normal stresses.

Geogrid GG1 provided better performance than the other geosynthetics, while marginal improvement was obtained using GG3. In addition, the geogrid GG1 and geomembrane GC2 performed better, in spite of having lower ultimate tensile strengths compared to GG2 and GC1. The interface shear resistance (k_τ) between subballast and different geosynthetics was measured, and a generalised empirical formulation was developed to predict the shear strength of unreinforced and reinforced subballast. Based on the experimental results, friction angle and dilatancy angle were decreased by increasing effective normal stress. Also, the stress ratio (τ/σ_n) was decreased significantly by increasing the shear displacement rate (S_R). On other hand, the magnitude of τ/σ_n was improved by increasing the relative density (D_R). The laboratory results confirmed that a relative density of D_R = 77 % is sufficient to obtain optimum benefit of the geomembrane.

The impact of OA on the passive and frictional resistance in a reinforced subballast was studied. Despite having lower passive resistance, geomembrane GC1 provided the highest frictional resistance in reinforced subballast. As a result, the geomembrane GC1 could be selected for forming the geocell mattress for performing experiments on the geocell-reinforced subballast using the large-scale prismoidal triaxial.

CHAPTER 4

4. BEHAVIOUR OF UNREINFORCED AND GEOCELL-REINFORCED SUBBALLAST SUBJECTED TO CYCLIC LOADING IN PLANE STRAIN CONDITION

4.1 General

To minimise the vertical and lateral deformation of subballast, the behaviour and performance of unreinforced subballast under different confining pressures and frequencies, must be understood in order to develop a safe and economical rail transport.

A series of drained triaxial tests at different lateral confining pressures and various frequencies were carried out using the large-scale process simulation prismoidal test apparatus (PSPTA). It is well recognized that geocell has a significant influence on soil. The laboratory testing program aimed at investigating the performance of unreinforced and geocell reinforced subballast under cyclic loading. In this chapter, the methodologies and apparatus are discussed. Also, the details of instrumentation used to record the stresses and deformations, including the data acquisition techniques, are provided. Moreover the experimental results are discussed and an optimum confining pressure to reduced excessive lateral and vertical displacement is defined. Much of the work presented in this chapter was published earlier in the Journal of Geotechnical and Geoenvironmental Engineering (ASCE), and have been reproduced in this thesis with kind permission from ASCE.

4.2 Testing Materials

4.2.1 Geocell mattress

The geocells used in previous studies were made from geogrid (Dash et al. 2003; Sireesh et al. 2008; Biswas et al. 2013). The effectiveness of the geomembrane in terms of frictional resistance was discussed in the previous chapter. In addition, lower percentage of aperture size helps the infill material remains confined in the geocell pocket made from geomembrane. Thereby, the Geoweb geocells used in this study were made from strips of polyethylene material welded together at the joints to create the three-dimensional cellular form as shown in Figure 4.1. One of the most important parameters considered in determining the load bearing capacity is the tensile strength of geocell mattress. Tensile testing of the seam and bulk section of the geocell pocket was carried out using the tensile strength equipment (Instron machine) at the University of Wollongong. Two, 200 mm wide metal clamps were used to hold the test specimens; they were wide enough (200 mm) to cover the entire width of the specimen. The specimen was 150 mm wide and 200 mm long, and it was hooked to the top plate and the base plate, as shown in Figure 4.2. The specimen was aligned accurately in parallel to the applied force. A constant strain rate of 10% per min was maintained during testing. Tensile testing was conducted at room temperature of about 23°C. The load and displacements were recorded using the data logger connected to the computer, and loading continued until the specimen ruptured (Figure 4.3).

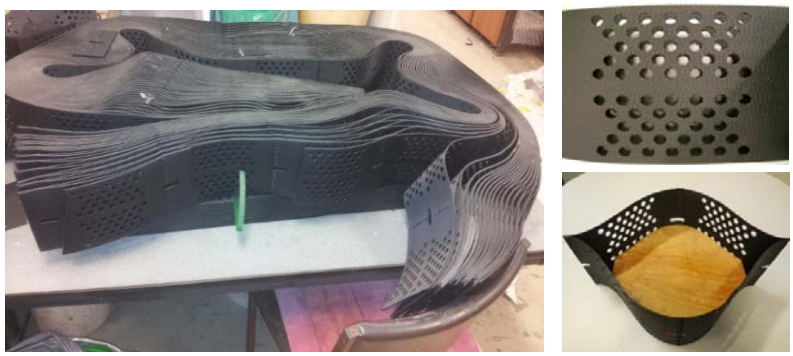

Figure 4.1. Geocell mattress before placing in the PSPTA

The ultimate tensile strength was determined using:

$$\alpha_f = \frac{F_f}{W_s} \qquad 4.1$$

where α_f is the tensile strength (N/m), F_f is the ultimate force that caused the geocell to tear, and W_s is the width of the specimen (mm).

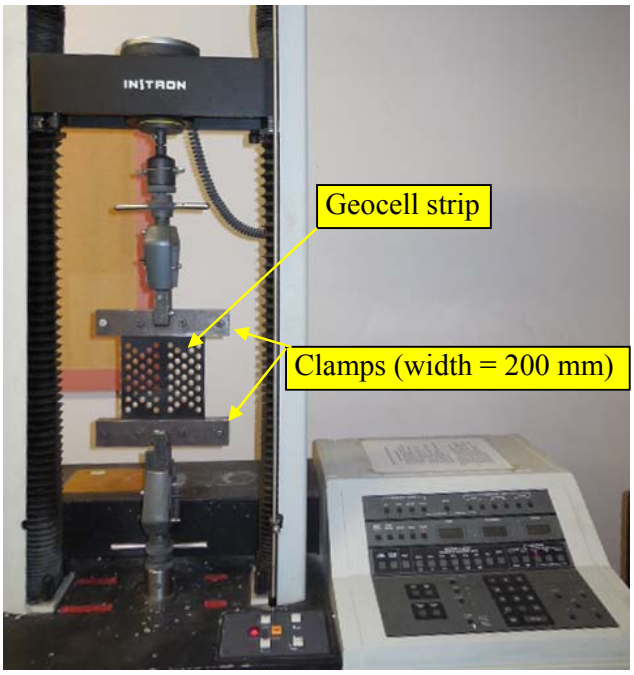

Figure 4.2. Instron machine used for tensile testing

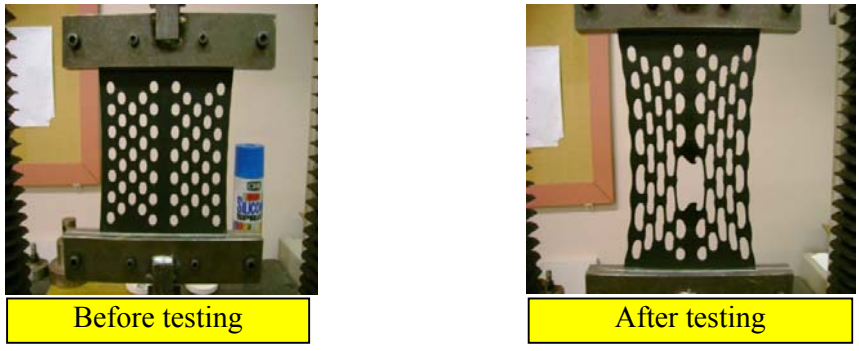

Figure 4.3. Tensile testing of the geocell membrane

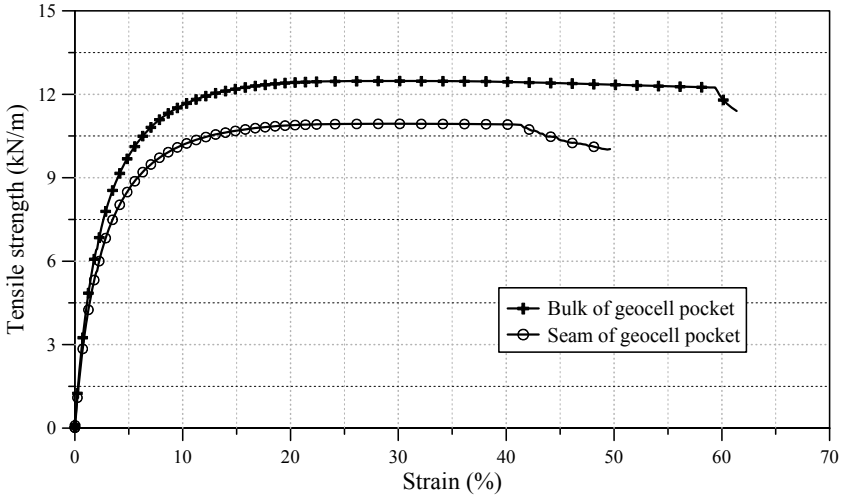

Figure 4.4. Tensile strength of the geocell membrane, bulk, and seam used in this experiment

The experimental results are plotted and shown in Figure 4.4. As shown in this figure, the bulk section of the geocell pocket had a higher ultimate strength than the seam. The tensile strength for the bulk and welded section of geocell were 12.5 and 11 kN/m according to ASTM D-4885 and ASTM D-4437. The geocells were examined prior to the experiment to determine their strength. The geocells were then cut to the required dimensions for the experimental in a mattress form, as shown in Figure 4.5. The geocell properties are summarised in Table 4.1.

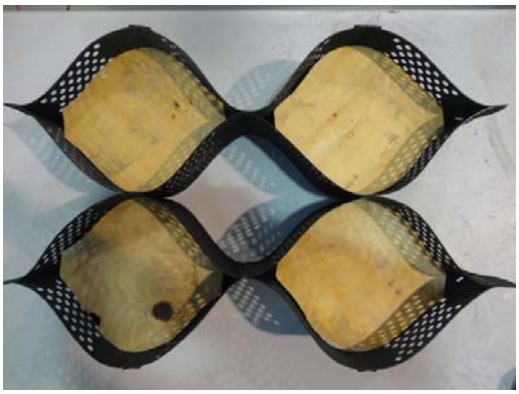

Figure 4.5. Geocell mattress prior the experiment

Table 4.1. Physical characteristics and technical specifications of geocell used for the study

Characteristics	Properties	Values/Details
Physical	Material	Polyethylene
	Aperture size (mm) (Length X Width)	320 × 287
	Wall type	Perforated, textured
	Percentage cell wall open area (%)	16.8
	Nominal area (mm^2)	46×10^3
	Cells per m^2	21.7
	Cell depth (mm)	150
	Weld spacing (mm)	445
	Thickness (mm)	1.3[a]
	Color	Black – from carbon black (1.5-2 % by weight)
Technical	Ultimate tensile strength (kN/m)	—
	Bulk material	9.5[b]
	Seam	8[c]
	Minimum cell seam strength (kN/m)	2.13
	Density (g/cm^3)	0.95[d]

Note: [a]ASTM (2012); [b]ASTM (2011); [c]ASTM (2013); [d]ASTM (2010)

4.3 Large-Scale Cubical Triaxial

4.3.1 Prototype Process Simulation

The area of the prototype Process Simulation Test Apparatus (PSPTA) replicates the influence zone or the unit cell area defined in Figure 4.6 (a & b) for a standard gauge Australian heavy haul track. The influence zone is defined by the following dimensions: (i) in the transverse direction, 400 mm symmetrically on each side of one rail (i.e. 800 mm) which is equal to L /3, where L is the total length of a sleeper given as 2400 mm (also termed as an effective sleeper length, i.e. L_e = L/3 e.g. Jeffs and Tew 1991), (see Figure 4.6(a); and (ii) in the longitudinal direction of train passage, a distance equal to the sleeper spacing (S_s) of 600 mm (see Figure 4.6(b). Thus, the PSPTA with movable sides does not suffer from reduced scale effects or adverse boundary effects, unlike conventional geotechnical equipment with a fixed rigid boundary. The boundary conditions at its sides may vary slightly from the field condition. For instance, due to symmetry, the lateral movements on each side of the unit cell in the direction of perpendicular to the sleeper is approximately the same, whereas in reality, lateral movement at the edge of the sleeper (i.e. side *AD* in Figure 4.6(b) is expected to be slightly greater than that at side *BC* which was subjected to higher confinement.

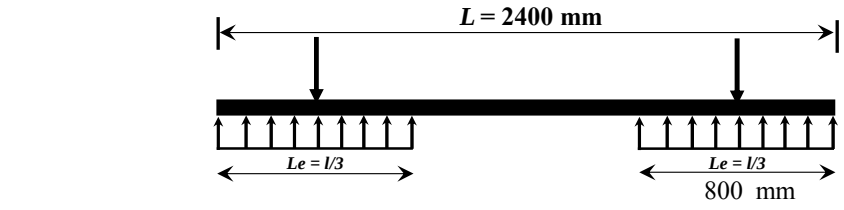

(a)

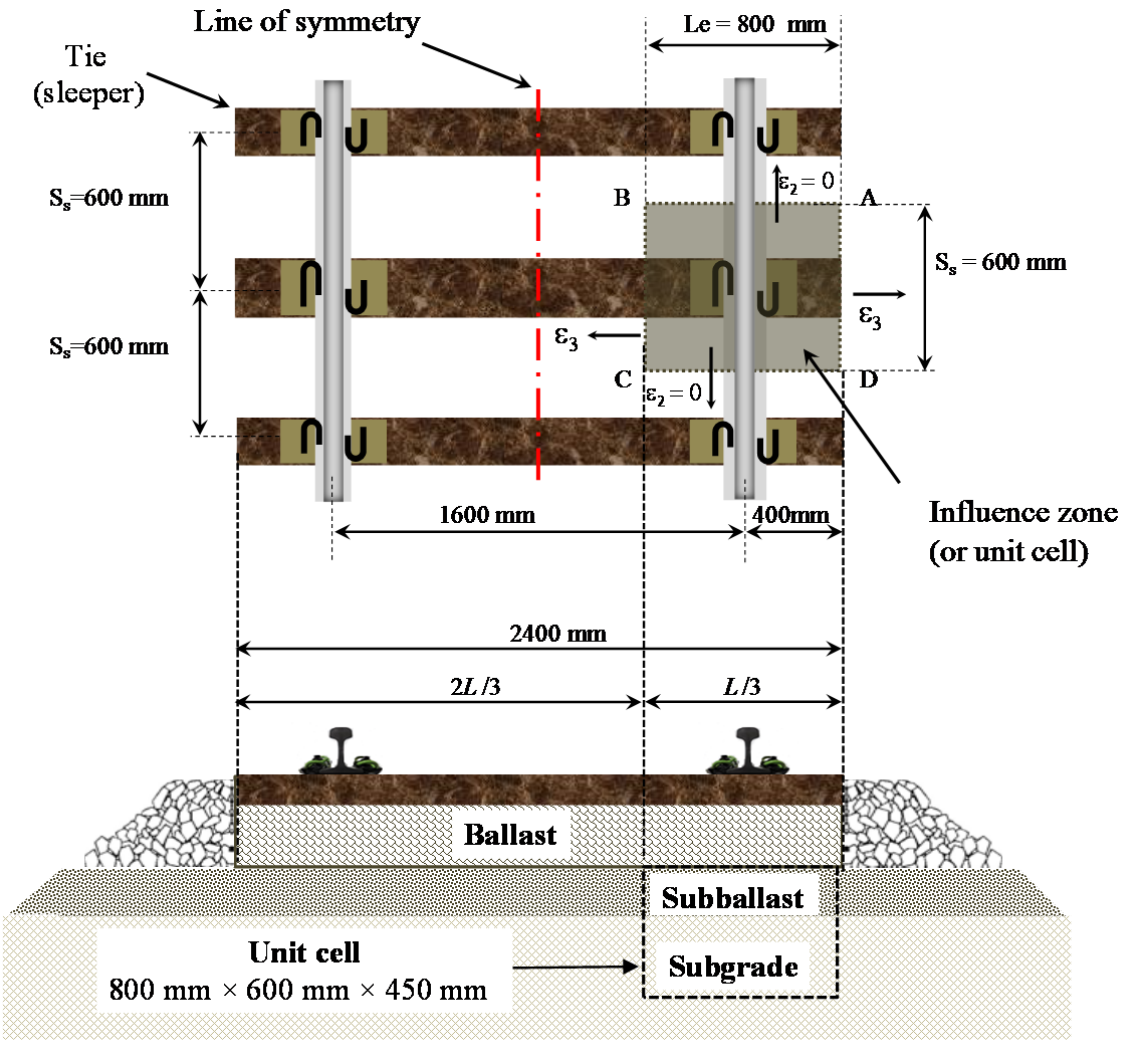

(b)

Figure 4.6. (a) Simplified track geometry for sleeper/ballast contact pressure assessment (Modified after Jeffs and Tew, 1991) and (b) the typical track substructure arrangement considered in this study

4.3.2 Methodology

In this study, a total of 30 cyclic tests were carried out, as summarised in Table 4.2, using PSPTA (800 mm long, 600 mm wide and 600 mm high), as shown in Figure 4.7. A predetermined amount of oven dried subballast was placed and compacted in several layers with a vibratory hammer to achieve a representative field density of about 2100 kg/m^3 (relative density (D_R) of 77 %, initial void ratio (e_0) = 0.29), as shown in Figure 4.8. A smooth frictionless plate was used to minimise disturbing the particles of mixed subballast as the cubical box was being filled. In the reinforced specimens, the test arrangement consisted of five geocells filled with subballast.

Table 4.2. Summary of cubical triaxial testing program on subballast

Material Type	Mean pressure q_{mean} (kPa)	q_{cyc}, q_{max}-q_{min} (kPa)	Confining pressure $\sigma_3^{'}$ (kPa)	Frequency f (Hz)
Subballast	104	125	5 10 15 20 30	10, 20, 30
Geocell + subballast	104	125	5 10 15 20 30	10, 20, 30

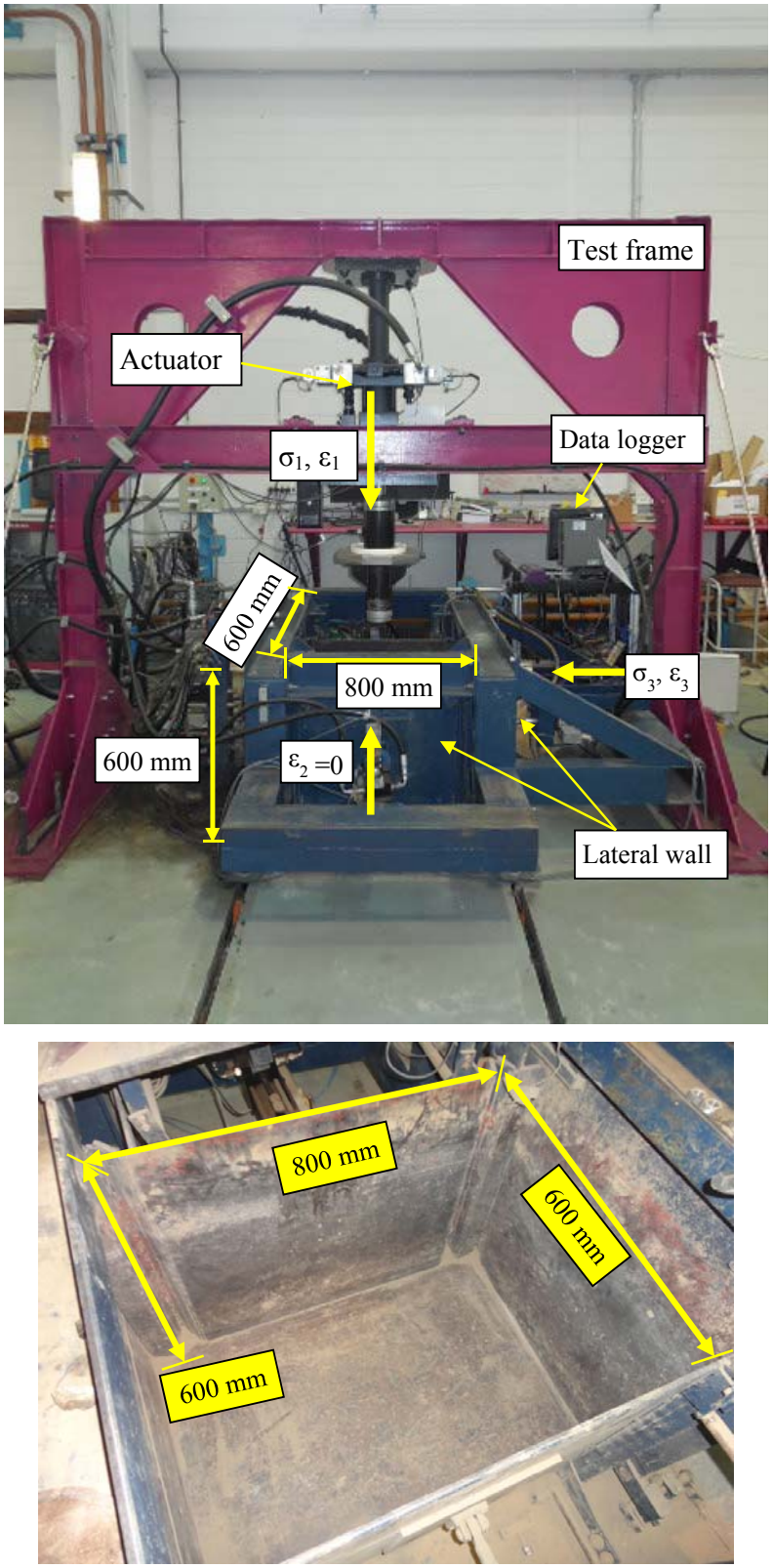

Figure 4.7. Process simulation Prismoidal Triaxial Apparatus (PSPTA) designed and built at University of Wollongong

Figure 4.8. Process of sampling of subballast in the PSPTA

For the reinforced subballast, geocell mattress was placed on top of the subballast, beneath the top solid platen, as shown in Figure 4.9. In the field, the same number of geocell pockets would be used under a rail track within the same area of influence. Also, the width of the test chamber (W_{box}) to the geocell diameter ratio (D) (i.e., W_{box}/D = 2.5) was on par with recommended NSW RailCorp practices (Choudhury 2009). Wooden templates were used to form semi-elliptical pockets in the geocell mattress, and then granular subballast material was placed into the PSPTA to a depth of 450 mm, as shown in Figure 4.9. The specimens were oven dried prior to the experiment.

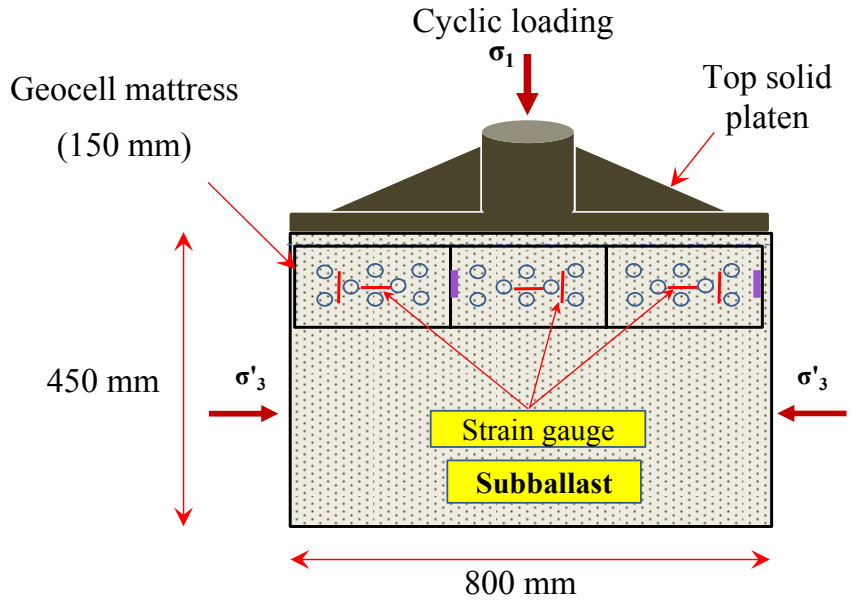

Figure 4.9. Schematic of geocell reinforced subballast in the PSPTA (modified after Indraratna et al. 2015)

Ten strain gauges with gauge length (L_{sg}) of 20 mm were attached to the strips at the mid-height of the geocell pocket (75 mm, see Figure 4.10) to measure the axial and circumferential strains. The surface of the geocell was brushed lightly with cleaner and degreaser, and an industrial adhesive was applied before mounting the strain gauges. The strain gauge was pressed into the adhesive with an overlying thin plastic film with care to remove all the entrapped air. Flexible sealant followed by

waterproofing tape was used to cover the strain gauges to protect them from being damaged by vibratory compaction and subsequent deformation of the geocells; the cable leads were also encased and covered in flexible conduits to protect them. Five miniature stainless steel pressure cells were placed in the geocell mattress to measure the lateral pressure on the geocell strips (t_{pc} = 10 mm, D_{pc} = 50 mm, range = 500 kPa, accuracy =99.7 %), as shown in Figure 4.10.

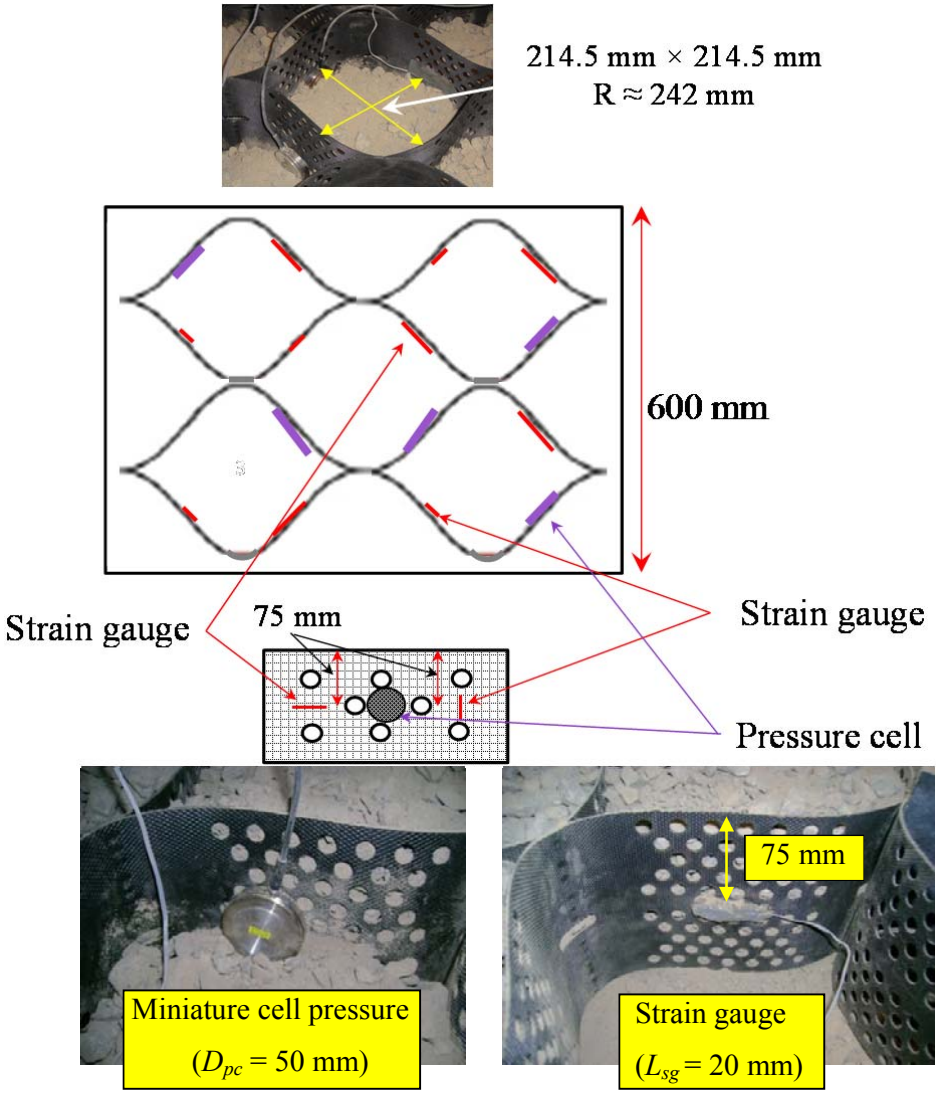

Figure 4.10. Schematic of pressure and strain gauges used in this study (Modified after Indraratna et al. 2015)

After placing the geocell mattress in position, the pockets were carefully filled with the subballast and compacted to the required density, as shown in Figure 4.11 (a & b). Two, 400 × 600 × 10 mm thick plates were placed on top of the subballast. A servo-hydraulic actuator with a maximum capacity of 100 kN provided the axial cyclic loading, which was transmitted to the subballast through a 100 mm diameter steel ram and a solid top platen (800 mm long × 600 mm wide × 12 mm thick), as shown in Figure 4.12.

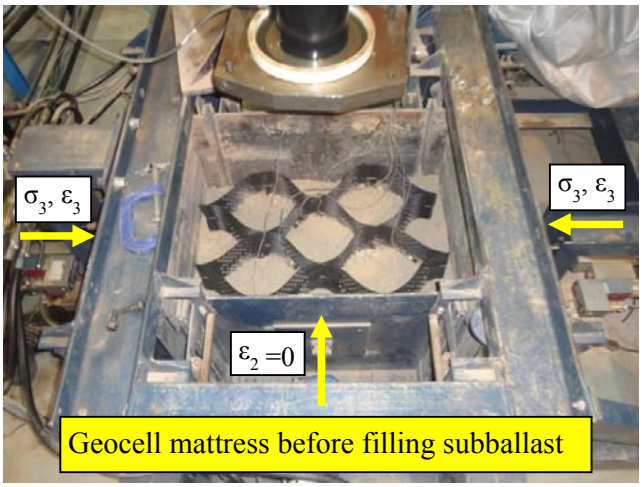

(a)

(b)

Figure 4.11. Geocell mattress (a) before and (b) after filling with subballast in PSPTA

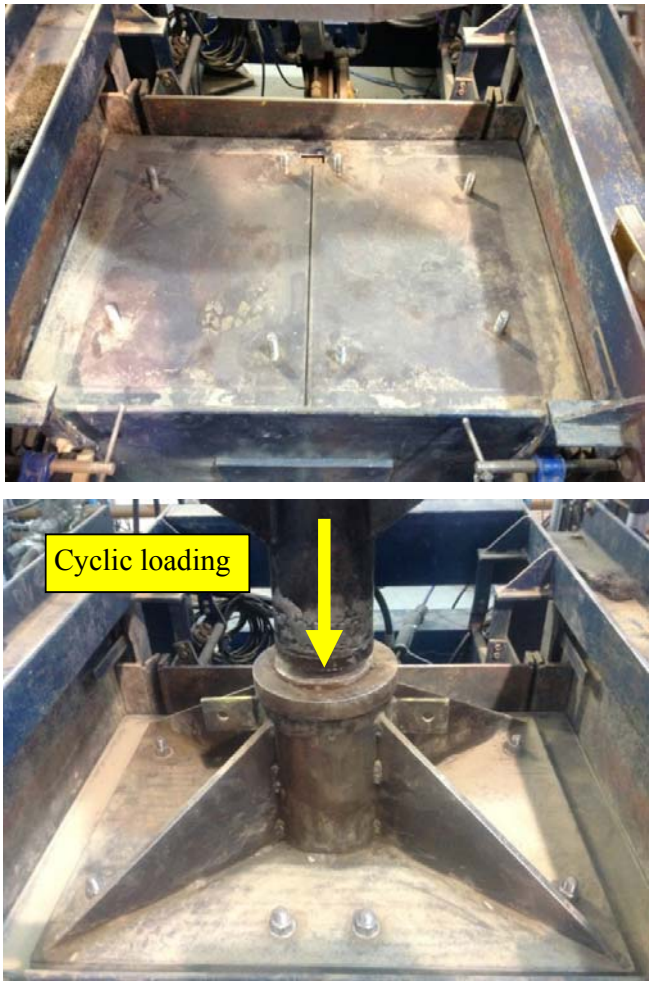

Figure 4.12. Top solid plates used on subballast

To mimic the lateral pressure available in the field, which in a real track is generated by the weight of the crib and shoulder ballast, a minor principal stress (σ_3') was applied to the vertical walls of the triaxial chamber via the horizontal jacks. To simulate a realistic plane strain condition along the long straight section of track, any lateral movement of the vertical walls in the direction of the intermediate principle stress (σ_2') was prevented by locking the castors (i.e. $\varepsilon_2 = 0$). However, the vertical walls in the orthogonal (i.e. transverse) direction of minor principle stress (σ_3') were allowed to move laterally. Lateral spreading (ε_3) was recorded by a linear voltage differential transformer (LVDT). The vertical load, axial and lateral displacement, and lateral confining pressure were recorded during the test using separate load cells,

as shown in Figure 4.13. The capacity of the lateral load cells were enough [10 and 50 kN in direction of parallel (σ_3') and perpendicular (σ_2') to the sleeper respectively] to carry out the experiments with the required confining pressures.

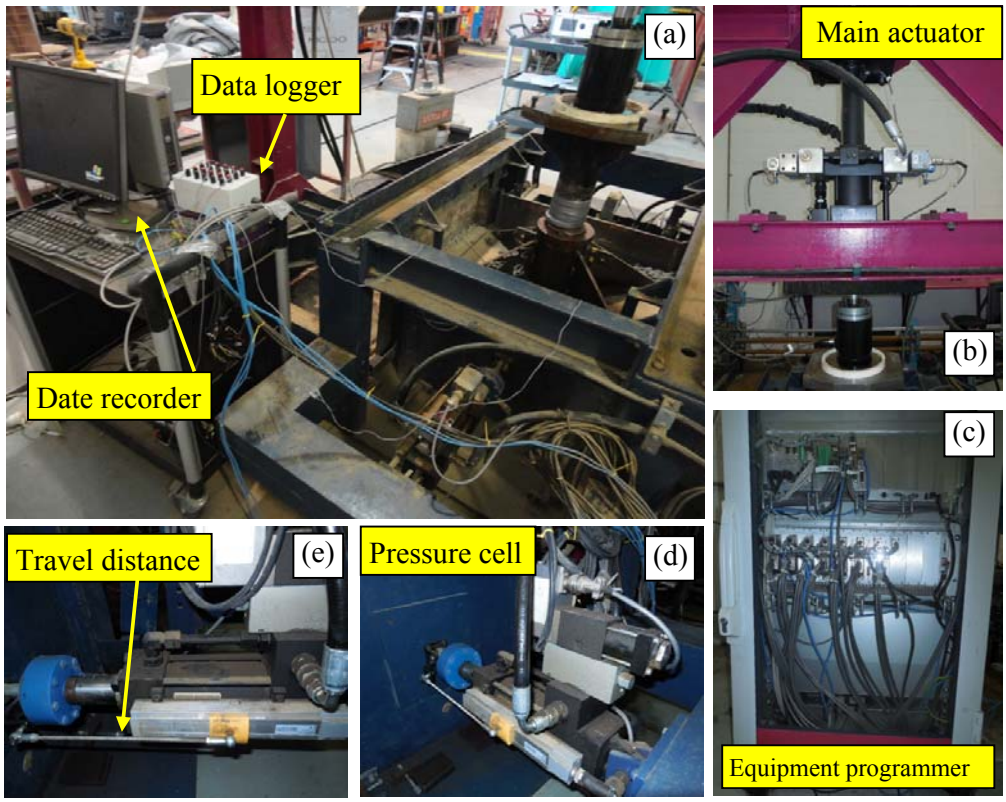

Figure 4.13. Schematic of PSPTA (a), recording system, (b) main actuator, (c) PSPTA programmer, (d) lateral pressure cell and (e) typical travel distance of lateral pressure cell

To carry out the test, initially, a monotonic strain-controlled load was applied at a rate of 1 mm/min until the mean level of cyclic deviator stress was attained. Then a cyclic load with a maximum (q_{max}) and minimum amplitude (q_{min}) of about 166 kPa and 41 kPa was superimposed over the monotonic load to produce a comparable mean contact stress of σ_1' = 160-170 kPa developed by train passes at the subballast-ballast interface. The maximum contact pressure on the surface of the subballast was determined as an input parameter for cyclic testing. To calculate this pressure, a nominal axle load of 294 kN [four axles in NSW heavy haul (30 tonnes)] was assumed, which is equivalent to a axial pressure of 147 kN. Based on

recommendations by the American Railway Engineering Association (AREA), the design wheel load can then be calculated using (Li and Selig 1998):

$$P_d = \phi \cdot P_s \tag{4.2}$$

where P_d = the design wheel load (kN), P_s = the static wheel load (kN), and ϕ = the impact factor (dimensionless) given as (Indraratna et al. 2011):

$$\phi = 0.0052V \Big/ D_W + 1 \tag{4.3}$$

By substituting a train speed (v) = 73 km/h (corresponding to f = 10 Hz, see Figure 4.14), and a wheel diameter D_w = 0.97 m, the design wheel load P_d was determined as being 204 kN. Considering that half of the pressure is transmitted to the adjacent sleepers (varies from 50-60 % as shown by Atalar et al., 2001), the rail seat load (q_r) was calculated as 102 kN. Assuming a uniform distribution of stress, the contact pressure at the ballast-sleeper interface (P_a) can then be computed as (Jeffs and Tew 1991):

$$P_a = \frac{q_r}{B_s \times L_e} F_2 \tag{4.4}$$

where L_e = the effective length of the sleeper, B_S = the width of the sleeper (B_S = 260 mm), L = the total length of the sleeper (L = 2400 mm) and F_2 = a factor depending on track maintenance and sleeper type (F_2 = 1). By assuming the effective length of sleeper as one third of the total sleeper length (Jeffs and Tew 1991), Eq [(4.4] becomes:

$$P_a = \left(\frac{3q_r}{B_s \times L} \right) F_2 \tag{4.5}$$

Based on Japanese Track Standards; considering $L_e = 2d_S$, where d_S = distance between the rail head center and the edge of the sleeper (d_S = 500 mm), the following equation can be used to obtain P_a (Atalar et al. 2001):

$$P_a = \frac{q_r}{2dB_s} F_2 \tag{4.6}$$

Considering Eqns. (4.4), (4.5) and (4.6), a maximum of P_a (i.e. P_a = 490.4 kPa) was considered. Considering the sleeper area (L_e = 800 mm, B_S = 260 mm) and a 300 mm depth of ballast, the stress on top of subballast can then be determined as 166 kPa using Boussinesq's elastic theory. A minimum amplitude q_{min} of 41 kPa was selected to represent the in situ unloaded state of the track (such as the weight of the rails, sleepers and ballast), and to prevent any undesirable behaviour by the actuator (i.e., impact loading).

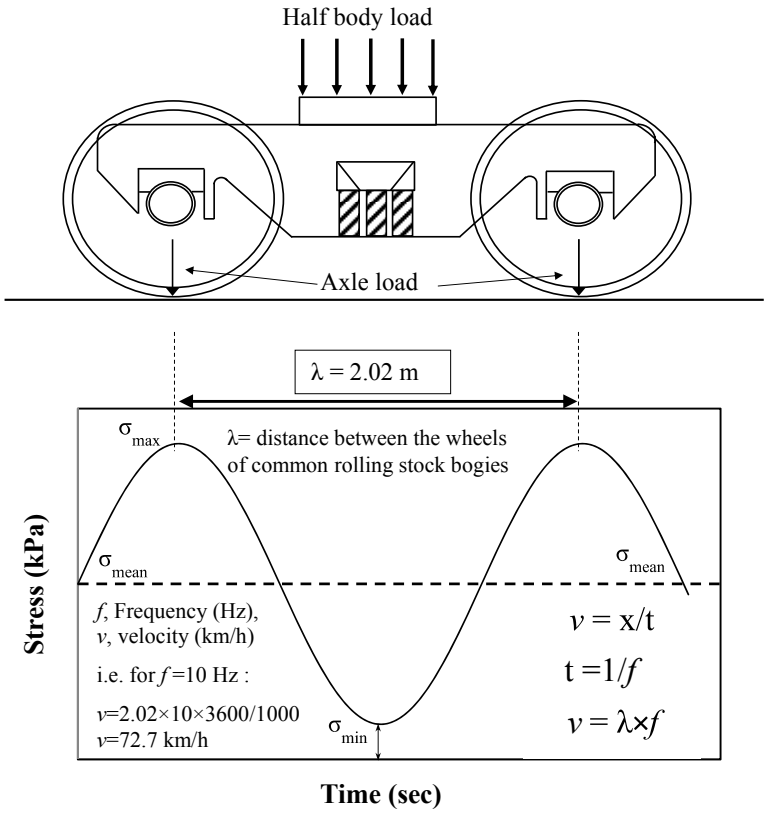

Figure 4.14. Typical schematic of axle load to the track (Modified after Indraratna et al. 2015)

The cyclic loads in a stress-controlled fashion were applied using a periodic, positive full-sine waveform, and the corresponding geostatic stresses were simulated using a

constant confining pressure, as shown in Figure 4.14. The subballast medium was allowed to spread laterally parallel to the sleepers, while the plane strain condition (ε_2 = 0) was maintained. To study the impact of frequency (f) and confining pressure (σ_3') on the behaviour of subballast, cyclic drained triaxial tests were conducted at σ_3' = 5, 10, 15, 20, 30 kPa and f = 10, 20, and 30 Hz. The load frequency of a train is expressed as $f = v/\lambda$, where v is train speed and λ is the characteristic length between the axles. A typical freight wagon has multiple axles (e.g. four axles in NSW heavy haul) that impart independent load cycles. Since the axle distance is much smaller than the bogie distance, the two rear axles of a leading wagon and two front axles of a trailing wagon would generate maximum frequency (Indraratna et al. 2015). Therefor a cyclic load frequency (f) of 10 Hz represents a train travelling at about 74 km/h a for an axle distance just exceeding 2 m, as shown in Figure 4.14. In order to consider the effects of increased train speeds (e. g. v = 145, 220 km/h) appropriate frequencies of f = 20 and 30 Hz were selected, respectively. A physical examination of geocells excavated from the subballast after testing revealed minor surface damage, but no rupture at the seams or joints, as shown in Figure 4.15 (a, b & c).

Figure 4.15. Physical examination of (a) geocell mattress (b) bulk and (c) seam of the pocket at the end of *N*=500,000 cycles.

The volumetric strain was calculated by summing the lateral strains measured in each vertical wall along the direction of σ_3' and vertical strains along the direction of σ_1. Since there were no failures, the magnitudes of vertical strain and volumetric strain were obtained at the end of a certain number of cycles *N*. Half a million cycles were applied to each test. Except at very high frequencies, any permanent deformation of subballast was usually caused by frictional rearrangement and volumetric compaction, (i.e. cyclic densification) rather than by actual breakage (Suiker and de Borst, 2003). Within the scope of this study, particle breakage was not considered for this subballast.

4.4 Vertical strain of subballast with and without geocell

4.4.1 Effect of number of load cycles (*N*)

Figure 4.16 and 4.17 present the vertical strains of unreinforced and reinforced subballast plotted against the number of load cycles (*N*) at different frequencies (*f*) and confining pressures (σ_3'). Based on these experimental results, the vertical strains (ε_l) increased rapidly during the first few thousand cycles due to initial particle rearrangement [(i.e. the unstable zone in Figure 4.16]. This strain rate increase decreased in the subsequent cycles beyond the unstable zone, and at a very high value of *N*, ε_l approached a constant. This zone where the strains (ε_l) stabilised is known as the 'stable zone', which was in accordance with studies reported elsewhere (Yu and Sloan 1997, Dahlberg 2001, Krabbenhoft et al. 2007, Trani and Indraratna 2010, Nimbalkar et al. 2012, Tafreshi et al. 2014). The experimental results for the unreinforced specimen did not exhibit a definite attainment of shakedown even after 500,000 cycles. However, almost a constant strain occurred at $\sigma_3' \geq 15$ kPa as *N* approached half a million cycles.

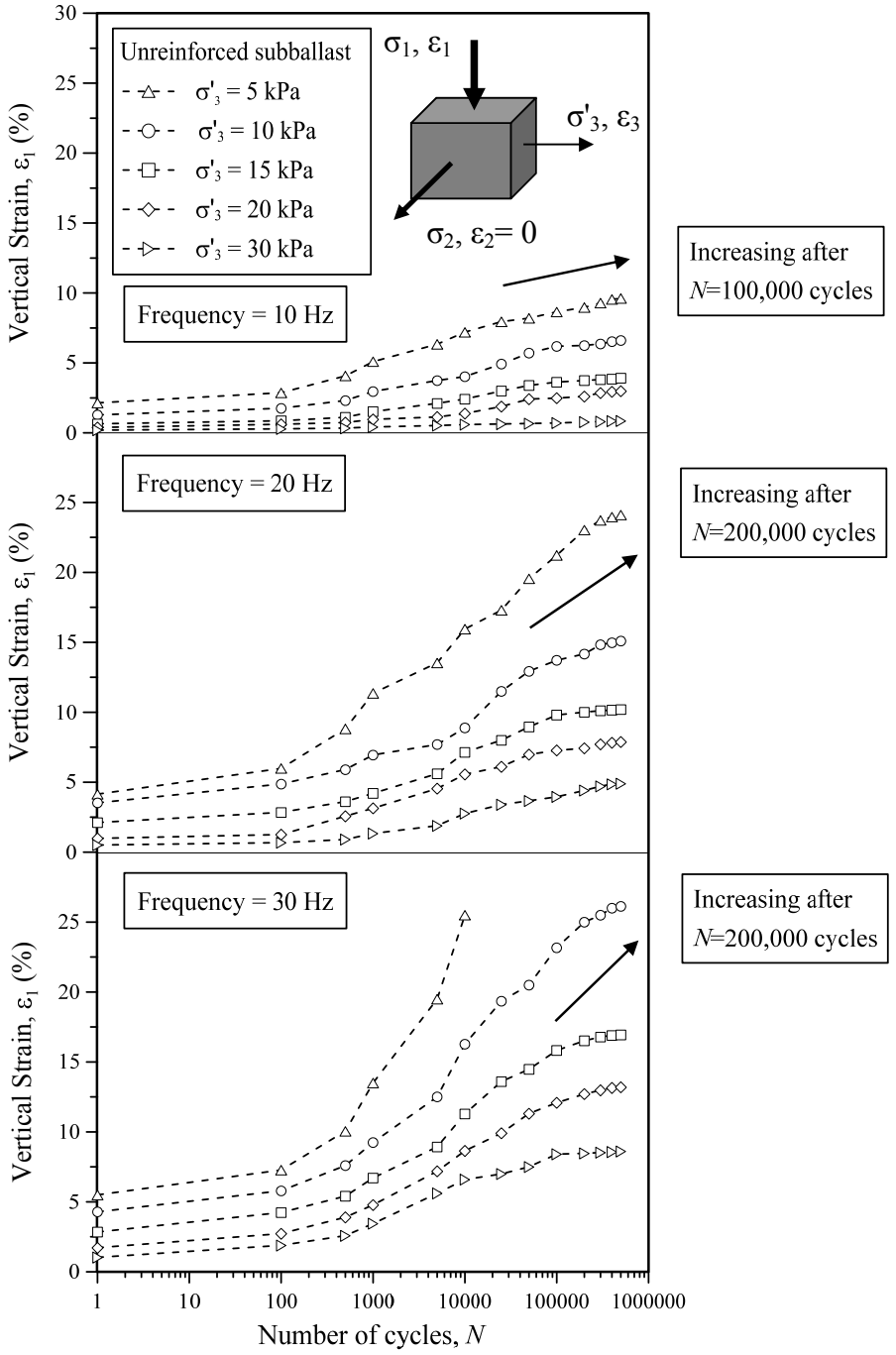

Figure 4.16. Variation of vertical strain (ε_1) against number of cycles (N) in unreinforced subballast (data sourced from Indraratna et al. 2015 with permission from ASCE)

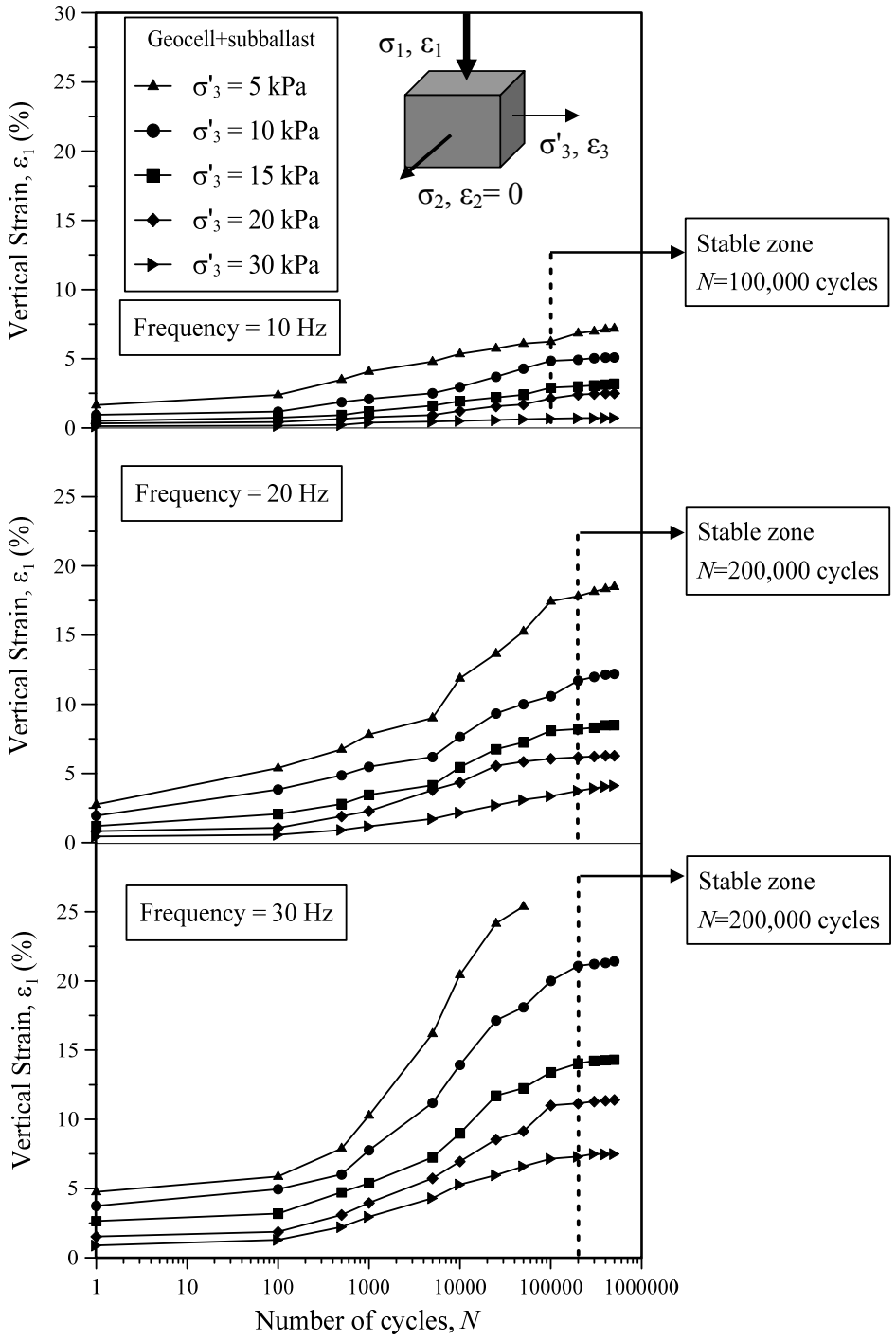

Figure 4.17. Variation of vertical strain (ε_1) against number of cycles (N) in reinforced subballast (data sourced from Indraratna et al. 2015 with permission from ASCE)

Undoubtedly, geocell reinforcement definitely improved the behaviour of subballast when it was reinforced with geocell. It was found that reinforced subballast approached the stable zone at less number of cycles than the unreinforced specimen [Figure 4.17]. It was observed that at a relatively low frequency ($f \leq 20$), both the unreinforced and reinforced subballast attained the shakedown zone at about N = 100,000 cycles. However, at a very low confining pressure ($5 \leq \sigma_3' \leq 15$) and a higher frequency ($f \geq 20$), the reinforced specimen reaches the stable zone at about N = 200,000 cycles. Nevertheless, the rate of vertical strain in the unreinforced subballast is still found to be increasing significantly. Providing the geocell as reinforcement, induced additional confinement that resulted in a quasi-rigid mattress that arrested the lateral movement of infilled subballast (Huang and Tatsuoka 1990). This confirmed that the reinforced composite material had a higher load bearing capacity with reduced vertical deformation under cyclic loading, as shown in Figure 4.17.

4.4.2 Effect of confining pressure (σ_3')

Substantial vertical strains developed in the unreinforced subballast when a relatively very low confinement was applied ($5 \leq \sigma_3' \leq 15$ kPa). These results also showed that the geocells had markedly reduced the strain rates of specimens tested at lower confining pressure ($\sigma_3' \leq 15$ kPa). It was observed that the rate of strain decreased at a higher confining pressure ($\sigma_3' \geq 20$ kPa). Reinforced-subballast tested at higher confining pressure (σ_3' = 20-30 kPa) resulted in much less or even negligible vertical strain for different frequencies, as shown in Figure 4.17. Marginal difference was observed between the unreinforced and reinforced subballast at σ_3' = 30 kPa, indicating that this optimum confining pressure is enough to control the strains, a result that is in agreement with a previous study (Lackenby et al. 2007).

4.4.3 Effect of frequency (f)

At low frequency (f = 10 Hz) the unreinforced subballast caused considerable vertical strain at a very low confining pressure ($5 \leq \sigma_3' \leq 15$ kPa). This behavior was more profound when a higher frequency was applied. As Figures 4.16 and 4.17 show, by increasing the frequency ($f \geq 20$ Hz), the vertical strains (ε_1) increased significantly, especially at low confining pressure ($\sigma_3' \leq 15$ kPa). These results also revealed that geocells provided a pronounced impact on the subballast tested at higher frequencies, (i.e. f = 20-30 Hz), as shown in Figure 4.17. This can be explained because when these specimens yielded a significant lateral strain, which in turn mobilised a higher tension in the geocell strips. As result, geocells generated a substantial additional confining pressure that was more effective at a higher applied frequency.

4.5 Lateral spreading of subballast with and without geocell

4.5.1 Effect of number of load cycles (N)

Perhaps the most significant impact of the geocell mattress is reducing the lateral spreading (S_L) of infill materials. Figure 4.18 shows the variation of lateral spreading for the unreinforced specimen against the number of cycles (N) for different confining pressures and frequencies. As this figure shows, bigger lateral spreading was observed in the first number of cycles. This was in accordance with previous studies (Indraratna et al. 2006). Moreover, lateral spreading continued even after number of cycles of about N = 100,000 cycles. However, lateral spreading minimised markedly after a geocell mattress was placed in the subballast, as shown in Figure 4.19. As this figure shows, geocell reinforcement effectively seized lateral deformation of subballast at an early stage of cyclic loading ($N \leq 1000$ cycles), unlike the unreinforced specimens.

4.5.2 Effect of confining pressure ($\sigma_3^{'}$)

It is well known that the cyclic behaviour of rail track substructure is governed in the field by the confinement exerted by the ballast shoulder. As Figure 4.18 shows, by applying cyclic loading and increasing the number of cycles, subballast experienced a considerable amount of lateral spreading due to the very low confinement. As expected, at a very low confining pressure ($\sigma_3' \leq 15$ kPa), unreinforced subballast experiences extensive lateral spreading. The degree of lateral spreading was reduced by increasing σ_3'. Moreover, at a confining pressure of about $\sigma_3' = 30$ kPa, the unreinforced specimen didn't show any major lateral spreading. However, the lateral deformation of subballast at very low confining pressures ($\sigma_3' \leq 15$ kPa) were reduced by utilising the geocell mattress in the specimen, as shown in Figure 4.19. Nevertheless, the reinforcement was not as effective at higher confining pressures ($\sigma_3' \geq 20$ kPa).

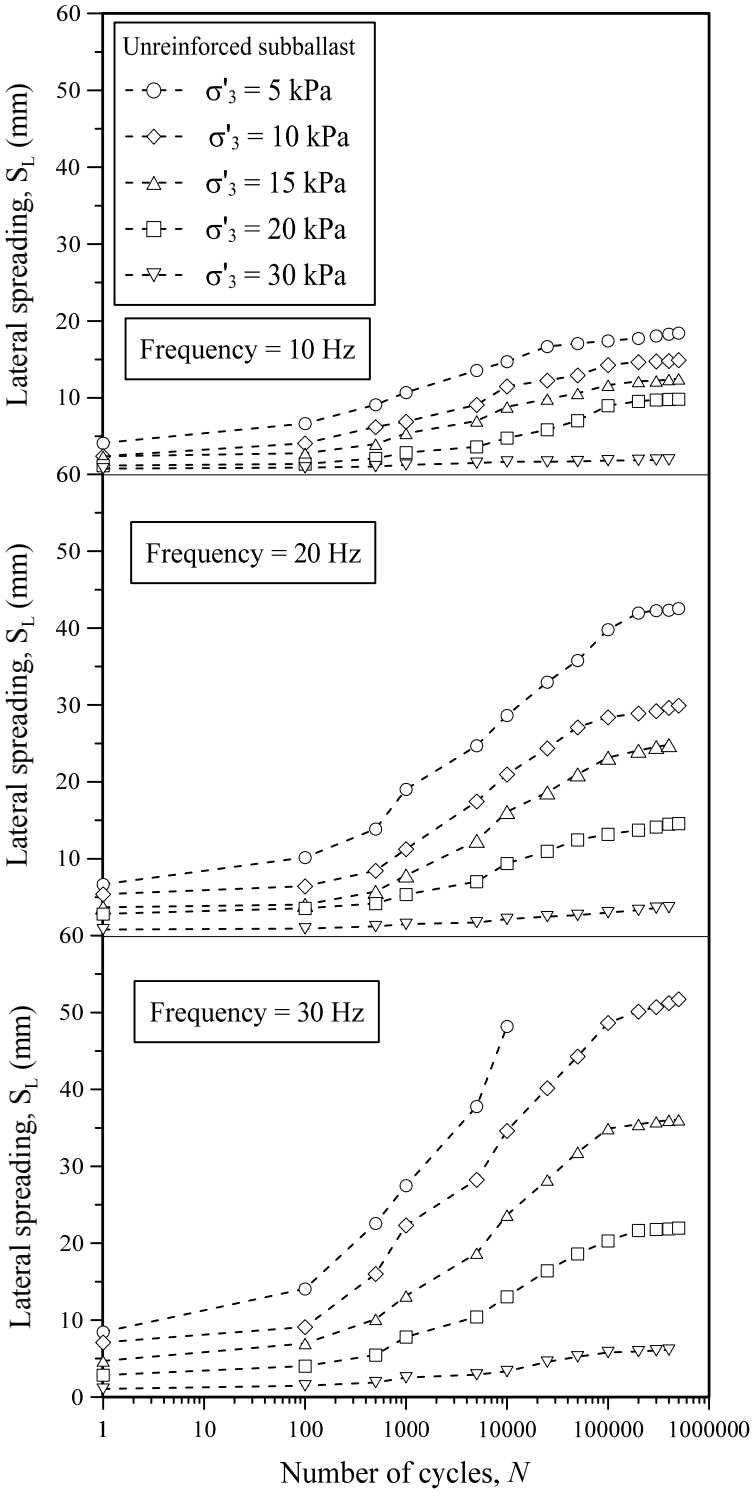

Figure 4.18. Variation of lateral spreading of unreinforced subballast against number of cycles (N) in unreinforced subballast

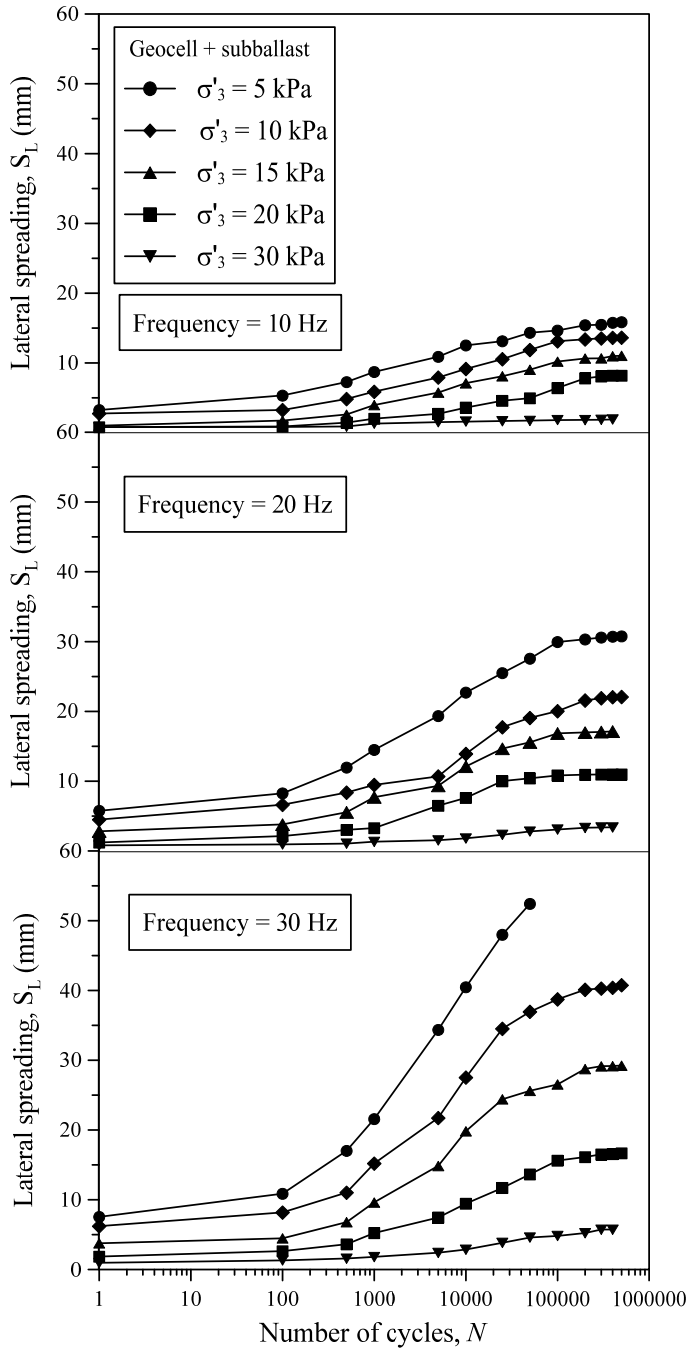

Figure 4.19. Variation of lateral spreading of unreinforced subballast against number of cycles (*N*) in reinforced subballast

4.6 Volumetric strain of subballast with and without geocell

4.6.1 Effect of number of load cycles (*N*)

The lateral deformations were recorded parallel to the minor principal stress ($\sigma_3^{'}$), but in the orthogonal lateral direction, a plane strain condition was maintained (i.e. ε_2 = 0). The complementary strain invariant, i.e. volumetric strain ε_v was defined by Timoshenko and Goodier (1970) as:

$$\varepsilon_v = \varepsilon_1 + \varepsilon_2 + \varepsilon_3 \tag{4.7}$$

For the non-axisymmetric triaxial specimens in a special case of plane strain, the strain invariants ($\sigma_2' \neq \sigma_3'$ and $\varepsilon_2 = 0$) were expressed as:

$$\varepsilon_v = \varepsilon_1 + \varepsilon_3 \tag{4.8}$$

In concurrence with a previous study (Suiker et al. 2005), during the first few thousand cycles, unreinforced subballast experienced a steady increase in volumetric strains until it reached the 'stable zone' shown in Figures 4.20 and 4.21. Nevertheless, the rates at which the increments of volumetric strain increased decreased markedly as the number of cycles increased.

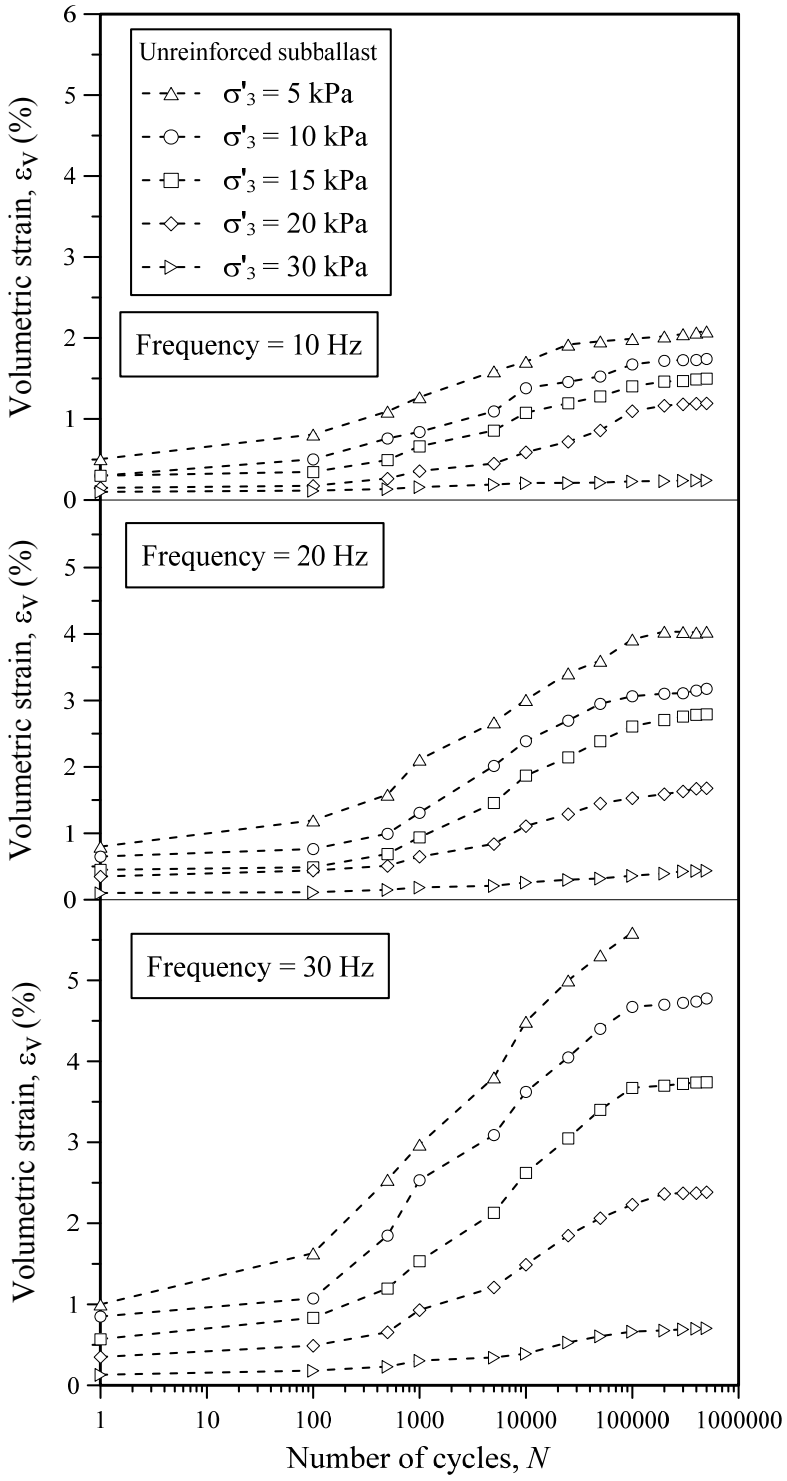

Figure 4.20. Variation of volumetric strain (ε_v) against number of load cycles of unreinforced subballast (data sourced from Indraratna et al. 2015 with permission from ASCE)

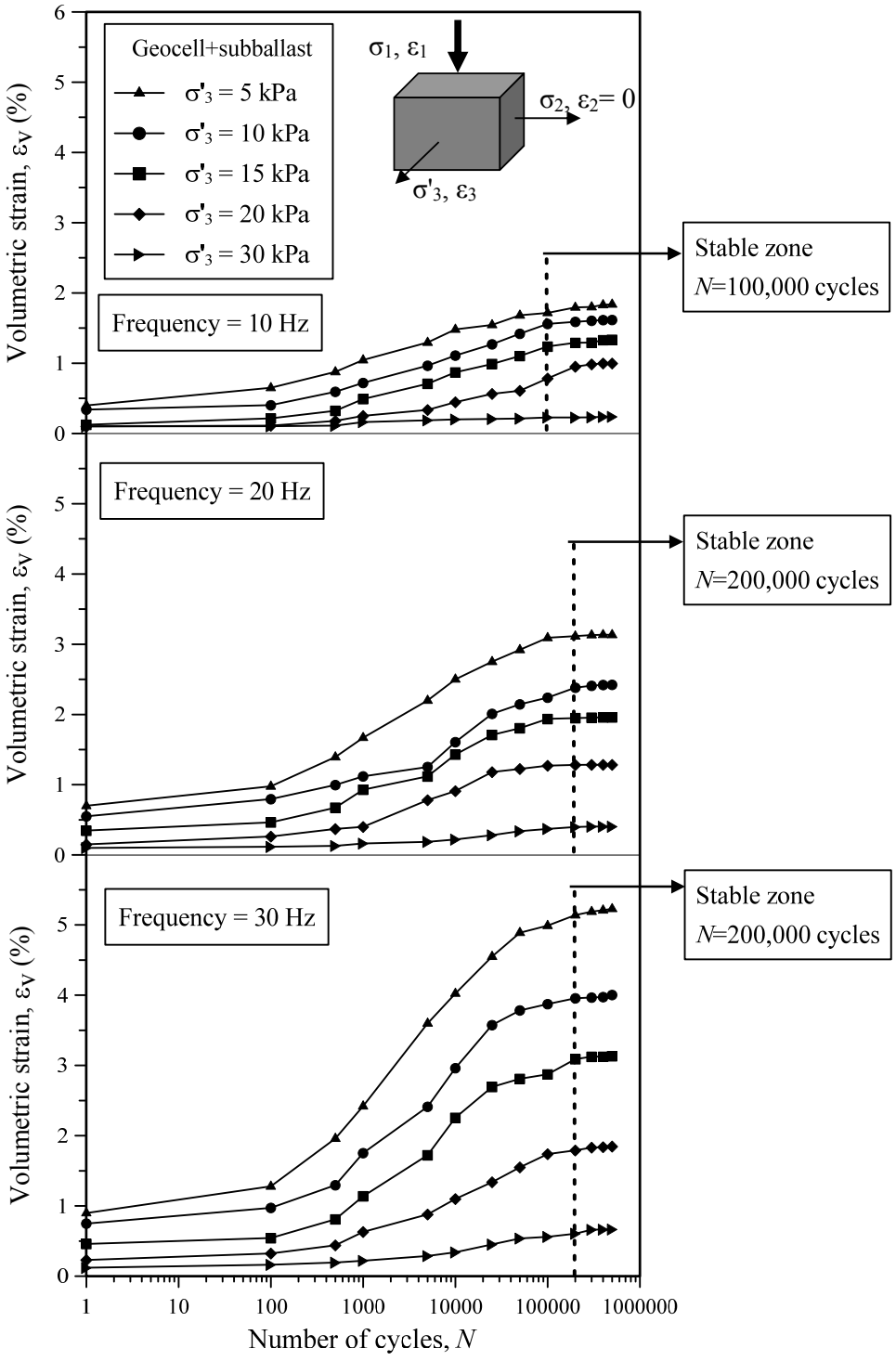

Figure 4.21. Variation of volumetric strain (ε_v) against number of load cycles of reinforced subballast (data sourced from Indraratna et al. 2015 with permission from ASCE)

4.6.2 Effect of confining pressure (σ_3') and frequency (f)

Cyclic loading reorients the subballast and results in volumetric strain (i.e. compression or dilation) depending upon the initial condition of the material. In this current study the dilative volumetric strain was considered to be positive. As Figures 4.20 and 4.21 show, the confining pressure (σ_3') significantly influenced the volumetric strain of the subballast such that at very low confinement ($\sigma_3' \leq 15$ kPa), excessive dilation developed in the unreinforced subballast at the same frequency. Moreover, the results also revealed that specimens with $\sigma_3' \geq 20$ kPa were not influenced as much, even at higher frequencies, which indicated that a confinement of $\sigma_3' \geq 20$ kPa was large enough to prevent the subballast from excessive dilation.

Based on the outcome of this current study, the geocell-reinforced granular medium varies significantly depending upon the applied cyclic frequencies (f). For instance, a higher frequency loading ($f \geq 20$ Hz) initially caused increased lateral spreading of the material, which in turn induced tension in the geocell wall and an associated increase in additional confinement. This increased confinement and geocell tension would then create a 'self-stabilising ring' of infill material. Under low frequencies ($f \leq 20$ Hz), the geocells would still provide some confinement. However, the cellular assembly is not fully activated until the hoop stress attains a threshold value at an increased frequency. Moreover, increasing the frequency induced significant volumetric strains into the specimen, but when geocell reinforcement was provided the volumetric dilation decreased to an acceptable degree. Moreover, in unreinforced and geocell-reinforced subballast no compression behaviour was observed.

4.6.3 Final vertical and volumetric strains

The influence of confining pressures on the permanent strains of subballast can best be presented by comparing the final values of vertical (ε_1) and volumetric (ε_v) strains at N = 500,000. Figure 4.22 (a & b) shows the beneficial use of geocells for a subballast tested at low confining pressure and at different frequencies. Indeed the

results show that increasing the confining pressure to σ_3' = 20-30 kPa at the desired frequency markedly reduced the strains (ε_l and ε_v) for unreinforced and reinforced subballast. As [Figure 4.22(a)] shows, the vertical strain of the specimens increased to about 25-30 % after the frequency increased from 10 to 30 Hz at a given confining pressure (σ_3' = 5 kPa). Nevertheless, the percentage reduction of vertical strains decreased markedly by increasing the confining pressure from σ_3' = 5 to 30 kPa at a given frequency.

Figure 4.22 (b) shows that utilising geocell as a cellular confinement led to significant reduction in the volumetric strain. As shown here, for a desired frequency at σ_3' = 5-10 kPa, geocell reinforcement reduced the volumetric strain by 15-25 % compared to the unreinforced subballast. These results confirmed that geocells performed best at relatively low confining pressure ($\sigma_3' \leq$ 15 kPa). This means that geocell reinforcement is an ideal technique for use in rail tracks where the confinement of ballast and subballast has not been increased by other methods such as side restraints and altered sleeper shapes, as proposed by Lackenby et al (2007).

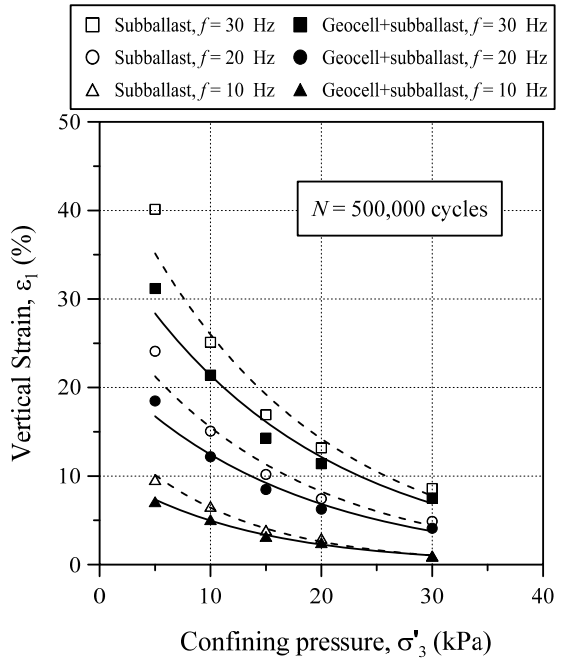

(a)

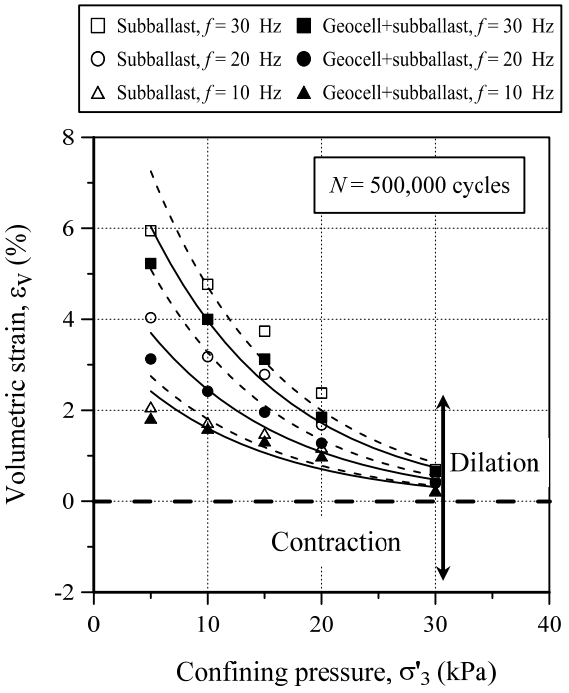

(b)

Figure 4.22. Final (a) vertical strain (ε_1) and (b) volumetric strain (ε_v) at 500,000 cycles (N) at different confining pressure (σ_3')(data sourced from Indraratna et al. 2015 with permission from ASCE)

4.7 Resilient modulus of unreinforced and reinforced subballast

Under cyclic loading, the resilient modulus (M_R) is defined as (AASHTO T274-82):

$$M_R = \frac{q_{cyc}}{\varepsilon_1^e} \tag{4.9}$$

where q_{cyc} = cyclic deviator stress, and ε_1^e = elastic vertical strain during unloading. The influence of the number of cycles (N), confining pressure (σ_3') and frequency (f) on the resilient modulus of unreinforced and geocell reinforced subballast was evaluated in this study. It was observed that the resilient modulus (M_R) improved with the increasing number of cycles (N). Figure 4.23 shows typical response of unreinforced and geocell-reinforced subballast under cyclic loading at very low confining pressure (σ_3' = 5 kPa) and relatively high frequency (f = 20 Hz). As shown here, at early number of load cycles, unreinforced subballast experiences significant densification. The rate of densification was reduced by increasing the number of cycles. Nevertheless, at N = 100,000 cycles, the magnitude of M_R in unreinforced subballast, still is increasing, indicating that the material has not reach stable zone. On the other hand, the due to cellular confinement, rate of densification in the reinforced subballast was much greater than unreinforced specimen. Based on the test results, the reinforced subballast attained stable zone at about N = 100,000 cycles.

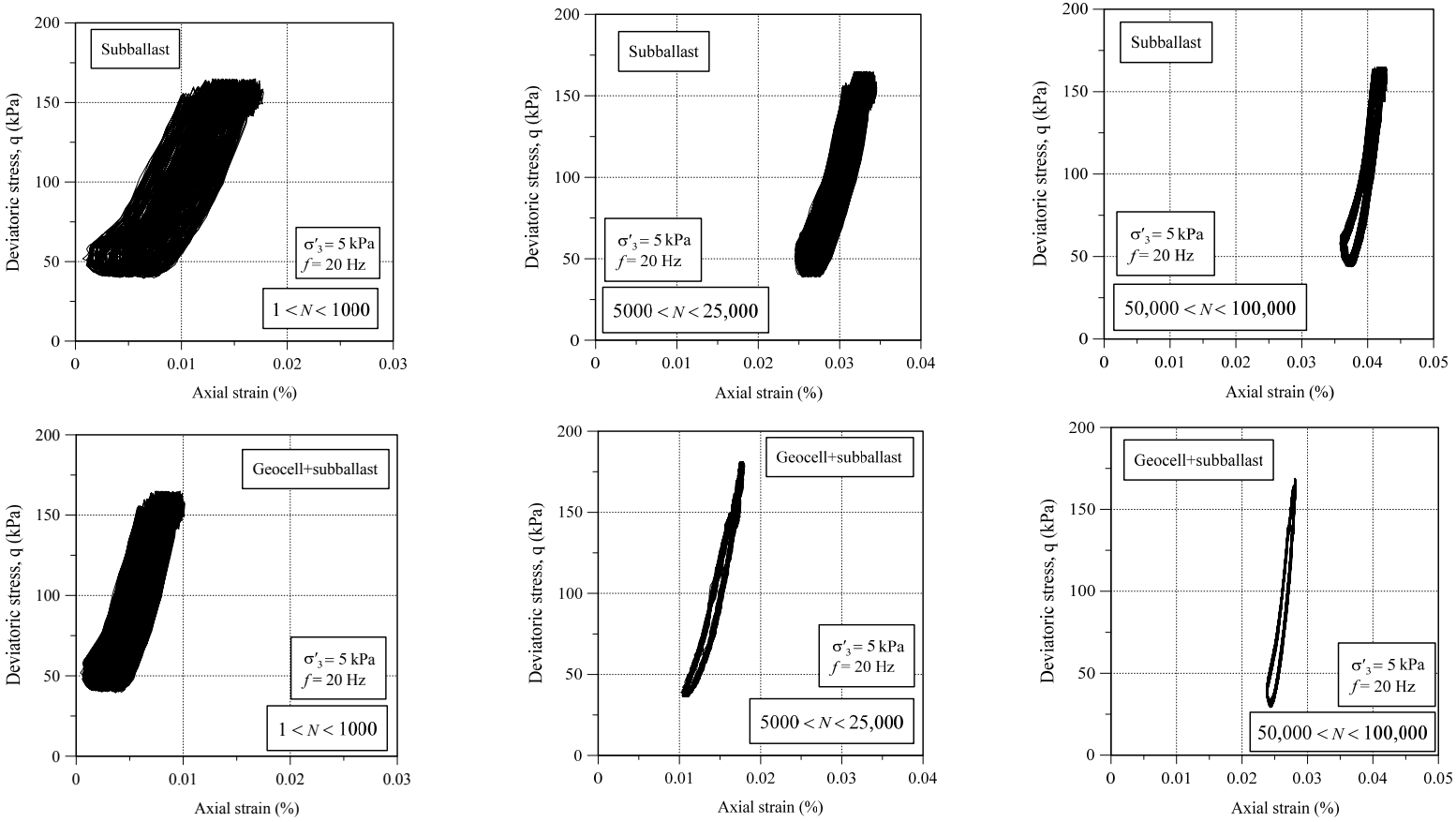

Figure 4.23. Variation of Resilient modulus (M_R) of the unreinforced and reinforced subballast at different number of load cycles (N)

To highlight the influence of geocell on the resilient modulus of subballast, the degree of M_R is plotted for confining pressure of σ_3' = 20 kPa at different frequencies against the number of cycles (N). The magnitude of plastic deformation of unreinforced and reinforced subballast decreased significantly after a very large number of cycles ($N \geq 100{,}000$), indicating a constant value of M_R. The results also showed that the M_R for reinforced subballast increased by 10-18 % compared to unreinforced subballast, as shown in Figure 4.24.

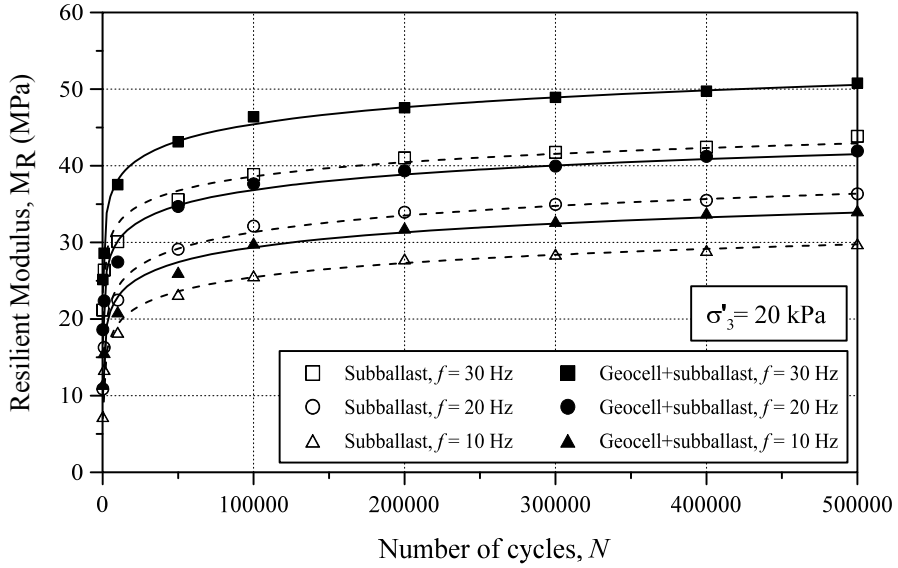

Figure 4.24. Variation of Resilient modulus (M_R) of the unreinforced and reinforced subballast at different frequency against number of load cycles (N) (data sourced from Indraratna et al. 2015 with permission from ASCE)

Figures 4.25 (a) and 4.26 (a) show the effect of confining pressure and frequency on the observed results at the number of cycles of N = 500,000 cycles. By increasing σ_3' and f, the magnitude of M_R for unreinforced and geocell-reinforced subballast increased by about 20 %. It was found that frequency influences the M_R of the specimen reinforced with geocells slightly more than the unreinforced specimen. This can be explained as the geocells help to stabilise the infill subballast under high frequency cyclic loading, which improves its resilient modulus.

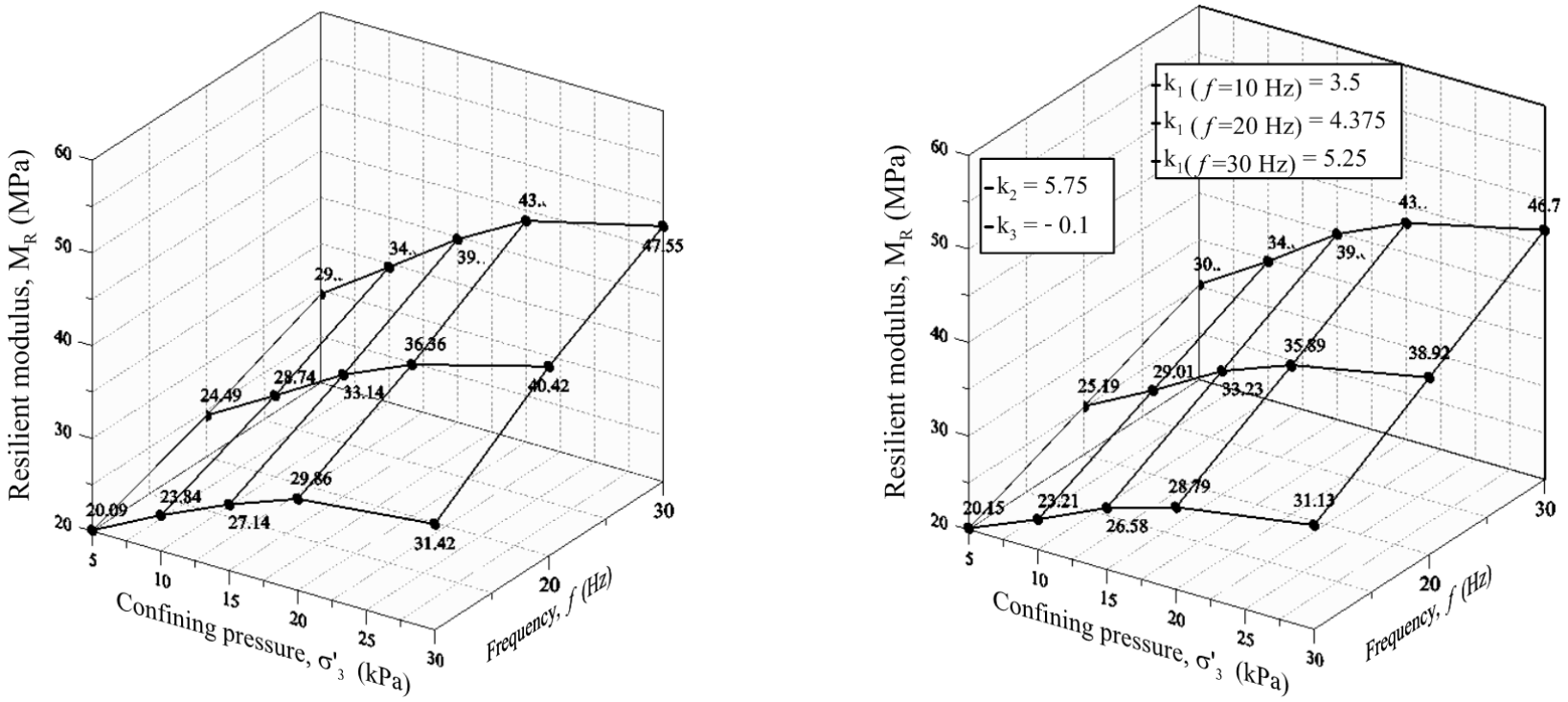

Figure 4.25. Variation of resilient modulus against different confining pressure (σ_3') and given frequency (*f*) of (a) experimental results of unreinforced subballast (b) model prediction of unreinforced subballast (data sourced from Indraratna et al. 2015 with permission from ASCE)

It is well known that the resilient modulus of granular material can be determined by (Uzan, 1985):

$$M_R = k_1 P_{atm} \left(\frac{\theta}{P_{atm}} \right)^{k_2} \left(\frac{\tau_{oct}}{P_{atm}} + 1 \right)^{k_3} \tag{4.10}$$

where p_{atm} = atmospheric pressure, τ_{oct}= the shear stress and θ = the bulk stress of the subballast, as defined by:

$$\theta = \sigma_1 + \sigma_2 + \sigma_3 \tag{4.11}$$

$$\tau_{oct} = \frac{1}{3}\sqrt{(\sigma_1 - \sigma_2)^2 + (\sigma_1 - \sigma_3)^2 + (\sigma_2 - \sigma_3)^2} \tag{4.12}$$

k_1, k_2, and k_3 = the experimental parameters. A best fit regression analysis was performed to back-calculate the values of these empirical parameters using the experimental data (coefficient of regression, $r^2 \geq 0.97$). Figures 4.25 (b) and 4.26 (b) show the predicted values of the resilient modulus of unreinforced and reinforced subballast based on the empirical model [Eq. (4.10)]. The predictions made by the empirical model agreed with the experimental data obtained from the plane strain condition. This means the model can capture variations in the resilient modulus for different σ_3' and f.

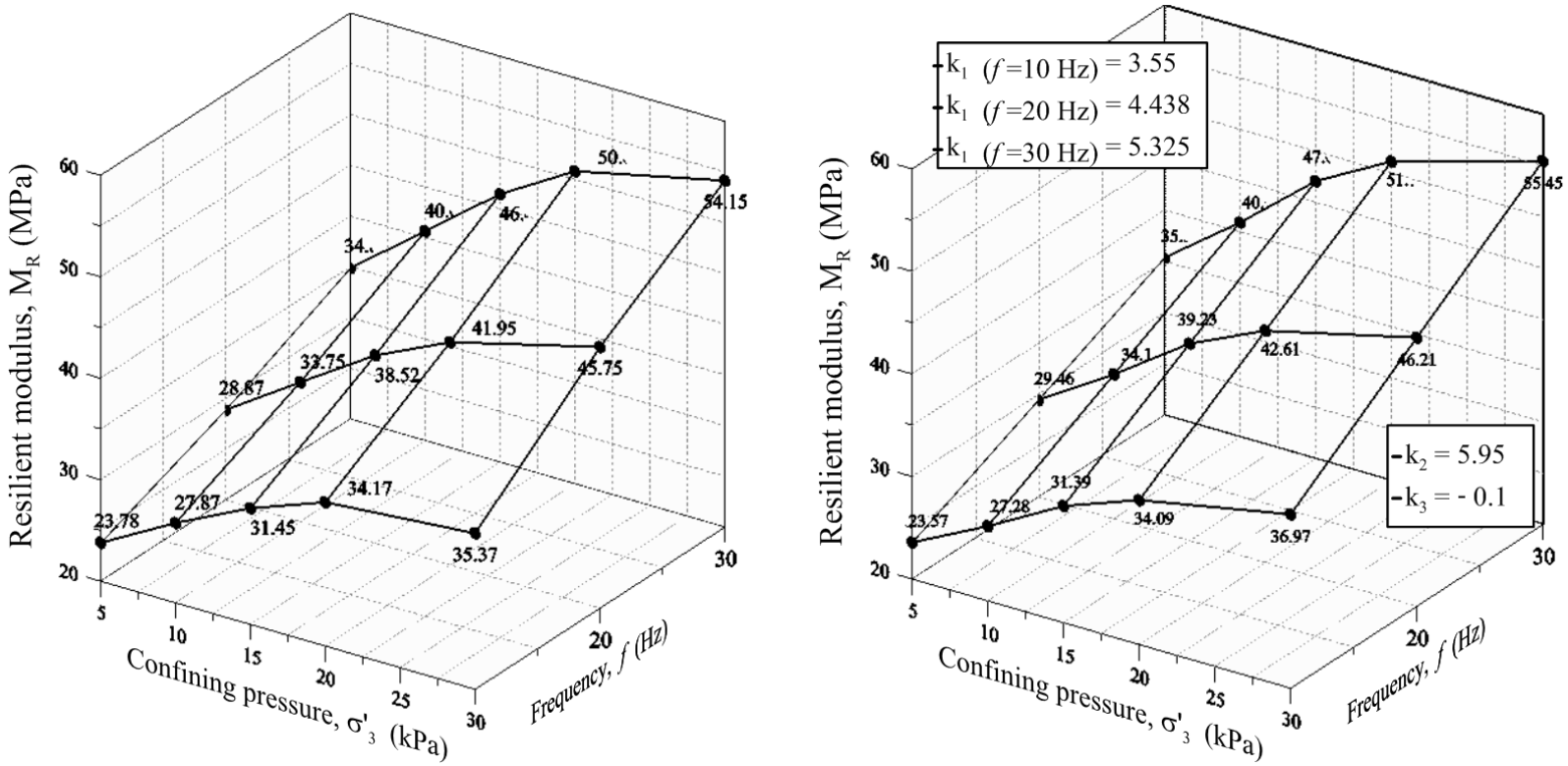

(a) (b)

Figure 4.26. Variation of resilient modulus against different confining pressure (σ'_3) and given frequency (f) of (a) experimental results of reinforced subballast (b) model prediction of reinforced subballast (data sourced from Indraratna et al. 2015 with permission from ASCE)

4.8 The angle of friction ϕ_m and dilatancy ψ_m

Based on the results obtained, it was found that the friction angle and dilatancy angle are not constant during cyclic loading. As result, the mobilised friction angle and angle of dilatancy can be measured by (Bolton, 1986):

$$\sin\phi_m = \frac{\sigma_1^{'} - \sigma_3^{'}}{\sigma_1^{'} + \sigma_3^{'}} \tag{4.13}$$

$$\sin\psi_m = \frac{d\varepsilon_1^P + xd\varepsilon_3^P}{d\varepsilon_1^P - xd\varepsilon_3^P} = \frac{d\varepsilon_v^P / d\varepsilon_1^P}{2 - \left(d\varepsilon_v^P / d\varepsilon_1^P\right)} \tag{4.14}$$

where σ_1' = normal stress (kPa), σ_3' = the confining pressure (kPa), ψ_m = the mobilized dilation angle (degree), ϕ_m = the mobilised friction angle (degree), ε_1^p = the plastic vertical strain at the required number of cycles (N), ε_v^p = the plastic volumetric strain, and the value of x = 1 for plane strain condition (Indraratna and Nimbalkar, 2013). In a previous study (Leshchinsky and Ling 2013) the effect of confining pressure on the angles of friction or the angle of dilation was ignored. However this study revealed that σ_3' and f have a significant influence on the friction angle and angle of dilatancy.

Figure 4.27 and 4.28 show that the mobilised friction angle and the angle of dilation decrease as the confining pressure and frequency increase within the range of 38°-44°. The reinforced subballast had a lesser value of ϕ_m and ψ_m than the unreinforced aggregates due to induced additional confinement. Nevertheless, increasing the confining pressure to 30 kPa, the difference between ϕ_m of unreinforced and reinforced became marginal because the geocells were ineffective. As expected, the variation of ϕ_m with σ_3' was relatively smaller than the variation of ψ_m due to the low confining pressures adopted in this study. Under higher confining pressures (20

$\leq \sigma_3'$), the friction angle could decrease substantially and render a more prominent non-linear variation (e.g., Indraratna et al. 1998). Assessing track stability using the strain-based approach (dilation angle preferred over friction angle) would be more appropriate when the tracks are subjected to almost uniform stress, albeit being sensitive to deformation due to insufficient confining pressure and high frequency loading. The results in Figure 4.28 imply that for a real rail track with geocell confinement, and with σ_3' equal to 30 kPa, subballast dilation can be controlled effectively, even at higher speeds ($f \geq 20$ Hz).

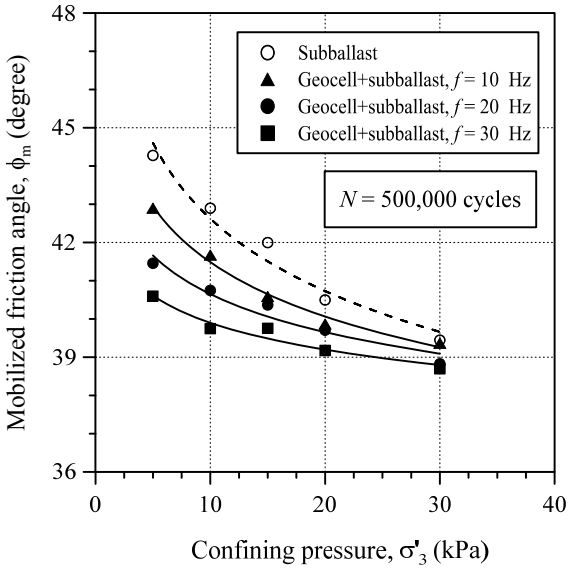

Figure 4.27. Variation of mobilised friction angle ($\varnothing_m$) at different confining pressures (σ_3') (data sourced from Indraratna et al. 2015 with permission from ASCE)

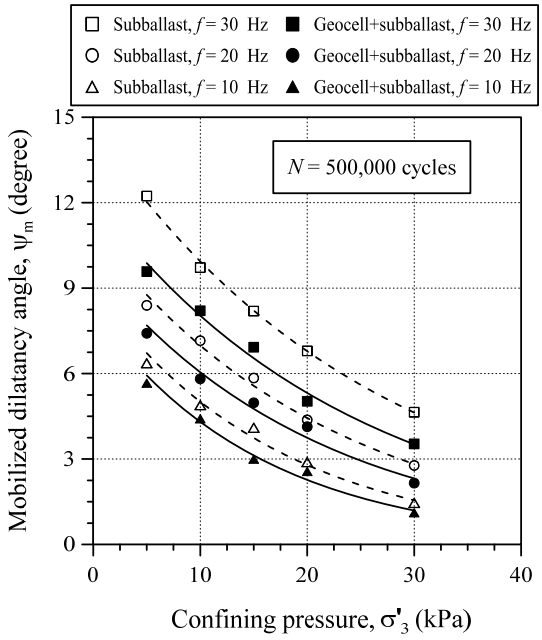

Figure 4.28. Variation of mobilised angle of dilatancy (ψ_m) at different confining pressures (σ_3')(data sourced from Indraratna et al. 2015 with permission from ASCE)

4.9 Axial strain and lateral pressure mobilised in geocells

Variation of axial strains recorded by strain gauges attached to the geocell strips are plotted against the number of cycles (*N*) as shown in Figure 4.29. An increase in axial strain occurred with an increasing *N*, which implies the occurrence of vertical (axial) compression coupled with lateral (outward) expansion of the geocell pocket. Moreover, increased strains occurred at higher frequencies. Figure 4.29 also shows that a lower axial strain was measured by strain gauges at a higher confining pressure (σ_3' = 30 kPa). Again, this indicates that at the confining pressure of σ_3' = 30 kPa, there will be an insignificant axial deformation in the specimen, highlighting the ineffectiveness of geocell mattress at a higher confinement.

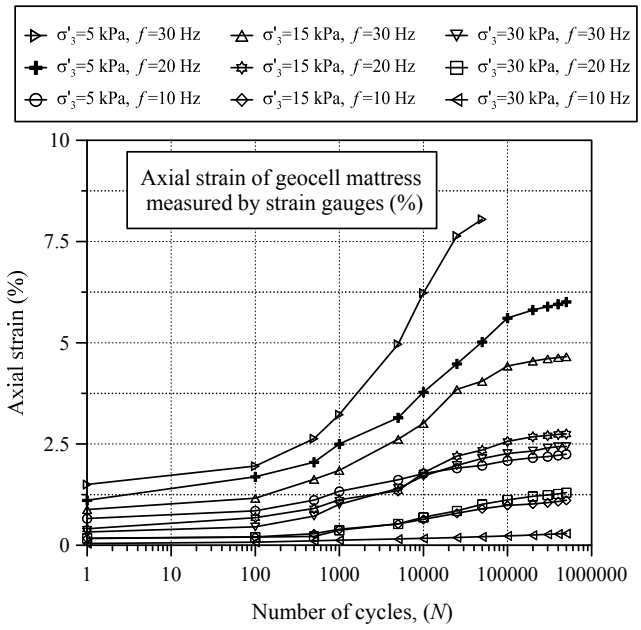

Figure 4.29. Axial strain recorded by strain gauges (data sourced from Indraratna et al. 2015 with permission from ASCE)

4.10 Effect of the intermediate stress

The effect of intermediate principal stress cannot be ignored in any analysis of railway foundation, including ballast or subballast. Perhaps one of the parameters that governs the subballast performance is the intermediated principal stress (σ_2'), which was investigated in this study. According to the experimental results, by increasing the stress to mean stress (q_{mean}), the granular material in an unreinforced subballast attempts to spread isotropically in each direction. Nevertheless, in plane strain condition, the subballast can move vertically or spread laterally in the direction of major (σ_1') and minor principal stress (σ_3') as lateral movement in direction of intermediated principal stress (σ_2') was prevented. The laboratory results show that the magnitude of σ_2' increases markedly when a mean pressure of q_{mean} = 104 kPa is reached, as shown in Figure 4.30. The results also show that σ_2' increased as the confining pressure increased, because, the lateral spreading was restricted, hence σ_2' accumulated at higher confining pressures. However, in geocell-reinforced subballast the magnitude of σ_2' was slightly different. The results showed that the degree of σ_2' in reinforced subballast was slightly more than the unreinforced specimen. This occurred because the geocell minimised the subballast from spreading laterally in the direction of minor principal stress, leading to a higher σ_2' than the unreinforced subballast.

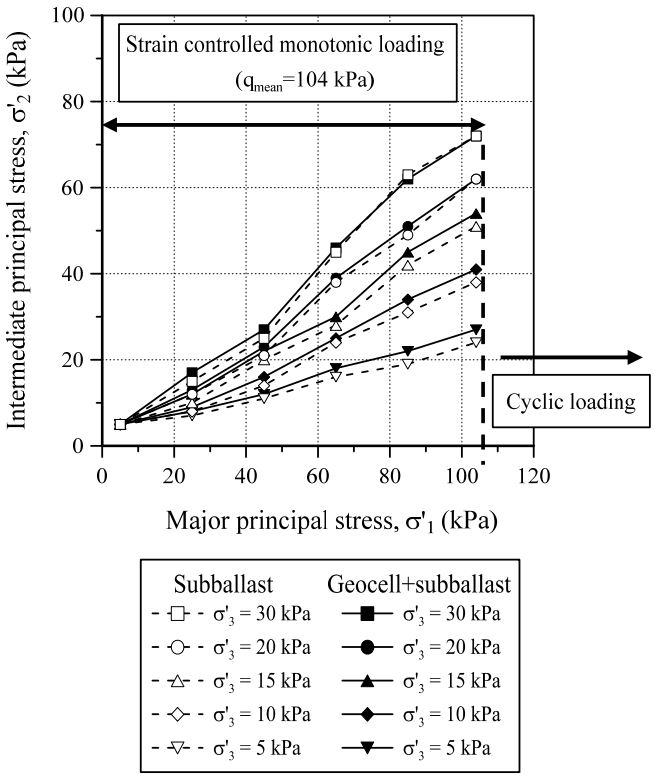

Figure 4.30. Variation of Intermediate principal stress (σ_2') with externally applied confining pressures (σ_3')

Based on the laboratory results, the magnitude of σ_2' was more profound at lower confining pressure and higher frequencies. This could be explained by the fact that at $\sigma_3' \leq 15$ kPa and $f \geq 15$ Hz, there would be a significant degree of additional confinement induced by the geocell mattress, which would lead to an increase of σ_2'. Figure 4.31 shows the values of σ_2' at the loading stage (q_{max} = 166 kPa) for different confining pressures and frequencies. As expected, the magnitude of σ_2' increased at higher frequencies. Table 4.3 summarises the ratio of σ_2'/σ_3' for different confining pressures and frequencies.

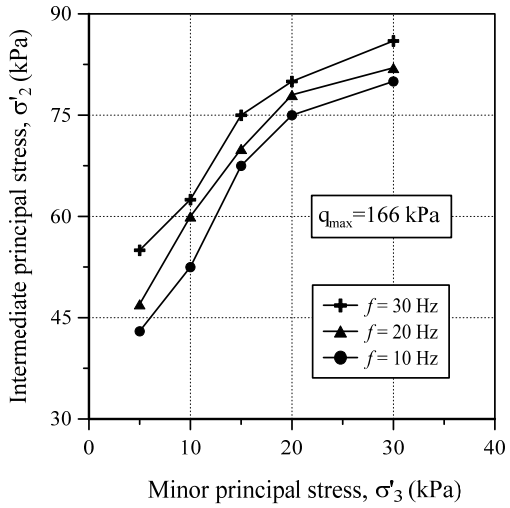

Figure 4.31. Comparison of intermediate principal stress at different confining pressures (σ_3') and frequencies (*f*) in unreinforced subballast

Table 4.3. The ratio of σ_2'/σ_3' obtained based on experimental results

	Confining pressure σ_3' (kPa)	Frequency (Hz)		
Subballast		**10**	**20**	**30**
	5	9.80	10.20	11.80
	10	5.80	6.20	6.60
	15	4.53	4.87	5.13
	20	3.85	3.90	4.10
	30	2.77	2.97	3.00
Geocell +subballast				
	5	11	11.40	13
	10	6.25	7	7.25
	15	5.17	5.33	5.67
	20	4.20	4.40	4.45
	30	3	3.07	3.20

4.11 Summary

In this chapter, a laboratory investigation to study the resilient and permanent displacement of railway subballast in both unreinforced and geocell-reinforced subballast under high speed cyclic loading was presented. The effectiveness of geocell reinforcement on the subballast performance was highlighted by studying several key factors including: the vertical and lateral displacement, the volumetric deformation, the confining pressure, the frequency and the number of load cycles, angle of shearing resistance (friction), dilation angle and the resilient modulus.

At all confining pressures ($5 \leq \sigma_3' \leq 30$ kPa) and frequencies ($30 \geq f \geq 10$ Hz), most of the particle rearrangement occurred at the initial cycles ($N \leq 10{,}000$ cycles). The rate of densification was diminished during the subsequent cycles. Unreinforced subballast did not show any stable behaviour even after N = 100,000 cycles. However, by confining infill granular material, geocell accelerated the rate of densification in reinforced subballast. All of the geocell-reinforced subballast at different confining pressures and frequencies attained a stable state at N = 100,000 cycles.

At very low confining pressure ($\sigma_3' \leq 15$ kPa), unreinforced subballast experienced significant vertical and lateral displacement. This behavior was more profound at higher frequencies ($f \geq 20$ Hz). The magnitude of deformations was markedly reduced by increasing the confining pressure to $\sigma_3' \geq 20$ kPa. Nevertheless, reinforcing subballast with the geocell significantly reduced the vertical and lateral deformation of subballast. The geocell mattress was more effective at very low confining pressure and higher frequency. This was attributed to higher tensile strength mobilised in the geocell. Marginal improvement was observed in the geocell-reinforced subballast compared to unreinforced subballast at higher confining pressure ($\sigma_3' \geq 20$ kPa). The test series confirmed that a confining pressure

of σ_3' = 30 kPa was sufficient to reduce excessive volumetric dilation of the subballast under different frequencies.

The friction angle (ϕ_m) and the angle of dilatancy (ψ_m) were shown to decrease with increasing confining pressure. This implies that under cyclic loading, ψ_m and ϕ_m are not constant. Higher friction and dilation angles were observed at higher frequencies.

The intermediate principal stress (σ_2') was significantly higher than the minor principal stress (σ_3'). This difference was more profound at lower confining pressure. The rate of increment of σ_2' was reduced by increasing the confining pressure.

CHAPTER 5

5. ANALYTICAL MODEL FOR CALCULATING THE ADDITIONAL CONFINEMENT INDUCED BY GEOCELL

5.1 General

The use of cellular confinement over low strength subgrade has gained much popularity. In various studies the improved performance of geocell-reinforced soil has been attributed to the apparent cohesion mobilised between infill soil and geocell, while the soil friction angle remains constant (Bathurst and Karpurapu 1993; Rajagopal 1999; Latha and Murphy 2007). However, it has been proven that the improved performance of geocell-reinforced soil is associated with the additional confinement $\Delta\sigma_3'$ induced by the geocell pockets. Additional confining pressure mobilised in the geocell mattress effectively confines the soil enclosed in the pocket and minimises lateral spreading. Accordingly, developing an analytical model is necessary to predict the behaviour of reinforced soil. In this chapter a semi-empirical model for determining the additional confinement induced by a geocell mattress is proposed. Also the results from this model were compared with other models established in practice. Much of the work presented in this chapter was published earlier in the Journal of Geotechnical and Geoenvironmental Engineering (ASCE), and have been reproduced in this thesis with kind permission from ASCE.

5.2 Background

Only a limited amount of researchers have developed an analytical model to predict the additional confinement to pocket by infill material under cyclic loading; most available models only capture additional confinement, known as hoop stress, under monotonic loading. However, due to difficulty to consider various soil and reinforcement parameters, most available models only capture limited soil and geocell factors. One of the earliest studies devoted to additional confining pressure was based on hoop tension theory (Henkel and Gilbert 1952). However, due to the limited number of input parameters (M, D and ε_a), this model cannot predict the actual additional confining pressure developed by geocell mattress. In a recent study carried out on unbound granular material, an analytical model that can predict the additional confining pressure induced by geocell mattress (Yang and Han 2013) was proposed as follows:

$$\Delta\sigma_3 = \frac{M}{D}\left[-\frac{\Delta\sigma_3}{M_{r,1}} + \frac{\sigma_1 - (\sigma_3 + \Delta\sigma_3)}{M_{r,2}}\right] \times \left(\frac{\varepsilon_0}{\varepsilon_r}\right) e^{-(\rho''/N_{\lim it})^{\beta''}} \left(\frac{1+\sin\psi}{1-\sin\psi}\right) \qquad (5.1)$$

where $\Delta\sigma_3$ is the additional confining pressure, σ_1 and σ_3 are the external stresses, ψ is the dilatancy angle, $\varepsilon_0/\varepsilon_r$, ρ'' and β'' are the permanent deformation parameters, Mr is the resilient modulus and D is the diameter of the sample. However, the effect of the number of cycles and the frequency was ignored. It is well recognised that the behaviour of geocell-reinforced soil under cyclic loading is distinct from monotonic loading. In the past, no attempt was made to quantify the degree of additional confinement with respect to important governing rail track parameters (i.e., frequency, number of cycles and relatively low confining pressure), so developing a model which predicts $\Delta\sigma_3'$ under cyclic loading at a different number of cycles, is inevitable.

5.3 Model formulation

Based on the elastic behaviour of a geocell mattress, hoop tension theory can be used to calculate the additional confinement offered by geocell. In this chapter the derived equations are based on the mobilised strength for an ideal, elastic, and isotropic material in terms of the stress component given by Hook's law. In these equations the empirical parameters for axial and lateral strain based on the stress dilatancy approach were adopted. By considering Hook's law, the circumferential stress offered by geocell is described as:

$$\sigma_c = \frac{M_m}{(1+\nu_g)\cdot(1-2\nu_g)}\cdot\left[(1-\nu_g)\varepsilon_c + \nu_g\left(\varepsilon_3+\varepsilon_z\right)\right] \tag{5.2}$$

where σ_c is the circumferential stress using a cylindrical polar coordinate system, ν_g is Poisson's ratio of geocell, M_m is the mobilised geocell modulus at a different number of cycles, ε_c and ε_3 are the circumferential and radial strains. For a plane strain condition ($\varepsilon_2 = 0$), Eq. (5.2) can now be simplified to:

$$\sigma_c = \frac{M_m}{(1+\nu_g)(1-2\nu_g)}\left[(1-\nu_g)\varepsilon_c + \nu_g\varepsilon_3\right] \tag{5.3}$$

Referring Figure 5.1 (a), additional confinement can be presented as:

$$\Delta\sigma_3^{'} = \frac{2\sigma_c}{D} \tag{5.4}$$

where D = diameter of an equivalent circular area of the geocell pocket.

In the current analysis a constant ratio between circumferential and lateral strains was assumed for a given deflection profile [see Figure 5.1 (a & b)] in a plane strain condition [i.e. $\varepsilon_c = k.\varepsilon_3$].

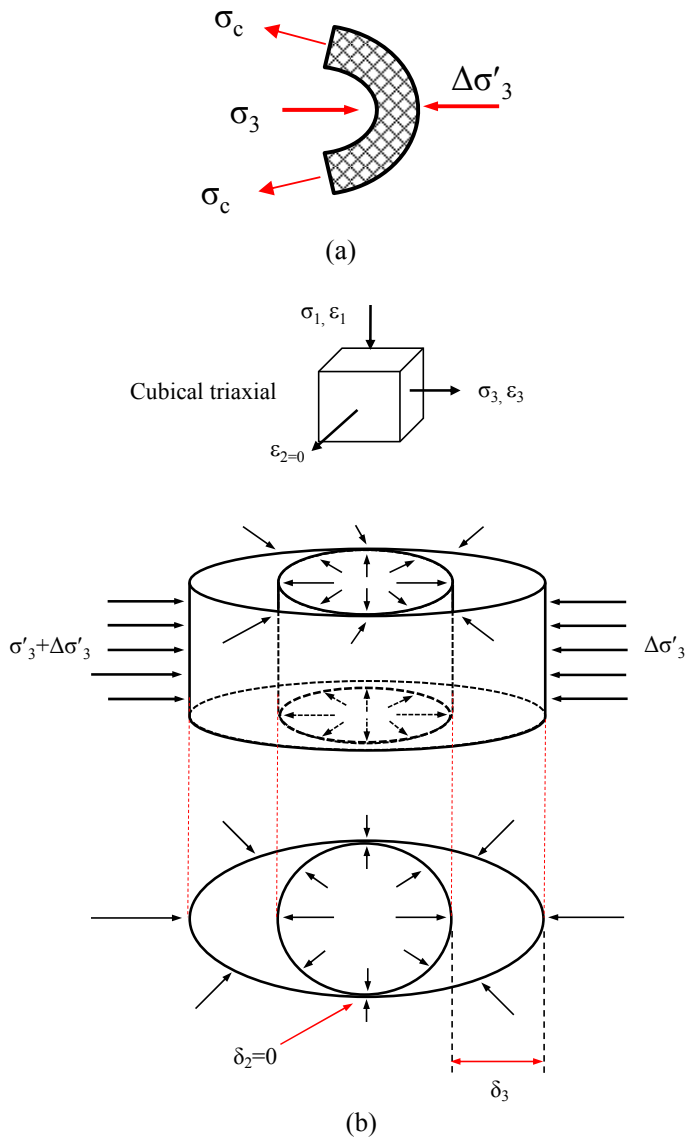

Figure 5.1. (a) Stress profile and (b) deflection profile of geocell under plane strain environment (modified after Indraratna et al. 2015)

By substituting Eq. (5.3) in Eq. (5.4), the additional confinement stress $\Delta\sigma_3'$ for a geocell mattress can be presented as:

$$\Delta\sigma_3^{'} = \frac{2M_m}{D}\frac{\left[(1-\nu_g)k+\nu_g\right]}{(1+\nu_g)(1-2\nu_g)}(-\varepsilon_3) \tag{5.5}$$

where $\Delta\sigma_3'$= the additional confining stress (kPa) in each pocket, k = the ratio $(k = \varepsilon_c^p / \varepsilon_3^p = 0.45)$. The total strain rate $d\varepsilon_{ij}$ is the sum of a plastic, non-reversible component $d\varepsilon_{ij}^p$ and the elastic, reversible component $d\varepsilon_{ij}^e$ as indicated by e and p respectively, such that

$$d\varepsilon_3 = d\varepsilon_3^e + d\varepsilon_3^p \tag{5.6}$$

The lateral elastic strain ε_3^e can be expressed as $\nu_g\varepsilon_1^e$. The elastic strain rate $d\varepsilon_3^e$ is:

$$d\varepsilon_3^e = \frac{\nu_g\sigma_{cyc}}{dM_R} \tag{5.7}$$

By using the dilatancy equation (5.7), the plastic strain rate $d\varepsilon_3^p$ can be defined as:

$$-d\varepsilon_3^p = d\varepsilon_1^p\left(\frac{1+\sin\psi_m}{1-\sin\psi_m}\right) \tag{5.8}$$

By substituting equations (5.7) and (5.8) into the differential form of equation (5.5), an additional confining pressure for a geocell mattress can be obtained as:

$$d\left(\Delta\sigma_3^{'}\right) = \frac{2M_m}{D}\cdot\frac{\left[(1-\nu_g)k+\nu_g\right]}{(1+\nu_g)(1-2\nu_g)}\cdot\left[-\frac{\nu_g\sigma_{cyc}}{dM_R}+d\varepsilon_1^P\times\left(\frac{1+\sin\psi_m}{1-\sin\psi_m}\right)\right] \tag{5.9}$$

By extending the relationship for cyclic loading proposed by Indraratna and Nimbalkar (2013), the permanent vertical strain can be defined in terms of the load cycles as:

$$\varepsilon_1^P = \varepsilon_{1,1}^P \left(1 + a \log N + 0.5b \log N^2\right) \tag{5.10}$$

where $\varepsilon_{1,1}^p$ is the settlement of the granular material after the first load cycles, and a and b are the empirical coefficients representing the stable and unstable zones respectively. By differentiating Eq. (5.10) and rearranging Eq. (5.9), the equivalent additional confinement in a geocell mattress can be proposed by:

$$\Delta\sigma_3^{'} = \int_{N=1}^{N=N_{\lim}} \frac{2M_m}{D} \cdot \frac{\left\lfloor (1-\nu_g)k + \nu_g \right\rfloor}{(1+\nu_g)(1-2\nu_g)} \cdot \left[-\frac{\nu_g \sigma_{cyc}}{dM_R} + \varepsilon_{1,1}^P \left(\frac{a^{'}}{N} + \frac{b^{'}}{N} \right) \right] \times \left(\frac{1+\sin\psi_m}{1-\sin\psi_m} \right) dN \tag{5.11}$$

where N_{lim} is the number of cycles required to reach the stable zone. In the proposed model an additional confining pressure $\Delta\sigma_3'$ can now be determined by integrating Eq. (5.11) and considering the properties of unreinforced subballast (i.e. ψ_m and $\varepsilon_{1,1}^p$) along with M_m and D for a geocell mattress at the desired number of load cycles, confining pressure, and frequency.

5.4 Model prediction

Unlike other models available in the literature (Yang and Han 2013), in the proposed model the geocell modulus (M_m) and angle of dilation (ψ_m) were not assumed to be constant during the test. Accordingly, in a geocell reinforcement, the mobilised angle of dilation decreased as the tensile strength increased with respect to the number of cycles. For a given cyclic stress (σ_{cyc}), by considering the variation of the resilient

modulus (M_R) and the dilation angle (ψ_m) against the number of cycles (N), the current model could provide more accurate predictions than the model proposed by Henkel and Gilbert (1952). To highlight how additional confinement can affect reinforced specimens, the normalized additional confinement is defined by a dimensionless ratio as:

$$k_\sigma = \frac{\Delta\sigma_3^{'}}{\sigma_3^{'}} \tag{5.12}$$

where $\Delta\sigma_3'$ is the calculated additional confinement (kPa) and σ_3' is the applied confining pressure (kPa). The comparison between $\Delta\sigma_3'$, determined by the proposed model and that of Yang and Han (2013) is presented in Figure 5.2. The current model predicts a higher confining pressure initially than Yang and Han (2013). This can be justified because the modulus (M_m) mobilised under cyclic loading reaches a higher value initially, and then an ultimate value depending on the strains is reached during cyclic loading. The model by Yang and Han (2013) also has some limitations: (i) it ignored the effect of frequency, and (ii) it ignored variations in the resilient modulus and the dilation angle against the number of load cycles. The present model incorporates these variations in the mobilised modulus (M_m) and the angle of mobilised dilatancy (ψ_m) under varying frequency and load cycles (N). The input parameters used to compare the current model and the model proposed by Yang and Han (2013) is summarised in Table 5.1.

Table 5.1. Input parameters for geocell-reinforced subballast

Input parameter	Current model	Model by Yang and Han (2013)
Frequency, f (Hz)	20, 30	-
Confining pressure, σ_3' (kPa)	σ_3' = 5, 10	σ_3' = 5, 10
Sample diameter, D (cm)	0.24	0.24
Geocell height, h (mm)	150	150
a'	0.55	-
b'	0.85	-
$d\varepsilon_o/d\varepsilon_r$	-	50
ρ''	-	1000
β''	-	0.2
Geocell modulus, Mm (kN/m)	328 (ultimate) 600 (initial) #	328
k_1	3.5 (f = 10 Hz)	3.5
	4.375 (f = 20 Hz)	
	5.25 (f = 30 Hz)	
k_2	5.75 ($10 \leq f \leq 30$ Hz)	5.75
k_3	- 0.1 ($10 \leq f \leq 30$ Hz)	- 0.1
Poisson's ratio (ν)	0.3	-
Number of cycles, N_{lim}	N = 500,000	N = 500,000

It should be noted that the geocell modulus varies from the initial to the maximum value depending on the strains reached during each stage of cyclic loading. As shown in Figure 5.2, geocell mattress offers maximum additional confinement at σ_3' = 5 kPa

at any given frequency. As expected, by increasing the confining pressure (σ'_3 = 20-30 kPa), the value of $\Delta\sigma'_3$ decreased by about 40 % at a given frequency.

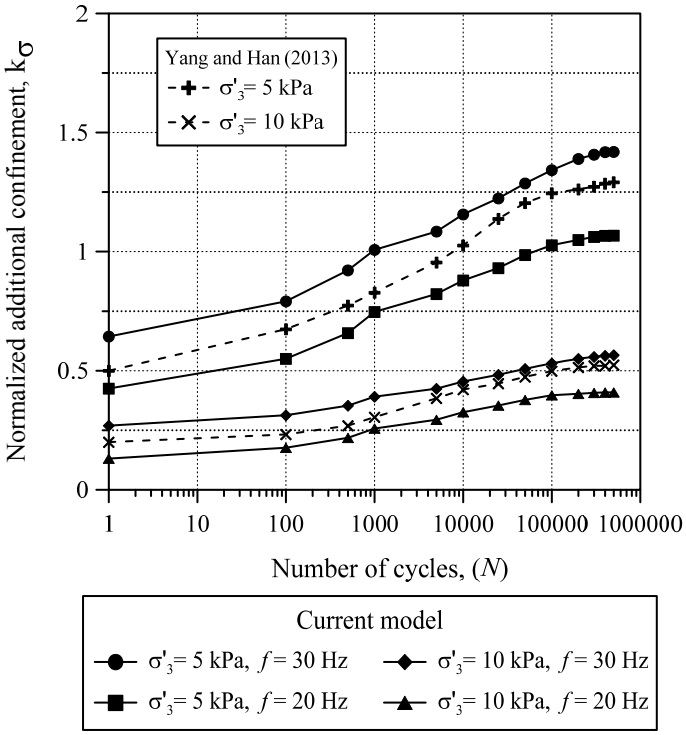

Figure 5.2. Comparison of additional confinement present study with the model by Yang and Han (2013) (k_σ) for reinforced subballast at *N*=500,000 cycles (test data vs. model predictions) (data sourced from Indraratna et al. 2015 with permission from ASCE)

Figure 5.4 shows that the frequency has a pronounced influence on $\Delta\sigma'_3$, such that increasing the frequency led to an increase in k_σ. As a result, the apparent confining pressure applied to the sample increased as:

$$\sigma'_{3(effective)} = \sigma'_{3(apparent)} + \Delta\sigma'_3 \tag{5.13}$$

It should also be noted that the proposed mechanistic approach Eq. (5.11) can be applied for a wide range of material and stress levels.

The superiority of the current model over conventional models used by researches can be highlighted by comparing with models available. Figure 5.3 shows the normalised values of $\Delta\sigma_3'$ that were predicted based on the model proposed by Henkel and Gilbert (1952). In this prediction the parameters of M and D and ε_a are assumed to be constant. As a results, the magnitude of predicted additional confinement is expected to be much smaller than the actual $\Delta\sigma_3'$ induced by the geocell.

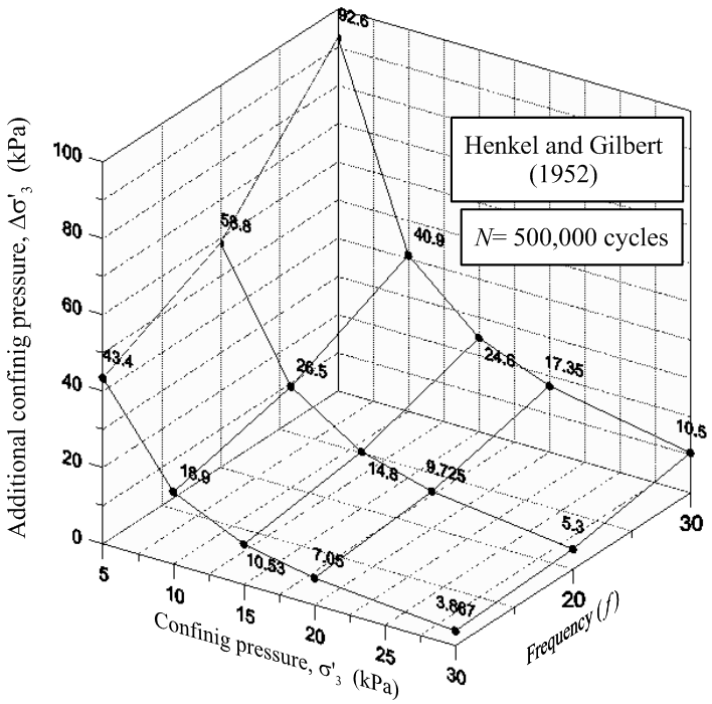

Figure 5.3. Normalised additional confinement (k_σ) for reinforced subballast at N=500,000 cycles

Figure 5.4 presents the values of normalised additional confinement in the geocell mattress. A comparison between the measured data and the extra confinement predicted by using geocell reveals that the analytical model proposed in the current study (Figure 5.4) was accurate enough.

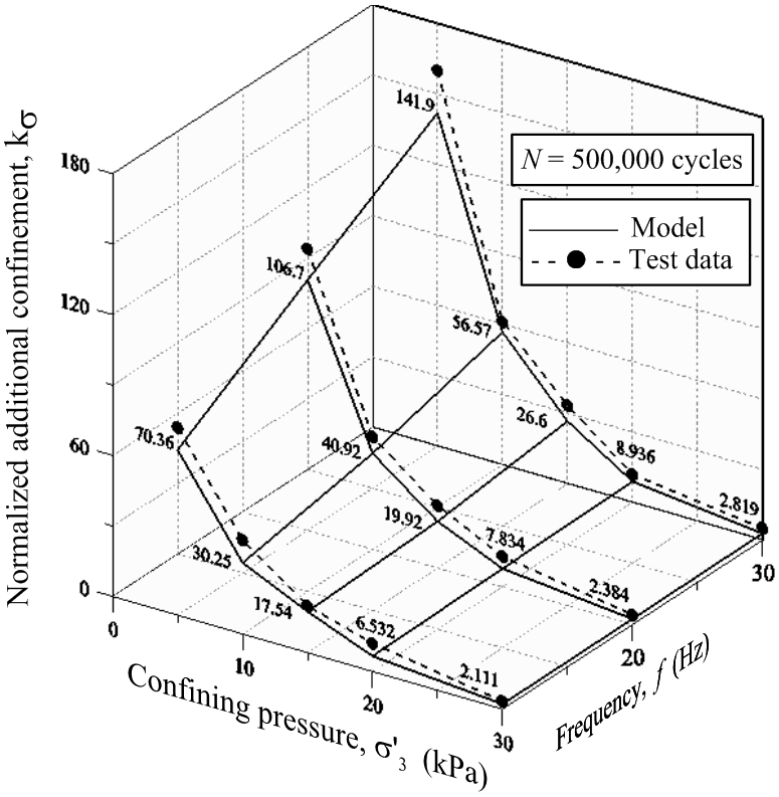

Figure 5.4. Normalised additional confinement (k_σ) for reinforced subballast at N=500,000 cycles (test data vs. model predictions) (data sourced from Indraratna et al. 2015 with permission from ASCE)

The impact of additional confining pressure on the performance of subballast can best be evaluated by comparing the mobilised friction and mobilised dilatancy angle in the unreinforced and geocell-reinforced subballast. As shown in Figure 5.5 increasing σ_3' reduced the mobilised friction angle and dilatancy angle. However the

degree of reduction in geocell-reinforced subballast was higher than the unreinforced subballast. This can be justified based on additional confinement induced by the cellular mattress, which confines infill materials and arrests excessive lateral spreading; hence the substantial reduction in the dilatancy angle. As shown, the impact of geocell was diminished by increasing the σ_3', which in turn minimised $\Delta\sigma_3'$.

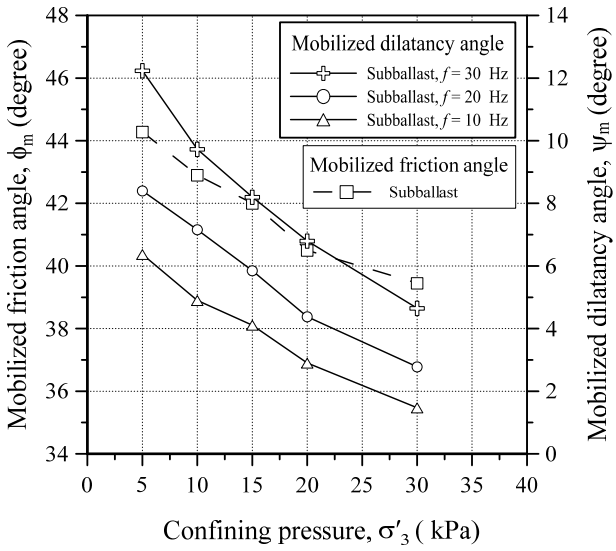

Figure 5.5. Friction and dilatancy angle in unreinforced subballast at different confining pressure (σ_3')

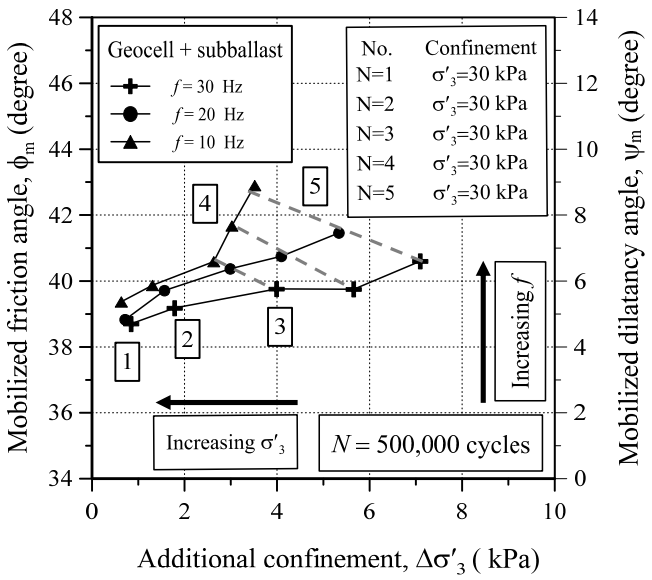

Figure 5.6. Variation of mobilised friction angle and dilatancy angle vs. additional confinement ($\Delta\sigma_3'$)

5.5 Practical Implications

The outcome of this study is certainly valuable for constructing or modernising rail track on subgrade material with low shear strength and insufficient confinement. Indeed the results of this current study proved that by using geocell reinforcement, the subballast can be confined to the degree required for enhanced track performance, including increased train speeds. This study has shown that geocells can develop maximum additional confinement ($\Delta\sigma_3'$), and thus a significant improvement in track performance at a very low confining pressure of ($\sigma_3' \leq 15$ kPa) that is otherwise available in the field. Furthermore, geocells also improved the vertical and lateral stability (i.e., increased the resilient modulus, reduced the angle of dilatancy, and reduced the vertical deformation) of tracks.

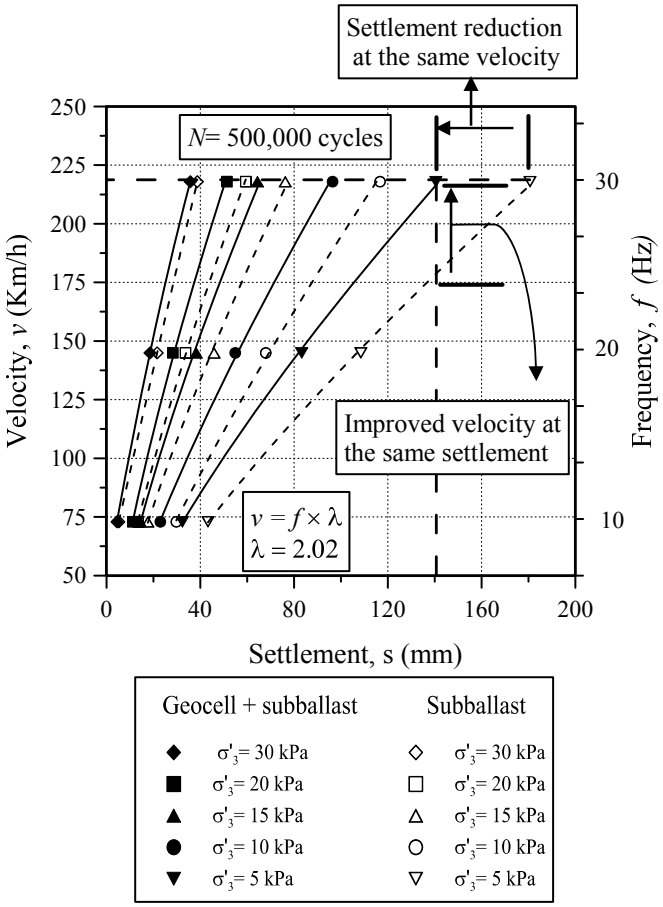

Figure 5.7. Variation of velocity and subballast settlement (data sourced from Indraratna et al. 2015 with permission from ASCE)

The frequency-velocity relationship described earlier was used to obtain the train speed at the corresponding frequency of cyclic loading. Figure 5.7 shows the variation between train speed (and frequency) and settlement at a given number of load cycles (N = 500,000). It is evident that using geocells can decrease settlement at the same confining pressure and frequency, and furthermore, a train with a much higher speed can be allowed on track with reinforced subballast at a given confining pressure and allowable settlement, as shown in Figure 5.7.

To highlight the influence of additional confinement on the performance of subballast, the improved resilient modulus [$F(M_R)$], settlement reduction ratio [$F(S_{a,p})$], and speed improvement factor (F_v) are plotted against the k_σ, shown in Figure 5.8. The relative increase in $F(M_R)$ helps to decrease the value of $F(S_{a,p})$, and the associated increase in train speed. The $F(M_R)$ shows a rapid increase followed by a dramatically decreasing rate at higher values of k_σ, which implies the subballast was stiffer as a result of using geocells. The percentage decrease in settlement and percentage increase in train speed follow the same trend. This implies that train speeds can be increased substantially by using geocells due to increasing lateral restraints. Following equation can be proposed by performing a regression analysis on the test data to predict the ratio of improved speed, and it is given below:

$$F_v = 4.0928\ln(k_\sigma) + 22.089 \tag{5.14}$$

By using this simple analytical approach, it is now feasible to predict the improvement in speed for a given rail track based on the additional confinement pressure obtained from Eq. (5.11), when it is stabilised with geocells at any given confining pressure.

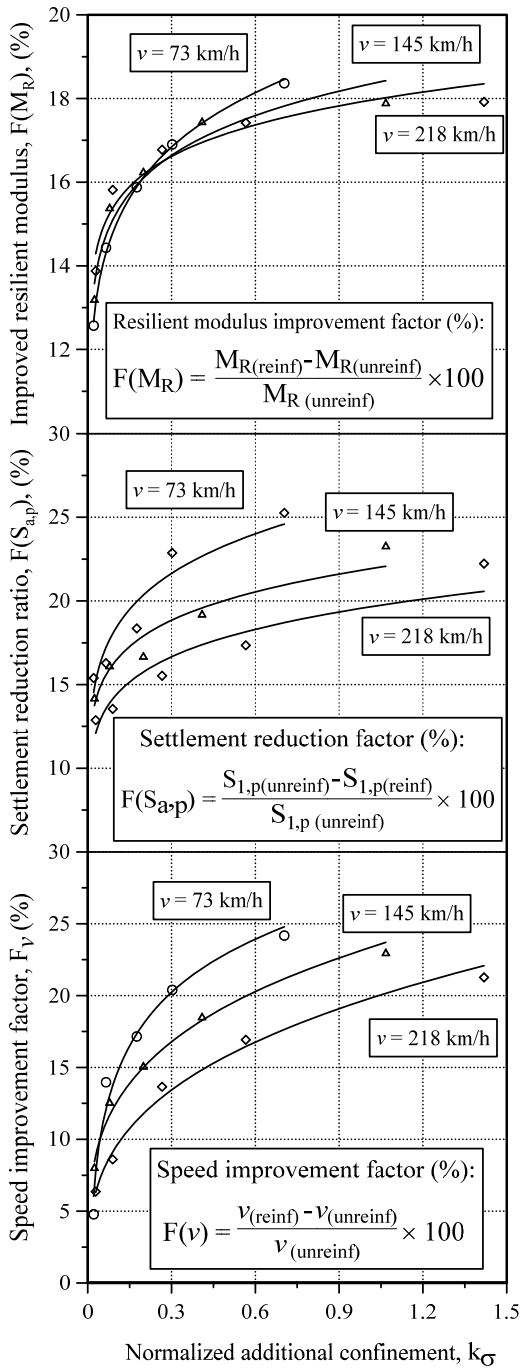

Figure 5.8. Normalised additional confinement (k_σ) against variation of (a) settlement reduction factor (Fs), resilient improvement factor $F(M_R)$ and speed improvement factor (F_v) for geocell-reinforced subballast at given velocity (data sourced from Indraratna et al. 2015 with permission from ASCE)

5.6 Summary

A new analytical model based on Hook's law was proposed for geocell-reinforced subballast under cyclic loading. Hoop tension theory was used to include the additional confining pressure induced by the geocell. The model described important factors such as the number of cycles, the mobilised friction angle, and the mobilised dilatancy angle. The model's predictions were influenced by the test environment, the apparent confining pressure, frequency, and the number of cycles. Also model predictions are in decent agreement with the laboratory outcome. The predictions were compared with the models available in the literature. Using the model's prediction, the permissible train speed as a speed improvement factor for geocell-reinforced subballast was therefore proposed.

CHAPTER 6

6. FEM SIMULATION OF GEOCELL-REINFORCED SUBBALLAST UNDER CYCLIC LOADING

6.1 General

Understanding the performance of geocell reinforcement under cyclic loading is the key requirement needed for its design and application in ballasted rail track. The development of a numerical model is inevitable in order to establish proper design guidelines based on safety and economic considerations. The performance of geocell mattress with different types of infill soil has already been analysed under monotonic loading (Saride et al. 2009; Yang et al. 2010; Wang et al. 2013). The equivalent composite approach has been used to model geocell-reinforced soil in a 2-D environment (Bathurst and Knight 1998; Madhavi Latha and Somwanshi 2009; Hegde and Sitharam 2013; Mehdipour et al. 2013). By modelling geocell-reinforced soil as a new layer of soil with higher shear strength, its behaviour has effectively been investigated. Moreover, the performance of geocell-reinforced soil in 3-dimnesional framework under monotonic loading has been investigated (Hegde and Sitharam 2014). However, there is very limited number of studies that investigated the influence of geocell mattress on railway substructure under cyclic loading are available (Leshchinsky and Ling 2013). In this chapter, applications of finite element techniques to investigate effectiveness of geocell reinforcement on the railway substructure are presented. This numerical approach is calibrated and validated against the results of large-scale laboratory tests.

6.2 Finite element analysis

6.2.1 Unit cell geometry

Generally, due to easier and faster developing, a two-dimensional (2-D) model has gained more popularity than the three-dimensional (3-D) model. However, due to unique shape of the geocell mattress (honeycomb like structure), a 2-D model cannot accurately capture the additional confinement developed through circumferential strains, that are mobilised along the geocell walls. The current model simulates the behaviour of geocell-reinforced media subjected to cyclic loading in 3-D condition in plane strain condition. This unit cell geometry was selected based on the Australian standard railway substructure. The size of the specimen represents the effective sleeper length (l = 800 mm) and distance between two adjacent sleepers (tie in North America) (b = 600mm) with a depth of h = 450 mm, as shown in Figure 6.1. The cyclic loading stress caused by a train and exerted beneath the ballast, was applied directly onto the subballast. As result, no ballast or sleeper (tie) was considered in this simulation. Due to variation of subballast thickness, a total of 450 mm thickness was considered for the subballast and subgrade. Lateral movement in the direction of intermediate stress ($\varepsilon_2 = 0$) was prevented, while the subballast was free to move in direction of the minor principal stress ($\varepsilon_3 \neq 0$).

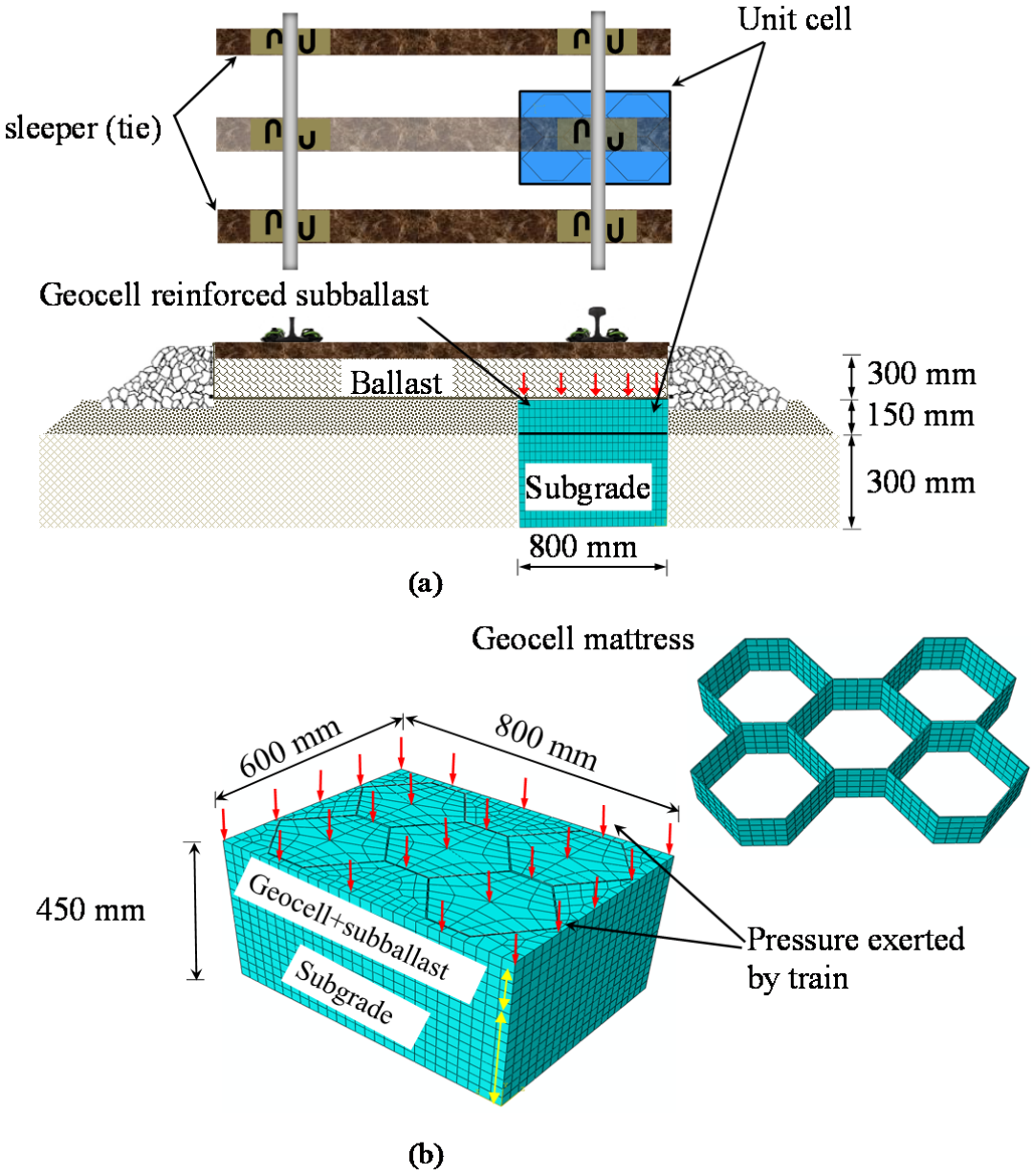

Figure 6.1. Finite element idealisation of typical rail environment

6.2.2 Material properties

An elasto-plastic material with non-associative behaviour was considered for the subballast and subgrade. In order to capture the plastic behaviour of subballast and subgrade the Drucker-Prager yield criterion was used. The strength parameters (i.e., ϕ, ψ) were obtained from the PSPTA under cyclic loading (Indraratna et al. 2015).

To model geocell mattress, a linear elastic-perfectly plastic material was used. The elastic properties of the geocell strips had been determined in chapter three and were then deployed in ABAQUS. Hexagonal cells were created to provide a more uniform stress distribution that was close to the actual curvature of geocell mattress available in the field. In order to apply a uniform pressure to the subballast (i.e. axial load and lateral confining pressure), plats with linear elastic were modelled. A summary of the material properties is provided in Table 6.1. Due to the time required to run this simulation under cyclic loading at a large number of cycles, all the simulations were only performed up to 10,000 cycles.

Table 6.1. Finite element properties of subballast and geocell used in this study

Material	**Subballast**	**Subgrade**	**Geocell**	**Plate**
Friction angle (degrees)	39	39	–	–
Angle of dilation (degrees)	9	9	–	–
Elastic modulus (MPa)	7	7	300	200,000
Poisson's Ratio	0.3	0.3	0.3	0.3
Density (kg/m^3)	1955	1955	950	2000

6.2.3 Boundary conditions and Mesh size justification

In order to simulate railway field conditions, plane strain condition was applied to the model. During the simulation, vertical boundaries in the direction of the intermediate principal stress (σ_2') were constrained. However, the model was allowed to move in the direction of the major (σ_1) and minor principal stresses (σ_3'), respectively. Moreover, the base of the model was restricted to any displacement, as shown in Figure 6.2.

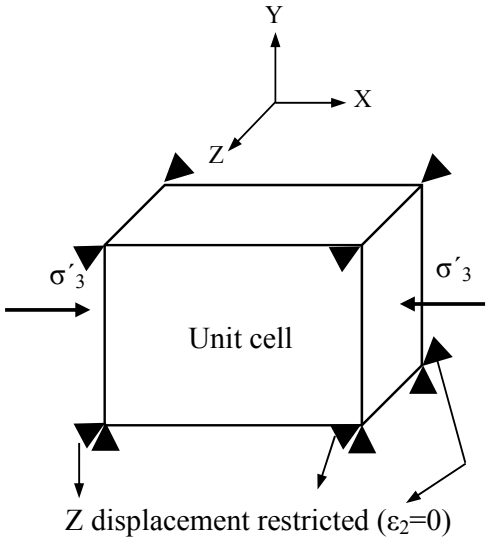

Figure 6.2. Typical boundary condition for unit cell

In this investigation, the whole foundation was modelled. In order to obtain the optimum size mesh, several models with different number of elements were modelled. A sensitivity analysis was carried out to determine the density of the mesh, as shown in Figure 6.3. The vertical settlement of reinforced subballast with different number of elements were compared at N = 1000 cycles, as shown in Figure 6.4. The results showed that the by increasing the number of elements, the vertical displacement (S_V) was improved. Nevertheless, the axial displacement improved slightly by increasing the number of elements beyond 9380. As result, a model with

9380 elements was selected to simulate the performance of the subballast in this study.

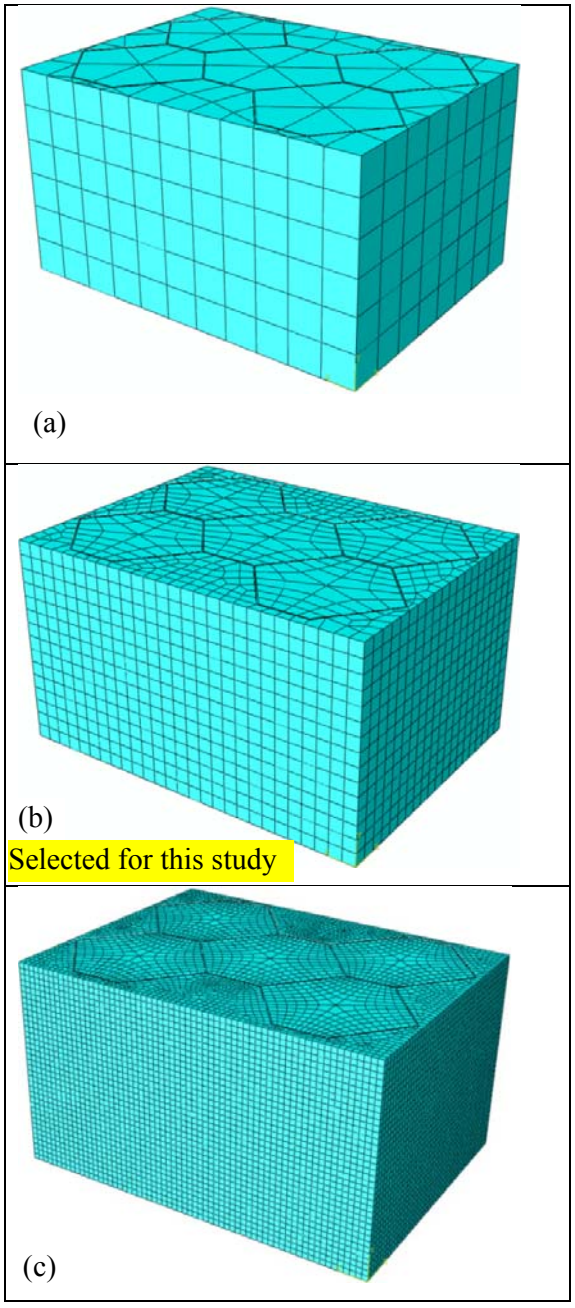

Figure 6.3. Unit with different number of elements: (a) 976 Coarse, (b) 9380 intermediate FE model and (c) 99708 fine

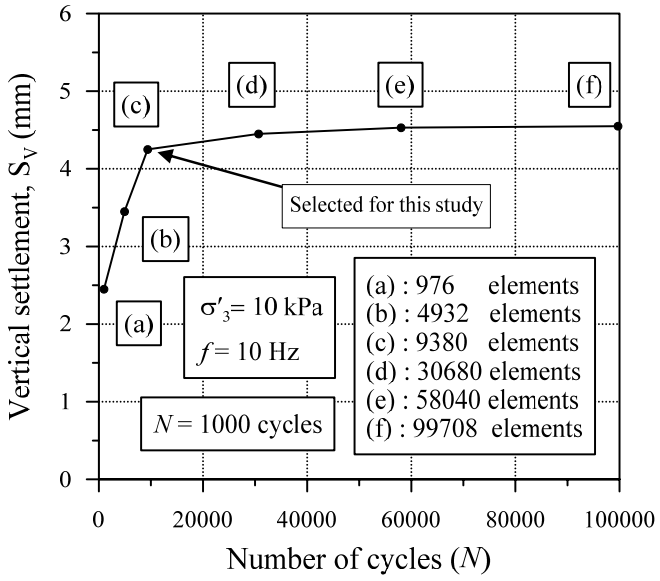

Figure 6.4. Vertical settlement predicted by FE model with different number of elements

The reinforced model was created from 9380 elements and 12624 nodes. The material represented by C3D8R was due to the geometry of the unit cell used in this simulation. The interaction between subballast and geocell strips was modelled with contact elements, including a hard normal contact (Leshchinsky and Ling 2013). Given the highly random nature of particle orientations within the subballast assembly, it was assumed that the angle of shearing resistance between the aggregates and the membrane in a geocell mattress was isotropic, considering that the membrane texture is usually uniform. As a result, the interface contact for both horizontal and vertical direction was modelled assuming 2/3 of the interface friction angle (ϕ = 39 degree).

6.2.4 Loading condition

In order to have uniform deformation, a constant confining pressure was applied to the unit cell to simulate the mean pressure due to the geostatic stresses inherent in a railway track. For the computation of additional confinement, proposed model (discussed in Chapter 5), was incorporated in FEM ($5 \leq \sigma_3' \leq 30$ kPa). Subsequently, mean stress was applied onto the top of the specimen. The mean stress was chosen to provide the most critical scenario of stress that could be applied to the subballast. By calculating and comparing different approaches, a magnitude of σ_{mean} = 104 kPa was selected and applied onto the top of the subballast (Indraratna et al. 2015).

After completing the static loading, a cyclic load was superimposed onto the monotonic loading at different confining pressures. During this cyclic loading, each load cycle was returned to full unloading to represent a passing train wheel. Unlike the popular approach such as the equivalent cyclic load, which only considers the performance of the soil specimen just at maximum amplitude, a cyclic load with a periodic and positive full-sine waveform was applied to the unit cell. The cyclic load was performed in a stress controlled mode with a frequency of f = 10 Hz. The maximum and minimum applied amplitude were 166 kPa and 41 kPa respectively, as shown in Figure 6.5.

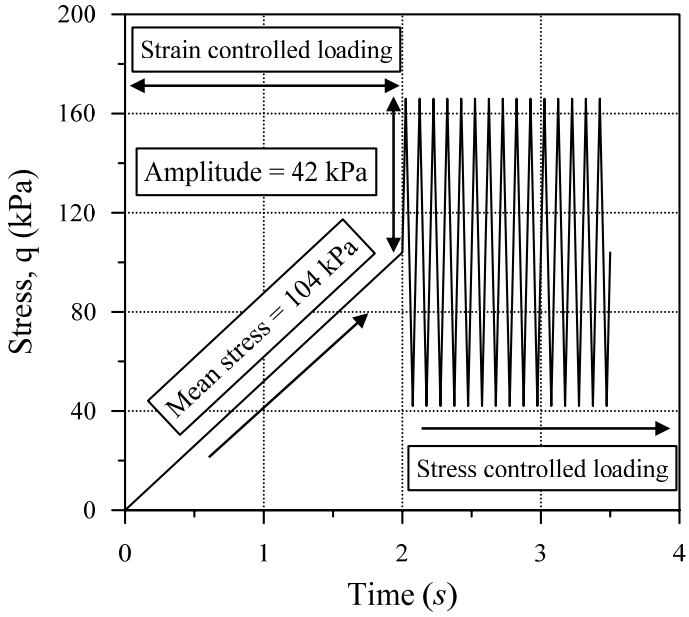

Figure 6.5. Schematic illustration of cyclic loading

6.3 Results and Discussions:

6.3.1 Axial deformation

Figure 6.6 shows the axial deformation of an unreinforced specimen at a confining pressure of σ_3' = 10 kPa under cyclic loading with a frequency of f = 10 Hz and a number of cycles where N = 10,000. As this figure shows, the top layer of the soil, which is in direct contact with the footing, experienced the maximum and almost uniform vertical deformation (S_V = 8.45 mm). The magnitude of vertical displacement decreased deeper down. From this, it can be concluded that the optimum location for a geocell mattress is directly beneath the foundation where the cyclic stress is at a maximum.

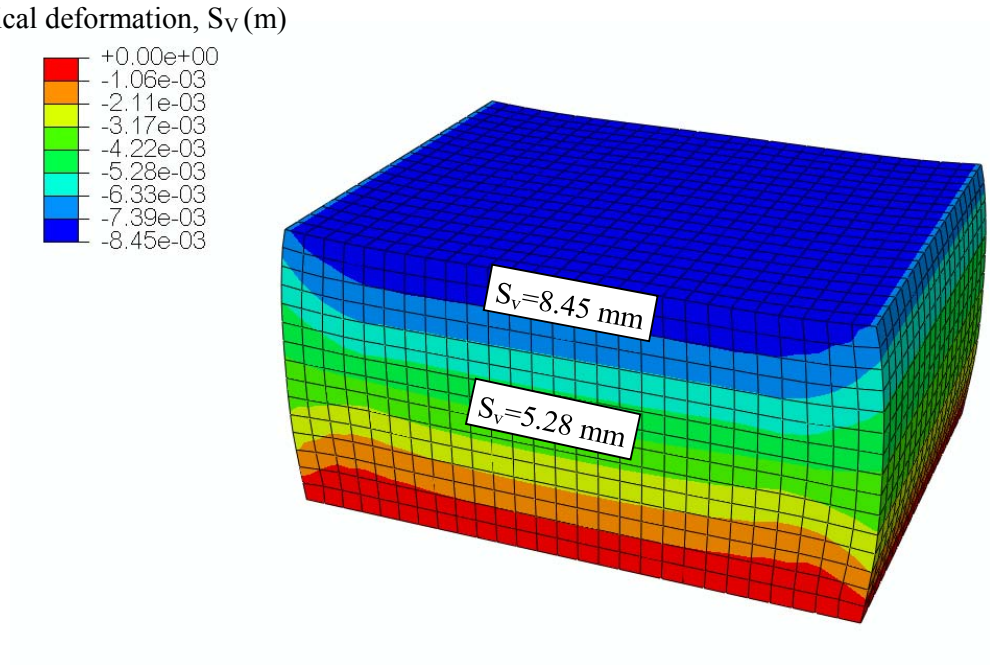

Figure 6.6. FEM predicted vertical displacement of unreinforced subballast

Figure 6.7 shows the vertical displacement of a reinforced specimen. The figure shows that placing a geocell mattress on top of the specimen reduced the magnitude of axial deformation in reinforced subballast quite significantly. As result, in reinforced specimen, the degree of axial deformation transferred to the soil beneath the geocell reinforcement layer was much less than in the unreinforced subballast. Maximum vertical displacement occurred at the edge of the specimen where the granular material was outside of the cellular mattress; nevertheless the axial displacement at the centre of the geocell mattress was less. This implies that geocell reinforcement effectively increased the stiffness of the subballast, while substantially reducing settlement under the track. Unlike the unreinforced specimen (S_v = 5.28 mm), the magnitude of vertical displacement was significantly reduced in the soil under the reinforced layer (S_v = 1.71 mm). This indicates the effectiveness of the geocell for reducing the vertical stress in the lower layer of soil and hence reducing vertical displacement.

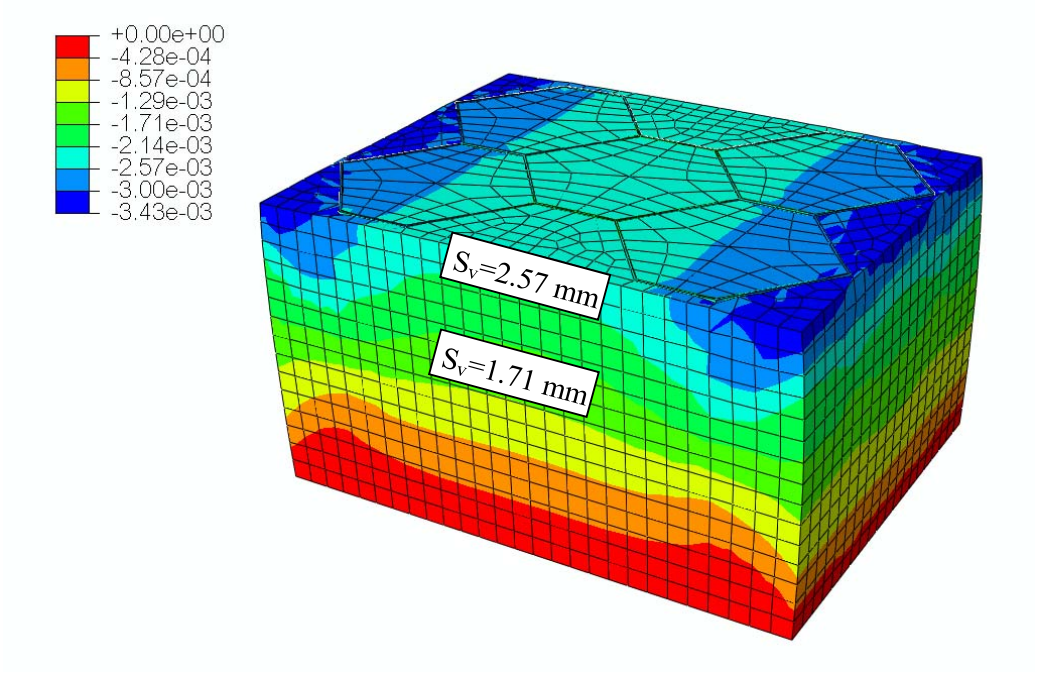

Figure 6.7. FEM predicted vertical displacement of geocell-reinforced subballast

In order to compare the experimental and numerical results, the vertical deformation (S_V) of unreinforced and geocell-reinforced subballast are plotted against the number of cycles for different confining pressures, and f = 10 Hz, as shown in Figure 6.8 and Figure 6.9. As shown in Figure 6.8, by applying cyclic loading, unreinforced subballast undergoes a substantial vertical deformation (S_V). Based on the results, the maximum S_V occurred in the early stage of loading ($N \leq$ 10,000 cycles). The rate of increment was diminished as N increased. The numerical and experimental results both confirmed that the magnitude of S_V decreased by increasing σ_3'. As Figure 6.8 shows, the specimen with σ_3' = 10 kPa, experienced a vertical displacement of about S_V = 17.5 mm. Moreover, the model prediction and the laboratory results showed that the degree of S_V decreased as the confining pressure increased to σ_3' = 20 kPa.

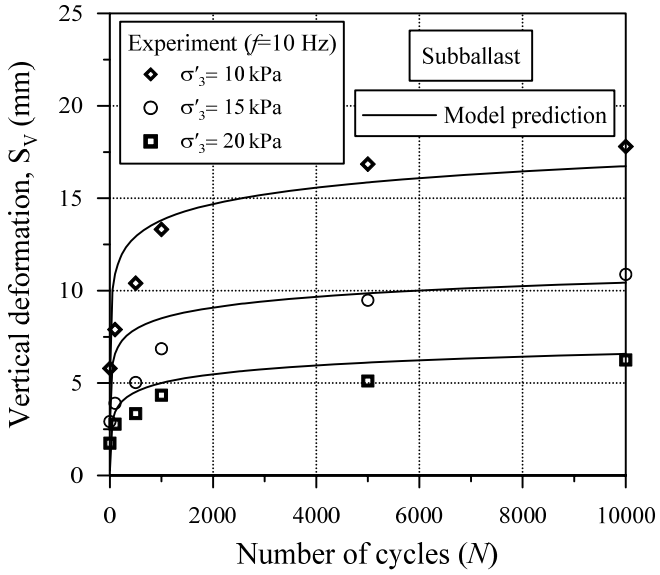

Figure 6.8. Vertical deformation of subballast against the number of cycles (N): laboratory measurements vs. model predictions

Nevertheless, the magnitude of S_V was markedly reduced in the reinforced specimen (S_V < 12.5 mm), as shown in Figure 6.9. By comparing the experimental and numerical results it can be seen that geocell had the highest effect on the specimens at a lower confining pressures ($\sigma_3' \leq 15$ kPa). Accordingly, at a confining pressure of $\sigma_3' = 20$ kPa, the effectiveness of reinforcement decreased and the performance of the unreinforced and reinforced specimens was almost similar.

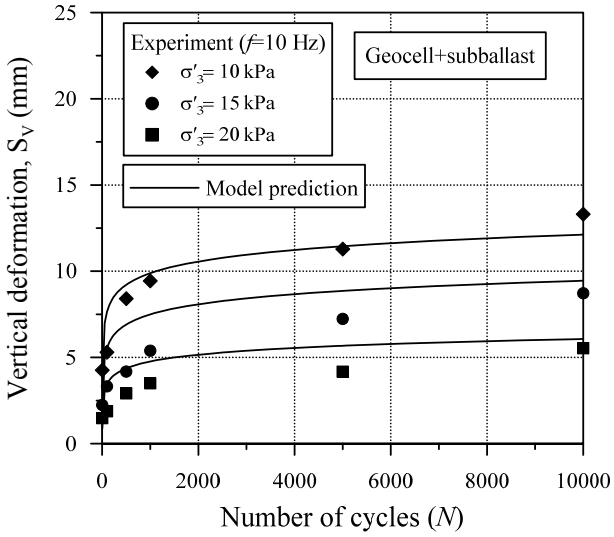

Figure 6.9. Vertical deformation of geocell- reinforced subballast against number of cycles (N): laboratory measurements vs. model predictions

6.3.2 Lateral spreading

Figure 6.10 shows the lateral spreading (S_L) of unreinforced subballast at a confining pressure of σ_3' = 10 kPa and a frequency of f = 10 Hz at different heights. The figure shows that due to the very small degree of σ_3', lateral spreading started from directly beneath the footing and increased in magnitude as the depth of the specimen increased, and as the number of cycles (N) increased. A maximum magnitude of S_L occurred at subballast and subgrade interface, at a depth of about h = 250-300 mm, while the magnitude of S_L decreased at a lower depth (h < 200 mm). A similar trend occurred at a different number of cycles. Marginal spreading occurred at the base of the foundation (h = 0).

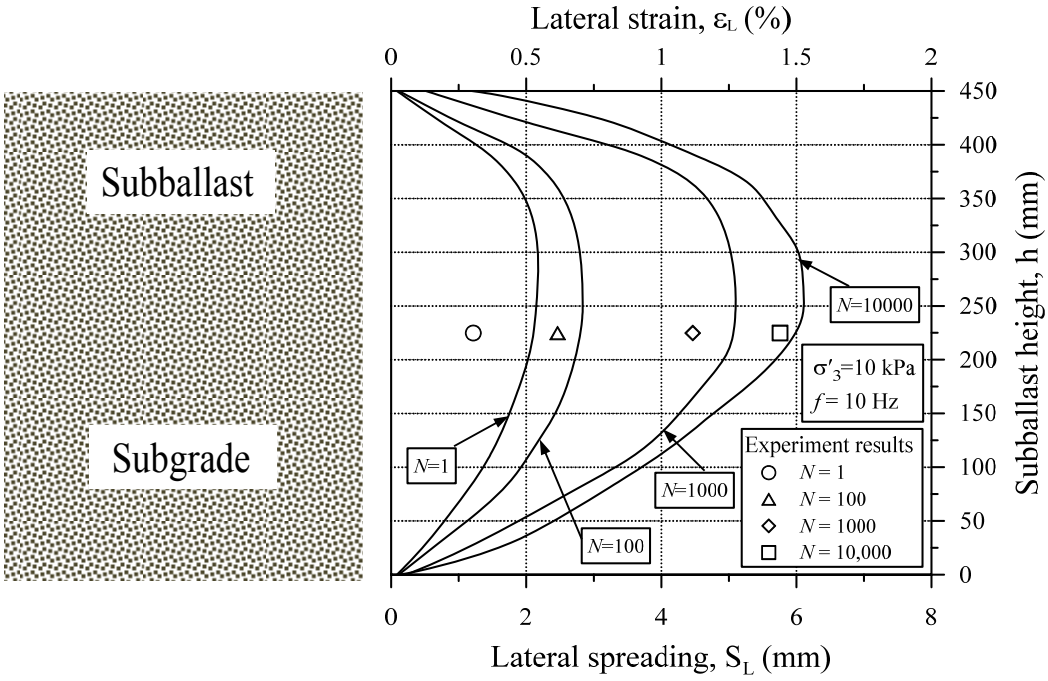

Figure 6.10. Typical lateral deformation profile of unreinforced subballast

The benefit of geocell can be highlighted in terms of reducing excessive lateral spreading, as shown in Figure 6.11. As shown in this figure, all of the lateral spreading of subballast was successfully arrested by the geocell mattress. This figure also shows that the degree of S_L was markedly minimised for the unreinforced subballast beneath the reinforced layer. Relatively, small degree of S_L observed beneath the interface of the subballast and subgrade which indicated that geocell effectively improves the performance of the layer of reinforced soil and the unreinforced soil beneath the reinforced soil as well. This figure also shows that most of the subballast in the unit cell remained stable and did not experience any lateral deformation, apart from at the edge of the specimen. As a result, the specimen became more rigid as a result of utilising geocell, hence helped to improve the performance of the subballast under cyclic loading. This indicated the effectiveness of a geocell mattress placed beneath the footing where the maximum degree of cyclic stress will be applied.

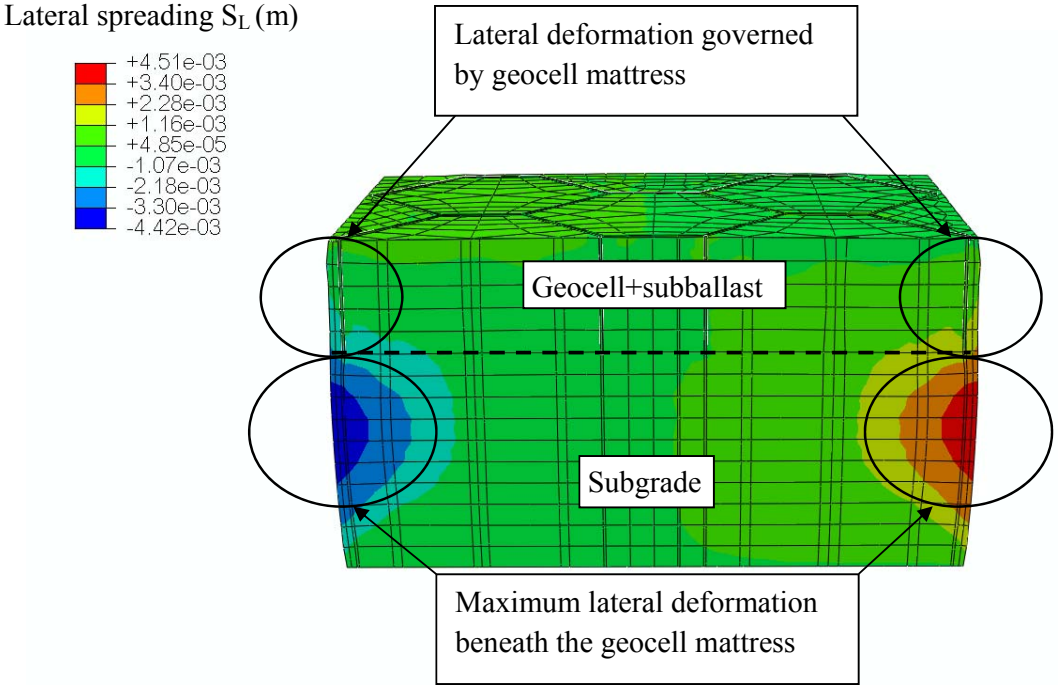

Figure 6.11. Illustration of typical lateral spreading of reinforced subballast predicted by FEM

The influence of the geocell mattress on the S_L is shown in Figure 6.12 by comparing the experimental and numerical results at f = 10 Hz and σ_3' = 10 kPa at different heights of subballast. This figure shows that, the reinforced layer remained almost stable, without any lateral spreading at any desired number of cycles (N). Moreover, lateral spreading started below the reinforced layer. As expected, the magnitude of lateral spreading was higher at the initial cycles (N) but the rate of increase decreased as the number of cycles (N) increased. However, the magnitude of S_L was much lower than the unreinforced specimen. A similar trend was also observed in previous study (Leshcninsky and Ling 2013). The maximum degree of S_L occurred at a depth of about h = 200-250 mm of the height of the specimen.

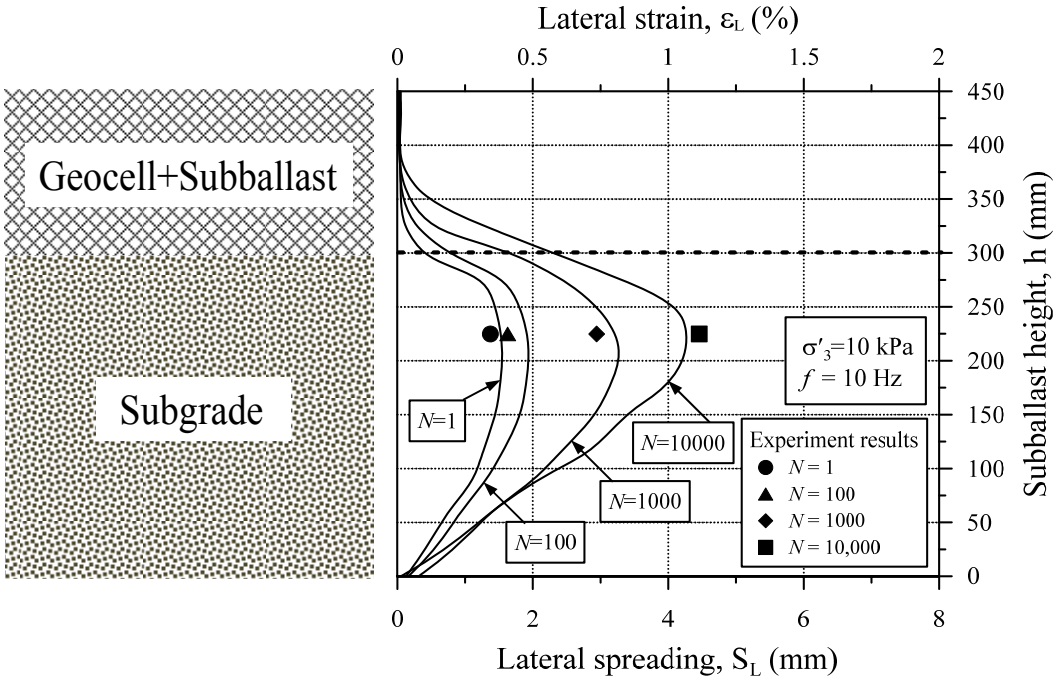

Figure 6.12. Typical lateral deformation profile of reinforced subballast at different depth and number of cycles

The beneficial use of geocell reinforcement can best be highlighted by comparing the experimental and numerical results of unreinforced and reinforced subballast for different confining pressures at f = 10 Hz, as shown in Figure 6.13 (a & b). As shown in Figure 6.13 (a), under a low confining pressure σ_3' = 10 kPa, the experimental and numerical results showed that the specimen experience excessive lateral deformation, but the degree of S_L decreased by increasing σ_3' > 10 kPa. However, in the reinforced specimen, the increment rates decreased compared to the unreinforced subballast. There was a marginal improvement at a higher confining pressure σ_3' = 20 kPa, indicating that this confining pressure was enough to minimise any excessive lateral spreading Figure 6.13 (b). The effectiveness of geocell reinforcement can also be illustrated by comparing the lateral spreading of reinforced subballast at σ_3' = 10 kPa with unreinforced subballast at σ_3' = 15 kPa. As Figure 6.13 (a & b) shows, the

reinforced specimen performed better than the unreinforced specimen even with higher σ'_3.

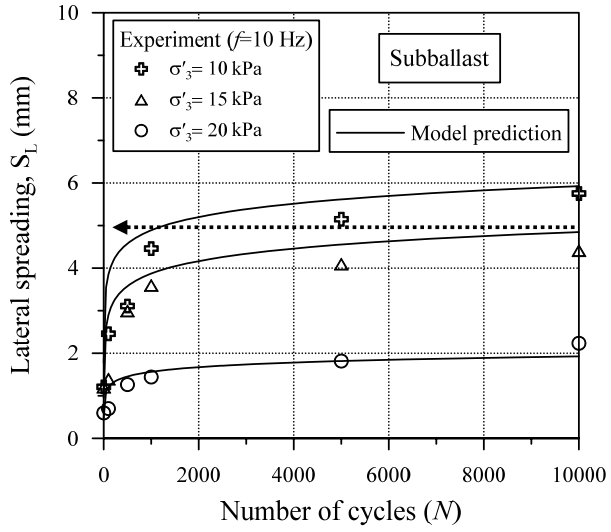

(a)

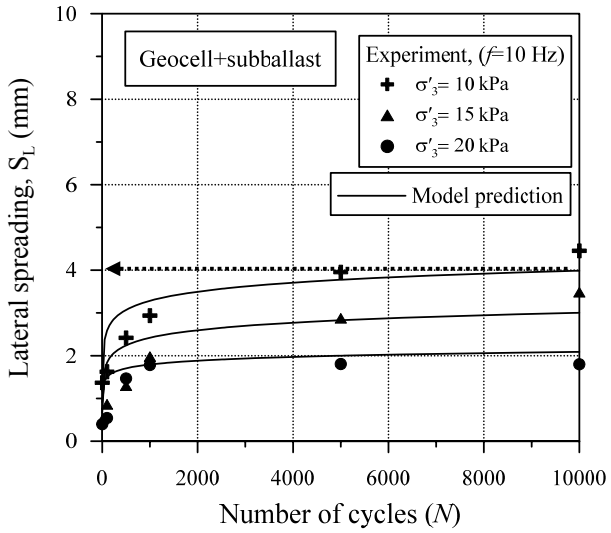

(b)

Figure 6.13. Lateral displacement of (a) unreinforced and (b) unreinforced subballast again number of cycles (N): laboratory measurements vs. model predictions

Based on the results obtained from the numerical simulation, the vertical (I_V) and lateral (I_L) deformation reduction factors are provided for different confining

pressures, as shown in Table 6.2. The maximum beneficial effect of geocell reinforcement can be seen at a lower confinement.

Table 6.2. A summary of I_L and I_S obtained from the numerical results.

Factor	**Frequency** f (Hz)	**Confining pressure**, σ'_3 (kPa)				
		5	**10**	**15**	**20**	**30**
Settlement reduction factor, I_S (%) $I_S = \frac{S_{unrein} - S_{rein}}{S_{unrein}} \times 100$	**10**	31.25	25	14.55	12.67	10.5
Lateral displacement reduction factor, I_L (%) $I_L = \frac{L_{unrein} - L_{rein}}{L_{unrein}} \times 100$	**10**	34.75	30.32	31.91	22.5	16.25

6.3.3 Distribution of Stress in the subballast

Perhaps the best way to investigate the behaviour of reinforced subballast, is to understate the loading mechanism in the unit cell. The stress contours of geocell-reinforced subballast in the unit cell at a confining pressure of σ'_3 = 10 kPa and a frequency of f = 10 Hz is shown in Figure 6.14 (a & b). Figure 6.14 (a) shows that during loading (σ_{max} = 160-170 kPa), the concentration of horizontal stress (parallel to the direction of σ'_3) occurred inside the geocell pockets [point (C)]. This was expected because the subballast was confined inside the pocket, which prevented any lateral spreading. Figure 6.14(a) shows that the degree of horizontal stress was much less at the pocket located in the middle of the mattress [point (D)]. As shown in this figure, during loading, the degree of stress increased slightly at the centre of the specimen just below the reinforced layer in unreinforced subballast (point A & B). This can be attributed to the impact of intermediate stress (σ'_2) and boundary condition in a plane strain condition. However, for the rest of the specimen, the geocell mattress successfully captured the intensity of applied cyclic loading and transferred less stress to the lower layer of soil. Again, this confirmed the

effectiveness of a geocell mattress placed beneath the footing, where there is a maximum degree of applied cyclic stress.

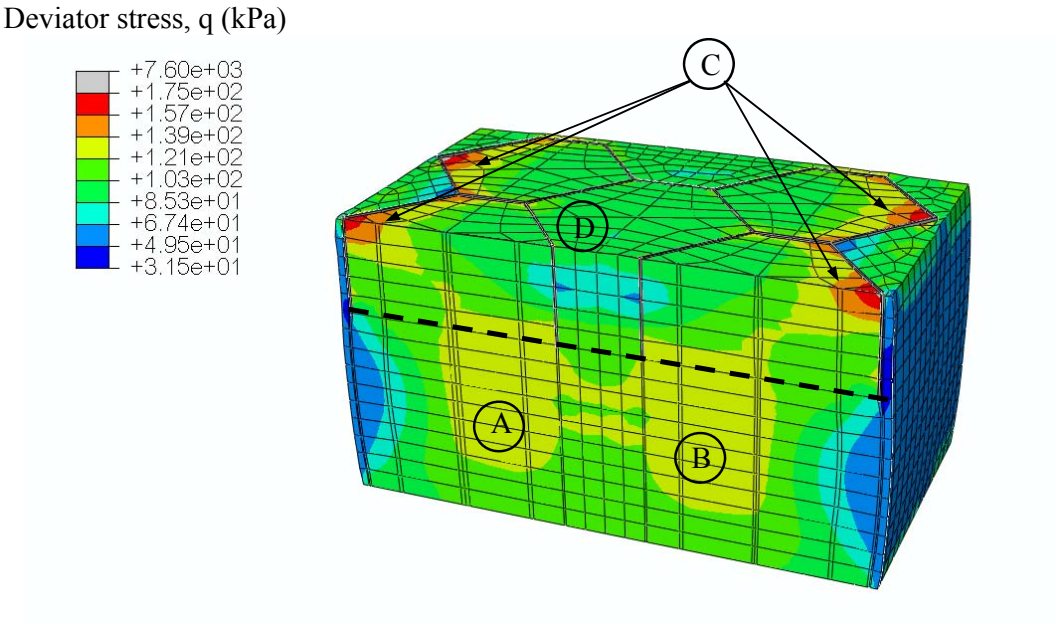

(a)

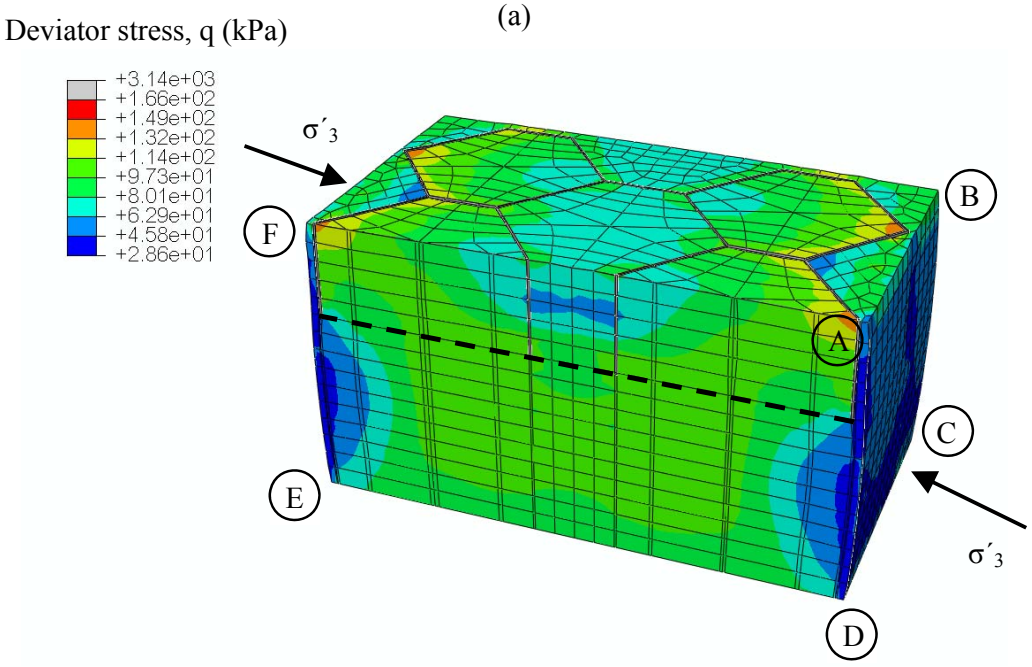

(b)

Figure 6.14. Stress distribution in during (a) loading and (b) unloading of unit cell in a geocell-reinforced subballast

Moreover, based on the numerical results, the degree of horizontal stress varied at the loading stage (i. e. loading and unloading). Figure 6.14 (b) shows there was less horizontal stress in the unloading stage. This figure also show the magnitude of pressure developed on the specimen by cyclic loading, in the direction parallel to σ_3' (side ABCD) was about 50-66 kPa, which was much higher than the confining pressure (σ_3' = 15 kPa). The magnitude of pressure on the ABCD side decreased as applied confining pressures σ_3' increased. One of the beneficial effects of numerical modelling is investigating the effect of intermediate stress (σ_2'). The numerical results showed that the magnitude of stress that developed in the direction of σ_2' (side ADEF) was much higher than σ_3', which was about σ_2' = 60-80 kPa. This can be justified as the effect of boundary condition which led to the accumulation of stress in this direction. In conventional design criteria, the degree of intermediate stress is usually assumed to be equal to the minor principal stress ($\sigma_2' = \sigma_3'$), but this simulation showed there was a remarkable dissimilarity between σ_3' and σ_2' when the experiment carried out in plane strain condition, which is similar to field conditions.

6.3.4 Distribution of Stress in geocell mattress

The behaviour of a geocell mattress under cyclic loading was investigated in this study. As an important parameter, the tensile stress of the reinforcement has a significant impact in the design criteria. Based on the available studies and conventional design criteria, the tensile strength of geocell is usually assumed to be constant. However, this simulation showed that during cyclic loading, the tensile stress had changed considerably at the loading stage (i.e. loading or unloading). Figure 6.15 (a & b) shows the mobilised tensile stress at the loading and unloading stages. Based on the numerical results, the maximum and minimum tensile stress was observed at the max (loading) and min (unloading) amplitude respectively.

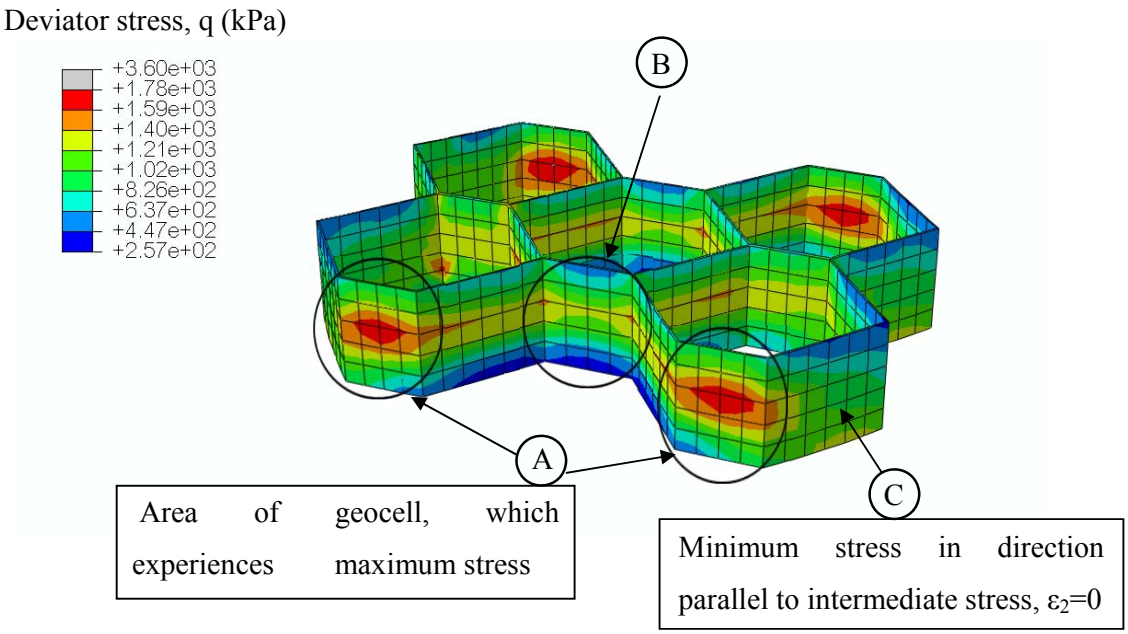

(a)

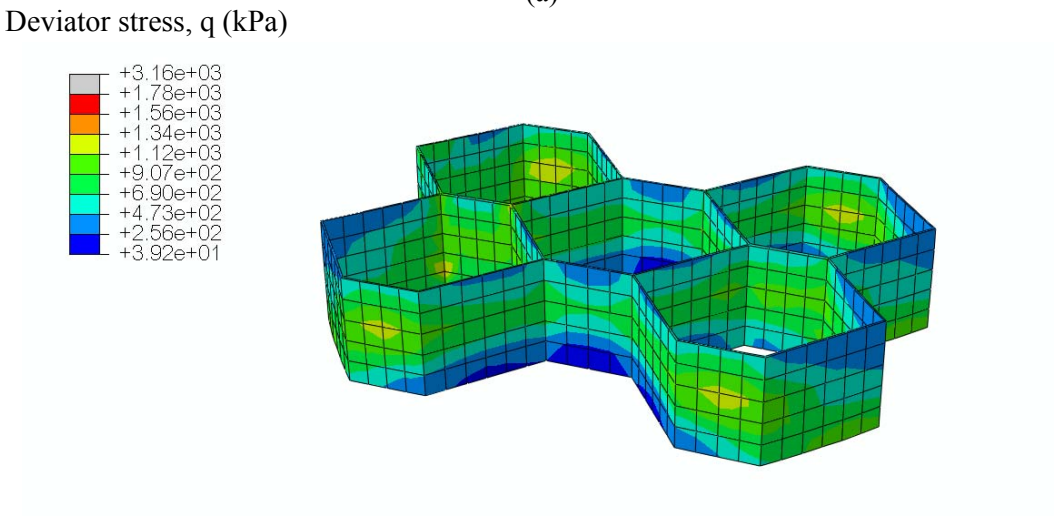

(b)

Figure 6.15. Tensile stress mobilised in geocell mattress (a) loading and (b) unloading stage subjected to cyclic loading.

Figure 6.15 (a) shows that by preventing the infill subballast from excessive lateral spreading, a significant amount of the tensile stress was mobilised in the geocell mattress. It was also found that in the middle of the geocell strip (point A), in direction parallel to the minor principal stress (σ_3') was subjected to the largest amount of tensile stress in the loading and unloading stages. Nevertheless, the mobilised tensile stress in the middle pocket (Point B) was much less than the surrounding pockets. Unlike a conventional assumption which considers a uniform distribution of stress over geocell wall, it can be concluded from these results that the stress over the geocell strip is not distributed uniformly. Moreover, this investigation showed that the ultimate tensile stress of the geocell mattress was never reached during cyclic loading. This implies that the improved performance of geocell-reinforced subballast was only governed by mobilised tensile stress of the reinforcement. Figure 6.15 (a) also shows that the minimum tensile strength was mobilised in the direction parallel to the intermediate principal stress (σ_2') (Point c). This can be explained by the fact that due to simulated condition ($\varepsilon_2 = 0$), the geocell mattress only allowed it to move only in the direction parallel to the minor principal stress.

The influence of confining pressure on the mobilised tensile stress in the geocell was also investigated and is presented in Figure 6.16. This figure shows that the developed tensile stress reached its highest magnitude at a very low confining pressure ($\sigma_3' \leq 5$ kPa). The degree of tensile stress decreased markedly as the confining pressure increased. The minimum tensile stress occurred at the higher confining pressure ($\sigma_3' = 30$ kPa), which indicated that the beneficial impact of geocell with respect to the confining pressure available in the rail track environment.

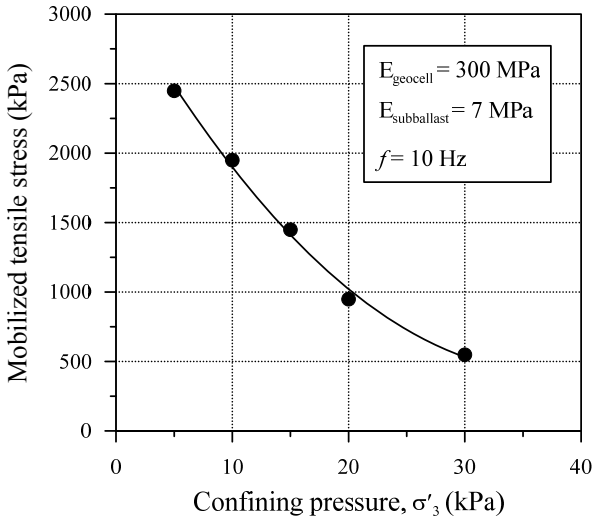

Figure 6.16. Mobilised tensile stress at the geocell in reinforced subballast at different confining pressures σ_3'

6.4 Parametric study

6.4.1 Subballast strength

Perhaps the greatest advantage of numerical analysing is that it provides an insight into the behaviour of specimens with different properties. Since the supply of aggregates with required quality is limited, the use of granular material with higher or lower shear strength is inevitable. Thereby it is important to understand how geocell will impact on infill material with different strengths. Figure 6.17 (a & b) shows the impact of the subballast shear strength on the performance of unreinforced and reinforced specimens. The effectiveness of the subballast strength was highlighted by varying its modulus $E_{subballast}$ from relatively low to high stiffness ($4 \leq E_{subballast} \leq 40$ MPa), as presented in Figure 6.17 (a & b). The stiffness of 4 to 40 MPa were selected to mimic the behaviour of very soft soil and very stiff aggregate used as infill material.

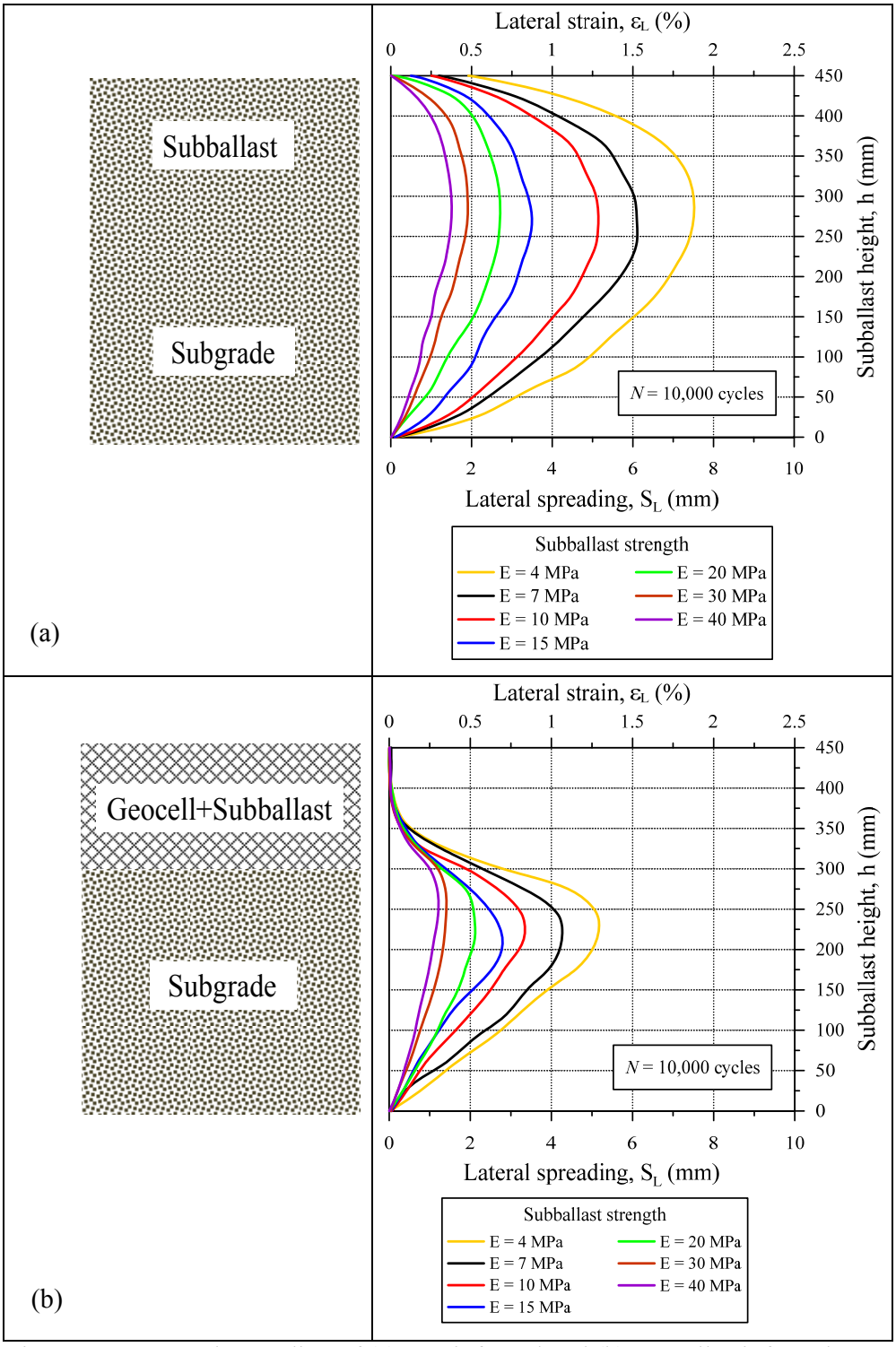

Figure 6.17. Lateral spreading of (a) unreinforced and (b) geocell-reinforced subballast at different strengths

As Figure 6.17 (a) shows, based on the numerical results, during cyclic loading the specimen with very low strength experienced excessive lateral displacement (S_L = 7.50 mm). As expected, the performance of material improved by increasing its strength ($4 \leq E_{subballast} \leq 40$ MPa). However, as Figure 6.17(b) shows, the geocell reinforcement reduced lateral spreading of specimen better for soil with a relatively low strength ($E_{subballast} \leq 10$ MPa). The maximum performance occurred in softer soil, with $E_{subballast}$ = 4 MPa; this indicated the beneficial effect of geocomposite when low quality soil was used as infill material. This can be justified because there was more lateral spreading in the soil, and hence a higher tensile strength was mobilised in the geocell. As expected, by increasing the strength of the subballast this influence was reduced substantially. There was also a marginal improvement in the reinforced subballast compared to the unreinforced ballast at a higher modulus (30 MPa $\leq E_{subballast}$).

6.4.2 Geocell stiffness

Due to the variety of polymeric material available, it was necessary to investigate the influence of geocell stiffness in geocell-reinforced subballast, when the cost of the construction is a major concern. The outcome of this study will help practicing engineers use geocell made from lower material quality while still having an acceptable performance with relatively a lower manufacturing cost. As a result, the influence of the geocell modulus was investigated from a wide range of 0.3 GPa to 5 GPa, as shown in Figure 6.18. As expected, increasing the stiffness of geocell improved the performance of reinforced subballast in all cases by stopping the subballast from excessive lateral spreading. This result shows the impact of a geocell mattress in terms of reducing the lateral spreading of lower layers of soil. As this figure shows, the magnitude of lateral spreading of unreinforced soil beneath the reinforced layer was reduced further by increasing the stiffness of geocell.

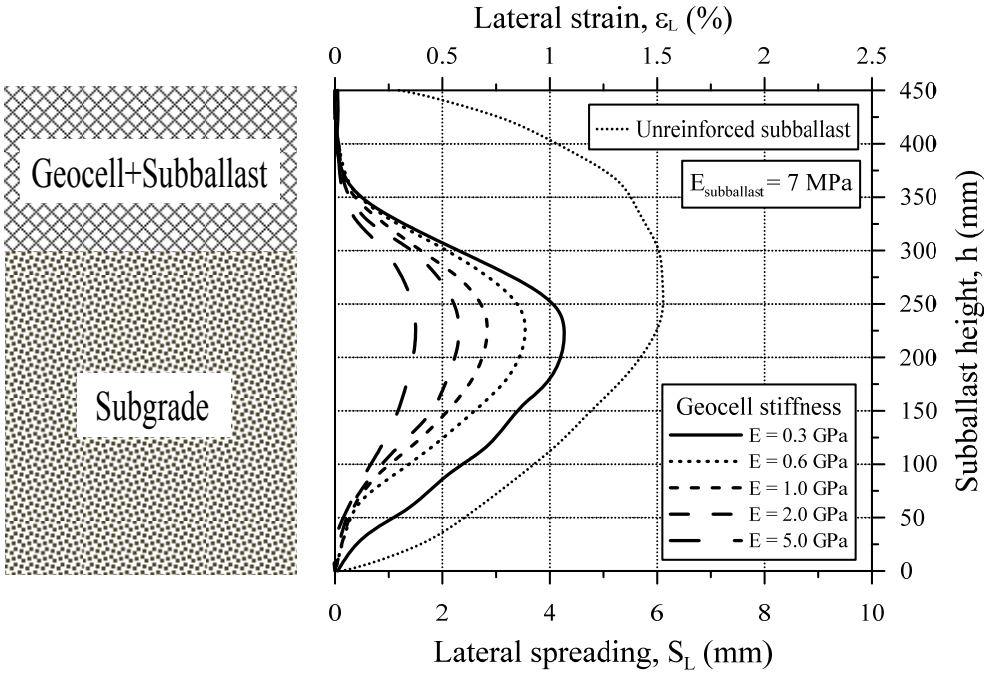

Figure 6.18. Comparison of lateral spreading of unreinforced and geocell-reinforced subballast at different geocell stiffness

The influence of the strength of infill material and the stiffness of geocell can best be evaluated by comparing the reduction factor (I_L) of lateral spreading in reinforced subballast. Figure 6.19 shows the magnitude of I_L for different geocell stiffness and subballast strength at σ_3' = 30 kPa and N = 10,000 cycles. It was found that the degree of I_L varied between 20 % < I_L < 32 %, when soil with different strengths was modelled. As this figure shows, the maximum value of I_L > 30 % occurred at $E_{subballast} \leq$ 10 MPa. In addition, for the soil with relatively high strength, still I_L = 20 % can be achieved. Again, this emphasises the advantage of geocell when it is used for soil with low strength. However, this figure also shows that the reinforced specimen encountered a wider range of I_L according to variations of $E_{geocell}$. According to the numerical results, even at a very low stiffness geocell ($E_{geocell}$ = 300 MPa), a significant degree of about I_L = 30 % occurred. This indicates the

effectiveness of cellular confinement regardless of the stiffness of the geocell. As expected, the results show that the rate of increasing in I_L decreased by increasing $E_{geocell}$.

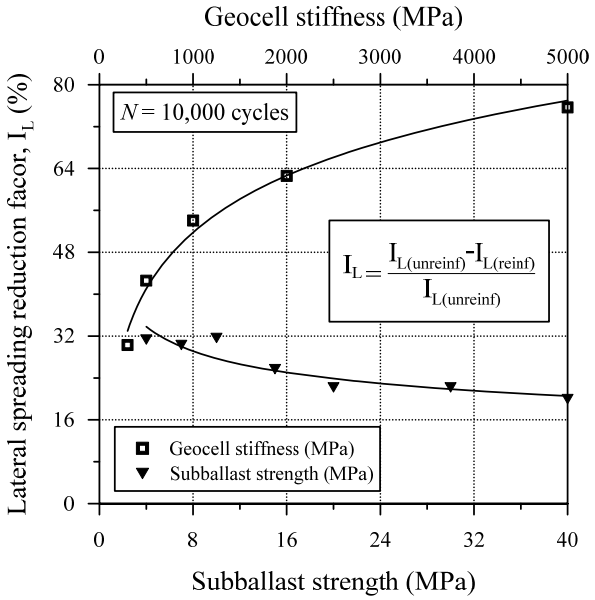

Figure 6.19. Reduction factor of lateral spreading for geocell-reinforced subballast

6.5 Model validation

By using the proposed analytical model discussed in chapter 5, the model results compared well with different sets of experimental data reported elsewhere (Leshcninsky and Ling 2013). The simulation was carried out on both unreinforced and geocell-reinforced material. A new hexagonal shaped geocell mattress was developed to reinforce granular material, as shown in Figure 6.20, where a single layer of 200 mm thick geocell mattress was used. The loading amplitudes for the unreinforced and reinforced specimens were $35 \leq q \leq 175$ kPa and $70 \leq q \leq 350$ kPa respectively. The axial load applied on top of embankment through a plate with dimension of 356 × 356 × 25 mm. The internal friction angle and dilatancy angle of granular material was 45 and 15 degrees respectively. With the meshing, the base of the embankment was restricted from displacing vertically, so a rigid concrete

foundation was modelled (Leshcninsky and Ling 2013), but the sides of the embankment were free to move laterally of vertically.

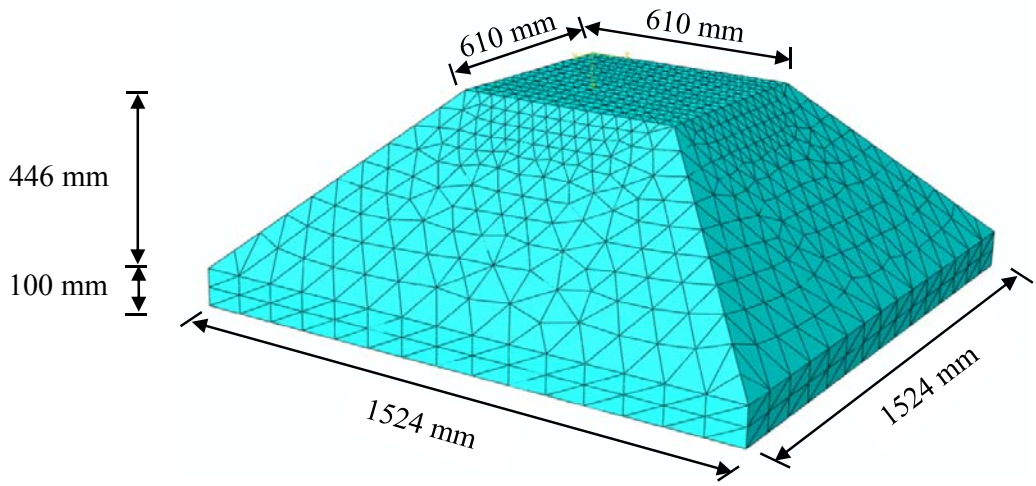

(a)

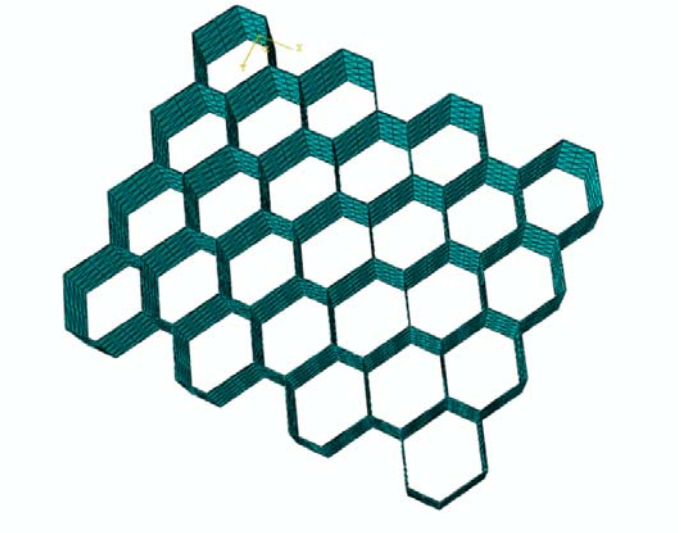

(b)

Figure 6.20. Typical illustration of (a) geometry of model and (b) geocell mattress used for validation

The model was validated by the experimental and numerical results for the unreinforced and geocell-reinforced material. Figure 6.21(a) shows the laboratory outcomes and model prediction of vertical displacement.

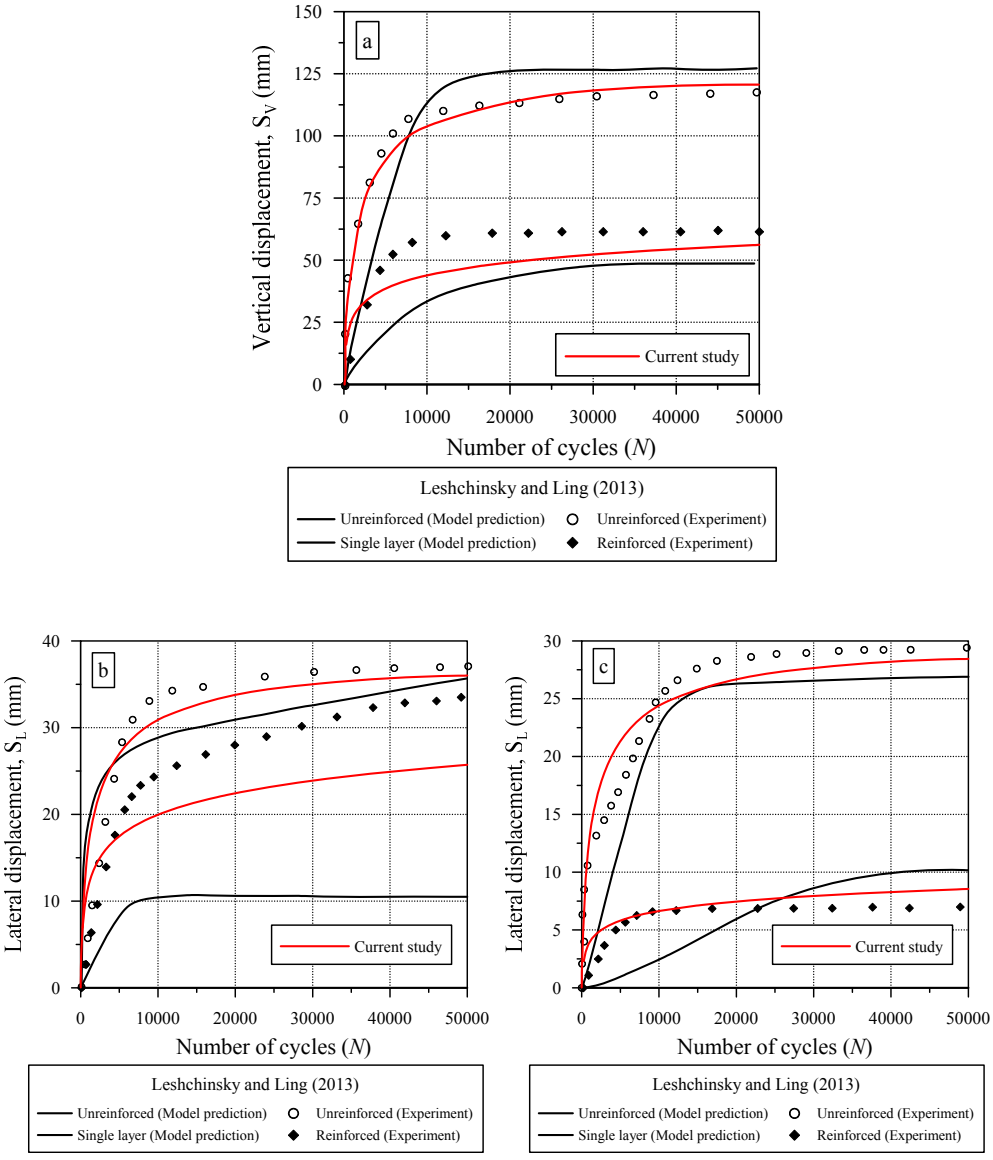

Figure 6.21. Model prediction compared with experiment and numerical results of (a) vertical and lateral deformation at (b) the top and (c) bottom of the embankment

The vertical displacement for unreinforced specimen was about S_V =120 mm. As expected, a lower performance observed in unreinforced specimen. However, the embankment performed better after a geocell mattress was utilised. As this figure shows, the current study provides a better prediction than the numerical simulation performed by Leshchinsky and Ling (2013). As current model predicted, most of vertical settlements occurred in the initial cycles and the rate were decreased by increasing number of cycles.

Also, the lateral displacements at the top and bottom of the embankment were compared, shown in Figure 6.21 (b & c). In all cases, the model predicted carried out by current study provided higher initial modulus for both unreinforced and reinforced specimen. This result occurred due to a more accurate confining pressure that was calculated by the proposed model. For the reinforced specimen, it also can be justified by using a hexagonal shaped geocell mattress that was similar to the actual shape used in the field. Using hexagonal shaped could be led to better distribution of stress in the geocell mattress, hence mobilised higher and more uniform tensile stress in the geocell strips. Also, it confirmed that using geocell with hexagonal shaped was more effective to arrest lateral spreading of material.

6.6 Implication of current numerical analysis

This study provides an insight into the loading mechanism and deformation of unit cells with respect to cyclic loading. Geocell was placed directly under the footing where the maximum cyclic pressure was applied to the foundation. The outcome of current numerical analysis can be used by the railway industry as a guideline for constructing new tracks or stabilising exist rail track for heavier traffic commuting on subgrade with low shear strength, while still having a safe and economic design. In the absence of granular material of the required quality, the numerical simulation presented in this study can be deployed for a wide range of granular material and geocell mattresses with different strengths and stiffness. This can be highlighted by

simulating the influence of the strength of subballast ($E_{subballast}$) on the behaviour of the reinforced specimen. Figure 6.22 shows the mobilised tensile stress in the geocell ($E_{geocell}$ = 300 MPa) and lateral spreading (S_L) in the reinforced specimen at the loading stage (q_{max} = 166 kPa), with different strength subballast ($4 \leq E_{subballast} \leq 40$ MPa). This figure shows that the maximum degree of tensile strength occurred on the subballast with lower strength ($E_{subballast}$ = 4 MPa). This is because the rigidity of infill subballast was improved by transferring the cyclic loading as hoop stress (mobilises tensile stress) to the geocell, indicating that lowering the stiffness of infill material enables a higher tensile stress to be mobilised in the geocell mattress. This can be valued by practicing engineers when granular material with the required strength is not available. Accordingly, the magnitude of tensile strength decreased significantly by increasing $E_{subballast}$. In all cases the lateral spreading was reduced significantly.

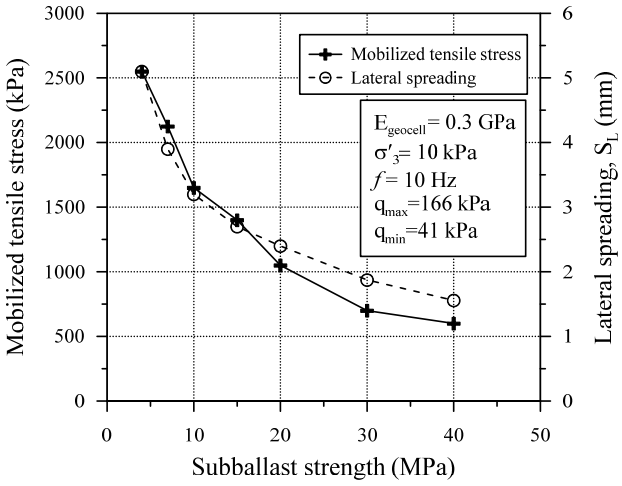

Figure 6.22. Mobilised tensile stress at the geocell in reinforced subballast with different strength

6.7 Summary

Using the finite element procedure (ABAQUS), the simulation and practical implication of geocell-reinforced subballast subjected to cyclic loading was carried out in the actual geometry of subballast that was similar to rail track in the field. The model was compared with the experimental data obtained from a series of laboratory tests on unreinforced and reinforced subballast, carried out by large scale prismoidal triaxial equipment. The numerical results were validated by the available field data. This simulation can be effectively used to predict the performance of subballast and subgrade when the subballast is reinforced with a geocell mattress. By considering the agreement between the laboratory results and the numerical simulation, the following conclusions can be drawn from this study:

1- The performance of subballast can be improved markedly by using a geocell mattress as reinforcement. By acting as a stiff slab, the geocell restrained surface failure and reduced the intensity of pressure to the lower layer of soil, layer. Accordingly, it minimised the vertical and lateral displacement of soil under cyclic loading.

2- The maximum vertical displacement (S_V) occurred directly under the footing where there cyclic loading was at its maximum. The intensity of S_V decreased at a lower depth. The numerical results also showed that the maximum lateral displacements in the unreinforced specimen occurred at the top 450-250 mm. As a result, utilising geocell in the subballast layer can effectively reduce excessive axial and lateral deformations. The optimum place for geocell was directly under the footing.

3- The maximum effect of geocell reinforcement can be achieved when soil with a low strength is used as infill material. This highlights the importance of $E_{subballast}$ for designing purposes, where a weak foundation is available. Also the performance of the subballast was improved further by increasing the stiffness of the geocell.

4- The tensile stress varied during loading and unloading under cyclic loading, and the ultimate tensile stress of the geocell mattress was never reached during cyclic loading. Moreover, the numerical simulation also showed that the highest concentration of stress occurred in the geocell mattress at the middle height of the pockets. This fact can be emphasised when manufacturing mattresses that are higher than normal.

CHAPTER 7

7. CONCLUSION AND RECOMMENDATIONS

7.1 General

There is an urgent need in Australia to design rail tracks capable of operating trains that can travel at higher speed, imposing an immense challenge to the stability and load bearing capacity of track substructures. To achieve this goal, a relatively rigid track foundation, including the ballast and subballast is needed. Accordingly, rail operators must discover a unique and relatively cost effective way of constructing or modernising rail tracks for high speeds train. A properly designed layer of geocell-reinforced subballast can act as a rigid mattress to reduce differential settlement and excessive lateral spreading, with positive implications in terms of enhancing track stability and reducing maintenance costs. Moreover, the cost of construction and/or maintenance could be reduced significantly if appropriate reinforcement is used to stabilise the subballast. The benefits of geocell are more pronounced in coastal areas where the subsoil is weak. To date, no guideline or technical specification is available in Australia to specify whether train speeds can be increased when geocell is used to reinforce subballast. If additional confinement induced by geocell can be determined, lateral deformation and settlements can be significantly reduced and trains can be operated at higher speeds.

This study was focused on providing a design guideline in terms of allocation of permissible train speeds by stabilising subballast using geocells. To achieve this, various factors having considerable influence on the behavior of subballast reinforced with a geocell mattress, have been investigated. A series of large-scale laboratory tests were carried out using a process simulation prismoidal triaxial apparatus designed and built at the University of Wollongong. The interface shear strength of subballast with and without geocells was also assessed using large scale direct shear box apparatus. The following sections highlight major conclusions drawn from the current study with regards to the effectiveness of geocell in improving the performance of subballast. Recommendations for future investigation are also provided. The salient aspects of this thesis are highlighted below.

7.1.1 Interface shear strength under direct shear testing

The performance of unreinforced and reinforced subballast was investigated using large-scale direct shear box apparatus under low effective normal stresses ($1 \leq \sigma_n \leq$ 45 kPa). Also, the impact of the relative density, shearing displacement rate and open area of geosynthetics were investigated. The interface shear resistance (k_τ) between the subballast and different geosynthetics was measured, and a generalised empirical formulation was developed to predict the shear strength of unreinforced and reinforced subballast. The results confirmed that the interface shear strength was governed by effective normal stress, the shearing displacement rate (S_R), the relative density of the material (D_R), and the open area of the geosynthetic (OA). The results showed that the interface shear resistance was substantially different, depending on the type of geosynthetic.

Irrespective of the size and shape of the apertures, all the reinforcements helped to improve the performance of the subballast, and interface shear strength ratio (k_τ) > 1 was always observed. However, for OA > 80 %, there was a rapid decrease in

effectiveness. The value of k_τ was higher for the triaxial geogrid than the biaxial grids. Indeed the highest value of k_τ was provided by GG1, which varied in the range of k_τ = 1.22-1.29. It was also found that geomembrane GC1 provided relatively low k_τ values (k_τ = 1.03-1.08), indicating they were not as effective as geogrids.

In essence, the geogrids GG1 and GG2 performed better than the geomembrane (GC1 and GC2), when placed in a horizontal direction. However, in practice the geomembrane (GC1) would still provide enough interface friction for geocells made with this material. Considering the opening area, the frictional resistance mobilised against a vertical wall in a geocell mattress made from geomembrane (GC1) was much more than for a geocell made from geosynthetics and with larger size aperture. In fact, increasing the frictional resistance due to less *OA* in the geomembrane (GC1) will induce a higher confining stress for the encased rockfill.

On the basis of the results obtained from the present study, the key factors that have a significant influence on the subballast interface behaviour can be summarised as follows:

1. *Relative density* (D_R). An increased relative density substantially improved the shear strength of subballast. However, at D_R > 77 %, the influence of relative density decreased for the unreinforced and reinforced subballast.

2. *Shear displacement rate* (S_R). At a lower shear displacement rate, the specimen exhibited higher strength. However, the magnitude of the shear strength of subballast decreased considerably as the shearing displacement rates (S_R > 2) increased.

3. *Open Area (OA)*. There was a significant improvement in interface shear resistance when the open area of geosynthetics was increased. The shear strength of GC2-reinforced subballast was higher than GC1 owing to more favourable size of the apertures maximising the particle interlock. The

percentage of open area could provide a better insight into evaluating the interface shear strength of subballast with a relatively small D_{50}.

4. *Passive resistance* (τ_{pass}). Compared to geomembranes, geogrids provided a greater value of passive resistance owing to their transverse ribs, but the mobilised passive resistance decreased with an increase in *OA*. The triaxial grids offered more passive resistance than the biaxial geogrid.

5. *Frictional resistance* (τ_{fric}). Frictional resistance had a profound impact on the total shear strength of reinforced subballast with geomembrane (GC1).

7.1.2 Behavior of geocell-reinforced subballast under cyclic triaxial testing

In order to investigate the role of geocell reinforcement under high frequency cyclic loading, a series of laboratory investigations were carried out using the large-scale process simulation prismoidal triaxial apparatus (PSPTA) as discussed in Chapter 4. The cyclic loading was applied to specimen at low confining pressures ($5 \leq \sigma_3' \leq 30$ kPa) to simulate a track environment. A high frequency ($10 \leq f \leq 30$ Hz) cyclic loads were applied to study the performance of unreinforced and geocell-reinforced subballast under high speeds. All experiments were conducted under a stress controlled mode with a large number of cycles (N = 500,000 cycles), and the vital parameters that govern the performance of unreinforced and geocell-reinforced subballast were investigated in detail. The parameters that influence the performance of subballast under cyclic loading were also studied in detail.

1. *Number of cycles* (N). The maximum rate at which vertical and lateral deformation increased, occurred during the initial stage of cyclic loading. The incremental rate of deformations was reduced by increasing N. Unreinforced subballast requires a higher number of cycles to reach a stable zone, and the

geocell helped the subballast to reach shakedown at a lower number of cycles.

2. *Confining pressure* (σ_3'). An increased confinement offered by geocells helped to reduce the vertical and volumetric strains of subballast. The benefit obtained from geocell was mainly observed at low confining pressure ($\sigma_3' \leq$ 15 kPa) and at higher frequency ($f \geq 20$ Hz). The geocells had relatively no impact on the behaviour of subballast at an optimum confining pressure (σ_3' = 30 kPa), but it was sufficient to reduce dilation. At this confining pressure no tensile strains were mobilised in the geocell (i.e. no extra confinement).

3. *Frequency* (*f*). Increased frequency led to higher vertical strain at the same number of cycles. At higher frequencies, the zone of stable shakedown in the subballast was attained at a higher number of cycles. While unreinforced samples did not reach a level of stable shakedown even after half a million cycles, the geocell-reinforced specimen reached shakedown depending on the frequency. At a higher confining pressure (σ_3' = 30 kPa), frequency had less effect on the behaviour of unreinforced and reinforced subballast.

Key parameters that were influenced under cyclic loading were studied, and summarised as follow:

1. *Mobilised friction angle* (ϕ_m) *and mobilised dilatancy angle* (ψ_m). Despite the conventional assumption that the friction angle and angle of dilatancy remains constant, the laboratory outcomes showed that under cyclic loading ϕ_m and ψ_m are mobilised with respect to the number of cycles, confining pressure, and frequency.

2. *Geocell modulus* (M_m). The ultimate tensile strength of geocell reinforcement was never reached. Accordingly, a "mobilised modulus" of geocell mattress

was presented that occurs when the specimen is subject to cyclic loading. The maximum modulus occurred at the initial cycles, where the rate of vertical strains was found to be at its maximum.

3. *Resilient modulus* (M_R). The resilient modulus was increased as a result of increase in the confining pressure and frequency with respect to the number of cycles. As a consequence, the rigidity of reinforced subballast improved and the reinforced soil layer acted like a stiff mattress with a higher load bearing capacity, and there was also a substantial reduction in vertical and lateral deformation.

7.1.3 Development of a semi-empirical analytical model

An additional confinement offered by cellular confinement under cyclic loading is important to better assess the behavior of geocell-reinforced subballast. It was thereby inevitable to develop an analytical model that can predict the confining pressure in terms of variations in the number of cycles, pocket size, and levels of stress. A semi-empirical mathematical model that could determine the additional confinement pressure induced by the geocell mattress under cyclic loading was also proposed and formulated. Additional confinement were predicted based on mobilised geocell modulus, mobilised dilation angle at required number of cycles. The additional confinement ($\Delta\sigma_3'$) predicted by the proposed model confirmed that the inclusion of geocell can significantly minimise lateral spreading and the axial settlement of infill subballast under cyclic loading, and thus improve track stability. The magnitude of $\Delta\sigma_3'$ was higher at lower confining pressure (σ_3') and higher frequency (*f*), which highlighted the effectiveness of geocell reinforcement when it was used in rail track substructure, and where a relatively low σ_3' is available. The

magnitude of $\Delta\sigma_3'$ was reduced significantly at higher confining pressure ($\sigma_3' \geq 20$ kPa), indicating.

7.1.4 Development of three dimensional numerical modelling

A comprehensive three dimensional finite element model implemented in ABAQUS was used. The unit cell was numerically modelled to study the effects of cyclic loading mechanism on settlement and lateral spreading. The cyclic loading with a periodic and positive full sine waveform was applied at a frequency of f = 10 Hz. The proposed model for the computation of additional confinement as discussed in Chapter (5) was incorporated in FEM. The model was calibrated by laboratory outcomes for unreinforced and geocell-reinforced subballast described in Chapter 4. The maximum effect of geocell reinforcement could be achieved when soil with a low strength was used as infill material. This highlights the importance of $E_{subballast}$ for designing purposes, where a weak foundation is available. Also, the maximum vertical displacement (S_V) occurred directly under the footing where there cyclic loading was at its maximum. The numerical modelling was successfully validated against results of large-scale model studies published elsewhere.

7.1.5 Practical implications of this study

One of the most important outcomes of this study is providing practical guidelines in terms of permissible train speeds. By analysing the outcome of the proposed analytical model at different factors (σ_3' and f), the comprehensive practical implications were presented in terms of speed improvement ratio. Also, an empirical equation was proposed to predict the speed improvement ratio. The current model can predict the permissible speed of a train travelling on rail track supported by

geocell-reinforced subballast. It was shown that by reinforcing the subballast with geocells, the allowable train speed could be increased by about 5-25 % to that applicable for track that usually has a low confinement in the field. Geocells were found to have a profound influence on improving resiliency (i.e. increasing the resilient modulus) and decreased the corresponding settlement by about 12-25 % compared to unreinforced subballast.

7.2 Recommendations

The lack of experimental data for geocell-reinforced subballast under cyclic loading in plane strain condition was the main motivation for this current study. The beneficial use of cellular confinement in subballast has been highlighted. Due to several limitations, some other aspects of this investigation required more in depth study. The following is a summary of the recommendations that may be useful for further research on geocell-reinforced subballast.

1. In this investigation, confining pressure applied to the specimen was assumed equal on each side, parallel to the sleeper. However, the degree of σ_3' maybe slightly greater on the wall that faced the line of symmetry of the rail tracks.

2. The assessment of particle breakage was not within the scope of this study. Due to its relatively small particles, subballast is not expected to have significant particle breakage, but depending on the parent rock type, breakage may become considerable.

3. All of these experiments were carried out in a dry condition, which may not always represent the actual field conditions. The impact of pore pressure on the degree of additional confinement induced by the geocell was not investigated. Further study is needed to investigate how the moisture content

would affect the performance of geocell-reinforced subballast under cyclic loading.

4. The subgrade underneath the layer of subballast had the same PSD of subballast. In the field usually granular material with finer particle size distribution and lower shear strength is generally used. Further studies might be needed to investigate the behaviour of geocell-reinforced subballast on top of the subgrade.

5. The assessment of durability of geocell was not within the scope of this study. All of the experiments were conducted up to N = 500,000 cycles. The durability of geocell should be investigated for a very large number of cycles, ($N \geq 1$ million cycles).

6. In this experiment a uniform confining pressure was applied to the specimen, but this might slightly differ from the actual confinement available in the field. In a typical railway environment, the magnitude of σ_3' might change slightly at a different height, so in the field, a uniform lateral displacement of the specimen may not occur.

REFERENCES

AASHTO T274-82 (1986), Standard method for testing resilient modulus, American Association of State Highway and Transportation Officials, Washington, D. C.

Allen, J. J. and Thompson, M. R. (1974). Resilient response of granular materials subjected to time-dependent lateral stresses. *Transportation Research Record* (510).

Al-Qadi, I. L., Dessouky, S., Tutumluer, E. and Kwon, J. (2011). Geogrid mechanism in low-volume flexible pavements: accelerated testing of full-scale heavily instrumented pavement sections. *International Journal of Pavement Engineering* **12**(2): 121-135.

Andrei D. (1999). Development of a harmonized test protocol for the resilient modulus of unbound materials used in pavement design. M.S. Thesis, University of Maryland- College Park.

Anubhav and Basudhar, P. K. (2010). Modelling of soil–woven geotextile interface behavior from direct shear test results. *Geotextiles and Geomembranes* **28**(4): 403-408.

Arulrajah, A., Rahman, M., Piratheepan, J., Bo, M. and Imteaz, M. (2014). Evaluation of interface shear strength properties of geogrid-reinforced construction and demolition materials using a modified large-scale direct shear testing apparatus. *Journal of Materials in Civil Engineering* **26**(5): 974-982.

ASTM. (2010). Standard test method for density of plastics by the density-gradient technique. D1505, West Conshohocken, PA.

ASTM. (2013). Standard practice for determining the integrity of field seams used in joining flexible polymeric sheet geomembranes. D4437, West Conshohocken, PA.

ASTM. (2011). Standard test method for determining performance strength of geomembranes by the wide strip tensile method. D4885, West Conshohocken, PA.

ASTM. (2012). Standard test method for measuring the nominal thickness of geosynthetics. D5199, West Conshohocken, PA.

Atalar, C., Das, B.M., Shin, E.C. and Kim, D.H. (2001). Settlement of geogrid-reinforced railroad bed due to cyclic load. *Proc. 15th Int. Conf. on Soil Mech. and Geotech. Eng., Istanbul*, **3**, 2045–2048.

Bacas, B. M., Konietzky, H., Berini, J. C. and Sagaseta, C. (2011). A new constitutive model for textured geomembrane/geotextile interfaces. *Geotextiles and Geomembranes* **29**(2): 137-148.

Bathurst, R. J. and Knight, M. A. (1998). Analysis of geocell reinforced-soil covers over large span conduits. *Computers and Geotechnics* **22**(3–4): 205-219.

Bathurst, R. J. and Karpurapu, R. (1993). Large-scale triaxial compression testing of geocell-reinforced granular soils. *Geotechnical Testing Journal* **16**(3): P296–303.

Bathurst, R. J. and Jarrett, P. M. (1988). Large-scale model tests of geocomposite mattresses over peat subgrades. *Transportation Research Record*, **36**(1188): 28-36.

Been, K. and Jefferies, M. (2004). Stress-dilatancy in very loose sand. *Canadian Geotechnical Journal* **41**(5): 972-989.

Bergado, D. T., Chai, J. C., Abiera, H. O., Alfaro, M. C. and Balasubramaniam, A. S. (1993). Interaction between cohesive-frictional soil and various grid reinforcements. *Geotextiles and Geomembranes* **12**(4): 327-349.

Biabani, M. M., Indraratna, B. (2015). An evaluation of the interface behavior of rail subballast stabilized with geogrids and geomembranes. *Journal of Geotextiles and Geomembranes* **43**(3): 240-249.

Binquet, J. and Lee, L. K. (1975). Bearing capacity tests on reinforced earth slabs. *International journal of rock mechanics and mining sciences & geomechanics abstracts* **13**(3): 1241–1255.

Bishop, A. W. and Henkel, D. J. (1962). The measurement of soil properties in the triaxial test. London, E. Arnold.

Biswas, A., Krishna, A. M. and Dash, S. K. (2013). Influence of subgrade strength on the performance of geocell-reinforced foundation systems. *Geosynthetics international* **20**(6): 376-388.

Bolton, M. D. (1986). The strength and dilatancy of sands. *Géotechnique* **36**(1): 65-78.

Brown, S. and Pell, P. (1967). An experimental investigation of the stresses, strains and deflections in a layered pavement structure subjected to dynamic loads. *Intl. Conf. Structural Design Asphalt Pavements*.

Brown, S. F., Kwan, J., and Thom, N. H. (2007). Identifying the key parameters that influence geogrid reinforcement of railway ballast. *Geotextiles and Geomembranes*, **25**(6), 326–335.

Bush, D. I., Jenner, C. G. and Bassett, R. H. (1990). The design and construction of geocell foundation mattresses supporting embankments over soft grounds. *Geotextiles and Geomembranes* **9**(1): 83-98.

Cazzuffi, D, Picarelli, L, Ricciuti, A, Rimoldi, P. (1993). Laboratory investigations on the shear strength of geogrid reinforced soils. Geosynthetic soil reinforcement testing procedures (pp. 119-137), West Conshohocken, PA 19428-2959.

Charles, J. A., and Watts, K. S. (1980). The influence of confining pressure on the shear strength of compacted rockfill. Geotechnique, London, U.K. **30**(4), 353-367.

Chen, Q., Abu-Farsakh, M. and Sharma, R. (2009). Experimental and analytical studies of reinforced crushed limestone. *Geotextiles and Geomembranes* **27**(5): 357-367.

Choudhury, J. (2009). Track reconditioning guidelines. TMC 403 Engineering manual-Geotechnical Version 1.2: 1-30.

Cole, D., Bently, D., Durell, G., and Johnson, T. (1986). Resilient modulus of freeze-thaw affected granular soils for pavement design and evaluation: Part 1, laboratory tests on soils from Winchendon. *Massachusetts, test sections. USA Cold Regions Research and Engineering Laboratory Report* 86–4, Hanover, NH.

Cowland, J. W. and Wong, S. C. K. (1993). Performance of a road embankment on soft clay supported on a Geocell mattress foundation. *Geotextiles and Geomembranes* **12**(8): 687-705.

Dahlberg, T. (2001). Some railroad settlement models-a critical review. *Proceedings of the Institution of Mechanical Engineers* **215**(4): 289.

Dash, S. K. (2010). Influence of relative density of soil on performance of geocell-reinforced sand foundations. *Journal of Materials in Civil Engineering* **22**(5): 533-538.

Dash, S. K., Krishnaswamy, N. R. and Rajagopal, K. (2001). Bearing capacity of strip footings supported on geocell-reinforced sand. *Geotextiles and Geomembranes* **19**(4): 235-256.

Dash, S. K., Krishnaswamy, N. R. and Rajagopal, K. (2007). Behaviour of geocell-reinforced sand beds under strip loading. *Canadian Geotechnical Journal* **44**(7): 905+.

Dash, S. K., Rajagopal, K. and Krishnaswamy, N. R. (2001). Strip footing on geocell reinforced sand beds with additional planar reinforcement. *Geotextiles and Geomembranes* **19**(8): 529-538.

Dash, S. K., Sireesh, S. and Sitharam, T. G. (2003). Model studies on circular footing supported on geocell reinforced sand underlain by soft clay. *Geotextiles and Geomembranes* **21**(4): 197-219.

Dunlap, W. A. (1963). A report on a mathematical model describing the deformation characteristics of granular materials. Texas Transportation Institute Texas A & M University, College Station Tex.

Emersleben, A. and Meyer, M. (2010). The influence of hoop stresses and earth resistance on the reinforcement mechanism of single and multiple geocells. *9th International Conference on Geosynthetics, Brazil*: 713-716.

Esveld, C. (2001). Modern Railway Track. The Netherlands, MRT Productions.

Ezzein, F. M. and Bathurst, R. J. (2014). A new approach to evaluate soil-geosynthetic interaction using a novel pullout test apparatus and transparent granular soil. *Geotextiles and Geomembranes* **42**(3): 246-255.

Fatahi, B. and Khabbaz, H. (2011). Enhancement of ballasted rail track performance using geosynthetics. *Advances in Pile Foundations, Geosynthetics, Geoinvestigations, and Foundation Failure Analysis and Repairs, ASCE*. 222-230

Garg, N. and Thompson, M. R. (1997). Triaxial characterization of Minnesota road research project granular materials. *Transportation research record* (1577): 27-36.

Haeri, S. M., Noorzad, R. and Oskoorouchi, A. M. (2000). Effect of geotextile reinforcement on the mechanical behavior of sand. *Geotextiles and Geomembranes* **18**(6): 385-402.

Han, J., Pokharel, S., Yang, X., Manandhar, C., Leshchinsky, D., Halahmi, I. and Parsons, R. (2011). Performance of geocell-reinforced RAP bases over weak subgrade under full-scale moving wheel loads. *Journal of Materials in Civil Engineering* **23**(11): 1525-1534.

Haque, A., Bouazza, A. and Kodikara, J. (2004). Filtration behaviour of cohesionless soils under dynamic loading. *Proceeding of the 9th ANZ conference in Geomechanics, Aukland*, vol.2, 867-873.

Hebeler, G.L., Frost, J.D., Myers, A.T. (2005). Quantifying hook and loop interaction in textured geomembrane-geotextile systems. *Geotextiles and Geomembranes* **23**, 77-105.

Hegde, A. and Sitharam, T. G. (2014). 3-Dimensional numerical modelling of geocell reinforced sand beds. *Geotextiles and Geomembranes*: 1-11.

Hegde, A. M. and Sitharam, T. G. (2014). Effect of infill materials on the performance of geocell reinforced soft clay beds. *Geomechanics and Geoengineering*: 1-11.

Henkel, D. J. and Gilbert, G. D. (1952). The effect measured of the rubber membrane on the triaxial compression strength of clay samples. *Géotechnique* **3**(1): 20-29.

Hicks, R. G. and Monismith, C. L. (1971). Factors influencing the resilient properties of granular materials. *Highway Research Record*, (345), 15–31.

Huang, C. C. and Tatsuoka, F. (1990). Bearing capacity of reinforced horizontal sandy ground. *Geotextiles and Geomembranes* **9**(1): 51-82.

Huang, C. C. and Menq, F. Y. (1997). Deep-footing and wide-slab effects in reinforced sandy ground. *Journal of Geotechnical and Geoenvironmental Engineering* **123**(1): 30-36.

Huang, C. C. and Tatsuoka, F. (1988). Prediction of bearing capacity in level sandy ground reinforced with strip reinforcement. *Proceedings of the international symposium on theory and practice of earth reinforcement, Fukuoka, Kyushu, Japan* **27**(3): 191–196.

Indraratna, B., Biabani, M. and Nimbalkar, S. (2015). Behavior of geocell-reinforced subballast subjected to cyclic loading in plane-strain condition. *Journal of Geotechnical and Geoenvironmental Engineering* 141(1): 04014081-16

Indraratna, B., Hussaini, S. K. K. and Vinod, J. S. (2012). On the shear behavior of ballast-geosynthetic interfaces. *Geotechnical Testing Journal* **35**(2): 305-312.

Indraratna, B., Vinod, J. S. and Lackenby, J. (2009). Influence of particle breakage on the resilient modulus of railway ballast. *Géotechnique* **59**(7): 643-646.

Indraratna, B., Ionescu, D. and Christie, H. (1998). Shear behavior of railway ballast based on large-scale triaxial tests. *Journal of Geotechnical and Geoenvironmental Engineering* **124**(5): 439-449.

Indraratna, B., Lackenby, J. and Christie, D. (2005). Effect of confining pressure on the degradation of ballast under cyclic loading. *Géotechnique* **55**(4): 325-328.

Indraratna, B., Ngo, N. T. and Rujikiatkamjorn, C. (2011). Behavior of geogrid-reinforced ballast under various levels of fouling. *Geotextiles and Geomembranes* **29**(3): 313-322.

Indraratna, B. and Nimbalkar, S. (2013). Stress-strain degradation response of railway ballast stabilized with geosynthetics. *Journal of Geotechnical and Geoenvironmental Engineering* **139**(5): 684-700.

Indraratna, B., Nimbalkar, S. and Neville, T. (2014). Performance assessment of reinforced ballasted rail track. *Proceedings of the ICE - Ground Improvement* 167, 24-34

Indraratna, B., Rujikiatkamjorn, C., Vinod, J. S. and Khabbaz, H. (2009). A review of ballast characteristics, geosynthetics, confining pressures and native vegetation in rail track stabilisation. *Transport Engineering in Australia* **12**(1): 25-36.

Indraratna, B., Salim, W. and Rujikiatkamjorn, C. (2011). Advanced rail geotechnology – ballasted track, CRC Press/Balkema.

Indraratna, B., Wijewardena, L. S. S., Balasubramaniam, A. S. and Mostyn, G. (1993). Large-scale triaxial testing of grey wacke rockfill. *Géotechnique* **44**(3): 539-544.

Indraratna, B., Salim, W. and Christie, D. (2006). Geotechnical properties of ballast and the role of geosynthetics in rail track stabilisation. *Proceedings of the ICE - Ground Improvement* **10**(3): 91-101.

Indraratna, B., Rujikiatkamjorn, C. and Christie, D. (2006). Stabilization of ballasted rail tracks and underlying soft formation soils with geosynthetic grids and drains. *GeoShanghai Internatonal Conference, Shanghai, China*.

Jeffs, T. and Tew, G.P. (1991). A review of track design procedures, Vol. 2, Sleepers and Ballast. Railways of Australia.

Jewell, R. A. (1990). Reinforcement bond capacity. *Géotechnique* **40**(3): 513-518.

Jewell, R. A. and Milligan, G. W. E. (1984). Interaction between soil and grids. *In Proceedings of Symposium on Polymer Grid Reinforcement*: 18-29.

Jewell, R. A. and Wroth, C. P. (1987). Direct shear tests on reinforced sand. *Géotechnique* **37**(1): 53-68.

Jha, k. and Mandal, J.N. (1988). A review of research and literature on the use of geosynthetics in the modern geotechnical world. *Proceedings of the First Indian Geotextiles Conference on Reinforced Soil and Geotextiles*: 85-93.

Karasahin, M. (1993). Resilient behaviour of granular materials for analysis of highway pavements, PhD thesis, Dept. of Civil Engineering, University of Nottingham, Nottingham, England.

Khedkar, M. S. and Mandal, J. N. (2009). Pullout behaviour of cellular reinforcements. *Geotextiles and Geomembranes* **27**(4): 262-271.

Kief, O., Schary, Y. and Pokharel, S. K. (2014). High-modulus geocells for sustainable highway infrastructure. *Indian Geotechnical Journal*: 1-12.

Koerner, R. (1998). Designing with geosynthetics.

Kolisoja, P. (1997). Resilient deformation characteristics of granular materials. PhD thesis, Tampere University of Technology, Publ. No. 223, Tampere, Finland.

Krabbenhoft, K., Lyamin, A. V. and Sloan, S. W. (2007). Bounds to shakedown loads for a class of deviatoric plasticity models. *Computational Mechanics* 39, 879-888.

Krishnaswamy, N. R., Rajagopal, K. and Latha, G. M. (2000). Model studies on geocell supported embankments constructed over a soft clay foundation. *Geotechnical Testing Journal* **23**(1): 45-54.

Lackenby, J., Indraratna, B., McDowell, G. and Christie, D. (2007). Effect of confining pressure on ballast degradation and deformation under cyclic triaxial loading. *Géotechnique* **57**(6): 527-536.

Latha, G. M. and Murthy, V. S. (2007). Effects of reinforcement form on the behavior of geosynthetic reinforced sand. *Geotextiles and Geomembranes* **25**(1): 23-32.

Latha, G. M., Rajagopal, K. and Krishnaswamy, N. R. (2006). Experimental and theoretical investigations on geocell-supported embankments. *International Journal of Geomechanics* **6**(1): 30-35.

Lee, K. M. and Manjunath, V. R. (2000). Soil-geotextile interface friction by direct shear tests. *Canadian Geotechnical Journal* **37**(1): 238-252.

Lekarp, F., Isacsson, U. and Dawson, A. (2000). State of the Art. I: Resilient response of unbound aggregates. *Journal of Transportation Engineering* **126**(1): 66-75.

Lekarp, F., Isacsson, U., and Dawson, A. (2000). State of the art. II: Permanent strain response of unbound aggregates. *Journal of Transportation Engineering ASCE*, **126**(1), 76–83.

Leshchinsky, B. and Ling, H. (2013). Effects of geocell confinement on strength and deformation behavior of gravel. *Journal of Geotechnical and Geoenvironmental Engineering* **139**(2): 340-352.

Leshchinsky, B. and Ling, H. I. (2013). Numerical modelling of behavior of railway ballasted structure with geocell confinement. *Geotextiles and Geomembranes* **36**(0): 33-43.

Leshchinsky, B. A. (2012). Enhancing ballast performance using geocell confinement. Ph.D thesis, Columbia University.

Li, D. and Selig, E.T. (1998). Method for railroad track foundation design, I: Development. *J. of Geotechnical and Geoenvironmental Engineering, ASCE*, **124**(4), 316–322.

Liu, C. N., Ho, Y. H. and Huang, J. W. (2009). Large scale direct shear tests of soil/PET-yarn geogrid interfaces. *Geotextiles and Geomembranes* **27**(1): 19-30.

Liu, C., Zornberg, J., Chen, T., Ho, Y. and Lin, B. (2009). Behavior of geogrid-sand interface in direct shear mode. *Journal of Geotechnical and Geoenvironmental Engineering* **135**(12): 1863-1871.

Madhavi Latha, G., Dash, S. and Rajagopal, K. (2008). Equivalent continuum simulations of geocell reinforced sand beds supporting strip footings. *Geotechnical and Geological Engineering* **26**(4): 387-398.

Madhavi Latha, G. and Somwanshi, A. (2009). Effect of reinforcement form on the bearing capacity of square footings on sand. *Geotextiles and Geomembranes* **27**(6): 409-422.

Mandal, J. N. and Gupta, P. (1993). Stability of geocell-reinforced soil. *Construction and Building Materials* **8**(1): 55-62.

Mandal, J. N. and Sah, H. S. (1992). Bearing capacity tests on geogrid-reinforced clay. *Geotextiles and Geomembranes* **11**(3): 327-333.

Marachi, N. D., Chan, C. K., and Seed, H. B., 1972. Evaluation of properties of rockfill materials. *J. Soil Mech. and Found. Div., ASCE*, 98, 95-114.

Marsal, R. J., 1967. Large scale testing of rockfill meterials. *J. Soil Mech. and Found. Div., ASCE*, **93**(2), 27-43.

Mehdipour, I., Ghazavi, M. and Moayed, R. Z. (2013). Numerical study on stability analysis of geocell reinforced slopes by considering the bending effect. *Geotextiles and Geomembranes* **37**(0): 23-34.

Mello, V. F. B. D. (1977). Reflections on design decisions of practical significance to embankment dams. *Géotechnique* 27, 281-355

Mengelt, M., Edil, T. B. and Benson, C. H. (2006). Resilient modulus and plastic deformation of soil confined in a geocell. *Geosynthetics International* **13**(5): 195-205.

Mohamed, M. H. A. (2010). Two dimensional experimental study for the behaviour of surface footings on unreinforced and reinforced sand beds overlying soft pockets. *Geotextiles and Geomembranes* **28**(6): 589-596.

Monismith, C. L., Seed, H. B., Mitry, F. and Chan, C. (1967). Predictions of pavement deflections from laboratory tests. *Second International Conference on the Structural Design of Asphalt Pavements*.

Moraci, N. and Recalcati, P. (2006). Factors affecting the pullout behaviour of extruded geogrids embedded in a compacted granular soil. *Geotextiles and Geomembranes* **24**(4): 220-242.

Murthy, B. R. S., Sridharan, A. and Bindumadhava (1993). Evaluation of interfacial frictional resistance. *Geotextiles and Geomembranes* **12**(3): 235-253.

Nataatmadja, A., and Parkin, A. K. (1989). Characterisation of granular materials for pavements. *Canadian Geotechnical Journal*, 26, 725–730.

Nataatmadja, A. (1992). Resilient modulus of granular materials under repeated loading. *Proc., 7th Int. Conf. on Asphalt Pavements, Univ. of Nottingham, Nottingham, U.K.*, 1, 172–185.

Nimbalkar, S., Indraratna, B., Dash, S. and Christie, D. (2012). Improved performance of railway ballast under impact loads using shock mats. *Journal of Geotechnical and Geoenvironmental Engineering* **138**(3): 281-294.

Palmeira, E. M. (2009). Soil–geosynthetic interaction: Modelling and analysis. *Geotextiles and Geomembranes* **27**(5): 368-390.

Patra, C. R., Das, B. M. and Atalar, C. (2005). Bearing capacity of embedded strip foundation on geogrid-reinforced sand. *Geotextiles and Geomembranes* **23**(5): 454-462.

Puppala, A. J. (2010). Geotechnical Special Publication. *Ground improvement and geosynthetic*. Reston, VA, USA, ASCE. Volume 207

Perkins, S. W., Christopher, B. R., Cuelho, E., Eiksund, G., Hoff, I., Schwartz, C., Svanø, G. and Watn, A. (2004). Development of design methods for geosynthetic reinforced flexible pavements. Report prepared for the US Department of Transportation Federal Highway Administration, Washington, DC, FHWA Report Reference Number DTFH61-01-X-00068, 263p.

Pezo, R. F. (1993). A general method of reporting resilient modulus tests of soils – A pavement engineer's point of view. *Proceedings of 72nd Annual Meeting of the transportation Research Board, Washington, D.C., USA*.

Pokharel, S. K., Han, J., Leshchinsky, D., Parsons, R. L. and Halahmi, I. (2010). Investigation of factors influencing behavior of single geocell-reinforced bases under static loading. *Geotextiles and Geomembranes* **28**(6): 570-578.

Radampola, S. S. (2006). Evaluation and modelling performance of capping layer in rail track substructure, PhD thesis, Central Queensland university.

Rajagopal, K., Krishnaswamy, N. R. and Madhavi Latha, G. (1999). Behaviour of sand confined with single and multiple geocells. *Geotextiles and Geomembranes* **17**(3): 171-184.

Raymond, G. P. (2001). Failure and reconstruction of a gantry crane ballasted track. *Canadian Geotechnical Journal* **38**(3): 507-529.

Rea, C. and Mitchell, J. K. (1979). Sand reinforcement using paper grid cells. *Proc., ASCE Spring Convention and Exhibit, Pittsburg,* ASCE, New York, 24-28

Rowe, P. W. (1962). The stress-dilatancy relation for static equilibrium of an assembly of particles in contact. *Proceedings of the Royal Society of London. Series A. Mathematical and Physical Sciences* **269**(1339): 500-527.

Salim, W. and Indraratna, B. (2004). A new elastoplastic constitutive model for coarse granular aggregates incorporating particle breakage. *Canadian Geotechnical Journal* **41**(4): 657-671.

Saride, S., Puppala, A. J., Sitharam, T. G. and Gowrisetti, S. (2009). Numerical simulation of geocell-reinforced sand and clay. *Proceedings of the Institution of Civil Engineers. Ground improvement* **162**(4): 185-198.

Sayeed, M. M. A., Ramaiah, B. J. and Rawal, A., 2014. Interface shear characteristics of jute/polypropylene hybrid nonwoven geotextiles and sand using large size direct shear test. *Geotextiles and Geomembranes* **42**(1), 63-68.

Schanz, T. and Vermeer, P. A. (1996). Angles of friction and dilatancy of sand. *Geotechnique* **46**(1), 145-151

Schlosser, F., Juran, I. and Jacobsen, H. Moust (1983). Soil reinforcement. *General Report, VIII European Conference on Soil Mechanics and Foundation Engineering, Balkema, Helsinki*, 83–103

Seed, H. B., Mitry, F. G., Monismith, C. L., and Chan, C. K. (1967). Prediction of flexible pavement deflections from laboratory repeated-load tests, Highway Research Board National Research Council National Academy of Sciences-National Academy of Engineering.

Selig, E. T. (1987). Tensile zone effects on performance of layered systems. *Géotechnique* **37**(3): 247-254.

Selig, E. T. and Waters, J. M. (1994). Track Geotechnology and Substructure Management, Thomas Telford, London.

Sieira, A. C. C. F., Gerscovich, D. M. S. and Sayão, A. S. F. J. (2009). Displacement and load transfer mechanisms of geogrids under pullout condition. *Geotextiles and Geomembranes* **27**(4): 241-253.

Sireesh, S., Sitharam, T. G. and Dash, S. K. (2008). Bearing capacity of circular footing on geocell–sand mattress overlying clay bed with void. *Geotextiles and Geomembranes* **27**(2): 89-98.

Sitharam, T. G. and Hegde, A. (2013). Design and construction of geocell foundation to support the embankment on settled red mud. *Geotextiles and Geomembranes* **41**(0): 55-63.

Smith, W. S., and Nair, K. (1973). Development of procedures for characterization of untreated granular base coarse and asphalt treated base course materials. *Report No. FhWA-RD-74-61, Federal Highway Administration*, Washington, D.C., 1973

Soleimanbeigi, A. and Hataf, N. (2006). Prediction of settlement of shallow foundations on reinforced soils using neural networks. *Geosynthetics International* **13**(4): 161-170.

Sridharan, A. and Deepankar Choudhury, D. (2000). Shear Strength of fine grained soil and concept of cohesion. *Proc. of Indian Geotechnical Conference, IGC-2000*, December 13-15, 2000, IIT Bombay, India, Vol.1, pp. 93-94.

Stark, T. D., Williamson, T. A. and Eid, H. T. (1996). HDPE geomembrane/geotextile interface shear strength. *Journal of geotechnical and geoenvironmental engineering* **122**(3): 197-203.

Suiker, A. S. J. and de Borst, R. (2003). A numerical model for the cyclic deterioration of railway tracks. *International Journal for Numerical Methods in Engineering* **57**(4): 441-470.

Suiker, A. S. J., Selig, E. T. and Frenkel, R. (2005). Static and cyclic triaxial testing of ballast and subballast. *Journal of Geotechnical and Geoenvironmental Engineering* **131**(6): 771-782.

Swan, R. H., Bonaparte, R., Bachus, R. C., Rivette, C. A. and Spikula, D. R. (1991). Effect of soil compaction conditions on geomembrane-soil interface strength. *Geotextiles and Geomembranes* **10**(5–6): 523-529.

Sweere, G. T. H. (1990). Unbound granular basis for roads.

Tafreshi, S. N. M., Khalaj, O. and Dawson, A. R. (2014). Repeated loading of soil containing granulated rubber and multiple geocell layers. *Geotextiles and Geomembranes* **42**(1): 25-38.

Tanyu, B. F., Aydilek, A. H., Lau, A. W., Edil, T. B. and Benson, C. H. (2013). Laboratory evaluation of geocell-reinforced gravel subbase over poor subgrades. *Geosynthetics International* 20, 47-61

Tatlisoz, N., Edil, T. and Benson, C. (1998). Interaction between reinforcing geosynthetics and soil-tire chip mixtures. *Journal of Geotechnical and Geoenvironmental Engineering* **124**(11): 1109-1119.

Tetsudo Gijutsu, K. (1994). Study on properties of road bed reinforced with geocell. Quarterly reports 35: 23-31.

Thallak, S., Saride, S. and Dash, S. (2007). Performance of surface footing on geocell-reinforced soft clay beds. *Geotechnical and Geological Engineering* **25**(5): 509-524.

Thom, N. and Brown, S. (1988). The effect of grading and density on the mechanical properties of a crushed dolomitic limestone. *Australian Road Research Board (ARRB) Conference, 14th*, 1988, Canberra.

Timoshenko, S. P. and Goodier, J. N. (1970). Theory of elasticity. McGraw-Hill, New York.

Trani, L. and Indraratna, B. (2010). Assessment of subballast filtration under cyclic loading. *Journal of Geotechnical and Geoenvironmental Engineering* **136**(11): 1519-1528.

Uzan, J. (1985). Characterization of granular material. *Transportation research record*: 52-59.

Vidal, H. (1969). The principle of reinforced earth. *Geotechnical special publication* **123**(118): 1331 - 1346.

Wang, G. Y., Zhang, J. P. and Zhao, J. W. (2013). Numerical analysis of geocell protective slope stability, Trans Tech.

Wang, Y. M., Chen, Y. K. and Liu, W. (2008). Large-scale direct shear testing of geocell reinforced soil. *Journal of Central South University of Technology* **15**(6): 895-900.

Webster, S. L. and Alford, S. J. (1978). Investigation of construction concepts for pavements across soft ground, Soil and Pavement Laboratory, U.S. Army Engineer Waterways Experiment Station.

Webster, S. L. and Watkins, J. E. (1977). Investigation of construction techniques for tactical bridge approach roads across soft ground. US Army Waterways Experiment Station, Technical Report, 77-1.

Wesseloo, J., Visser, A. T. and Rust, E. (2009). The stress–strain behaviour of multiple cell geocell packs. *Geotextiles and Geomembranes* **27**(1): 31-38.

Woodward, P. K., Woodward, P. K., Thompson, D. and Banimahd, M. (2007). Geocomposite technology: reducing railway maintenance. *Proceedings of the Institution of Civil Engineers. Transport* **160**(3): 109-115.

Yang, X. (2010). Numerical analyses of geocell-reinforced granular soils under static and repeated loads. 3422690.

Yang, X. and Han, J. (2013). Analytical model for resilient modulus and permanent deformation of geosynthetic-reinforced unbound granular material. *Journal of Geotechnical and Geoenvironmental Engineering* **139**(9): 1443-1453.

Yang, X. and Han, J. (2013). Geocell-reinforced granular fill under static and cyclic loading: A synthesis of analysis. *Geotechnical engineering* **44**(4): 17-23.

Yang, X., Han, J., Parsons, R. L. and Leshchinsky, D. (2010). Three-dimensional numerical modeling of single geocell-reinforced sand. *Frontiers of Architecture and Civil Engineering in China* **4**(2): 233-240.

Yang, X., Han, J., Pokharel, S. K., Manandhar, C., Parsons, R. L., Leshchinsky, D. and Halahmi, I. (2012). Accelerated pavement testing of unpaved roads with geocell-reinforced sand bases. *Geotextiles and Geomembranes* **32**(0): 95-103.

Yu, H. S. and Sloan, S. W. (1997). Finite element limit analysis of reinforced soils. *Computers & Structures* **63**(3): 567-577.